Spring 2012

Glycerin reformation in high temperature and pressure water

Jason W. Picou

Department: Chemical and Biochemical Engineering

GLYCERIN REFORMATION IN HIGH TEMPERATURE AND PRESSURE WATER

by

JASON WADE PICOU

A DISSERTATION

Presented to the Faculty of the Graduate School of the

MISSOURI UNIVERSITY OF SCIENCE AND TECHNOLOGY

In Partial Fulfillment of the Requirements for the Degree

DOCTOR OF PHILOSOPHY

IN

CHEMICAL ENGINEERING

2012

Approved by

Dr. Sunggyu Lee, Advisor
Dr. Douglas Ludlow, Co-Advisor
Dr. Yangchuan Xing
Dr. John Sheffield
Dr. David Retzloff

ABSTRACT

The noncatalytic reformation of glycerin in supercritical water was studied in a Haynes 282 tubular reactor. In order to determine which parameters were the most influential, a 2^3 experimental matrix was conducted, with temperatures of 500 and 700°C, water/glycerin molar ratios of 3:1 and 13:1, and residence times of 30 and 90 seconds, all at a pressure of 24 MPa. It was found that temperature had the largest effect on the two gasification parameters deemed most important, gasification percentage and hydrogen yield. Based on this, the effect of temperature was further investigated by looking at 50°C intervals from 500 to 800°C. From this it was determined that a temperature of 700 to 750°C was most conducive to glycerin reformation. The results were compared to equilibrium, as calculated by Gibbs free energy minimization. It was found that at temperatures from 750°C to 800°C; most of the results were at equilibrium. Based on this, kinetic models were developed for experiments not in equilibrium. The first model is a pseudo first order model of the gasification, which compares favorably with other studies. The second kinetic model takes into account the carbon containing gaseous species. Three reactions are used to model the gaseous products: Complete gasification of the glycerin into carbon monoxide and hydrogen, water gas shift of the resulting carbon monoxide, and a reaction in which glycerin and hydrogen combine to produce methane. Other reaction pathways were tested, and they either did not fit the data as well, or were thermodynamically impossible. The reactions are also capable of predicting hydrogen production for most conditions.

ACKNOWLEDGEMENTS

Many people and institutions have contributed to the work outlined in the following pages. I would like to thank them for their support, experience and trust. I would like to express my gratitude to my advisor, Dr. Sunggyu Lee, for all the opportunities and guidance he has given me in my academic and personal development. My Co-Advisor, Dr. Ludlow, who remained steadfast that I deserved a chance to earn this degree. I've been financially supported by the U.S. Army under PE Number 0602705A via a subcontract from DRS Technical Services Inc. and by the U.S. Department of Education's GAANN fellowship program. My thanks to all my friends in Dr. Lee's group, especially Michael Stever, Dr. Jonathan Wenzel, and Melody Mueller, who provided insights, encouragement and have made my graduate school experience very enjoyable. Of course, I have to thank my family for their support, love and motivation throughout the years.

TABLE OF CONTENTS

Page

LIST OF FIGURES

LIST OF TABLES

1. INTRODUCTION

1.1. RESEARCH OBJECTIVES

The object of this research is to reform glycerin into hydrogen and carbon monoxide non-catalytically using supercritical water. The major variables in any reformation project include temperature, pressure, water-to-fuel ratio, residence time, catalyst, and reactor type. This study will focus on temperature, water-to-fuel ratio and residence time. A 2^3 factorial design is used to determine which variable is most important to gasification, and further in-depth research is conducted in that direction. The objective is to produce hydrogen or a mixture of hydrogen and carbon monoxide known as synthesis gas. These product gases can be used in a variety of petrochemical and fuel applications.

Also, this supercritical water system is of a small pilot plant scale, while most other studies into supercritical water reformation use micro-reactors. A larger scale reactor investigation, such as the current study, offers more realistic reactor, heat transfer and flow conditions compared to micro-reactors. This is important for new process development as well as scale-up of the process system. These two insights, the most important parameters and the feasibility of scale-up, offer opportunities to maximize the process and scale-up further to industrial applications

1.2. MOTIVATION OF RESEARCH

Glycerin is the major by-product of biodiesel production, being 10% by weight of the product stream. Biodiesel production is increasing worldwide, leading to an increase

in the production of glycerin whose conventional market is not expanding at the same rate. Having a process by which glycerin can be converted into value added products would increase the profit margin of biodiesel production, thus making it more sustainable. Furthermore, hydrogen and carbon monoxide are currently produced from fossil fuels, while glycerin is derived from a biological, renewable source.

The motivations for using supercritical water in glycerin reformation have to do with the properties of glycerin and supercritical water. First, glycerin is hygroscopic, and absorbs up to 20% water from the atmosphere. Glycerin itself has a low calorific value, approximately 40% of that of gasoline per mass basis. These facts make it less desirable for direct combustion. Also, the crude glycerin from the biodiesel plant contains impurities that make it more costly to purify to use as a livestock feed, food preservative or cosmetics, which are currently some of the major end uses of glycerin. Using supercritical water negates the water absorption problem because water is used in the process, and the noncatalytic reforming in supercritical water is less affected by the impurities found in crude glycerin. The properties of supercritical water also make it an effective and efficient method of reformation. Supercritical water reformation produces gasses at high pressure, which is useful for efficient storage, transportation or subsequent reactions.

Some studies have examined obtaining products from glycerin other than hydrogen and carbon monoxide, specifically liquid products like acrolein, propylene glycol, formaldehyde, and methanol, among others. The formation of hydrogen and carbon monoxide was emphasized in this study because they are building block chemicals, from which a variety of products can be produced. They are simple to

separate from the liquid effluent, and easier to characterize. In future studies crude glycerin may be used, which could have impurities that hinder some of the liquid products or decrease their yield. In order to have greater future application, the simplest and highest yield components, the gaseous products, were investigated.

2. BACKGROUND

2.1. INTRODUCTION

The purpose of this dissertation is to study the reformation of glycerin in supercritical water. Therefore, the purpose of this background is to explain the components and provide an overview of research conducted in similar areas. It begins with a review of supercritical fluids, then specifically supercritical water. Next, glycerin is discussed, its properties and how and why it is produced. Then the products of reformation, synthesis gas and hydrogen, are discussed. Finally, a literature review of atmospheric, subcritical and supercritical reformation of glycerin is given, as well as some of the catalytic effects observed in glycerin reformation.

2.2. SUPERCRITICAL FLUIDS

A supercritical fluid is a unique state of matter that occurs for any fluid that is above its critical temperature and pressure. In general, if the temperature of a liquid is raised at constant pressure it becomes a gas, or if the pressure on a gas is increased at constant temperature it becomes a liquid. At a point called the critical point, if the temperature or pressure is raised the boundary between the liquid and vapor phase disappears and the fluid is no longer a gas or a liquid but is a supercritical fluid. This continuity of the liquid and gas states, and the existence of the critical point, was discovered in 1861 by Thomas Andrews (*1*). The mathematical definition of a critical point is where both the partial derivative and its second partial derivative of pressure with respect to volume at constant temperature equal zero (*2*, *3*).

Supercritical fluids have properties that are usually intermediate from those of either liquids or gases, and these properties can be finely tuned around the critical point (*4*). Theoretically, all compounds have a critical point, but some such as polymers degrade before reaching it (*5*). A supercritical fluid, as compared to a liquid, has a higher molecular diffusivity, a lower viscosity and no surface tension at all. The molecular diffusivity in a supercritical fluid is between that of a liquid and a gas, but closer to that of a gas, so that reactions that are diffusion limited in the liquid phase can become faster in the supercritical region (*6*). The density is highly dependent on temperature and pressure near and beyond the critical point, thus allowing a wide variability (*7*). These properties, especially the higher diffusivity, make supercritical fluids applicable and potent solvents. Supercritical fluids are also simple to regenerate because by cooling and depressurizing the fluid it loses its supercritical solvent capabilities and the solute precipitates out, leaving the solute and solvent separated (*3*, *7*). When conducting chemical reactions at supercritical fluid conditions, the above properties allow for greater solubility of reactants and products, the elimination or alleviation of interphase transport limitations on the reaction rate, the reduction of carbon deposition on heterogeneous catalysts, and the integration of reaction and separation unit operations (*6*). Carbon dioxide and water are the fluids most frequently used in supercritical applications. Both are environmentally benign and readily accessible. The properties of supercritical CO_2 and the ease with which its critical point is reached means it could replace some halogenated or aromatic solvents (*6*, *8*). Supercritical fluids have been used to decaffeinate coffee and tea, to extract the nicotine from tobacco, textile dying and dry cleaning, cleaning and etching silicon wafers, wastewater treatment, remediation of

contaminated soil, supercritical fluid chromatography, production of fine powders, extraction from and impregnation of polymers, polymerization and graft copolymerization, natural food extracts and fragrances, vitamin and antioxidant extraction, among other applications (*5*, *9–13*). This section will begin with an introduction into the physical properties of supercritical water, then cover some of the unique advantages of using supercritical water in reformation or gasification processes.

2.2.1. Supercritical Water. "*In no other solvent can the properties near or above the critical point be changed more strongly as a function of pressure and temperature than in water*" (*14*). Figure 2-1 is a pressure/temperature graph of pure water, which illustrates the supercritical region for water, the critical point for which is 647.3 K and 22.06 MPa (*3*, *5*). The addition of any impurities to the water would change its phase behavior, including the critical point. The diffusivity, density, dielectric constant, heat capacity, organic and inorganic solubility, and viscosity all change significantly for water going from ambient temperature to supercritical (*2*, *3*, *5*).

Table 2-1 presents these important physical properties of water as a function of temperature and pressure, in order to compare the differences between ambient, sub-critical, and supercritical water and superheated steam. The density of supercritical water is between that of ambient water and superheated steam, and can be varied continuously from high, liquid-like values to low, gas-like values, without phase transition as a function of temperature and pressure. Supercritical water is distinct from ambient water in that the hydrogen bonding of supercritical water is almost entirely disrupted, making it more like an organic solvent than ambient water (*15–17*).

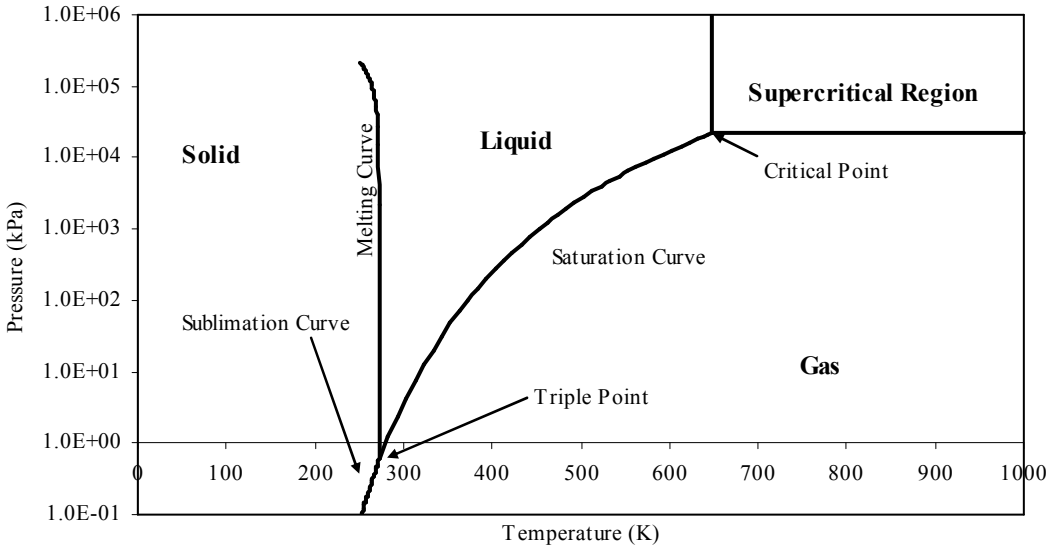

Figure 2-1. Phase diagram including supercritical region for water.

Table 2-1. Physical properties of water (*18–20*).

	Ambient Water	**Superheated Steam**	**Subcritical Water**	**Supercritical Water**		
T (°C)	25	400	250	400	800	400
P (MPa)	0.1	0.1	24	24	24	50
ρ (kg/m3)	997.05	0.32	819.97	148.55	50.64	577.79
ε	78.41	1.00	28.06	2.28	1.22	11.98
pK_w	14.0	N.A.	11.0	19.4	24.2	11.9
c_p (kJ/kg °C)	4.14	2.07	4.65	10.80	2.63	6.79
η (μPa s)	890.08	24.45	111.39	28.19	41.92	67.99

The disrupting of the hydrogen bonding gives supercritical water a low dielectric constant, meaning supercritical water is completely miscible with non-polar compounds like hydrocarbons and chlorofluorohydrocarbons, while being immiscible to inorganic

salts. The dielectric constant of water at 25°C is 78, while it is about 6 at the critical point. As can also be seen in Table 2-1, the heat capacity of supercritical water at 400°C is larger than ambient water or superheated steam. The ionic product of water, K_w, is another property that is tunable with changes in temperature and pressure in the sub- to supercritical region, which is useful for optimizing acid/base reactions. The dynamic viscosity, η, at supercritical conditions is a ten to twenty times lower than the viscosity of ambient water, leading to advantages where reaction rates are limited by mass transfer, such as heterogeneously catalyzed reactions (*21*, *22*).

Figures 2-2, 2-3 and 2-4 illustrate how the density, gas solubility and inorganic solubility changes as a function of temperature at 23.44 MPa (*23*). The dashed line at 374°C is the temperature at which pure water becomes supercritical. The density changes gradually around the critical point, so that variations in temperature or pressure can have controllable variations in the density. The solubility of permanent gases has a more dramatic change at the critical point, as shown in Figure 2-3. Gases such as oxygen are 100% soluble in supercritical water, as are other permanent gases such as carbon monoxide and methane (*24*). The solubility of permanent gases in supercritical water can overcome inter-phase transport limitations, increasing mass transfer, while also simplifying downstream separation and purification (*6*, *25*). If the water is cooled below the critical point, the gases and water would separate, leaving high pressure gaseous products. Hydrocarbon and organic solubility follows a similar pattern (*10*, *23*, *26*). Figure 2-4 illustrates the miscibility of salts in supercritical water.

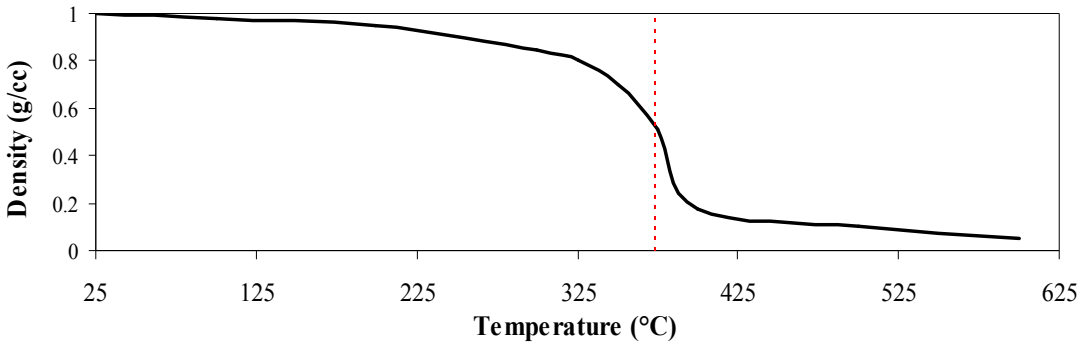

Figure 2-2. Density change of water as a function of temperature at 23.44 MPa (*20*).

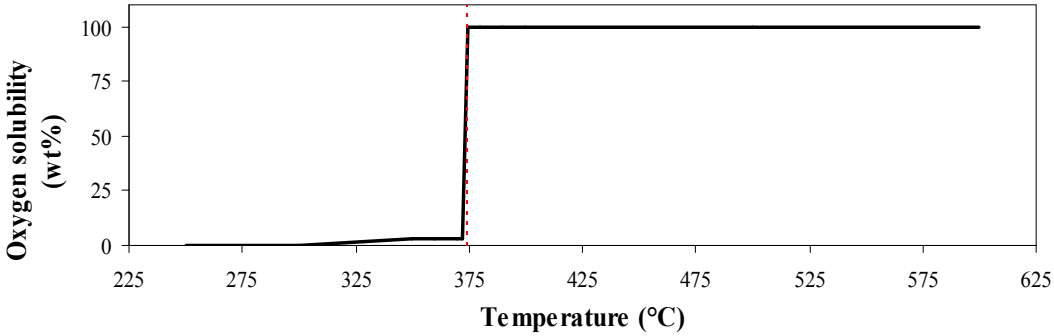

Figure 2-3. Oxygen solubility in water as a function of temperature at 23.44 MPa (*23*).

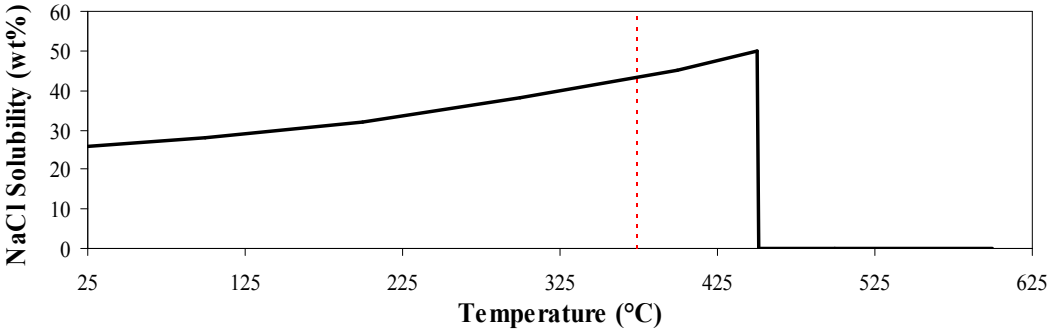

Figure 2-4. Sodium chloride solubility in water as a function of temperature at a pressure of 23.44 MPa (*23*).

The reason that the solubility increases gradually after the critical point then suddenly decreases at about 450°C is because the salt changes the critical point of water, just as it changes the boiling and melting point of water. The dashed line represents the pure water critical point, but the steep decline in solubility at about 450°C is the actual critical point for this mixture (*23*). These properties of supercritical water are the complete opposite to some of the properties of ambient water, which is largely immiscible to oils, dissolves salts and can only dissolve a small amount of permanent gases

2.2.2. Applications and Advantages of Supercritical Water. Supercritical water reformation and supercritical water oxidation have been investigated for years as a medium for waste disposal, depolymerization, geochemical reactions, and the reformation of various hydrocarbons and biomass (*5*, *27–32*). The first industrial use of supercritical water was in a deep-shaft wastewater reactor developed by Vertox in 1975, which used a deep shaft drilled into the earth to develop high pressure. A wastewater stream and air were pumped down the shaft, which became supercritical due to the energy liberated *in situ* by oxidation and the high pressures due to the weight of the water above. The waste in the water was oxidized to water and carbon dioxide (*5*). The first aboveground supercritical water reactor was developed by Modell and coworkers at the Massachusetts Institute of Technology in 1979 to investigate the reformation of various organics and the destruction of wastes (*5*, *33*, *34*). Since then, numerous studies have been conducted into the applications of supercritical water.

The supercritical phase reformation has the advantage of not requiring energy-intensive vaporization of water to generate steam (*35*). The enthalpy of supercritical

water at 700°C and 30 MPa is 3744 kJ/kg, steam at 700°C and 1 atm has an enthalpy of 3929 kJ/kg, a difference of 5%. While this in itself is not a large difference, supercritical water leads to more compact and efficient heat exchange. Since the driving force of a heat exchanger is the difference between hot and cold, evaporation or vaporization reduces the efficiency of heat exchangers because energy must be transferred without a temperature change (*14*). Supercritical water negates this problem. Efficient heat exchange is one of the design features that are essential to system efficiency and performance when dealing with supercritical water gasification (*36*).

Supercritical water oxidation or partial oxidation has been studied as a means of de-polymerizing polymers, gasifying biomass and high-weight hydrocarbons, and destroying such wastes as rocket propellants, chemical warfare agents, waste sludge, concentrated municipal sewage and organic waste (*5*, *31*, *32*, *37–44*). The advantages include fast reaction times because oxygen is completely soluble in supercritical water, and the high temperatures lead to fast reactions. This solution to waste disposal does not have some of the problems associated with standard incineration, which includes only partial combustion of the waste and the formation of dangerous incineration byproducts (IBP's) like dioxin. The lower temperatures in supercritical water oxidation leads to nitrogen containing compounds producing mainly nitrogen gas, so that NO_x production is not a problem (*45*). Partial oxidation of biomass or hydrocarbons leads to higher conversions of the hydrocarbons into gas and in-situ heat generation, leading to autothermal gasification (*37*, *38*, *46*). Additionally, water can function as a catalyst as well as a reactant in numerous reactions (*25*, *47–52*).

When the goal is to gasify biomass, supercritical water gasification has the advantage of not having to dry the biomass, which can have a water content of 80 wt% or more (*14*). The water in the biomass acts as a solvent and a reactant (*26*). Also, supercritical water accelerates the depolymerization of biomass such as cellulose, and leads to faster gasification rates then subcritical water (*53*). The intermediates are highly soluble in SCW, which inhibits tar and coke formation (*6*, *54*). Another advantage of supercritical water gasification is that the product gas is produced at high pressures, making it easier to store or transfer. Carbon dioxide can be separated from the other permanent gases because it is more soluble in high pressure, ambient temperature water. Supercritical or near-critical water can also function as a solvent in chemical processing, so that organic solvents would not have to be used (*51*).

The largest current commercial application of supercritical water oxidation is its use for the gasification of sewage sludge and hazardous waste. A hydrothermal oxidation system in Harlingen, Texas uses a patented process from HydroProcessing, L.L.C. to gasify up to 9.8 dry tons per day of municipal sludge. The process is autothermal, so that all of the energy needed is generated by the exothermic oxidation reaction (*43*). They employ a tubular reactor that operates up to 700°C, as well as a patented process to depressurize the solid containing effluent (*55*, *56*). A pilot plant in Karlskoga, Sweden was built in 1998 and based on technology developed by Chematur Engineering AB called the Aqua-Critox system, and capable of processing 250 kg wet sludge per hour (*40*). Supercritical water oxidation plants have been used in Japan and Germany to dispose of wastes from pharmaceutical and semiconductor manufacturers (*41*). Numerous companies have built or proposed of plants that use supercritical water

oxidation for the destruction of hazardous waste on US Army bases and US Navy ships, including VX nerve gas and high explosives (*41*).

The ability to use a single phase during heat transport has led to the investigation of using supercritical water in nuclear reactors. The system is characterized by low flow rates, high enthalpy rise and single phase cooling, which allows thermal efficiency up to 44% for the plant. Because supercritical water is such an efficient heat transport medium, the supercritical water nuclear reactor can have a power density similar to liquid metal-cooled reactors, which leads to a more compact vessel size. The high power density, smaller size and the simplicity of having only one phase leads to capital cost reduction. Supercritical water nuclear reactors are one of the candidates for the Generation IV nuclear reactor system (*57*, *58*). Fossil fuel power plants can also achieve higher thermodynamic efficiency and heat transfer by using supercritical or high pressure water instead of steam (*59*, *60*).

While supercritical water does have numerous advantages, there are also challenges. The most basic is a reaction system that can operate at the temperatures and pressures necessary for supercritical water, which entail higher investment costs. There are some problems with corrosion using supercritical water, which is greatly increased for supercritical water oxidation or when halides are present, as these can form acids (*61*–*65*). Recent advances in metallurgy, such as the high nickel alloys, mitigate these problems. The lack of kinetic and thermodynamic data in supercritical water reactions is a fundamental disadvantage, because only a few binary or ternary systems have been investigated (*25*, *66*, *67*). When gasifying biomass, there can be problems with salts plugging the reactor, since the solubility of salts is reduced in supercritical water. (*42*,

68–70). This is more of a problem with catalytic reactors since the free diameter in the reactor is smaller (*69*). Salts, along with any nitrogen or sulfur containing compounds, can poison the catalysts in some processes (*71–73*). In other work, it has been shown that alkali salts act as a catalyst in supercritical water, increasing biomass gas yields (*54*, *74*). At lower temperatures, char or coke can also lead to reactor plugging (*69*, *75*).

2.3. GLYCERIN

Glycerin, also known as glycerol, glycerine, or 1,2,3-propanetriol is a colorless, nontoxic, viscous liquid with the chemical formula $C_3H_5(OH)_3$ (*76*). The name 1,2,3-propanetriol better describes the compound as a three carbon backbone compound with a hydroxyl group bonded to each carbon, which accounts for its hygroscopic nature and solubility in water and simple alcohols. Some of the physical properties of glycerin are listed in Table 2-2, while Appendix A has information about the physical properties of glycerin/water mixtures.

Table 2-2. Physical properties of glycerin at 25°C and 100 kPa (*77–80*).

Molecular Weight (g/mol)	92.09
Density (g/cm^3)	1.26
Melting Point (°C)	17.8
Boiling Point (°C)	290
Critical Temperature (°C)	577
Critical Pressure (atm)	74.02
Acentric factor	0.5163

Among its many uses, glycerin is found in cosmetics and personal care products, pharmaceuticals, as a lubricant and in the production of nitroglycerine. Cosmetics and personal care products include soap, lotions, hair products, oral care products, personal lubricants, deodorants and suppository laxatives (*76*). The hygroscopic and non-toxic nature of glycerin is the reason for its being used so heavily in the personal care industry, because it acts as a moisturizer. Due to glycerin's sweet taste and non-toxicity, it is used in many food and tobacco applications. Toothpastes, cough syrup, lozenges, mouthwash, and cookies can contain it. The hygroscopic nature of glycerin is used in the tobacco industry to keep cigarettes and other products at the correct moisture content (*76*). The high viscosity of glycerol makes it a perfect thickening agent for food and beverages (*81*).

Glycerin can be polymerized and form polyglycerol esters, which have a wide variety of characteristics based on the length of the polyglycerol and the hydrocarbons used during esterification. Polyglycerol esters are widely used in pharmaceuticals and cosmetics, as well as food processing as an emulsifying agent, crystal inhibitor, anti-clouding agent and as a viscosity reducing agent in the manufacture of chocolate (*82–84*). Along with fatty acids, glycerin is used when producing some esters and as an ingredient in alkyd resins (*82*, *85*). A long list of other applications for glycerin could be compiled, but these are the most prevalent. As of 2003, the world market for glycerin was 600 million kg (*86*). Table 2-3 shows how this glycerin is used by various industries and in what percentage. Glycerin is the backbone of most of the natural oils and animal fats; three fatty acids esterified to glycerin constitute a triglyceride. Before the advent of a major biodiesel industry, glycerin was a byproduct of other industries that wanted to

extract the fatty acids from oils, such as the soap industry. Glycerin is also produced synthetically from various petroleum products, such as propylene, which was used due to glycerin shortages but is now mostly used to make ultra-high purity glycerin (*76*). Currently, most glycerin is the byproduct of the biodiesel industry (*86*).

Table 2-3. Worldwide glycerin consumption by various industries (*87*).

Industry	Percentage consumption (%)
Drugs, pharmaceuticals	18
Personal care	16
Polyglycerol esters	14
Food	11
Other	11
Triacetin	10
Alkyd resins	8
Tobacco	6
Detergents	2
Cellophane	2
Explosives	2

Biodiesel is a hydrocarbon fuel produced from plant oil, algae oil, or animal fat that is meant to be a renewable fuel that can be blended with or replace diesel derived from petroleum (*88*, *89*). Biodiesel can completely displace diesel with only minor modifications to the engines or fuel systems of the diesel fleet, with no infrastructure change or transportation difficulties beyond ordinary diesel (*86*, *90*). Diesel and biodiesel can be blended at any percentage, commonly 5% biodiesel, known as B5, or 20% (B20).

This is because no engine modification is needed up to 20% biodiesel. It has a higher cetane number (CN) and lubricity than petroleum derived diesel, but with a lower energy content, leading to a 2-8% decrease in fuel economy (*88*). Rudolph Diesel, when writing about using vegetable oils as fuels in 1912, said "In any case, they make it certain that motor-power can still be produced from the heat of the sun, which is always available for agricultural purposes, even when all our natural stores of solid and liquid fuels are exhausted" (*91*). Biodiesel is industrially produced by the transesterification reaction, given below in Equation 1, of triglyceride with an alcohol, usually catalyzed by an acid or base, to form the alkyl esters which constitute biodiesel. The reaction below uses methanol as the alcohol, but any alcohol can be used and will affect the resulting biodiesel.

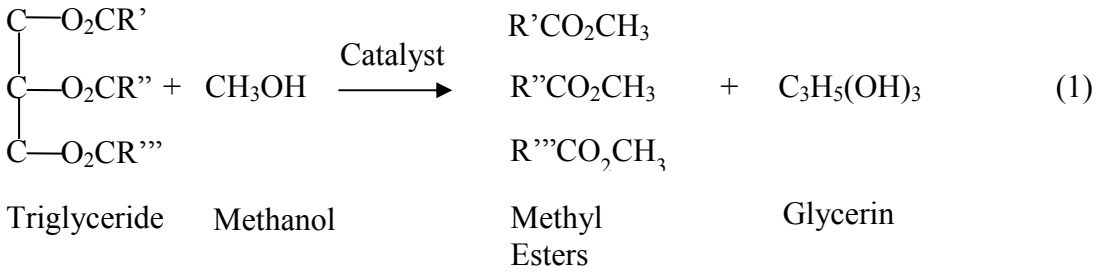

In the above reaction, the hydrocarbon chains of the triglyceride are represented by R', R" and R'". If the triglyceride has different length hydrocarbon chains, then the resulting fatty acids would reflect this. The triglyceride used need to have hydrocarbon chains of similar length and properties as diesel in order to be blended with or replace it. The best starting material for biodiesel is refined vegetable oils such as canola, palm, soybean and rapeseed oils, although animal fats and tallow can also be used (*88*). The most common feed stocks are rapeseed in the EU, palm oil in tropical countries, and

soybean oil in the U.S (*89*). Waste triglycerides that could be used include yellow grease, which is waste oil from restaurants, and trap grease, which is collected at wastewater treatment plants (*89*, *92*). The feedstock costs decrease from canola oil > soybean oil > tallow and lard > yellow grease > trap greases (*89*). While trap grease is least expensive, it is contaminated and must first be purified to be used, increasing its cost. The current industrial production of biodiesel is conducted at temperatures from 50 to 70°C at atmospheric pressure, in either batch or continuous reactors (CSTR or plug flow), depending on the size of the plant (*93*). Excess alcohol is used, typically 50-200%, so that a complete reaction with yields of 99.7% are achieved (*89*). Methanol is commonly used, except perhaps in Brazil where there is a large source of inexpensive ethanol. Methanol has the advantage of having a higher reactivity and being non-hygroscopic, while ethanol is renewable and non-toxic (*94*). Water has a detrimental effect on the reaction because soaps can be formed, which cause problems in downstream separation. While both acids and bases can be used as a catalyst, base catalysts are 4000 times more active and cause less corrosion (*89*). Supercritical methanol can also be used for the transesterification of oils. This method does not require a catalyst, requires no pretreatment, and has a faster reaction rate because it is a homogeneous supercritical reaction that has no interphase mass transfer to limit the reaction rate (*95*, *96*). This method has seen limited use in Europe (*97*).

Currently biodiesel is produced only from commercial food crops such as soybeans or rapeseed, but research is being conducted that would have non-food plants produce oils with which to make biodiesel. Microalgae is seen as a promising replacement because it is not a food crop, does not require arable land, has very high

growth rates, and utilizes a large fraction of solar energy (*89*, *98*). Microalgae can be grown almost anywhere and require only sunlight, water and simple nutrients, although higher yields are obtained under more controlled conditions (*99*, *100*). Microalgae can be grown in water unfit for human consumption, such as wastewater or agricultural runoff (*98*, *99*). Certain stains of algae can produce 250 times the amount of oil per acre as soybeans, and are the highest yielding feedstock for biodiesel (*101*). Microalgae can contain from 7 to 54 dry wt% triglycerides (*102*). Efficient removal of the oil from the algae is still a focus of study, and could account for 20-30% of the total cost of algae to biofuel production (*103*). Options include sedimentation, centrifugation, filtration, belt filtering and flotation, among others (*98*, *103*). The remaining material can undergo anaerobic digestion to produce methane, burned to produce electricity, gasified to produce syngas or in some stains which produce large amount of starch, fermented to produce ethanol (*104*, *105*). Genetic engineering of microalgae may unlock even more potential (*106*). There are many questions still unanswered about the industrial scale production of microalgae, including what species of microalgae to use, where and how to grow it, what nutrients are needed, what predators or competitors might slow growth, and how to process the microalgae. Obviously there may be problems un-envisioned, since the commercial production of algae does not have a long history of progress like farming does. The current limitation of microalgae is the high production cost (*107*).

The production of biodiesel is increasing both in Europe and the United States. In 2010, U.S. biodiesel production was about 1 million metric tons, up from only 1700 metric tons in 1999 (*108*, *109*). This is far less than the European Union, which produced more than 9 million metric tons in 2009 (*110*). Biodiesel is the most important biofuel in

the E.U., representing 80% of biofuel production (*111*). The reason for the increase in biodiesel production is two-fold. With the rise in the price of crude oil over the past decade, non-petroleum sources of energy became economically viable. As well, the concern over domestic production of energy leads to subsidies for biofuels, as does concerns over climate change. In the U.S., the Energy Policy Act of 2005, the Jobs Act and the 1992 Energy Policy Act all provided incentives for biodiesel production (*112*). The European Commission has set a goal of having biofuels be 5.75% of the transportation fuels in the E.U. by 2010. Many E.U. countries give full tax exemption from normal fuel taxes for biofuels, and the U.K. gives a partial tax exemption. The E.U. provides a carbon credit of $54/ha for farmers who grow crops for biofuel production (*111*). Both the E.U. and U.S. have required the sulfur content of diesel to be reduced, which leads to a decrease in fuel lubricity. The addition of biodiesel increases the lubricity, leading to additional use (*113*). It has been modeled that the cost of biodiesel varies inversely and linearly with the price glycerin, so that the more valuable glycerin the less expensive biodiesel becomes (*114*).

As can be seen in Equation 1, for every three moles of biodiesel one mole of glycerin is made. This corresponds to crude glycerin making up about 10 wt% of the resulting products (*86*). Crude glycerin is the name given to the glycerin produced after transesterification, and contains 80-95 wt% glycerin with the balance being water and other contaminants such as methanol, fatty acids, and salts (*86*, *113*, *115–117*). The salts are a product of the catalysts used, usually sodium hydroxide or sodium methylate. Most of the sodium is recovered as sodium glycerate, sodium methylate and sodium soaps. The rest is treated with an acid to produce sodium salts, usually NaCl (*113*). Most of the

water comes either from the environment, since glycerin will absorb water from the atmosphere at concentrations above 80 wt% glycerin, or is added by the bio-diesel manufacturer to facilitate pumping of the viscous glycerin (*76*, *118*). The amount of crude glycerin produced, as well as its composition, is a function of both the feedstock bio-oil used to make the biodiesel and the processing method.

Crude glycerin can be processed to produce pure glycerin, but the recent increase in glycerin production has decreased its market value, making biodiesel production less profitable overall (*86*, *119*). The price of glycerin in Europe was $900 per metric ton in 1996, and as of 2006 the price was about $110 per metric ton (*120*). In 2006, 680 million kg of crude glycerin was produced in the E.U., and 50 million kg in the U.S. (*116*). The Department of Energy estimates that if the United States produced enough biodiesel to supplant 2% of the current diesel usage, an additional 364 million kilograms would be produced (*121*). Currently, crude glycerin is either refined enough to use as a supplement to animal feed or is mixed with fuel oil and burnt in boilers (*86*). The heating value of crude glycerin is about 20 MJ/kg, which is comparable to some other common biomass like palm shell or cane trash (*120*, *122*). When used as a boiler fuel, the salts found in crude glycerin lead to excess ash and the water decreases the heating value and leads to the blanketing of the flame at the burners and the formation of carbon. For these reasons, special burners must be used when co-combusting glycerin (*120*). In order to advance biodiesel production, crude glycerin needs to be transformed from a near-waste into a value added product.

Because biodiesel, and hence crude glycerin, have only recently been produced in such large quantities, there are only a few technologies to convert the excess glycerin into

other chemicals. Oxidation can be used to produce glyceric acid, tartronic acid, ketomalonic acid and dihydroxyacetone, although selectivity and yield are generally too low to be commercially viable (*86*, *119*, *123–126*). Glycerin can be reacted catalytically with carbon dioxide or urea to produce glycerol carbonate (4-hydroxymethyl-1,3-dioxolan-2-one), which has many potential applications (*127*, *128*). Some studies have been conducted to use glycerol tertiary butyl ether (GTBE) as a replacement for methyl tertiary butyl ether (MTBE) as a fuel additive (*129*). The glycerol is reacted with isobutylene with an acid catalyst to produce GTBE (*130*, *131*). Using glycerin to produce propanediols has received considerable attention, first mentioned in a 1933 patent. Most use carbon supported Ru, Rh, Pt, Ni or Pd catalysts (*132–135*). In that same 1933 patent, acrolein was produced from glycerin using a copper phosphate catalyst (*132*). Many studies have been published about the production of acrolein from glycerin, including using supercritical water (*136–145*). Acrolein is a versatile intermediate, used for the production of acrylic acid esters, polymers or detergents (*137*). It is important to note that glycerin decomposes into acrolein under sub- and supercritical conditions, and during pyrolysis in the absence of water. Acetaldehyde, formaldehyde, hydroxyacetone, allyl alcohol, methanol, ethanol and a variety of gaseous products are also produced from glycerin in sub- and supercritical water and during pyrolysis (*136*, *137*, *145–150*). Most of the processes are acid catalyzed, and when an acid catalyst is absent the decomposition of acrolein was faster than acrolein formation (*137*, *139*). For now, the conversion and selectivity of sub- or supercritical dehydration to acrolein are not economical routes for dealing with the excess glycerin (*137*).

Biological conversion of glycerin has also received wide attention. Yeast, mold and bacteria are all candidates for glycerin conversion, both aerobic and anaerobic. Anaerobic conversion has seen more research than aerobic because anaerobic processes do not require aeration and so have reduced operational expenses (*86*). Anaerobic conversion by various bacteria has produced 1,3-propanediol, acetic acid, butyric acid, lactic acid, butanol, ethanol and formate (*151–161*). The most promising product is 1,3-propanediol, which has the highest yield of all of the products listed above. Increases to conversion and yield could come about from genetic engineering of the microbes to specifically consume glycerin or produce a target product. The general drawbacks to microbial conversion are also apparent here, where the microbes must be given specific vitamins or minerals to optimally convert the glycerin. Also, some of the microbes used are classified as pathogens that are detrimental to human and animal health. To further complicate the situation, crude glycerin can contain a wide variety of contaminants due to the different refining process, bio-oil feedstock and glycerin refining procedures. This all affects the performance of the microbes and suggests that a particular microbe would only be applicable to particular refining techniques and feedstock. Currently, no commercially applicable results have been reported (*86*, *154–156*). Another way to increase the value of glycerin is to reform it into synthesis gas or hydrogen.

2.4. SYNTHESIS GAS AND HYDROGEN

The purposes of these experiments are to see how effectively glycerin could be gasified. The gases that are normally encountered in reformation or gasification studies are hydrogen, carbon monoxide, carbon dioxide, methane, other light hydrocarbons and

nitrogen/oxygen if air or oxygen is used. These gases, especially hydrogen and carbon monoxide, are the goal of any gasification study. This section reviews the different methods from which these gases can be made and the uses that they currently find and foreseeable future uses.

2.4.1. Synthesis Gas. A gas that contains mostly hydrogen and carbon monoxide is known as synthesis gas, or syngas. It is named this because of the large amount of chemicals that can be synthesized from it (*162*). While it can be produced from any carbon containing feedstock, currently industry utilizes either coal or natural gas due to economic considerations. Figure 2-5 gives an overview of the major fuels and chemicals produced from synthesis gas.

Natural gas is used in most applications to produce synthesis gas. This is due to the cleanliness of the gas, ease of transport and use, and cost (*162*, *163*). The natural gas can be steam reformed using steam over a catalyst, an endothermic reaction between methane and water to produce hydrogen and carbon monoxide in a 3:1 molar ratio. It is usually carried out at temperatures of 700 to 1100°C with a nickel catalyst on an alumina support (*164*, *165*). The natural gas must be cleaned of sulfur and chlorine before being reformed, because these species poison the catalysts. This is commonly done by absorption of these compounds on zinc oxide (*166*). These processes employ natural gas to heat the reaction vessels, typically high nickel alloy tubes packed with catalysts, and the burners themselves can have a variety of arrangements (*167*). The amount of natural gas consumed as fuel varies from 3 to 20% of all the natural gas used at the plant, depending mostly on subsequent energy requirements such as water gas shift or carbon dioxide removal (*166*, *168*). There are other processes similar to steam reforming that

use some oxygen to partially combust the methane, leading to better heat transfer and higher efficiency (*169*, *170*).

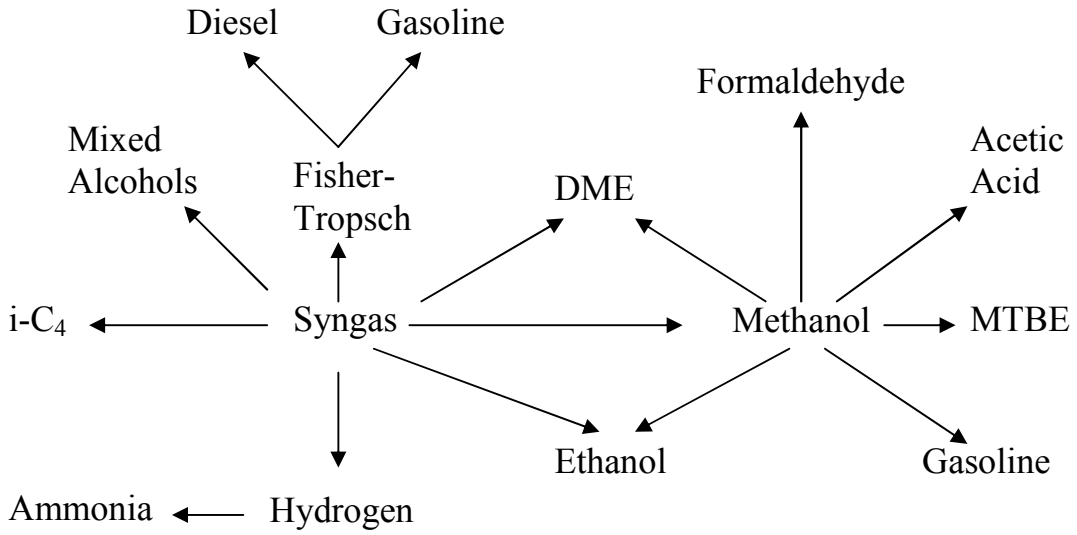

Figure 2-5. Fuels and chemicals that can be produced from synthesis gas, adapted from Spath and Dayton.(*171*).

Another method of producing synthesis gas is the gasification of coal (*169*). This process has been in use for over one hundred years; before natural gas was piped across the country city lights burned gas that was made from gasified coal called town gas (*172*). The process is similar to the partial oxidation of natural gas because the coal is heated under pressure and reacted with steam and oxygen to form hydrogen and carbon monoxide. There are a variety of processes to gasify coal, catalytic and non-catalytic, with temperatures varying from 620°C to 1500°C and pressures from atmospheric to 1250 psi. SASOL, a South African chemical company, is a leader in producing synthesis gas from coal (*172*). Reforming coal is difficult because of the large amount of impurities like ash and sulfur, and because coal is a solid, which makes it more difficult

to use in a reactor. This procedure may be able to produce hydrogen cheaply and efficiently, but requires a large, fixed operation and substantial investments of time and money (*173*). It has been successfully implemented only in regions that do not have access to natural gas. Because of the complexity of the coal gasification process, small scale plants are not economically feasible (*166*). These technologies can be partially applied to other hydrocarbon feed stocks such as biomass, but as of now all large-scale production of syngas is from fossil fuels.

The use of biomass to produce syngas, while not currently used on an industrial scale, is an important area of study because fossil fuels will run out, and syngas from biomass is nearly carbon neutral and sustainable. The ideal biomass would be a high yield crop that required little nutrients, fertilizers, and energy input (*89*). The biomass most often cited as potential hydrocarbon feed stocks for syngas are agricultural waste, lignocellulosic products such as cane, bagasse, or wood pulp, aquatic plants and algae, and food processing waste (*174*, *175*). This biomass falls in between the very wet biomass, such as sewage and animal waste that is currently recovered by microbial fermentation, and the dry biomass such as scrap wood and some garbage which is often burned directly as fuel. There are a few broad process routes from which synthesis gas can be produced from biomass. The biomass can undergo partial oxidation, similar to coal gasification, to produce a syngas (*176*, *177*). The major problem in biomass gasification is the formation of char and tars (*89*, *178*, *179*). Solar energy can even be used to supply the heat for the gasification process (*120*, *174*, *180*, *181*). Or it can undergo pyrolysis to produce a bio-oil, which is catalytically steam reformed to syngas (*182*, *183*).

Another form of reformation, called dry reformation, uses carbon dioxide to produce synthesis gas (*184–190*). The temperatures used are similar to those used in any reformation or gasification process, 600 to 1000°C. It has the advantage of using carbon dioxide, which may become plentiful if carbon capture is employed at a large scale. The reverse water gas shift reaction occurs during dry reformation, so that the carbon dioxide reacts with hydrogen to produce carbon monoxide and water. Therefore steam reformation would produce more hydrogen than dry reformation, and have a higher hydrogen to carbon monoxide ratio (*184*). There are significant problems with coking when using dry reformation, but it has been determined that the coke that is produced during dry reformation is in the form of multi-walled carbon nanotubes, itself an attractive product (*189*, *190*). Coke accumulation leads to catalyst deactivation and reactor plugging, and is the primary reason dry reformation is not used for gasification. Biomass can be digested microbially to produce hydrogen or synthesis gas, and much research is being performed in this area due to the success of genetically engineered microbes to produce desired products (*191–194*). As mentioned in Section 2.2.2, supercritical water has long been considered a mode of producing synthesis gas from biomass due to its natural moisture content (*28*, *69*, *89*, *195*). A number of other renewable energy sources exist, such as solar, wind and hydroelectric, but currently plant biomass is the only renewable source of carbon that can be readily used for liquid fuels and chemicals.

The uses for synthesis gas are numerous, so only the commercially important or most promising will be covered. The production of liquid or solid hydrocarbons from

syngas is the Fischer-Tropsch (F-T) process (*196*). The general chemical reaction is given by Equation 2 below.

$$CO + 2H_2 \rightarrow \text{—}CH_2\text{—} + H_2O \qquad (2)$$

This is a simplification of the complex reactions that occur, but is the overall idea of Fischer-Tropsch. The process produces straight chain alkanes, shown above as —CH_2—. The most uses catalysts for this process are iron or cobalt, depending on the temperatures used and the desired product. The high temperature F-T process is iron catalyzed at 300-350°C and is used for the production of gasoline and diesel. The high temperature process can also accommodate some carbon dioxide in the feed. The low temperature F-T (200-240°C) is iron or cobalt catalyzed and used mostly to produce linear waxes (*197*). The ratio of hydrogen to carbon monoxide can be changed using the forward or reverse water-gas shift reaction, since the steam reformation of methane results in a 3:1 hydrogen to carbon monoxide ratio while 2:1 is ideally need for Equation (2).

Industrially, the water gas shift reaction occurs at temperatures of 150 to 600°C, and is typically carried out over a catalyst of copper and zinc oxide on an alumina support (*198*, *199*). The high temperature F-T can accommodate some carbon dioxide because it is converted to carbon monoxide via the reverse water-gas shift (*197*). The process is traditionally a gas-phase reaction, and since the reaction is exothermic heat removal issues arise. This and other difficulties have led to research in F-T synthesis in liquids or even supercritical fluids like *n*-hexane (*6*, *200*, *201*).

The Fisher-Tropsch process can produce synthetic gasoline or high purity waxes and chemicals, and high quality, zero-sulfur diesel fuel. The production of diesel fuel is the best known, because the process is well suited to the production of straight chain

alkanes that make excellent diesel fuel. During World War II, fuels from the Fischer-Tropsch process provided 25% of all automobile fuels, and since the 1950's a large percentage of South Africa's diesel fuel was provided by this method (*197*, *202*). The economic viability of the Fisher-Tropsch process is linked to the price of crude oil, so that Fisher-Tropsch derived hydrocarbons become more viable as the price of crude oil rises. So far, it has been implemented on a commercial scale only in exceptional instances (*6*). Some oil companies use or are planning to use F-T to produce liquid fuels from natural gas in remote locations, instead of flaring off the gas (*89*). The most expensive section in a Fischer-Tropsch complex is the production of purified syngas, typically 60-70% of the capital and operational cost of the entire plant (*197*). Considering that the formation of synthesis gas from glycerin is endothermic, about 80 kcal/mol, but the conversion of synthesis gas to alkanes is exothermic, about -110 kcal/mol, the conversion of glycerol to alkanes is theoretically exothermic (*119*). If glycerin were converted to synthesis gas, then were to undergo Fisher-Tropsch conversion to a liquid alkane like octane, the process would theoretically be exothermic, with 63 kJ/mol of heat liberated per mole of glycerin reacted (*203*). Additionally, most synthesis gas produced from biomass requires either air or pure oxygen be used to facilitate gasification (*204*). This then requires a costly oxygen separation or leads to the dilution of the synthesis gas with nitrogen. Glycerin gasification would negate both of these problems.

Methanol is another important product made from syngas. Historically, methanol was produced from the destructive distillation of wood, which lead to the common name

of wood alcohol, but currently almost all is made via syngas (*205*). The main chemical reactions involved in methanol production are:

$$CO + 2H_2 = CH_3OH \quad (3)$$

$$CO_2 + 3H_2 = CH_3OH + H_2O \quad (4)$$

$$CO + H_2O = CO_2 + H_2 \quad (5)$$

The carbon dioxide in these reactions is either already present in the syngas, added to it or formed from it via the water gas shift reaction, Equation 5 (*206*). Carbon dioxide is usually added because the rate of methanol production is seven times higher for H_2, CO and CO_2 mixtures than just H_2 and CO (*207*). The most common method of methanol production now involves a $Cu/ZnO/Al_2O_3$ catalyst at temperatures of 250 to 300°C at 50 to 100 atm. Methanol is used as a feedstock in a diverse number of industries, as an automobile fuel, and can be converted to high octane gasoline (*206*). As of 2007, 40 million metric tons of methanol were produced worldwide, almost all of it used as a chemical feedstock for a variety of chemicals including formaldehyde, methyl tert-butyl ether, and acetic acid (*208*, *209*). Most of these chemicals are themselves feedstocks for many common products. Some prefer methanol to hydrogen as the fuel of the future, because of its ease of storage and transportation (*208*). Methanol can be used in internal combustion engines, and while it has about half of the energy density of gasoline, it has a higher octane rating. It has been used in automobile racing since the 1960's due to its fire safety over gasoline (*208*).

Dimethyl ether (DME) is another chemical produced either from syngas or methanol (*209–211*). The production of DME from the dehydration of methanol is carried out over an acidic catalyst (*208*, *211*). DME can be used in diesel engines as a

diesel fuel substitute. DME has a cetane number of 55-60, which is higher than the 40-55 of diesel fuel (*212*). While synthesis gas has many uses of its own, it is also the route by which almost all hydrogen gas is produced.

2.4.2. Hydrogen. Hydrogen is the most abundant element in our universe. It is estimated that hydrogen makes up about three quarters of the observed mass of the universe, and is the tenth most common element on earth, where it is found mostly as water. Because hydrogen gas is so buoyant it readily escapes from the atmosphere, meaning less than 1 part per million by volume of the atmosphere is free hydrogen gas (*213*). In 2010, world production of hydrogen gas was 31.3 million metric tons, and almost 95% of that is captive, in that large industrial chemical consumers produce the hydrogen onsite to satisfy the chemical needs of that industry (*166*, *214*). Of all the hydrogen produced in the U.S., only 2% comes from electrolysis, the rest comes from the gasification of coal, oil or natural gas into syngas, which undergoes the water gas shift reaction, Equation 5, to produce more hydrogen (*214*). Therefore, syngas is the largest current producer of hydrogen, and hydrogen produced from any hydrocarbon will first be synthesis gas.

Electrolysis uses electricity to break water into its constituents, hydrogen and oxygen. The cathode and anode, usually made from inert metal, are placed in the water and hydrogen is produced on the cathode and oxygen at the anode. Electrolysis is usually sped up by the addition of an electrolyte, such as potassium hydroxide, to the water (*166*). The energy required to produce hydrogen by electrolysis (assuming 1.23 V and atmospheric pressure) is between 33 and 47 kW•h/kg H_2. There are systems that first pressurize the water to about 7000 psi, then use electrolysis to produce hydrogen. This

process requires more energy (60 kW•h/kg H_2), but the hydrogen is already at an elevated pressure for storage and transport (*215*). The future use of electrolytic hydrogen will likely be practical only for niche applications due to the high cost of electricity. If, however, a large renewable electricity source such as wind or solar is constructed, electrolysis could be used to alleviate problems associated with the intermediate nature of renewable energy (*166*). Unlike electricity, hydrogen can be stored in various quantities for long periods, to be used when renewable energy is lax.

The United States produces 95% of its hydrogen from the steam reforming of natural gas followed by the water gas shift, which has already been described in the synthesis gas section. Following the reforming and water gas shift, the carbon dioxide can be removed by an alkaline-based solution via absorption, and the resulting hydrogen rich gas can be further purified via pressure swing adsorption (PSA) (*166*). The steam reforming of natural gas is currently the most economic source of hydrogen, as well as being well understood technologically (*166*). Other countries produce large amounts from coal or oil; worldwide 18% comes from coal and 30% from oil, while natural gas accounts for 50% (*214*). In oil refineries, there are catalytic reforming units that convert low-octane naphtha into higher octane products, and a byproduct of this process is hydrogen. The reaction ranges from 490°C to 530°C in temperature and 70 to 650 psi (*216*, *217*). This hydrogen is usually used within the refinery for fuel upgrading and hydrodesulfurization (*218*).

Sixty percent of the hydrogen produced was used to for ammonia production by the Haber process, which is in turn used mostly to make fertilizer. Twenty three percent was used by oil refineries to upgrade and remove sulfur from fuel, and the rest was used

in other chemical and metallurgical processes, as well as in the space program as a fuel. The Haber process is critical in sustaining food production, because nearly half of the world food supply would not exist without fertilizer produced via the Haber process (*219*). It was discovered by chemist Fritz Haber and chemical engineer Carl Bosch in 1908, and the first factory to use it was built in Germany in 1913 (*219*, *220*). At that time, Germany needed supplies of ammonia to produce dynamite for World War I, and Germany contained no natural supplies. Most natural supplies were in the form of guano, and were highly valued (*219*, *221*). With the Haber process, humanity was able to produce large quantities of ammonia, which when coupled with new hybrid crops and increased agricultural education lead to what has been called the green revolution (*222*, *223*). More food was produced, and human population increased dramatically after 1950, as seen in Figure 2-6 (*224*, *225*). Without these ammonia fertilizers, billions of people would starve (*219*).

The chemical industry currently produces more fixed nitrogen via the Haber process per year than the entire natural nitrogen cycle (*221*). In 2010, worldwide ammonia production was 131 million metric tons, 83% of which is used as fertilizer such as ammonium nitrate (*226*, *227*). Some of the other uses of ammonia include general purpose cleaner, explosive, refrigerant and an intermediate to almost all nitrogen containing chemicals (*226*, *227*). Because hydrogen is needed to make ammonia fertilizer, and most hydrogen is produced from natural gas, the price of ammonia and natural gas are closely linked (*228*). Higher fertilizer prices necessitate higher food prices, and the supply of natural gas is finite. Coupling the Haber process to renewable

energy and biological sources of hydrogen would release the ammonia supply from the price and quantity of natural gas.

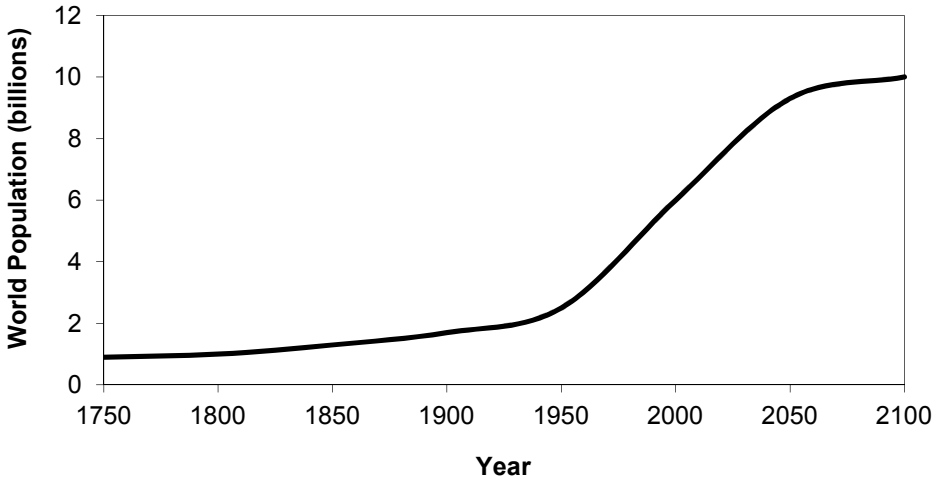

Figure 2-6. World population in billions from 1750 to now. Projected to year 2100 (*224*, *225*).

Hydrogen is the cleanest fuel, because when combusted with oxygen only water and energy is formed. Hydrogen can be used directly in specially designed internal combustion engines or in turbine engines (*229*). Hydrogen has a number of properties that makes it suitable for combustion engines, such as its ability to be burned with a low amount of oxygen, leading to lower temperatures, less pollution, greater fuel economy and more complete combustion. Also, hydrogen has a high diffusivity in air, leading to a uniform mixture of fuel and air and better combustion. The space program is by far the largest user of hydrogen for fuel, due to its high energy to weight ratio (*214*).

The fuel cell, which uses hydrogen and oxygen from the air to make water, heat and electricity, is another way to convert hydrogen to energy. Fuel cells are generally

more efficient than combustion engines or turbines, and have fewer moving parts and so have less likelihood of mechanical failure (*230*). There are a number of different types of fuel cells, such as the Polymer Electrolyte Membrane (PEM) fuel cell, the Solid Oxide fuel cell (SOFC), the Alkaline fuel cell (AFC), the Direct Methanol fuel cell (DMFC), and the Molten Carbonate fuel cell (MCFC), among others. Table 2-4 lists some of the common fuel cells and their capabilities (*230*).

Table 2-4. Properties of fuel cells in current use (*230*, *234*).

Fuel cell type	Operating Temperature	System Output	Peak Efficiency
Alkaline (AFC)	90 - 100°C	5 - 150 kW	60%
Phosphoric Acid (PAFC)	160 – 220°C	50 kW to 11 MW	80-85% overall with combined heat and power (CHP), 40% electric
Polymer Electrolyte Membrane (PEM)	50 - 120°C	5-250 kW	60% transportation, 35% stationary
Molten Carbonate (MCFC)	600 - 800°C	100 kW to 2 MW	85% overall with CHP, 50% electric
Solid Oxide (SOFC)	650 - 1000°C	100-250 kW	85% overall with CHP, 60% electric

Each fuel cell has characteristics that make it desirable in certain applications. The high temperature fuel cells like MCFC and SOFC can use small amounts of carbon monoxide as a fuel and SOFC can also process small amounts of methane (*230*, *231*). The higher operating temperature systems can use a combined heat and power (CHP) system to increase efficiency by making use of the waste heat. The largest hurdle that fuel cells must overcome is their sensitivities to impurities in the hydrogen gas stream, and the operating temperature and weight of the fuel cells (*230*). When fuel reformation to produce hydrogen is coupled with an engine or fuel cell, the waste heat can be used to supply heat to the reformer, increasing efficiency (*232*). There are downsides to using hydrogen as a transportation energy source, due to the high pressures and/or low temperatures needed to store enough hydrogen gas to practically use. This is because of the low energy density of hydrogen by volume compared to hydrocarbon fuels. Also, hydrogen gas has the propensity to leak from metal containers and causes weakness to metals. Therefore, other methods including storage as metal hydrides and chemical storage along with gaseous and liquid hydrogen storage are being researched (*233*).

It is obvious that hydrogen and synthesis gas have many important and possible uses, so the challenge lies in effective and sustainable production. Fossil fuels are used for almost all production, but their supply is finite and quickly being consumed, and are seen more as a medium term source of hydrogen. Electrolysis is promising, but may only have specific applications. The gasification of biomass is seen as an important step in sustaining the production of hydrogen and syngas after fossil fuels become prohibitively expensive.

2.5. GLYCERIN GASIFICATION

As explained above, the main byproduct of biodiesel production is crude glycerin, which is glycerin containing impurities such as alcohol, salts, heavy metals and water (*86*). This crude glycerin must be further purified to be used in many of the applications pure glycerin is used. Section 2.3 introduced the idea of using glycerin as a feedstock or reactant in the formation of liquid chemicals, while the rest of this section will review using glycerin to produce gaseous species.

The general idea of glycerin gasification, or the gasification of any hydrocarbon, is to react it with water at elevated temperatures to produce hydrogen, carbon monoxide, carbon dioxide, methane and perhaps other gaseous hydrocarbons (*235*). The liquid products that form, usually at lower temperatures, have been reviewed already in this section. Various chemical reactions, which will be discussed in more detail later, occur to produce this mixture of gases. Table 2-5 reviews some of the terminology used in various studies. This is not an exhaustive list, because many times the terms are used interchangeably or in a different manner by different groups or different countries.

For example, many times the terms gasification and reformation are used interchangeably. Usually reformation is reforming one gas into another, i.e. methane into syngas; while gasification is turning a liquid or solid into a gas, and usually uses oxygen (*89*). These two terms come from the long history of methane reformation and coal gasification. Because many of the reactions, reaction conditions and equipment are similar, the terms are used interchangeably, especially when dealing with compounds that are neither methane nor coal.

Table 2-5. Reaction nomenclature and description for the reactions involving water, oxygen and hydrocarbons.

Reaction	Description
Steam reforming (gasification)	Endothermic, T>350°C, with/without catalyst
Liquid phase (aqueous) reforming	Endothermic, T<350°C, high pressure, with/without catalyst
Partial oxidation	No water, includes oxygen, with/ without catalyst, T>800°C
Autothermal reforming (Wet oxidation)	Partial oxidation plus steam reforming, 500 to 800°C, no energy input needed
Supercritical water (SCW) reforming	High pressure, T > 374°C, with/without catalyst
Supercritical water partial oxidation	SCW reforming plus partial oxidation

Other terms that are frequently used are yield and gasification percentage. Yield, as defined here and in many other sources, is the molar flow of that particular gas out of the reactor divided by the molar inlet flow of the reactant. Hydrogen yield in this paper is molar flow of hydrogen out divided by molar flow of glycerin into the system. It is a dimensionless number. Other papers, usually when dealing with more complicated reactants (coal, sewage sludge, etc.) will define yield as gas flow out divided by carbon flow in, because the total carbon entering the system is easier to calculate. Gasification percentage is the carbon leaving the system as gas divided by the carbon that entered in the fuel. It represents how much of the reactant was converted to gaseous carbon. Sometimes this will be called carbon gasification or carbon conversion, or in this context, glycerin gasification or glycerin conversion. At other times, conversion is glycerin

converted into liquid and gaseous products, so care must be taken to determine what each author is using as a definition.

2.5.1. Sub-Critical Glycerin Gasification. Numerous studies have been conducted on the atmospheric or low temperature gasification of glycerin with steam or liquid water. Studies were conducted with and without catalysts, in batch and continuous operations, at various pressures, temperatures, residence times and glycerin concentrations. A number of these, especially those that are similar or relevant to the experiments performed in this work, are summarized here. This section will give a brief introduction into the current state of sub-critical glycerin gasification.

Before all of the studies are discusses, it should be mentioned that there is a company running pilot plant studies into glycerin steam reformation. The Linde Group, at a biodiesel facility in Leuna, Germany, have a catalytic process that operates at 30 bar and temperatures of 600 to 850°C. They first purify the glycerin by removing the salt, then dilute with water, pump up to pressure and heat to reaction temperatures. They do not give many specifics on the catalysts, reactor type, dilution, etc. The gas produced contains hydrogen, carbon monoxide, carbon dioxide, methane and other hydrocarbons. They use steam methane reforming and after cooling, they use the water gas shift reaction and pressure swing adsorption to produce pure hydrogen. They report hydrogen production of 4.4 kg/h. Linde Group announced the construction in 2009 and began producing hydrogen in mid-2010 (*120*, *236*).

Adhikari et al. tested fourteen different catalysts at temperatures from 700 to 900°C and determined that Ni/Al_2O_3 and $Rh/CeO_2/Al_2O_3$ had the highest hydrogen selectivity and glycerin conversion. These two catalysts were then used to test the effect

of glycerin concentration, feed flow rate and catalyst loading. The water to glycerin molar ratio was varied from 3:1 up to 9:1, while the feed flow rate went from 0.15 to 0.45 ml/min and catalyst metal loading from 1.5 to 3.5 wt% in a 19 mm ID tubular alumina reactor. The hydrogen yield and glycerin conversion increased with an increase in water/glycerin ratio and metal loading, and decreased with an increase in flow rate. It was determined that the lowest feed flow rate (0.15 ml/min) and the highest water to glycerin molar ratio (9:1) lead to the highest hydrogen yield (5.04) at 900°C with the Ni/Al_2O_3 catalyst. This condition produced a 90% glycerin conversion. The product gas was made up of only hydrogen, carbon monoxide, carbon dioxide and methane, but C_2-hydrocarbons were not able to be detected. Up to 94% glycerin conversion for both catalysts was found at the highest metal loading (*237*).

In a separate test of just nickel catalysts, Adhikari et al determined that Ni/CeO_2 was the best performing, with a hydrogen yield of 5.177 and glycerol conversion of 99% at a water/glycerin molar ratio of 12/1, a temperature of 600°C and a feed flow rate of 0.5 mL/min. Increases in temperature and water/glycerol ratio had positive effects on hydrogen yield and conversion, while increases in feed flow rate decreased yield and conversion (*238*). Nickel catalysts are commonly investigated because it facilitates C-C bond rupture (*239–242*). Adhikari and his colleagues have studied the steam reforming of glycerin in other journal articles, in which a thermodynamic analysis identified the theoretical optimum conditions for the production of hydrogen as greater than 630°C, atmospheric pressure and a water-to-glycerol ratio of 9/1, which are also the conditions Rossi et al. and Wang et al. found to be optimum (*243–246*). The theoretical maximum

hydrogen yield increased with an increasing water/glycerin ratio, but its effect was small at water/glycerin ratios above 9/1 (*246*, *247*).

The atmospheric catalytic reforming of glycerol was studied by Kunkes et al. at temperatures of 548-623 K over a Pt-based catalyst. A variety of platinum catalysts were tested at these temperatures, and it was found that a carbon-supported bimetallic Pt/Re catalyst was best the for glycerin reforming. Therefore a two-catalyst bed system was employed, the first bed using the Pt/Re catalyst to reform, and the subsequent bed using a $Pt/CeO_2/ZrO_2$ catalysts for the water-gas shift reaction. A 12.7 mm OD quartz reactor was used for all experiments. Concentrated glycerol solutions of 30-80 wt% were used, and carbon conversion was between 94-100% for these concentrations at 573 K and a 0.04 cm^3 min^{-1} glycerol flow rate using the PtRe/C and $Pt/CeZrO_x$ catalysts. The hydrogen yield was 6.19 for the 30 wt% glycerin solution, and 2.81 for the 80 wt%. These hydrogen yield results are the product of the two-catalyst bed system, which was used to promote water-gas shift. (*248*).

Hirai et al. used ruthenium catalysts at 500-600°C, a steam-to-carbon molar ratio of 3.3/1 and a contact time of 13.4 g_{-cat} h/mol. Ruthenium (Ru) was chosen after screening several other metals, such as Rh, Ni, Co, Pt, Pd, and others. It had the highest hydrogen selectivity, but Rh had a higher glycerin conversion. The ruthenium was then tested on a variety of supports, which have a dramatic effect on the performance. Ru/Y_2O_3 had the best results, and reported complete conversion to gas at 600°C and a 5.8 hydrogen yield. It is interesting to note that without a catalyst, the conversion was only 1.6% (*249*).

Zhang et al., using an Ir/CeO_2 catalyst, had 100% conversion at 400°C with a hydrogen yield of 5.99. The experiments were conducted at atmospheric pressure, with a volumetric ratio of $C_3H_8O_3/H_2O/He$ = 2/18/80 vol. % and a gas hourly space velocity of 11,000 $ml/g_{-cat}•h$, at temperatures from 250 to 550°C. Ir, Co and Ni catalysts were tested and Ir had the highest conversion and hydrogen yield. For Ir, conversion increased with temperature, from 40% at 250°C to 100% at 400°C, after which the hydrogen yield increased and conversion remained 100%. Hydrogen yield was 5.99 at 400°C and increased to 6.58 at 550°C, the highest measured. The other catalysts had similar trends but did not perform as well. The authors note that since the decomposition of glycerol to methane is highly favorable, the catalyst should be able to reform methane at the reaction conditions (*250*).

The steam reforming of crude glycerol with *in-situ* CO_2 sorption was evaluated by Dou et al., using crude glycerin with a composition of between 70-90% glycerin, with the remainder made up of water and methanol. The temperature was varied between 400 and 700°C at atmospheric pressure at a 4 mL/h flow rate and a 3.0/1 steam to carbon molar ratio. The experiments were conducted with and without a calcined dolomite CO_2-sorbent in a 344 cm^3 tubular reactor with a nickel catalyst (*251*). This work was compared against an earlier work by Dou et al. in which pure glycerin was reformed (*252*). Without sorbent, the crude glycerol conversion increased from 71% at 400°C to 100% at 600°C, while the pure glycerin increased from 63% at 400°C to 97% at 600°C. Conversion for both was near 100% at 700°C. The gas compositions of both pure and crude glycerin were also similar, with hydrogen being the dominant gas species, followed by carbon dioxide and carbon monoxide. The maximum hydrogen yield for pure and

crude glycerin was 6.6 at 700°C. There was significant methane at 400°C, but was negligible at 600°C and above. The CO_2 sorbent was able to decrease the amount of CO_2 and hence raise the hydrogen selectivity. The CO_2 sorbent lasted between 7 and 28 minutes before CO_2 breakout, depending on temperature. Dou et al. concluded that temperatures around 500°C are optimal for glycerol steam reforming with CO_2 removal, because around this temperature the hydrogen purity is highest and the CO_2 breakthrough time is the longest. In another work, Dou et al. investigated the kinetics of both pure and crude glycerol pyrolysis at atmospheric pressure, and determined that there are four distinct phases in glycerol decomposition, which can be modeled by a first-order power-law model. The most active phase for glycerin decomposition was the phase from 426 to 548 K, when about 67-70% of the glycerin decomposed to gas. The main gas components of the decomposition were CO_2, CH_4, CO and H_2 (*118*).

At ambient or near ambient pressures, a membrane can be used to separate the hydrogen produced during reformation from the other reactants and products. This was investigated by Iulianelli et al. in a Pd-Ag membrane reactor using a Co-Al_2O_3 catalyst. The experiments were conducted at 400°C, a H_2O/Glycerol molar ratio of 6/1, a weight hour space velocity (WHSV) of 1.01 h^{-1} and at pressures of 1 and 4 bars. At 1 bar, the glycerol conversion was 50% and at 4 bar it increased to 94%, the highest achieved for these experiments. The higher pressure, however, increased the production of methane, so that the hydrogen yield decreases with pressure. The efficiency of the membrane was measured by the percentage of CO-free hydrogen recovered, which was less than 5% at 1 bar but higher than 60% at 4 bar. The Co-Al_2O_3 catalyst is deactivated over time, with

glycerin conversion dropping irreversibly after a time on stream of more than 180 minutes (*253*).

Using a Pt/Al_2O_3 catalyst, Cortright et al. reformed various oxygenated hydrocarbons using liquid water (*35*). For glycerol, temperatures of 498 and 538 K were studied at 1 wt% and a feed rate of 0.008 g of glycerol per g of catalyst per hour, which lead to 83 and 99% gasification, respectively. The pressure was 29 bar at 498 K and 56 bar at 538 K. The gas phase composition was mostly hydrogen (57-65 mol. %) and carbon dioxide (30-32 mol. %), the rest being hydrocarbons. The highest conversion (99%) and hydrogen yield (5.64) was found at the highest temperature. There was a negligible amount of carbon monoxide produced at both conditions. A 10 wt% glycerin solution (molar ratio of $H_2O/C = 15$) had 77% conversion to gas and a hydrogen yield of 3.773 at 498 K.

A patent application by Cortright and Dumesic make use of a Pt-Re/C catalyst to produce synthesis gas from glycerin, and a Ru/TiO_2 catalysts to produce liquid hydrocarbons via Fischer-Tropsch synthesis (*254*). The preferred form of the patent has both catalysts present in a single bed, so that the energy needed for the endothermic reformation of glycerin is partially provided by the exothermic Fischer-Tropsch synthesis. Other versions of the process envision separate reactors for each reaction with heat exchange between them. The Pt-Re/C catalyst was chosen because it was found that the addition of Re enhanced hydrogen formation, and that other supports such as Al_2O_3, ZrO_2 and MgO/ZrO exhibited rapid deactivation (*203*, *248*). The process would be atmospheric, with temperatures less than or equal to 750 K. The glycerin gasification results given in the patent application are the same as those reported by Soares, Simonetti

and Dumesic, which are reviewed below (*203*). Cortright and Dumesic were able to produce FT liquids from the water/glycerin mixture using a combined bed of catalysts at 548 K, 5 bar and 80 wt% glycerin. Fourteen percent of the carbon entering the reactor left as organic liquid, with sixteen percent being organic liquids and the rest was present in the gas phase. Higher conversions to organic liquids, up to 50%, were seen with different feed stocks and conditions.

Soares, Simonetti and Dumesic used platinum-based catalysts to gasify glycerin at temperatures from 498 to 723 K at atmospheric pressure. They tested Pt supported on carbon, Al_2O_3, ZrO_2, CeO_2/ZrO_2 and MgO/ZrO_2 and found that Pt/C had the least deactivation, so was used for the subsequent experiments. Flow rates were varied from 0.06 to 0.64 cm^3/min, glycerin wt% from 20 to 50%, and the temperature from 573 to 723 K. The highest gasification percentage was 100% at 673 K, 30 wt% and a flow rate of 0.06 cm^3/min. However, after 3 hours, gasification fell to 72%. Higher temperatures led to lower conversion by catalyst deactivation. Higher concentrations and flow rates also lead to less gasification (*203*).

Lehnert and Claus used an aqueous-phase reforming process at conditions of 2 MPa, 250°C, 10 wt% glycerin to produce hydrogen from both pure and crude glycerin over various platinum catalysts. The catalysts used had similar results, with maximum glycerin conversion of 45% and a maximum hydrogen yield of 3.4 using pure glycerin. It was found that the catalyst support had a large effect on conversion and hydrogen yield. On a Pt/Al_2O_3 catalyst, a γ-Alumina support lead to 8% conversion, while a Puralox support had 57% conversion at the same conditions. Crude glycerin did not perform as well, with seven times less hydrogen produced compared with pure glycerin, and it was

found that the salt impurities in the crude glycerin lead to a loss of catalytic activity (*255*).

Huber et al. also used an aqueous-phase reforming process to produce hydrogen from oxygenated hydrocarbons. They used a Raney Ni-Sn catalyst at temperatures of 220 and 260°C, 2.5 to 5.1 MPa, 1 to 5 wt% glycerin, and had a maximum carbon gasification of 100% at the highest temperature and pressure and lowest glycerin concentration, with a maximum hydrogen yield of 5.32. The Raney Ni-Sn catalyst was chosen because it was not a precious metal, and because it decreased the rate of methane formation without inhibiting hydrogen production (*256*).

Menezes et al. conducted aqueous-phase reforming at 1wt% glycerin, 225°C, and 23 bar, in a Parr batch reactor over various platinum supported catalysts, Pt/Al2O3, Pt/CeO2 / Pt/ZrO_2 and Pt/MgO. The reaction time for all experiments was 3 hours. Conversion and hydrogen yield was low for all, with a maximum conversion of 26% and a hydrogen yield of 1.6 over the Pt/ZrO_2 catalyst. Liquid analysis found that propanone and ethanol were byproducts, but the concentrations were low, 2-732 ppm. As with Lehnert and Claus, they found that catalyst support plays a role in catalytic glycerol reforming (*257*).

Pompeo, Santori and Nichio used platinum catalysts for glycerol steam reforming at 250 to 450°C, 1 atm, and 10 wt% glycerin at a space time of 0.2 to 6.5 minutes in a quartz tubular reactor. The platinum catalysts were supported on SiO_2, ZrO_2, γ-Al_2O_3 and α-Al_2O_3 modified with Ce and Zr. They found that the Pt/SiO_2 catalyst was the most suitable, having the highest gasification and hydrogen yields and longest stability. Using this catalyst, at 350°C it was found that space times below 1.5 minutes resulted in liquid

intermediates, but above this time the glycerin was fully gasified. The liquid intermediates included mostly 2-propanone-1,3-dihydroxy, and in lesser quantities 2-propanone-1-hydroxy, propanal-2-oxo, 2,3-dihydroxy-propanal, 1,2-ethanediol and acetaldehyde. At a space time of 0.88 minutes the effect of increasing temperature found that complete gasification only occurred at 450°C. The maximum hydrogen yield, 6.7, was at the longest space time, 6.5 minutes and 350°C (*258*).

The reformation of both pure and crude glycerin was studied by Slinn et al., with the reformation of pure glycerin optimized first and then compared to crude glycerin. Experiments were conducted in a 4.8 cm^3 stainless steel tubular reactor with a platinum alumina catalyst at temperatures of 580 to 880°C, steam-to-carbon ratios of 0.5 to 2.5, flow rates of 0.03 to 0.59 mol/min glycerin per kg of catalyst, and at atmospheric pressure. With pure glycerin at 850°C, the gasification percentage remained near 100% for steam-to-carbon ratios between 0.5 and 2.5, but the hydrogen selectivity increased with increasing S/C ratios. The same trend is seen when increasing the glycerin flow rate. Increased methane production is seen at higher flow rates. For pure glycerin, the highest hydrogen yield, 5.5, was seen at the highest temperature, highest steam-to-carbon ratio and at a flow rate of 0.12 mol/min of glycerin per kg of catalyst. The crude glycerin was obtained from Green Biodiesel Ltd. and contained 40% fatty matter, 33% glycerol, 23% methanol, 3.8% ash and 3.2% water. The crude glycerin was more difficult to reform due to the large amount of long chain fatty matter, up to C_{18}, and was more likely to form carbon deposits on the catalyst. The gasification of crude glycerin was maximized at 90% at 800°C, and the maximum hydrogen yield was 4.9. In general, under the same reaction conditions the gasification and hydrogen yield of crude glycerin

was 70% that of pure glycerin. Also, the catalyst deactivated faster with the crude glycerin, due to impurities and increased coke formation (*232*).

The aqueous-phase reforming of various oxygenated hydrocarbons, including glycerol, was studied by Shabaker, Huber and Dumesic. They used platinum, nickel, and tin modified nickel catalysts. The Raney-Ni, Raney-NiSn, and Pt/Al_2O_3 catalysts displayed adequate stability, while the Ni/Al_2O_3 and $NiSn/Al_2O_3$ catalysts deactivated quickly due to sintering. Operating conditions included temperatures of 498 to 538 K, 1 wt% reactant, 26-51 bar, liquid hourly space velocities (LHSV) of 0.64 to 10.3 h^{-1}, in a stainless steel batch reactor. They reported a 100% carbon gasification at 538 K, 51 bar, a Raney-NiSn catalysts and a LHSV of 10.3 h^{-1}, but also had 4% carbon in the liquid. All the catalysts deactivated over time, and the best catalysts, Raney-NiSn, had 72% of its initial activity after 48 hours. The worst, Ni/Al_2O_3, lost 90% of its activity over 48 hours of operation (*259*).

Cheng et al. studied synthesis gas production from glycerol steam reforming over a Co/Al_2O_3 catalyst. They used temperatures from 450 to 550˚C, 30-60 wt% glycerin at atmospheric pressure in a stainless steel 10 mm ID tubular reactor. The cobalt was used because cobalt is a well-known Fisher-Tropsch catalyst, and in the future they hope to develop an integrated gasification and hydrocarbon synthesis reactor. The product gas was made up primarily of hydrogen and carbon dioxide, with less carbon monoxide and very little methane. The yield of all gasses increased with temperature, as did the gasification percentage. A larger percentage, 20 to 24%, of the carbon fed was deposited on the catalyst as coke (*260*).

The steam reforming of glycerol was studied using Ni/ZrO_2 or Ni/CeO_2 catalysts on α-Al_2O_3 supports by Buffoni et al. at temperatures of 450 to 600°C, 1 atmosphere, and a water/glycerin ratio of 6/1 in a 8 mm ID quartz tubular reactor. It was determined that the $Ni/CeO_2/\alpha$-Al_2O_3 was the most stable, and that the $Ni/ZrO_2/\alpha$-Al_2O_3 exhibited fast catalyst deactivation due to coking. At 450°C, both catalysts exhibited fast deactivation due to coking. As a function of time, both catalysts deactivated, but $Ni/ZrO_2/\alpha$-Al_2O_3 did so immediately, while $Ni/CeO_2/\alpha$-Al_2O_3 was stable up to eight hours. Gasification and gas yields increased with temperature. Hydrogen was the most abundant gas species, followed by carbon dioxide and carbon monoxide. Very little methane was formed (*241*).

The effectiveness of Pt/C and Pt-Re/C catalysts for glycerin reforming was investigated by King et al. at 225°C, 29 atmospheres, and 10 wt% glycerin in a tubular stainless steel reactor. A 3%Pt/C catalysts and two 3%Pt-Re/C catalysts with different Re loadings of 1 and 3% were used. The addition of Re significantly increases the conversion of glycerol, with gasification increasing from about 4% with 3%Pt/C to 52% with 3%Pt-3%Re/C catalysts. The addition of KOH decreased the gasification percentage for the Re catalysts but increased gasification with the Pt/C catalyst. Hydrogen yield was highest with the 3%Pt-3%Re/C catalyst. They propose a platinum catalysis pathway with ethylene glycol, propylene glycol, ethanol and methanol as the main liquid intermediates, based on the HPLC analysis (*261*).

The Sricharoenchaikul group from Chulalongkorn University in Thailand has been various catalysts for the gasification of crude glycerin. The first paper uses olivine ($LiFePO_4$) and nickel olivine catalysts at 500 to 800°C and one atmosphere in a 23 cm x

2.2 cm ID quartz tubular reactor. The crude glycerin was obtained from a local biodiesel manufacturer using palm oil as the feedstock. An elemental analysis on the crude glycerin found that it contained 36.40% carbon, 8.76% hydrogen, 0.67% sulfur and 54.17% oxygen. The analysis determined there were 13.56% moisture and 2.43% ash in the crude glycerin. No water was added during the gasification, so the steam to carbon ratio was 0.25, which is 87.2 wt% glycerin. This ratio is entirely due to the water present in the crude glycerin. They found that both olivine and Ni/olivine displayed excellent stability and high reactivity when compared to non-catalytic reformation. They found that gasification increases with temperature, and the liquid products decrease, while the solid component is stable at about 5 wt%. Reaction temperatures showed little effect on the solid component. The catalytic gasification increased from about 15% to 85% as temperature increased from 500 to 800°C, but the non-catalytic experiments only increased from about 4% to 32%. The hydrogen yield is not calculated, because that result is based on the ideal reaction of one mole of glycerin with three moles of water to produce seven moles of hydrogen. Since the chemical make-up of the crude glycerin is unknown, a yield for these types of experiments would not be comparable to the others using pure glycerin or known components. The production of hydrogen does increase with temperature, but the main gaseous component is methane (*122*).

The other Sricharoenchaikul group paper is crude glycerin gasification over perovkite-type oxide catalysts, in this instance $LaCoO_3$ and $LaNiO_3$ catalysts at the same reaction conditions as the above paper. This study used a 37 mm long and 30 mm OD quartz tubular reactor. The composition of the crude glycerin was also the same. The solid component was 4% to 17% of the product, and decreased with increasing

temperature. Gasification increased with temperature from 5% to 55% with the temperature increase. Hydrogen, carbon oxides and methane all increased with temperature. $LaNiO_3$ appeared to be more effective than $LaCoO_3$ because it produced more hydrogen and had slightly higher gasification (*262*).

Wen et al. conducted a catalysis test on hydrogen production by aqueous phase reforming of glycerin in a 3 cm I.D., 58 cm long stainless steel reactor. Mild temperatures and pressures were used, and both the supports and the metal catalysts were tested. The metals were Co, Ni, Cu and Pt, and it was found that Pt was highly stable and the most active. Then Pt was placed on six different supports and it was found that the activity of the support was as follows: SAPO-11 < active carbon < HUSY < SiO_2 < MgO < Al_2O_3. SAPO-11 and HUSY are both zeolite supports. The Pt/MgO and Pt/SAPO-11 deactivated with time the fastest. The other catalysts did deactivate with time, but more slowly. Gasification was low, 2-22% depending on the catalyst and support, as was hydrogen yield, 0.19-1.58. They found liquid products of methanol, acetaldehyde, ethanol, 1-hydroxy-2-propanone, acetic acid, 1-propanol, ethylene glycol, propanoic acid and 1,2-propylene glycol (*263*).

Wawrzetz et al. used Pt/Al_2O_3 catalysts in a stainless steel tube at 225°C, 25.7 to 44.4 atm and 10 to 30 wt% glycerin. They found that pressure had no effect on the glycerin conversion, but did push the reactants away from hydrogen and carbon dioxide and increased 1,2-Propanediol production. Very little carbon monoxide was produced for any experimental condition. Liquid products include methanol, acetaldehyde, ethanol, 1-hydroxy-2-propanone, acetic acid, 1-propanol, ethylene glycol, propanoic acid, propanal,

1,2-propylene glycol and 1,3-propylene glycol. The most common was 1,2-propylene glycol and ethanol (*264*).

Luo et al. also used Pt/Al_2O_3 catalysts in a stainless steel tubular reactor to study glycerin aqueous phase reformation. They found that hydrogen yield and gasification increased with Pt loadings of 0.9 wt% > 0.6 wt% ≈ 1.2 wt% > 0.3 wt%. Gasification and hydrogen yield increased with temperature from 180°C to 220°C, and decreased with increasing glycerin concentration from 5 wt% to 10 wt% glycerin. Catalytic deactivation occurred over time. They suggested a reaction pathway with liquid intermediates such as methanol, ethanol, acetone, acetic acid, 2,3 dihydroxylpropanal, propylene glycol and diglycerol, formed from dehydration and hydrogenation. The methanation reaction was also included in the reaction pathway (*265*).

The pyrolysis and steam gasification of glycerin was investigated in Valliyappan's M.S. thesis. Mainly the results of the steam gasification will be reviewed here. Pyrolysis always produced more char and less gasification than steam gasification. One temperature was used, 800°C, at three different steam to glycerin rations. The reactor was also packed with two different materials, either quartz or silicon carbide. Char was always produced, and was at a minimum of 10% at the highest dilution. With increasing water, the gasification and hydrogen yield increased. The major liquid products were methanol, acetone, and acetic acid. During pyrolysis, it was found that liquids were produced, and the majority, 97 wt%, of the liquid phase was water. It was concluded that the glycerin undergoes dehydration prior to any carbon-carbon bond breakage, at least during pyrolysis. Crude glycerin was also tested, and in general the gasification was more difficult due to the addition of salts, which produced more char. It

was determined that the crude glycerin contained 60 wt% glycerin, 31 wt% methanol, 7.5 wt% water and 1.5 wt% potassium hydroxide. The crude glycerin results are not given in the table below, only the pure glycerin results (*266*).

Table 2-6 summarizes the conditions used for the above sub-critical glycerin reformation journal articles, as well as the range of glycerol gasification and hydrogen yield. The hydrogen yield is defined as the moles of hydrogen gas in the product stream, divided by the moles of glycerin fed into the system. The glycerin conversion is the amount of carbon in the outlet gas phase divided by the carbon entering the system as glycerin. The Linde Group's commercial steam reformer is not included in the table, because too few facts about the process were given.

2.5.2. Supercritical Glycerin Gasification. As the above section was an overview of sub-critical glycerin gasification, this section is for supercritical glycerin gasification. Again, a variety of reactor types, catalysts, temperatures, pressures, and feed concentrations are used in these experiments, in order to illustrate the large variety of work done in this field.

Chakinala et al. investigated the non-catalytic gasification of glycerin in supercritical water using a 10 wt% glycerin solution, and found that the gasification percentage and the gas yields increased with temperature over the range 550 to 650°C at 25.0 MPa (*267*). The product gas was predominately hydrogen and carbon monoxide over the temperature range studied, with the highest hydrogen yield (2.5) and gasification percentage (92%) occurring at 650°C. Residence times between 4 and 11 seconds were studied, with the gasification percentage increasing linearly with time. They also conducted experiments with amino acids and alkali salts, and found that amino acids led

Table 2-6. Range of conditions used and maximum results for glycerin reformation via sub-critical water.

Reference	Reactor	Temperature (°C)	Pressure (atm)	wt.% glycerin	Catalyst	Glycerin Gasification %	H_2 yield
(*237*)	Alumina/tubular	700-900	1	36-63	Ni/Al_2O_3 and $Rh/CeO_2/Al_2O_3$	15-94%	0.50-5.04
(*238*)	SS/tubular	550-650	1	30-46	Ni/CeO_2, Ni/MgO and Ni/TiO2	49-99%	0.62-5.18
(*248*)	quartz/tubular	270-345	1	30-80	PtRe/C and $Pt/CeZrO_x$	30-100%	2.81-6.19
(*249*)	SS/tubular	500-600	1	34	various Ru	1.6-100%	0-5.80
(*250*)	quartz/tubular	250-550	1	31	Ir, Co and Ni/CeO_2	15-100%	0.5-6.58
(*251*)	quartz/tubular	400-700	1	36 Δ	Ni/Al_2O_3	71-100%	4.47-6.6
(*252*)	quartz/tubular	400-700	1	36	Ni/Al_2O_3	63-100%	3.97-6.6
(*253*)	SS/tubular	400	1-4	46	$Co-Al_2O_3$	41-94%	3.70-5.66
(*35*)	SS/tubular	220-260	28.6-55.3	1-10	Pt/Al_2O_3	77-99%	3.77-5.64
(*255*)	SS/tubular	250	19.7	10	Pt/Al_2O_3	8-57%	0.47-3.39
(*256*)	SS/tubular	220-260	25.7-50.3	1-5	$Ni-Sn/Al_2O_3$	81-100%	4.20-5.32
(*257*)	SS/batch	225	22.7	1	various Pt	13-26%	0.84-1.6
(*258*)	quartz/tubular	250-450	1	10	various Pt	22-100%	1.32-6.7
(*233*)	SS/tubular	580-880	1	40-77	Pt/Al_2O_3	40-100%	1.12-5.50
(*203*)	SS/tubular	225-450	1	20-50	Pt/C	17-100%	0.04-3.99
(*259*)	SS/batch	225-265	25.6-50.3	1	Pt/Al_2O_3, various Ni	83-100%	5.4-6.1

Δ Used crude glycerin only

Table 2-6. Range of conditions used and maximum results for glycerin reformation via sub-critical water. (cont.)

Reference	Reactor	Temperature (°C)	Pressure (atm)	wt.% glycerin	Catalyst	Glycerin Gasification %	H_2 yield
(*260*)	SS/tubular	450-550	1	30-60	Co/Al_2O_3	30-65%	0.7-2.8
(*241*)	quartz/tubular	450-600	1	46	$Ni/ZrO_2/\alpha$-Al_2O_3 & $Ni/CeO_2/\alpha$-Al_2O_3	40-100%	1.4-4.1
(*261*)	SS/tubular	225	28.9	10	Pt/C and Pt-Re/C	3.6-52%	0.2-1.5
(*122*)	quartz/tubular	500-800	1	87.2 Δ	$LiFePO_4$ and $Ni/LiFePO_4$	4-84%	N.A.
(*262*)	quartz/tubular	500-800	1	87.2 Δ	$LaCoO_3$ and $LaNiO_3$	5-55%	N.A.
(*263*)	SS/tubular	230	31.6	10	various	2-22%	0.19-1.58
(*264*)	SS/tubular	225	25.7-44.4	10-30	Pt/Al_2O_3	0-10.5%	0-0.42
(*265*)	SS/tubular	180-220	11.25-24.67	5-10	Pt/Al_2O_3	10-80%	0.35-4.9
(*266*)	Inconel/tubular	800	1	50-92	none	71.4-90%	2.3-3.7

Δ Used crude glycerin only

to significant coke formation and, in the case of L-proline, suppresses the gasification. Alkali salts enhances the gasification and promotes hydrogen production through the water-gas shift reaction.

Xu et al. used a 2.0 M glycerin solution, gasified with and without activated carbon catalysts at a temperature of 600°C, a 44 second residence time and a pressure of 34.5 MPa (*268*). The activated carbon catalyst was found to have no effect at these conditions, with complete gasification with and without catalyst and a product gas that contained mostly hydrogen and carbon dioxide. The maximum gas yield for hydrogen was 3.51.

Glycerol reforming in supercritical water over Ru/Al_2O_3 catalyst was studied by Byrd et al., with a temperature range of 700 to 800°C, 2.5 to 40 wt% glycerin, 24.1 MPa and short residence times of 1 to 5 seconds in a Inconel 600 tubular reactor (*269*). Glycerin was completely gasified at all conditions studied, producing a product gas of mostly hydrogen, carbon dioxide and methane. Shorter residence times lead to less methane production, and at dilute concentrations a hydrogen yield of 6.5 was achieved at 800°C. Operating at 700°C for feed concentrations over 5 wt% glycerin lead to reactor plugging, but this was not the case at 800°C. CHEMCAD 5.2.0 was used to determine the thermodynamic equilibrium by minimization of the Gibbs free energy using the Peng-Robinson equation of state. It was determined that the yields of H_2, CO, CO_2 and CH_4 are very close to equilibrium. The reaction was modeled as a reversible adsorption of glycerin onto the catalyst, then the reaction of water with the adsorbed glycerin to form an adsorbed complex molecule. The adsorbed complex molecule decomposed into intermediates that further decomposed into carbon dioxide and hydrogen. They made a

steady state assumption for the adsorbed intermediates and assumed that the decomposition of the absorbed molecule was rate limiting and that water was in excess. The rate constant was found using a regression on the rate of hydrogen production, and activation energy of 55.9 kJ/mol was found for the reaction.

Matsumura et al. found that temperatures below 600°C produced very low carbon conversions, and complete carbon conversion was only achieved around 700°C and glycerin concentrations of 3 wt% or less in a noncatalytic quartz capillary reactor (*270*). Hydrogen and carbon dioxide increase with temperature, while carbon monoxide decreases and methane remains unchanged. It was found that pressure had little influence on either the gas composition or carbon conversion over a wide range of pressures, 5 to 45 MPa. Concentrations higher than 10 wt% lead to a decrease in hydrogen yield and carbon conversion.

The fact that pressure has no effect on the conversion and product yield was also observed by Kersten et al., who performed noncatalytic and Inconel 625 catalyzed batch experiments using supercritical water in quartz reactors (*271*). Furthermore, it was determined that carbon conversion increases with temperature below 650°C, but increasing the temperature further to 800°C had little effect on conversion. Conversion is a strong function of concentration, with complete conversion only possible at 1 wt% dilutions. Hydrogen increases and carbon monoxide decreases with temperature due to the water gas shift reaction.

The decomposition of glycerol at temperatures of 344-470°C, 25-45 MPa, and residence times of 32-165 seconds was investigated by Buhler et al. It was found that gaseous products only form at higher temperatures, above 430°C, and gas production

decreases with decreasing pressure. The gas yields increased linearly with reaction time, meaning that the gas yield is independent of reaction time. It was also determined that the global glycerin decomposition rate has a reaction order in the range of 0.95-1.25, and so could be modeled as a first-order reaction. The gasification percentage was between zero and 3%, with hydrogen, carbon monoxide and carbon dioxide being the main components of the gas. The maximum hydrogen yield of 0.12 was obtained at the highest temperature. This study was focused more on the liquid produces than gasification, hence the almost negligible gasification and yields. The liquid products were methanol, acetaldehyde, propionaldehyde, acrolein, allyl alcohol, ethanol and formaldehyde. The authors concluded that at high pressures and/or lower temperatures, the degradation pathway consists of ionic reactions, while at lower pressures and/or higher temperatures a free radical pathway dominates. The ionic part of the reaction mechanism is totally based on assumptions, while there are some analogous reactions in the literature involving the free radical pathway. For the modeling of the decomposition of glycerol in supercritical water on the basis of elementary reactions, a combination of free radical and ionic pathways were used. The model was run in CHEMKIN II, and was optimized by comparing the experimentally measured concentrations of the main products with calculated values and then adjusting the kinetic parameters At the highest temperatures in this study, the reaction can be considered to behave Arrhenius-like and yield activation energy of about 150 kJ/mol with a pre-exponential factor of about 10^{18} s^{-1} (*136*).

The catalytic gasification of glycerin by May et al. was studied at 510-550°C, 35 MPa, 5 wt% glycerin, residence times of 2 to 10 seconds and both inert ZrO_2 particles

and a 1% Ru/ZrO_2 catalyst. Liquid products included acetaldehyde, acetic acid, hydroxyacetone and acrolein, along with gaseous products H_2, CO, CO_2, CH_4 and traces of C_2H_4. They concluded that the liquid intermediates were unstable under hydrothermal conditions because of the increased gasification and decrease in the liquid products, and that glycerin reacts to form liquids faster than those intermediate liquids react to form gases. A pseudo first-order kinetic model was used to describe the overall reaction rate for glycerin conversion, with rate constants of 0.034 and 0.385 s^{-1} at 510 and 550°C, respectively. Carbon deposition was seen on the inert ZrO_2 particles put not on the Ru/ZrO_2 catalyst. A maximum hydrogen yield of 0.55 and glycerin gasification percentage of 26% was found at a residence time of 8 seconds and at 510°C (*272*).

Xu et al. gasified 1 wt% glycine and glycerol in supercritical water, using a tubular Hastelloy C276 reactor from 380 to 500°C, 1 to 5 minutes, 25 MPa and a Na_2CO_3 catalyst. They found that the Na_2CO_3 catalyst had a negative effect on glycerin gasification and hydrogen yield. Glycerin was 98% gasified at 500°C, and produced 5.08 moles of hydrogen per mole of glycerin. The gaseous products were H_2, CO_2, CH_4, CO, and C_{2+}, with H_2 and CO_2 being the main components. Gas yields increased rapidly above 440°C. Gasification percentage increased with temperature, from 60% at 380C to 98% at 500°C. They assumed that the glycerin decomposes first to glycol and formaldehyde, which then reacts further to produce the gases seen (*273*).

Bennekom et al. investigated reforming of pure glycerin, crude glycerin and methanol, using a tubular Inconel 825 reactor at 450 to 650°C, 25.5 to 27 MPa, 3-20 wt% glycerin, and residence times of 6-173 seconds. The crude glycerin used in this study was a mixture of glycerin (~88 wt%), water (6.5 wt%), and NaCl (4.5 wt%), with other

cations and fatty acid methyl esters and monoglycerids making up less than 0.1 wt%. It was found that pure and crude glycerin had comparable glycerin gasification percentages. Gasification was near zero for a 10 wt% glycerin solution at 460°C, but increased to 91% at 613°C. For pure glycerin, the gasification percentage decreases slightly from 90% to 85% with increasing wt% glycerin from 5 to 20 wt% at a temperature of 619°C. Gasification of both crude and pure glycerin increases with residence time from 5 to 20 seconds, and levels off at higher residence times. They determined that water was a reactant when using crude glycerin, but a product due to glycerin dehydration when using pure glycerin. One mole of water is produced via dehydration per mole of glycerin fed. Hydrogen, carbon monoxide, carbon dioxide, methane and ethane were the main products, with trace amounts of ethene, propene and propane. The yield of hydrogen, carbon dioxide, methane and ethane increases with gasification percentage for both crude and pure glycerin. Carbon monoxide increases for pure glycerin, but for crude glycerin reaches a maximum yield of about 0.8 at a gasification percentage of 70%, and decreases thereafter. Hydrogen and carbon dioxide were the main products, and more hydrogen and carbon dioxide were produced from crude glycerin then pure. The presence of salt in the crude glycerin is believed to be the reason for the enhanced water-gas shift. Assuming pseudo first-order kinetics, the activation energies for glycerin conversion were 196 kJ/mol for pure glycerin and 183 kJ/mol for crude glycerin. They reported reactor plugging due to salt precipitation after several hours of operation when using crude glycerin (*75*).

Stever, in this 2011 master's thesis, investigated the effect of reactor liners on the reformation of glycerin in supercritical water. He used a 400 ml Haynes alloy 230

reactor at temperatures from 500 to 700°C, 17.6 to 63 wt% glycerin at 24.1 MPa with and without a Nickel 201 liner inserted into the reactor. The reactor liner was to determine the catalytic effects of metal walled reactors in supercritical reformation. Complete gasification was achieved at temperatures of 600°C and above and at glycerin weight percent of 27.5% and less. Hydrogen, carbon dioxide and methane yields increased with temperature, while carbon monoxide decreased. The Nickel 201 reactor liner did have an effect on the reformation, and increased glycerin gasification and hydrogen yield. Hydrogen yield was greatest at the most dilute glycerin loading and at the highest temperature with the Nickel 201 liner (*274*). Table 2-7 summarizes the conditions used for the above journal articles, as well as the range of glycerin gasification and hydrogen yield

2.5.3. Catalytic Effects of Metallic Reactors. The experiments conducted in this paper were done so non-catalytically; that is, no conventional heterogeneous catalyst was placed inside the reactor. However, it has been demonstrated that metallic reactor walls can potentially function as a catalyst in the gasification of hydrocarbons in sub and supercritical water (*24*, *271*, *275–280*). Kruse has postulated that there are three different reactor types that can be used to avoid or minimize catalysis by the reactor wall: Quartz reactors, seasoned or aged metallic reactors, and metallic reactors with ceramic liners. A seasoned metallic reactor is one that has been in use for a week or two, and is based on the observation that new metallic reactors have an effect that vanishes over time (*14*). Also, reactors that have seen use have a film of carbon deposited on the surface which may inhibit catalytic effects (*69*). As Kruse et al. explained "This does not necessarily mean that seasoned reactors have no catalytic effect; they rather show a lower and

Table 2-7. Range of conditions used and maximum results for glycerin reformation via supercritical water.

Reference	Reactor material/type	Temperature (°C)	Pressure (MPa)	wt% glycerin	Residence/Heating time	Catalyst	Glycerin gasification %	Hydrogen yield
(267)	Inconel 600/tubular	550-650	25	10	4-11 seconds	none	22-92%	0.74-2.5
(268)	Inconel 625/tubular	600	34.5	15.6	44 seconds	activated carbon	99-101%	3.15-3.51
(269)	Inconel 600/tubular	700-800	24.1	2.5-40	1-5 seconds	Ru/Al_2O_3	100%	2.0-6.5
(270)	quartz/batch	500-800	5-45	1-20	60 seconds	none	54-100%	0.2-2
(271)	quartz/batch	400-700	5-45	1-20	60 seconds	Inconel 625	22-100%	0.3-1.2
(108)	SS/tubular	344-470	25-45	1.7-5.0	32-165 seconds	none	0-3%	0-0.12
(272)	SS/tubular	510-550	35	5	2-10 seconds	Ru/ZrO_2	0-26%	0-0.57
(273)	Hastelloy-C276/tubular	380-500	25	1	60-300 seconds	Na_2CO_3	60-98%	1.4-5.08
(75)	Inconel 825/tubular	450-650	25.5-27	3-20	6-173 seconds	none	2-91%	0-2.9
(274)	Haynes 230/tubular	500-700	24.1	17.6-63	100 seconds	none	15-100%	0.1-4.4

constant catalytic effect, leading to more reproducible results". She added that it is not clear whether supercritical water gasification without an added heterogeneous catalyst is catalyzed on the surfaces or not (*14*). In another paper, Kruse et al. (2000) was studying the gasification of pyrocatechol, a model for lignin, with potassium hydroxide in supercritical water. They mention that deposition of the potassium salt on the tubular reactor surface are believed to improve the gasification (*195*).

During hydrogen production by glucose reforming in supercritical water, Yu et al. found that gas yields are strongly influenced by the reactor wall, with a new Hastelloy-C 276 reactor behaving differently and less effectively than a "corroded" Hastelloy-C reactor. It was also found that Inconel-625 strongly catalyzes the water gas shift reaction at the conditions tested, and that Inconel and Hastelloy behave similarly when reforming glucose (*275*). Arita et al. placed stainless steel (SS 316) and copper wires in a quartz reactor during the supercritical reformation of ethanol (1.0 M ethanol, 450°C, 30 min reaction time) and found that copper accelerated the reaction considerably, producing almost twice the amount of hydrogen gas than without catalyst, but that stainless steel showed little catalytic effect (*276*). Lachance postulated that the increased glucose degradation in his work, compared to other studies investigating the supercritical water gasification of glucose, could be the result of reactor wall material effects (*277*). Gadhe and Gupta, while investigating methane suppression during supercritical water methanol reforming, reported that the nickel present in the Inconel 600 tubular reactor used for the experiments catalytically increased the methanation reaction. They suggest the use of a Ni-Cu reactor to minimize the reactors methanation catalysis (*281*).

When studying the catalytic oxidation of p-chlorophenol in supercritical water, Yang and Eckert first ran noncatalytic experiments to determine a baseline. They found that the Inconel 600 reactor was being corroded, and that trace metals from this corrosion may have acted as catalysts (*278*). Bustamante et al. specifically studied the wall effects on the forward water-gas shift reaction. They conducted experiments in a quartz reactor, and then an Inconel 600 reactor, which exhibited substantially enhanced rates of reaction. The activation energy for the forward water-gas shift reaction in the quartz reactor was 288.3 kJ/mol, while for the Inconel 600 reactor it was 102.4 kJ/mol. The effect of a palladium or palladium-copper packing was also investigated, as this would be a typical choice for a hydrogen separating membrane. It was found that these metals did enhance the reaction, but not to the extent of the Inconel (*279*). In his 2011 master's thesis, Stever investigated the effect of reactor liners in the supercritical water reformation of glycerin. He found that the Nickel 201 liner increased the water gas shift reaction, and in certain conditions enhanced reformation, compared to the Haynes alloy 230 reactor (*274*). Boukis et al. used an Inconel 625 reactor for methanol reforming in supercritical water, and found that oxidation of the reactor with H_2O_2 prior to the experiment increased the reaction rate and decreased carbon monoxide and methane production (*24*). Of direct importance to this work, it has been shown, again using quartz reactors as a baseline, that Inconel 625 catalyzes the supercritical water gasification of glycerol. Kersten et al. demonstrated that Inconel 625 increased both the conversion and the yield when conducting experiments at 600°C, 30 MPa, residence time of 60 seconds and a 5 wt% glycerol/water solution. The addition of 6 gram of Inconel per gram of solution, compared to no Inconel present, increased the conversion from 60% to close to 90%,

while increasing the hydrogen yield from 0.25 to 1.2, while increasing the yields of the other gases less dramatically (*271*). These wall catalytic effects occur for various reactions and reactants in supercritical water, indicating it is a generalized phenomenon and not limited to specific reactants, reactions or conditions.

3. APPARATUS

3.1. INTRODUCTION

For water to be supercritical, it must be at a temperature above 374°C and at a pressure above 22.06 MPa, which requires a reactor able to withstand these conditions without mechanical stress failure or corrosion (*64*, *65*). Due to the fact that air is sometimes used to clean the reactor via supercritical water oxidation, it must also withstand an oxidation environment. Therefore, specialty metals must be used for the supercritical water reactor. Equipment is needed to pressurize and heat the reactants, then to cool, depressurize and separate the products. Temperature, pressure, and flow rate must be monitored and controlled during the experiment, and various safety precautions must be implemented due to the extreme conditions. To determine what the system is producing, analytical and measurement equipment is needed. This is what will be described in the following section.

3.2. MULTI-FUEL REFORMATION SYSTEM

The Multi-fuel Reformation (MFR) system consists of a liquid feed system, integrated heat exchanger, preheat, supercritical water reactor, reactor heaters, air feed system, sample collection system, and a data acquisition and control system, of which a schematic process flow diagram is illustrated in Figure 3-1. Unless noted otherwise, all of the tubing used in the supercritical water system is ¼" OD Swagelok 316 stainless steel tubing with a tubing wall thickness of 0.065", which has an ASTM allowable working pressure of 9600 psig as calculated from equations in ASME B31.3, code for

process piping typically found in petroleum refineries and other chemical processing plants. All of the thermocouples used to measure the temperature were Omega Type-K Chromega-Alomega® with either a 304 stainless steel or Inconel sheath. Most of the supercritical water reaction system is housed in a 60" tall, 66" long, and 36" wide welded ¼"-thick steel enclosure mounted on casters with two access doors on the back.

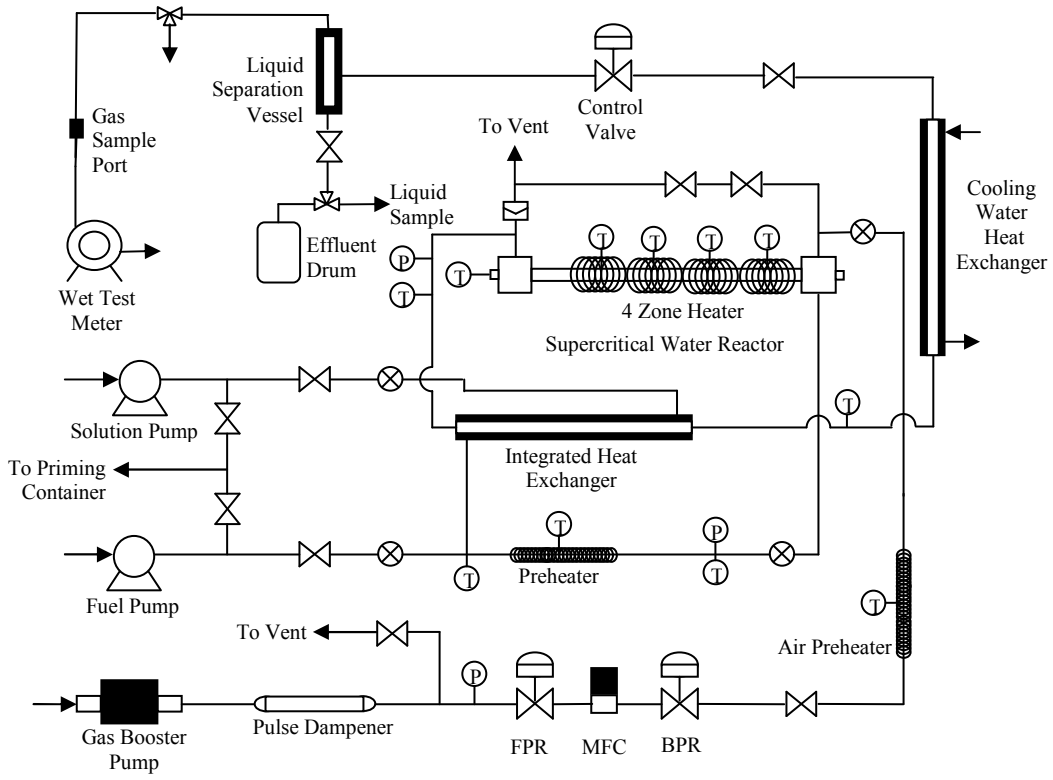

Figure 3-1. A schematic of the supercritical water multi-fuel reformer system.

3.2.1. Reactant Delivery and Preheat. The system begins with a 5 gallon HDPE plastic solution tank, which is on an Arlyn 620X industrial bench scale on the table behind the pump. The tank is on the table to facilitate easier, gravity assisted

priming of the pump, while the scale is used to measure the mass flow rate of the solution into the system. The system is capable of pumping two different fluids into the system with two different pumps, which is used when water and an immiscible hydrocarbon need to be fed together; with the hydrocarbon mixing with the water inside the system at a junction after the water goes through the integrated heat exchanger pictured in Figure 3-1. Because water and glycerin are miscible, and because pumping a water/glycerin mixture is easier than pumping glycerin separately, the second pump, labeled the fuel pump in Figure 3-1, is not used.

The solution enters the pump, an Eldex high pressure micro-metering pump model BBB, which is used to feed the liquid and bring it to pressure. The Eldex pump is a reciprocating three-piston pump that can deliver between 1.0 and 100 milliliters per minute of liquid, including corrosive liquids due to the corrosive-resistant wetted parts such as sapphire, ruby and stainless steel. After the pump, there is a Swagelok pressure relief valve set to 4600 psi, to make sure that the Eldex pump does not exceed its upper operation pressure of 5000 psi. The outlet of the pump then enters the steel enclosure, and will remain inside the enclosure until noted. The solution pump goes to two valves, one used for priming and the other for solution feed to the reactor. If the pump needs to be primed, the prime valve is opened while the reactor feed valve is closed, until all air has been removed from the line. This is performed at the beginning of the day before experiments are performed. After priming, the priming valve is closed and the reactor feed valve is opened. The solution goes through a check valve to prevent backflow out of the system, and then enters the integrated heat exchanger.

The integrated heat exchanger is a double-pipe heat exchanger that consists of a 48” long ¼” OD Hastelloy C-276 inner tube that will contain the product coming out of the supercritical reactor, and a ½” OD stainless steel outer tube containing the incoming reactants. The flow is counter-current to maximize heat recovery. After exiting the heat exchanger, the feed solution enters the preheating section. The preheat is a section of ¼” stainless steel line 42” long that is wrapped in Omega STH series ultra-high temperature heat tapes, which heat the incoming solution before it enters the reactor. The heat tapes are controlled by the LabVIEW computer software using proportional control based on a thermocouple that is downstream of the preheater and another thermocouple that ensures the temperature of the heat tape itself does not exceed 550°C, the highest operating temperature of this type of heat tape. This LabVIEW software records all of the temperatures, pressures, heater outputs and the on/off position of all switches in a data file two times every second. The preheating section and all sections leading up to the reactor have coned and threaded connections instead of the compression connections used in all other applications. The coned and threaded connections are not damaged by the high temperatures, so are used on the inlet and outlet of the reactor.

After the preheat, the feed solution passes through a cross to which a thermocouple and an Omega silicon on sapphire 0-6000 psi pressure transducer is connected, so that the inlet temperature and pressure can be measured. The inlet pressure transducer is located away from the reactor, because it cannot see the high temperatures of the inlet reactants. On the computer display this pressure transducer is called “SWR Pressure In”, and is synonymous with the reactor pressure. Also connected to this line is a pressure gauge mounted to the exterior of the steel enclosure, so that the pressure can

be monitored in case the pressure transducers were to fail. After this cross is a high temperature check valve so there is no backflow from the reactor into the preheater or integrated heat exchanger. Before the reactants enter the reactor, there is a tee connected to two valves in series. These are the inlet emergency depressurization valves, used in case the outlet emergency depressurization valves are unable to decrease pressure when needed. These valves are then connected to the expansion drum, a large steel drum that is vented to the atmosphere. The expansion drum is used for all depressurizations within the unit except when normally operating.

3.2.2. Air Feed System. The air feed system begins with an Airgas tank of breathing grade air which is connected externally to the MFR. The gas is regulated to a pressure of 1000 psi and passes through a check valve before entering the Haskel two-stage booster pump, which uses externally supplied compressed air to increase the pressure to 5500 psi. The compressed air for all the pneumatics is supplied by two 60-gallon air compressors. The air enters a 500 cm^3 pressure bomb which acts as a pulse dampener and storage vessel for the pressurized air. This pressure bomb is connected to a valve which can vent the contents of the bomb to the expansion drum if the air feed system needs to be depressurized, and also to a gauge mounted on the front of the unit. The bomb is also connected to a preset Swagelok pressure relief valve, so that if the pressure in the bomb were to rise above 6000 psi, the valve would vent the contents into the expansion drum.

The air passes through a 15 micron filter and proceeds to the control section of the air feed system. A Brooks mass flow controller, connected to the LabVIEW computer software which employs PID control, is calibrated for air flow and used to control the

flow of air into the reactor. The controller works best when the pressure drop across it is less than 100 psi, so there is a forward pressure regulator (FPR) and back pressure regulator (BPR) set 50 psi apart so that the pressure drop can be controlled. The pressure regulators are set at 4500 psi, because the mass flow controller is not rated for pressures above 5000 psi, and many components in the multi-fuel reformer such as the pressure gauges and transducers are not rated for pressures greater than 5000 psi. From here the air feed is controlled manually by an air shutoff valve and passes through another check valve. The air can be preheated using Omega high temperature heat tapes, and enters the reactor across from the liquid feed line at the inlet Inconel cross.

3.2.3. Supercritical Water Reactor. The reactor is a 42" long, ½" ID, 1" OD Haynes alloy 282 tube made by the High Pressure Equipment Company. It has conned and threaded connections on each end so that it can connect with the 4 1/8" x 4 1/8" x 1 ½" Inconel 625 cross, also manufactured by the High Pressure Equipment Company. The crosses are made to accept 1" conned and threaded fittings on two sides directly apart from each other and 3/8" conned and threaded fittings on the other two sides. One of the 1" conned and threaded fitting is connected to the reactor and the other is fitted to an adapter that allows a Parr Instrument's thermowell to extend into the middle of the reactor. This is illustrated in Appendix B, which also contains the Watlow heater diagrams. The crosses have reducers so that the ¼" conned and threaded feed and exit lines can be connected to the 3/8" fittings. The thermowell is a 52" long ¼" Inconel 625 tube with one end sealed. It is inserted into the top of the cross, goes through the cross and into the reactor. It is used so that thermocouples can be inserted into it and report temperatures for the inside of the reactor. Only one thermowell is used, the adapter at the

other end of the reactor is plugged. The reactor has a volume, minus the thermowell volume, of 101 ml.

Table 3-1. The nominal or limiting chemical composition of the alloys used in the multi-fuel reformer by weight percent (*282–284*).

Elements, wt%	Haynes 282	Hastelloy C-276	Inconel 625
Ni	57[a]	57[a]	58‡
Cr	20	16	20-23
Co	10	2.5*	1.0*
Mo	8.5	16	8.0-10.0
W	--	4	--
Ti	2.1	--	0.4*
Al	1.5	--	0.4*
Fe	1.5*	5	5*
Mn	0.3*	1*	0.5*
Si	0.15*	0.08*	0.5*
C	0.06	0.01*	0.1*
Others	B=0.005	V=0.35*	S=0.015*, P=0.015*, Nb+Ta=3.15-4.15

a = as balance, * = maximum, ‡ = minimum

The reactor, crosses and the tubing leading into and out of the reactor are made of high nickel alloys due to the high temperature and oxidative environment in the supercritical water reactor. The metals used are Hastelloy C-276, Inconel 625 and Haynes alloy 282. These are all high nickel alloys that can withstand the extreme environment. Stainless steel is well suited to lower temperatures or non-oxidative

conditions, but is not suitable here. The composition of the various alloys is given in Table 3-1. The stress-strain properties, as well as creep and rupture properties of Haynes alloy 282 allow the reactor to operate in an oxidative environment at 800°C and 5000 psi.

The heaters and insulation for the reactor were manufactured by Watlow Electric Manufacturing and comes in two pieces, the reactor heater and the outlet insulation. The reactor heater has four electric resistance heating zones, three of which are 7.75" long and the last is 7.69" long. All have ports for thermocouples which measure the skin temperature of the reactor. Each of the four zones is controlled by a reactor thermocouple, which is placed in the thermowell so that it is in the middle of the zone inside the reactor. The reactor thermocouples relay the temperature to the LabVIEW software, which using proportional control gives an output to the heaters, so that the temperature in the reactor may be controlled. The outlet cross has a separate piece of insulation manufactured by Watlow. Figure 3-2 below illustrates the reactor assembly, heater assembly, zone heater position and reactor thermocouple (RTC) position within the thermowell. The reactor, when mounted in the unit, is vertical, with the liquid and air feed at the bottom and the outlet at the top. Thermocouples 3 and 4 are averaged and this is the temperature that is reported as the reactor temperature.

3.2.4. Heat Exchange and Depressurization. Upon exiting the outlet cross, the product enters ¼" Hastelloy C-276 (HC-276) tubing which leads to a HC-276 cross. This cross has a thermocouple which measures reactor outlet temperature and another pressure transducer to measure outlet pressure. Both of the pressure transducers have to be some distance from the flow path because they cannot experience high temperatures, above 80°C. There is also a HC-276 rupture disc assembly at this point, which will rupture if

the pressure is over 6525 psig at 22°C or 6068 psig at 343°C. If this were to rupture, the product liquid and gases would go to the expansion drum, which is large enough to accommodate this rapid depressurization, and is vented to the atmosphere. The rupture assembly is one of many safety features which will be discussed later.

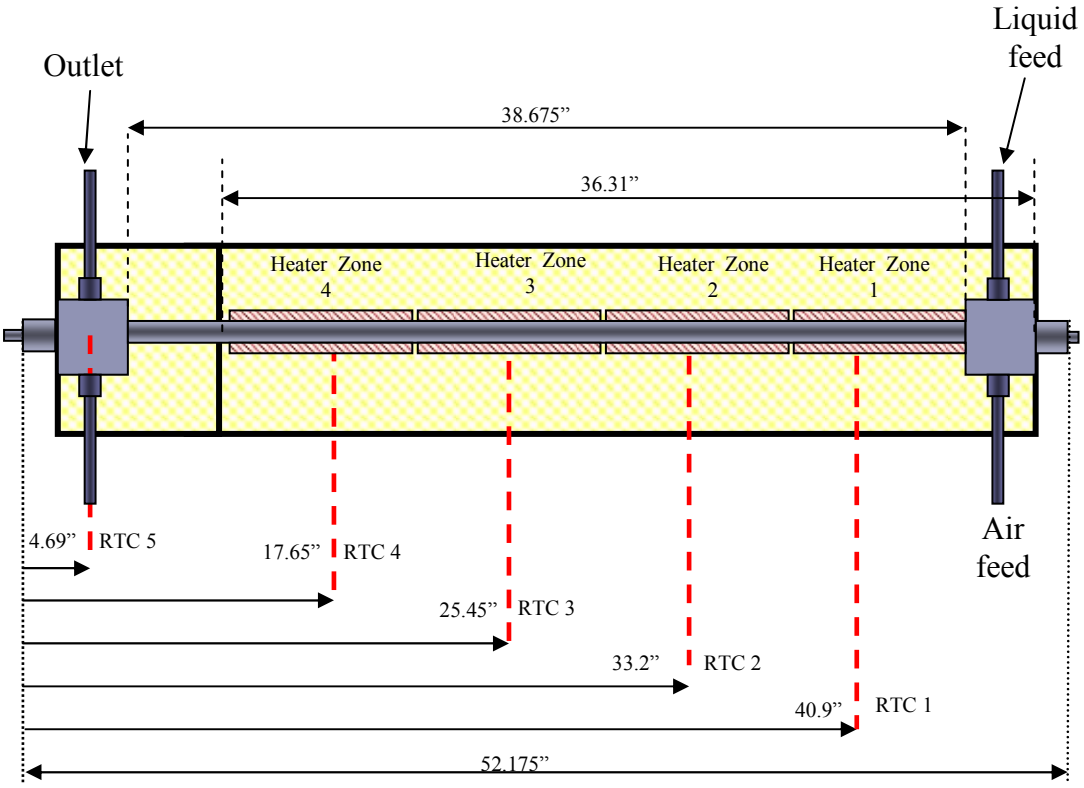

Figure 3-2. A diagram of the reactor and heaters on the MFR.

The product then enters the aforementioned integrated heat exchanger, where it is cooled by the incoming reactants, and then enters a 36” long stainless steel cooling water heat exchanger, which uses tap water to further cool the products to ambient conditions. This cooling water heat exchanger is not always used. The product enters a cross where there is a thermocouple to measure the temperature going into the control valve. The

normal process flow is for the product to go through an isolation valve, called the MFR outlet valve, through a 90-micron Swagelok filter and two 15-micron Swagelok filters in parallel before entering the control valve. Otherwise, the outlet emergency depressurization valves are connected here, so that the reactor can be depressurized through the outlet. This is the preferred way to manually depressurize the reactor because the effluent is cooler, which is better for long term valve function. The outlet emergency depressurization valves are also connected to the expansion drum

The filters are used so that the control valve does not become damaged by particulates. The control valve is a pneumatic Badger valve used to control the pressure in the system. It is computer controlled, with the computer receiving a pressure from the inlet pressure transducer, and using a proportional constant, sending a signal to the valve which is raised and lowed using pneumatic pressure. The product then enters the liquid separation assembly, where the liquid and gas products are separated. It consists of a 1000 cm^3 pressure bomb and ½" steel tubing to provide room for the liquid. The liquid exits from the bottom of the assembly, and the gas from the top, from which samples can be taken for analysis.

3.2.5. Process Sampling. The liquid is collected in the liquid separation assembly and is either drained to an in-process 5-gallon HDPE liquid effluent container, which is periodically emptied and sent to campus environmental health and safety for disposal, or liquid samples can be taken for later analysis. To take liquid samples, the liquid reservoir is completely drained and the time noted in the lab notebook. After a few minutes, dependent on the solution flow rate, the three-way valve is turned and the liquid reservoir is drained into a sampling bottle. The time is noted when done collecting the

sample, so that the mass flow rate of liquid out of the system can be measured. These samples are labeled and saved for later analysis.

The gaseous component remains in the system a little longer, and passes a three-way valve that allows the gases to be directed along the flow path or diverted into the expansion drum. The flow path leaves the enclosure and the gas passes a gas sampling port, where an air-tight Hamilton syringe is used for real time analysis on the GC. The gas samples are taken continuously throughout the experiment. From there, the gas enters a Precision Scientific wet test meter, where the gaseous flow rate is measure in liters per minute, the liter of gas being at room temperature and pressure. The gas is then vented out of the building via the ventilation system. The entire supercritical water reformation enclosure is ventilated using the same draw, as well as the expansion drum.

3.3. PROCESS SAFETY

Due to the high pressures and temperatures used in supercritical water reformation, as well as the combustible, poisonous and noxious gases that are evolved during reformation, safety is of the utmost concern. Safety begins with the construction of the supercritical water systems, being of welded ¼" steel with lockable doors on the back. This rugged construction protects the operators in case of any catastrophic failure of material or explosion. This enclosure is ventilated to ensure no effluent gases accumulate inside the enclosure if a leak were present. Also inside the enclosure is a SMC 200X series combustible gas monitor, which will detect any combustible gases and send out an alarm. This monitor is connected to the computer and the LabVIEW software, so that any alarm will automatically sound an alarm through the computer and

shut off all heaters, pumps and the air flow. The system would then be left to depressurize automatically or manually depressurized by the operators until the source of the alarm is determined. Outside of the system there are First Alert carbon monoxide detectors to alert the operators to the presence of carbon monoxide.

The outlet of the Eldex pump, as well as the air feed system, have Swagelok pressure relief valves, to make sure that the pump or the air feed system does not go over pressure and damage itself. Once inside the enclosure, the flow path contains multiple and redundant check valves, which ensures no backward flow. On the outlet of the reactor, there is a rupture disk assembly, rated to rupture at 6525 psig at 22°C or 6068 psig at 343°C Anywhere there are heaters on the system, there are thermocouples measuring both the internal and external temperatures, to ensure that the heaters are not exceeding their high temperature ratings or the ratings of the vessels. On the Watlow reactor heaters, there are thermocouples that measure the reactor skin temperature and report to the computer to ensure that the maximum reactor temperature is not exceeded, as well as thermocouples within the heaters to ensure the heater element itself does not exceed its maximum temperature of 1050°C. If this were to happen, an alarm on the computer would sound and the computer would turn off the heater until the temperature decreases. The inlet and outlet heaters, heater Zones 1 and 4, both have thermocouples to measure this temperature. A set of redundant thermocouples that are wired to a solid state relay and an independent control system, independent from the computer, ensure that in case of computer failures the reactor heaters will still turn off when needed.

There are both inlet and outlet emergency depressurization valves that the operators can use in case of overpressure. If the system goes 75 psi over the set pressure

of the Badger control valve, an alarm is sounded from the computer and all pumps, heaters and air flow is automatically stopped via the computer. Also, the Badger pneumatic pressure control valve is a fail-open device, meaning that without pneumatic pressure the valve will open and relieve pressure.

3.4. ANALYTICAL EQUIPMENT

The gas analysis is done using a HP 5890 gas chromatograph, with a Restek ShinCarbon 100/120 packed column 2 meters in length, 1/16" OD connected to a thermal conductivity detector, which uses 99.99% high purity argon as a carrier gas. The gas chromatograph is calibrated to detect hydrogen, nitrogen/oxygen, carbon monoxide, methane, carbon dioxide, acetylene, ethene, ethane, propene and propane. The gas chromatograph is connected to a computer which records and analyzes the results using a program called HP Chemstation. This software allows different run conditions to be saved and reused, and are called "methods". There are three methods used with the GC: Restek00, Restek01 and Restek02, which are adopted depending on the species to be detected. The GC was calibrated using tanks of pure gases supplied by Airgas. Appendix C lists the GC conditions and detectable species for each method, along with the elution time and calibration plot for each species. After every syringe injection a report is generated by HP Chemstation that gives the elution time and area of each peak, from which the species and number of moles can be determined. An example of the report generated by HP Chemstation is given in Appendix D.

4. EXPERIMENTAL METHODOLOGY

4.1. INTRODUCTION

The goal of this section is to explain how the equipment was used, what chemicals were used, what chemical reactions can occur, what experiments were performed and why. The materials used and their preparation is covered first. The apparatus was described in the previous section, so the operation section will draw on the terminology and flow path already described, while explaining the real time operation of the apparatus and analysis, along with start-up and shut-down procedures. The chemical reactions that occur during supercritical water reformation of glycerin are given, along with some analysis and description of the reactions. Details on how the residence time of the experiments are calculated is given, which is important when determining which experiments to be performed. The exploratory design of experiments will be described, the reason why the experiments were conducted and what they were designed to investigate.

4.2. MATERIALS

The water used for this study was deionized, and the glycerin used was 99.7% pure. The deionized water was supplied by a 12" Culligan mixed bed deionizer. The mixed cation-anion resin bed has a water quality of 2 megohm or higher with a neutral pH. The glycerin was purchased from TheChemistryStore.com and Sigma-Aldrich. The glycerin was first diluted with water to 75.0 wt% glycerin since glycerin above a purity of

80 wt% absorbs water from the atmosphere. Before the experiments were begun, the glycerin was further diluted to the weight percent used for those specific experiments.

4.3. OPERATING PROCEDURE

All components of operating the supercritical water reaction system will be detailed in this section. This includes the start-up of the system, the normal operation of the system throughout the day, gas analysis, air cleaning, system shut-down and routine maintenance. The supercritical water reaction system used is a rather large system, and requires significant time for start-up.

4.3.1. System Start-up. Experiments on the supercritical water reaction system are usually begun early in the morning, so that the operators can have the entire day to perform experiments while the reactor is up to temperature. The day is begun by opening National Instruments LabVIEW software and choosing the most up-to-date control file to use during operation. A data file is set up using the date of the experiment, a short description of the experiment. The data file is where all of the information that the LabVIEW control file collects during an experiment is stored. The temperature of each of the four heater zones is set. A switch on the control box must be switched on for each heater to be energized, as well as a button on the computer display. The air feed valve for the pneumatic Badger control valve is turned on, as is the ventilation system and the municipal tap water for cooling heat exchanger, if it is being used. As the reactor is heating up to operating temperature, the solution pump is primed with water to remove any air from the feed lines. Once the reactor is up to temperature, the preheat is turned on as well as the Eldex pump. The micrometers on the pump are set to give the desired

solution flow rate, and the reactor is pressurized. Water is pumped into the reactor until it is at operating temperature and pressure, and then the water tank is switched with the glycerin solution to be used for that experiment. Before an experiment is begun, the solution flow rate is confirmed by obtaining solution balance readings at five minute intervals, so that the flow rate is known and correct. If the flow rate is incorrect the micrometers are changed to obtain the correct flow rate. Once a steady temperature profile and pressure is established, the experiment can begin.

4.3.2. During an Experiment. The temperature and pressure are computer controlled, so after the operator sets the experimental conditions nothing more than occasional monitoring of the computer display is necessary. Throughout the experiment the solution flow rate is monitored to ensure the correct flow rate is maintained by recording the solution balance reading every fifteen minutes. The product gas flow rate is determined by taking wet test meter measurements continually throughout the experiment, so that the flow rate in ambient liters per minute is known. The content of the product gas is known in real time by taking syringe samples form the product stream and analyzing them on the HP 5890 gas chromatograph. The gas chromatograph can analyze a syringe sample in twenty minutes using method Restek01, or thirty minutes using Restek02. Restek00 is only used if prior syringe samples, analyzed with Reskek01, have shown there is no ethane or ethene in the product gas. The liquid reservoir must be continually monitored and drained of liquid, so that the gas sampling system is not flooded with liquid effluent. The liquid is drained into a removable in-process 5 gallon HDPE liquid effluent container. At least two liquid samples are taken during an experiment. An experiment is concluded when the GC results of three consecutive gas

syringe samples show no greater than one percentage point deviation between the three. After an experiment, the carbon conversion is calculated using the gas chromatograph results and product gas flow rates. If the conversion is less than 95%, the glycerin solution feed is stopped and water is fed into the reactor instead. Air is fed into the reactor via the high pressure air feed system, and the reactor is cleaned with supercritical water oxidation using air as the oxidant. Air cleaning is stopped when gas analysis shows no gaseous carbon in the product gas. With air cleaning done, the next experiment can begin. Once an experiment is concluded, or air cleaning if that is necessary, the conditions are changed to conduct the next experiment. During a typical day, four experiments are conducted.

4.3.3. Shut-down. After all of the experiments for that day are conducted, the reactor is cleaned with water and air as described above. The air flow and heaters are turned off and water only is pumped into the reactor for a few minutes to remove any air left in the system. When the water pump is shut off the reactor is depressurized by slowly opening the outlet emergency de-pressurization valves. After this the cooling water and the pneumatics are shut off, but the ventilation system is kept on so that any volatile components that may have come from the system during the depressurization are removed from the expansion drum. The LabVIEW computer display is stopped and about ten minutes after depressurization the ventilation system is shut down.

4.3.4. Maintenance. Once the reactor is cooled from the previous experiments, the system is pressure tested with air to ensure that the system is safe and ready to perform more experiments. The entire system up to the MFR outlet valve, which is immediately preceding the Swagelok filter assembly, is pressure tested. This is most of

the system that experiences high pressures and all of the system that experiences temperatures above ambient. The reactor is pressurized to 4500 psi and if the pressure drop is less than 30 psi per hour the system passes the check. If the pressure drop is more than that, different parts of the system are isolated and pressurized in order to determine the section that cannot hold pressure and begin the search for the leaking part. Other pieces that require regular maintenance are the Swagelok filters. If the previous experiments produced any tars or particulates, the filters can clog and produce pressure control problems, so they are replaced and cleaned before that can occur. The Eldex pump requires monthly oiling, and the liquid effluent tank is drained into a MS&T Environmental Health and Safety (EH&S) 55 gallon drum. Other maintenance occurs as needed.

4.4. CHEMICAL REACTIONS

The endothermic reformation of glycerin in supercritical water involves a complex reaction mechanism involving various intermediates and pathways. Many studies use the idealized decomposition of glycerin, Equation 6, combined with the water gas shift Equation 5,

$$C_3H_8O_3 \rightarrow 3CO + 4H_2 \quad (6)$$

$$CO + H_2O \Leftrightarrow CO_2 + H_2 \quad (5)$$

to simplify the reaction (*117*, *235*, *247*, *285*, *286*). The forward WGS reaction is equilibrium limited and thermodynamically favored at temperatures below 1090 K (*172*). When both of these reactions are combined, the overall reaction becomes

$$C_3H_8O_3 + 3H_2O \rightarrow 3CO_2 + 7H_2 \quad (7)$$

This is the maximum amount of hydrogen that could possibly be made from glycerin. While these reactions are important for determining the efficiency of the process, they do not represent all the products made during reformation, so it is important to understand how glycerin decomposes into intermediate products before undergoing further chemical reactions. First the decomposition of glycerin into liquid products will be reviewed. Various studies have shown that glycerin can decompose into acrolein at atmospheric pressures, with acetaldehyde being a major, secondary component (*140*, *141*, *143*, *144*). May et al. concluded that non-catalytic glycerin reformation in supercritical water involves both ionic and free-radical pathways. At lower temperatures ionic products include acetaldehyde, formaldehyde and acrolein. Higher temperatures lead to free-radical reactions that produce gases (*272*). It has been reported that the ionic reactions ins supercritical water begin with a proton produced from the dissociation of water (*1*, *52*, *287*).

Laino et al. used a technique called metadynamic simulation to explore the pyrolytic decomposition of glycerin. The mechanism they determined was that glycerin dehydrates into glycidol, which is the rate limiting step. Glycidol converts to 3-hydroxypropanal, which can decompose further to acrolein and water or into formaldehyde and acetaldehyde. The decomposition into formaldehyde and acetaldehyde is faster than the decomposition into acrolein and water under pyrolytic conditions, and that acrolein formation should only occur at higher temperatures (*288*). Nimlos et al. used quantum mechanical calculations and found similar mechanisms, differing in the intermediate species but producing the same final compounds, acrolein, formaldehyde and acetaldehyde (*149*).

Bennekom et al. concluded that glycerin reformation in supercritical water first begins with dehydration to produce liquid intermediates, and these intermediates further react to form the gaseous components. This was shown by performing an oxygen balance on the outlet products compared to the inlet glycerin. It was found that less oxygen exits the reactor in the gas phase than entered as glycerin, and from this it was concluded that the remaining oxygen exited the system as water due to the initial dehydration reaction. The reaction pathway Bennekom et al. describes is glycerin dehydration to liquid products, followed by gasification. The primary gas species would be hydrogen, carbon monoxide, methane and ethene. These gasses would react to form carbon dioxide via water gas shift, ethane via the saturation of ethene, and further methane via the methanation reaction (*75*).

Buhler et al. investigated the lower temperature ionic products and pathways of glycerol reformation in subcritical and supercritical water (*136*). The liquid products were methanol, allyl alcohol, acetaldehyde, acrolein, and formaldehyde. Also measured, though minor, were ethanol, acetone, ethane, ethene, propane, propene, butenes, and butanes. Acetaldehyde and acrolein were the major products of low temperature glycerin reformation in supercritical water in a variety of studies (*25*, *136*, *137*, *146*, *147*). The liquid pathway will focus on these two species.

Acrolein and water are formed from the decomposition of glycerol (*132*, *136*–*141*, *143*, *144*, *146*, *147*).

$$C_3H_8O_3 \longrightarrow C_3H_4O + 2H_2O \qquad (8)$$

The decomposition of acrolein produces a variety of chemical species, which in order of decreasing production include: carbon monoxide, ethene, hydrogen, methane, ethane, and

propene (*147*, *289*, *290*). To account for the four most abundant gas species, two different pathways for acrolein decomposition will be investigated. First, the reaction of acrolein with water to produce methane, carbon monoxide and hydrogen:

$$C_3H_4O + H_2O \longrightarrow 2CO + CH_4 + H_2 \quad (9)$$

The other reaction is acrolein decomposition into carbon monoxide and ethene.

$$C_3H_4O \longrightarrow CO + C_2H_4 \quad (10)$$

Water, acetaldehyde and formaldehyde are also produced from glycerin in sub and supercritical water (*136–138*, *147*, *148*).

$$C_3H_8O_3 \longrightarrow C_2H_4O + CH_2O + H_2O \quad (11)$$

In other studies of glycerin decomposition, it is noted that formaldehyde is an intermediate product that quickly decomposes in supercritical water (*136*, *273*). The decomposition of acetaldehyde, Equation 12, gives methane and carbon monoxide, and the decomposition of formaldehyde, Equation 13, produces carbon monoxide and hydrogen. (*25*, *136*, *147*, *276*, *291–293*).

$$C_2H_4O \longrightarrow CH_4 + CO \quad (12)$$

$$CH_2O \longrightarrow H_2 + CO \quad (13)$$

Overall, considering the gases made, there are two pathways for glycerin decomposition via liquid intermediates whether glycerin decomposes into acrolein or acetaldehyde and formaldehyde. As long as these liquid intermediates are produced via the above reactions, and decompose as given above, the two reactions for glycerin gasification via liquid intermediates are:

$$C_3H_8O_3 \longrightarrow CH_4 + 2CO + H_2 + H_2O \quad (14)$$

$$C_3H_8O_3 \longrightarrow C_2H_4 + CO + 2H_2O \quad (15)$$

Equation 14 is a product of either Equation 8 then 9 or Equation 11, then Equation 12 and 13. Whether glycerin decomposes to acrolein or acetaldehyde and formaldehyde, the end gaseous results are the same. Equation 15 is a combination of Equations 8 and 10. These two reactions describe all of the gaseous species seen in glycerin reformation except carbon dioxide, propane and ethane. The saturation of ethene,

$$C_2H_4 + H_2 \longrightarrow C_2H_6 \quad (16)$$

can explain the presence of ethane, while propene and propane will be neglected because they are not major components of the decomposition and were not major components of the experiments conducted for this work (*272*, *273*). Carbon dioxide can be formed in the presence of carbon monoxide and water by the water gas shift reaction, Equation 5, in supercritical water (*199*, *294–297*).

Another important chemical reaction seen during glycerin reformation is the exothermic methanation reaction, where carbon monoxide or carbon dioxide and hydrogen react to form methane and water (*199*, *258*, *265*, *298*). This reaction is undesirable since both hydrogen and carbon monoxide, the desired products, are consumed to form unwanted byproducts.

$$CO + 3H_2 \Leftrightarrow CH_4 + H_2O \quad (17)$$

$$CO_2 + 4H_2 \Leftrightarrow CH_4 + 2\,H_2O \quad (18)$$

Methanation is favored by lower temperatures, below 600°C, and requires a catalyst for commercial methanation. Most carbon monoxide methanation is done around 250°C, with carbon dioxide methanation being favored at higher temperatures (*299*). The reverse of the methanation reactions, the steam reforming of methane, would be

beneficial. Steam reformation is generally conducted at 700 to 1100°C, at ambient pressure, over a nickel catalyst. Methane can be formed by routes other than methanation, such as a decomposition product of the liquid intermediates.

Considering the reactions based on the intermediates, Equations 14 and 15, if all of the methane were reformed with steam reformation, and all the ethane or ethane reformed, and all the carbon monoxide underwent the water gas shift reaction, then the maximum amount of hydrogen seen in Equation 7 would be produced. Figure 4-1 is a generalized reaction pathway illustrating the various intermediates and how they decompose into the gases seen during supercritical water reformation of glycerin.

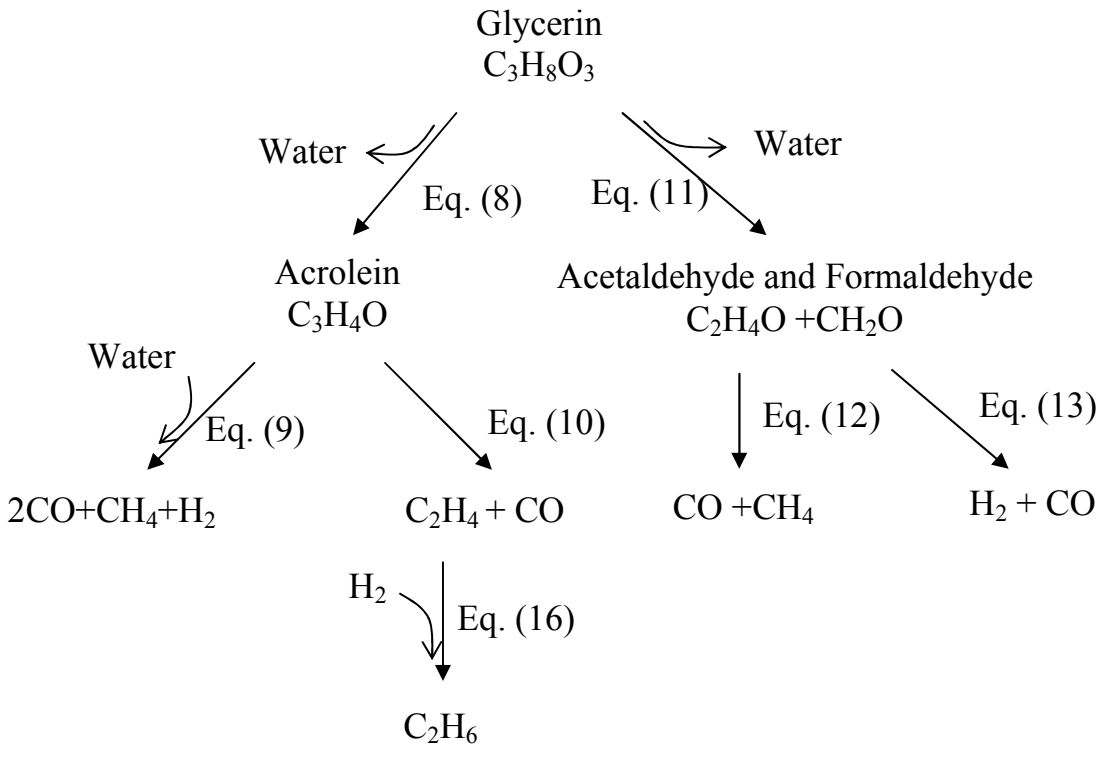

Figure 4-1. Possible reaction pathways for the reformation of glycerin by supercritical water.

The above pathway takes into account only a few of the possible liquid intermediates. Other reactions, such as the Boudouard reaction, methane decomposition, oxidation, methane dry reforming, hydrogenation or dehydrogenation, as well as many others are possible, but the discussion in this section will be limited to the above reactions due to their ability to describe and account for the product gases (*35*, *136*, *137*, *235*, *300*, *301*).

4.5. RESIDENCE TIME

Equations of state are the most thermodynamically consistent and computationally straightforward method for calculating properties in the supercritical region (*300*). After conducting a literature search, and comparing various equations of state, it was determined that the Peng-Robinson equation of state was the best for supercritical water and high-temperature, high pressure water mixtures involving nitrogen, carbon dioxide, methane and various hydrocarbons. The details of the selection process are given in Appendix E. Compared to the experimental data found in other studies, the error for the Peng-Robinson equation of state with van der Waals mixing rules was on average about 2% (*20*, *302*, *303*). The Peng-Robinson equation of state has been used by numerous studies working with supercritical fluids (*45*, *304–309*). The Peng-Robison equation of state will be used for the residence time calculations.

The residence time is defined here as the amount of time the reactants would remain in the reactor assuming no reactions took place. It is based on the volume of the reactor, the flow rate of the water/glycerin solution, the composition of the water/glycerin solution, the inlet pressure of the reactor and the average temperature of the reactor. This

definition of residence time is used because the profile of the reaction, when and what occurs along the length of the reactor, is unknown. It is calculated using the Peng-Robinson equation of state.

$$P = \frac{RT}{V - b} - \frac{a}{V(V+b) + b(V-b)} \tag{19}$$

The pressure used here is that recorded by the inlet pressure transducer, the temperature is the reactor temperature, R is the gas constant and V is the molar volume. Since this is a mixture of two species, a and b will be calculated using van der Waals mixing rules.

$$a = \sum_i \sum_j x_i x_j (1 - k_{ij})(a_i a_j)^{0.5} \tag{20}$$

$$b = \sum_i y_i b_i \tag{21}$$

Where a_i is the a parameter for species i, and a_j is the same parameter for species j, which are combined together by the Van der Waals mixing rule to make the composite a, with b being calculated similarly. The parameter k_{ij} is an interaction parameter between the two species, which is zero for these calculations. The values of x_i and x_j are the inlet mole fraction of each component. The values for a_i, a_j, b_i, b_j are calculated from

$$a_i = 0.457235(R^2 T_{ci}^2 / P_{ci})[1 + F_i(1 - T_{Ri}^{0.5})] \tag{22}$$

$$b_i = 0.07796(RT_{ci} / P_{ci}) \tag{23}$$

$$F_i = 0.37646 + 1.54226\omega_i - 0.26992\omega_i^2 \tag{24}$$

The parameter T_{ci} is the critical temperature of species i, P_{ci} is the critical pressure, and ω_i is the acentric factor. With a and b calculated for the mixture, the Peng-Robinson equation of state can be used to find V. The molar inlet flow rate is known, and by multiplying the inlet molar flow rate by the molar volume, the volumetric flow rate is

calculated. Dividing the volume of the reactor, 101 cm^3, by the volumetric flow rate in cm^3/min, gives the residence time in minutes.

This residence time is an approximation, because of the difficulties in determining the density of supercritical mixtures, as well as the reaction profile in the reactor. For binary and some ternary mixtures, the phase diagram can be classified into six main types in accordance with Van Konynenburg and Scott (*310*, *311*). For mixtures with more components, which is inevitable in reacting systems, the phase diagrams become increasingly complex (*312*, *313*). As for reacting systems, whose compositions change with time, the thermodynamic description of these systems is an unsolved problem (*25*, *281*). As such, this residence time, based on the mixture molar volume and hence on mixture density, is only as accurate as the equation of state and the mixing rules used to calculate it, and should function more as a descriptor of a relationship between the reaction conditions and not as an actual time. Since this is the method used by the majority of supercritical water researchers, it does facilitate comparison of data between research groups.

4.6. EXPLORATORY DESIGN OF EXPERIMENTS

There are many things that can be varied when supercritical gasification is to be studied. For these experiments it was determined that the three most important aspects of the supercritical water gasification of glycerin were: Temperature, water-to-glycerin ratio, and residence time. This is based upon the literature review that was conducted before these experiments, along with previous knowledge of the reformation/gasification of other hydrocarbons in supercritical water. Other variables seen in the literature are

pressure, reactor type/configuration, catalysis material, oxidant, heating time, and the addition of salts or other contaminants to the feed solution. Of these, the most viable candidate for study would have been the effect of pressure, but previous studies, as well as the literature review, indicated this would have less effect than the other three that were decided upon, especially in a range from 17 to 31 MPa (*268–271*, *300*, *314*). With three variables to be studied, it was decided that a 2^3 matrix would be employed. This is meant to be an exploratory design of experiment, so further study will be given to the variable(s) that have the most effect on the carbon conversion and hydrogen yield. Although carbon conversion and hydrogen yield are the most important responses, the response for all of the product gases will be calculated. Duplicate experiments will be performed to determine reproducibility and error, and the 2^3 factorial design will allow determination of the main effects, as well as the two-way and three-way interaction effects.

With a 2^3 matrix, high and low conditions for each of the variables are determined. For temperature, it was 500 and 700°C. For water/glycerin molar ratio it was 3/1 and 13/1, and for residence time it was 30 and 90 seconds. The temperature range was determined from the literature review and prior experience in hydrocarbon and glycerin reformation. The water/glycerin molar ratio of 3/1 was chosen because it is the stoichiometric ratio for complete glycerin gasification and complete water-gas shift, as shown in Equation 7. The ratio of 13/1 was chosen based on the literature review. The residence times are determined mostly by the equipment. Maintaining pressure and accurate solution feed rates is difficult at very high residence times. The solution pump and pressure control valve determine how low the residence time can be, so times of 30

and 90 seconds are median values which can still be lowered or increased if further study is needed. This is true of all of the variables, higher or lower temperatures or water/glycerin ratios could be employed, as well as a large range of intermediates. A 2^3 matrix results in eight design point experiments, which Table 4-1 shows. The temperature, water/glycerin ratio, and residence time are given, as well as the weight percent glycerin and solution flow rate. All experiments are performed at 24.1 MPa, which corresponds to 3500 psi. This pressure has been used for a number of experiments previous to these, as well as in the literature. This pressure is higher than that needed to have supercritical water, 22.1 MPa. The flow rates are determined for each residence time using the Peng-Robinson equation described above.

Table 4-1. The exploratory 2^3 matrix.

Temperature °C	Residence time Seconds	Water/glycerin ratio Moles/mole	Weight % glycerin	Solution Flow g/min
500	30	3/1	63.0	42.0
700	30	3/1	63.0	24.5
500	90	3/1	63.0	14.0
700	90	3/1	63.0	8.6
500	30	13/1	28.2	23.8
700	30	13/1	28.2	15.5
500	90	13/1	28.2	7.9
700	90	13/1	28.2	5.1

5. RESULTS AND DISCUSSION

5.1. RESULTS AND DISCUSSION OF EXPLORATORY MATRIX

A 2^3 matrix was implemented, in order to determine the effect of changing the residence time, temperature and water/glycerin ratio on carbon conversion and hydrogen yield. Based upon both prior range-finding experiments and the literature review, as well as the capabilities of the supercritical water system, it was determined to use temperatures of 500 and 700°C, water/glycerin molar ratios of 3/1 and 13/1, and residence times of 30 and 90 seconds at a pressure of 24.1 MPa. Analysis of this matrix will determine the focus of the later experiments.

5.1.1. Results. The 2^3 matrix involves eight experiments, but duplicates were conducted to determine the reproducibility and error. Eleven experiments were conducted from the original matrix. Once the matrix was analyzed, further experiments were conducted, and some matrix experiments were repeated. Therefore, the experiments are numbered in the order in which they were conducted, 1-11 being the originals, and 14 and 30 being conducted afterwards. Table 5-1 shows the experiment number, the temperature, pressure, solution flow rate, water/glycerin molar ratio, calculated residence time, and if the experiment was a repeat of a previous one. They are put in an order similar to Table 4-1, to illustrate the matrix design.

With the experiments conducted, the results can be determined. Table 5-2 shows the gas yield and carbon conversion for each experiment. These will be the results that are used to determine the most important variable of statistical significance. The gas yield is a dimensionless number defined as the moles of that particular gaseous species

exiting the system per minute divided by the number of moles of glycerin entering per minute. Yield is used so that variations in the inlet solution flow rate are taken into account, and to make comparing results with different flow rates or water/glycerin ratios easier.

Table 5-1. Experimental conditions for the exploratory matrix.

Experiment number	Temperature (°C)	Pressure (MPa)	Flow rate (g/min)	Water/ glycerin	Residence time (seconds)	Repeat of
10	500	24.3	42.8	3	29.6	
7	701	24.2	24.6	3	27.3	
8	701	24.3	24.5	3	30.0	7
11	701	24.1	24.5	3	29.8	7
9	502	24.3	14.5	3	86.3	
6	699	24.2	8.7	3	84.3	
14	701	24.2	8.6	3	85.3	6
29	701	24.2	7.9	3	91.9	6
4	498	24.4	23.6	13	30.6	
2	698	24.2	15.5	13	29.6	
5	698	24.3	15.6	13	29.6	2
3	500	24.5	7.9	13	91.3	
1	698	24.3	5.2	13	88.5	

The outlet gas composition is determined by the gas chromatograph, and the outlet gas flow rate from the wet test meter. Carbon conversion is the percentage of carbon that exits the system as gas divided by that which entered as liquid glycerin. It

should be noted that at times carbon conversions over 100% are encountered. This is due to analytical errors and does not mean that any carbon is generated in the process.

Table 5-2. Results of the exploratory matrix.

Experiment number	Gas Yield					Carbon conversion
	H_2	CO	CH_4	CO_2	C_2H_6	
10	0.03	0.15	0.03	0.04	0.00	7.6%
7	1.35	1.14	0.74	0.54	0.16	91.6%
8	1.37	1.11	0.74	0.56	0.16	91.2%
11	1.42	1.13	0.75	0.57	0.17	93.3%
9	0.09	0.31	0.08	0.12	0.01	17.8%
6	1.57	1.14	0.86	0.72	0.19	103.2%
14	1.38	1.18	0.89	0.68	0.21	105.9%
29	1.26	0.88	0.94	0.84	0.23	104.0%
4	0.02	0.03	0.01	0.01	0.00	1.6%
2	2.87	1.23	0.60	0.99	0.14	103.3%
5	2.73	1.00	0.59	1.08	0.15	99.3%
3	0.34	0.45	0.06	0.08	0.01	20.2%
1	3.48	0.35	0.79	1.79	0.10	104.3%

In Table 5-2, the ethene yield was not included, even though some of the experiments had ethane in the produced gas. Experiments 10, 9, 4, and 3 all contained some ethene, but the amount was so small the largest yield was only 0.01, and as such this was not included in the table. There is large variation in the results, with hydrogen yield going from 0.03 to 3.48, and carbon conversion from 1.6% to over 100%. This

indicates that the variables chosen for the matrix do affect the results. Using statistical methods, the effect of temperature, residence time and water/glycerin ratio on the hydrogen yield and carbon conversion can be determined, as well as an estimate of the error.

5.1.2. Analysis and Discussion. Figure 5-1 illustrates the eight experiments of the matrix as a cube, with temperature as one axis, residence time and water/glycerin ratio as the others. The corners of the cube are labeled 1 through 8, and these represent the results. When duplicate or triplicate experiments were conducted, the result is the average of all the experiments at that condition.

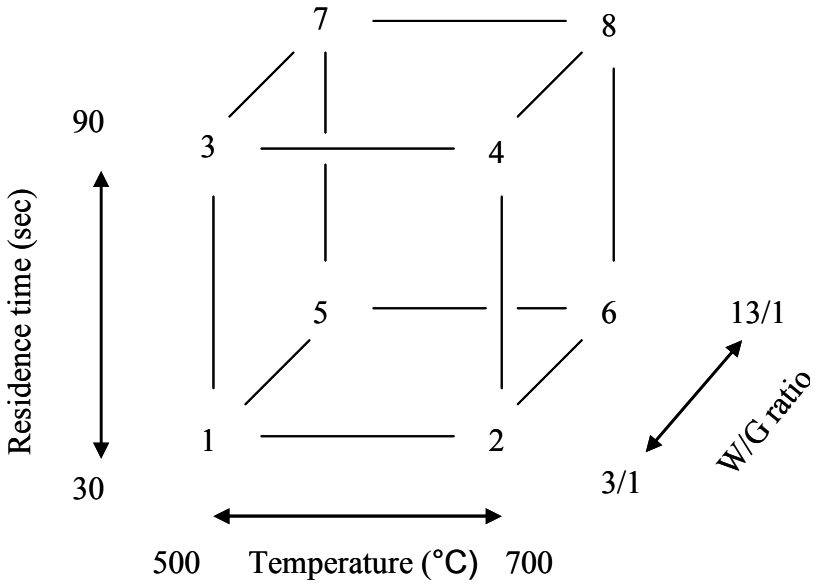

Figure 5-1. Visualization of the 2^3 matrix.

To determine the main effect of changing temperature, the conditions at different temperatures but with the other variables kept nominally constant were subtracted from each other, and the average of all these differences is the main effect of temperature. The

experiments are designated by E, then the number of the experiment. Using Figure 5.1, it would be the average of (E2-E1), (E4-E3), (E6-E5), and (E8-E7) to determine the main effect of temperature between 500 and 700°C. This was done for residence time and the water/glycerin ratio also. The two-factor and three-factor interaction effects are calculated similarly; the mathematics is given in Appendix F. All information about matrix design and evaluation came from "Statistics for Experimenters" by Box, Hunter and Hunter (*315*). Table 5-3 gives the main, two- and three-factor effects for carbon conversion and hydrogen yield.

Table 5-3. Calculated effects and estimated errors on carbon conversion and hydrogen yield for the 2^3 matrix.

	Effect on carbon conversion with estimated error	**Effect on hydrogen yield with estimated error**
Main effects		
Temperature, T	88 ± 2%	2.1 ± 0.1
Residence time, R	11 ± 2%	0.27 ± 0.1
Water/Glycerin ratio, W	1 ± 2%	0.94 ± 0.1
Two-factor interactions		
T x R	-3 ± 2%	0.1 ± 0.1
T x W	3 ± 2%	0.8 ± 0.1
R x W	0 ± 2%	0.2 ± 0.1
Three-factor interaction		
T x R x W	4 ± 2%	0.1 ± 0.1

An estimate of the standard error is given for all of the calculated effects, the mathematics of which is given in Appendix F. The calculated effects and estimated

standard error for the other gaseous species are in Appendix G. The results in Table 5-3 are clear, that over the ranges studied in this matrix, temperature had the largest effect upon carbon conversion and hydrogen yield. The conversion is higher by almost ninety percentage points between the two temperatures, going from an average conversion of 12% at 500°C to 100% at 700°C, while hydrogen yield increased from 0.1 to 2.3 over the same interval. The only other effect that comes close to temperature is the water/glycerin molar ratio, which had an effect of 0.94 for the hydrogen yield, less than half the effect of temperature. The two-factor and three-factor interaction effects are also small compared with the temperature main effect. For hydrogen yield, the temperature-water/glycerin ratio two-factor interaction is 0.8, the largest for the interaction effects. Appendix G shows that the largest effect on all of the gas yields was temperature. Based upon the results of this matrix, it was decided to conduct further experiments at different temperatures.

5.2. ANALYSIS OF TEMPERATURE

The conversion of any type of biomass is a strong function of temperature, with higher temperatures leading to higher conversions and less charring or polymerization (*75*). Gas yields will vary as well, due to the temperature effect on both the reaction rate and the equilibrium constants (*26*, *271*). Since the reaction rate would increase with temperature, overall reforming yield would be higher and would increase with temperature. Also, the complete conversion of glycerin to hydrogen is endothermic, while the methanation reaction is exothermic. Thus, according to the Le Chatelier principle, methane formation at equilibrium increases at lower temperatures. Methane

competes against hydrogen, and is not a desired product. Therefore, theoretically it is already known that high reforming temperatures are necessary. The temperature range for the matrix experiments was from 500-700°C. The upper operating temperature of the reactor is 800°C, so that was chosen as the upper limit on experimental temperature. The lower temperate that was chosen was 500°C, because it was found in the previous matrix that the carbon conversion was very low at this temperature, 20% or below. Further decreases in temperature would not be constructive. Experiments were conducted every 50°C between 500 and 800°C.

With the temperature range chosen, the other parameters, such as pressure, residence time, and water/glycerin ratio must be decided upon. The pressure was to remain at 24.1 MPa, since it was not varied in the matrix. It was determined to use the same residence times and water/glycerin ratios as the matrix, and just increase the temperature incrementally, every 50°C from 500 to 800°C. This would allow some of the original matrix experiments to be used again. Table 5-4 outlines the experiments conducted to determine the effect of temperature, and gives the temperature, residence time, water/glycerin ratio and solution flow rate. It is divided into sections based on what the residence time and water/glycerin ratio are.

5.3. RESULTS OF TEMPERATURE ANALYSIS

There are 28 experiments in Table 5.4, and in total 35 experiments were conducted due to repeat experiments. These 35 experiments include the ones conducted for the 2^3 matrix, and are numbered the same way, in the order in which they were conducted. All of these experiments were conducted over a span of 45 days. The

experiments will be analyzed in groupings based on their residence time and water/glycerin ratio, in the same way that Table 5-4 is divided. Table 5-5 shows the experimental conditions of the 35 experiments.

Table 5-4. The experiments to be conducted to investigate the effect of temperature.

Temperature °C	Residence time Seconds	Water/glycerin ratio Moles/mole	Solution Flow g/min
500	30	3/1	41.9
550	30	3/1	34.5
600	30	3/1	24.2
650	30	3/1	26.8
700	30	3/1	24.5
750	30	3/1	22.6
800	30	3/1	21.1
500	90	3/1	14.0
550	90	3/1	11.5
600	90	3/1	8.0
650	90	3/1	8.9
700	90	3/1	8.2
750	90	3/1	7.5
800	90	3/1	7.0
500	30	13/1	23.8
550	30	13/1	20.5
600	30	13/1	18.3
650	30	13/1	16.6
700	30	13/1	15.3
750	30	13/1	14.2
800	30	13/1	13.3
500	90	13/1	7.9
550	90	13/1	6.8
600	90	13/1	6.1
650	90	13/1	5.5
700	90	13/1	5.1
750	90	13/1	4.7
800	90	13/1	4.4

Table 5-5. Experimental conditions for the analysis of temperature.

Experiment number	Temperature (°C)	Pressure (MPa)	Flow rate (g/min)	Water/ glycerin	Residence time (seconds)	Repeat of
10	500	24.3	42.8	3	29.6	
13	546	24.2	33.7	3	31.0	
12	599	24.2	29.7	3	30.3	
15	600	24.2	29.4	3	30.6	12
17	649	24.2	27.4	3	29.4	
7	701	24.2	24.6	3	27.3	
8	701	24.3	24.5	3	30.0	7
11	701	24.1	24.5	3	29.8	7
16	749	24.3	22.0	3	30.9	
18	801	24.2	20.6	3	30.6	
9	502	24.3	14.5	3	86.3	
35	551	24.3	11.4	3	90.4	
34	600	24.4	9.7	3	93.1	
33	650	24.4	8.8	3	92.2	
6	699	24.2	8.7	3	84.3	
14	701	24.2	8.6	3	85.3	6
29	701	24.2	7.9	3	91.9	6
30	750	24.2	7.4	3	90.9	
31	799	24.3	7.0	3	90.4	
4	498	24.4	23.6	13	30.6	
20	547	24.2	20.8	13	29.7	
19	600	24.2	18.3	13	30.0	
23	650	24.2	16.0	13	31.0	
2	698	24.2	15.5	13	29.6	
5	698	24.3	15.6	13	29.6	2
21	750	24.1	13.8	13	30.9	
22	801	24.2	13.4	13	29.7	
3	500	24.5	7.9	13	91.3	
32	550	24.4	6.7	13	92.9	
28	599	24.4	5.8	13	96.1	
27	649	24.3	5.5	13	91.4	
1	698	24.3	5.2	13	88.5	
24	699	24.3	5.1	13	90.1	1
25	748	24.2	4.7	13	91.1	
26	764	24.3	4.5	13	93.4	

Table 5-5 lists the major experimental variables of the gasification, the temperature, pressure, flow rate, residence time, and water/glycerin ratio, as well as which experiments were repeats. As can be seen in Table 5-5, not all of the values are the same as those in Table 5-4, due to errors involved in the experiment. At times the solution flow rate into the reactor would be too high or low, and this would not be determined until after the experiment, leading to variations in the residence time from the desired 30 or 90 seconds.

5.3.1. Experiments at 30 Seconds, 3/1 Water/glycerin Ratio. The results of the experiments in the first section of Table 5-5 are illustrated in Figure 5-2, which shows the carbon conversion percentage and gas yield of hydrogen, carbon monoxide, methane, carbon dioxide and ethane. These are the main components of the product gas, but not the only ones. Ethene, propene and propane were also detected in some experiments, but not in all and in very low concentrations. The largest gas yield of the three was 0.04 for propene during experiment number 17 conducted at 650°C. All of these gases, ethene, propene and propane, only occurred for experiments in the 500 to 650°C range and were undetectable at the higher temperatures. The complete list of the results of the experiments: the experiment number, the wet test flow rate, the ambient temperature, the gas composition in mole percent, and the carbon conversion are given in Appendix H. For all duplicate experiments, the results are averaged and the standard error is given. The standard error is also included for the pressure and residence time, as these vary between each experiment. The lines used in the graphs to connect experimental data points are visual aids to allow the reader see trends in the data.

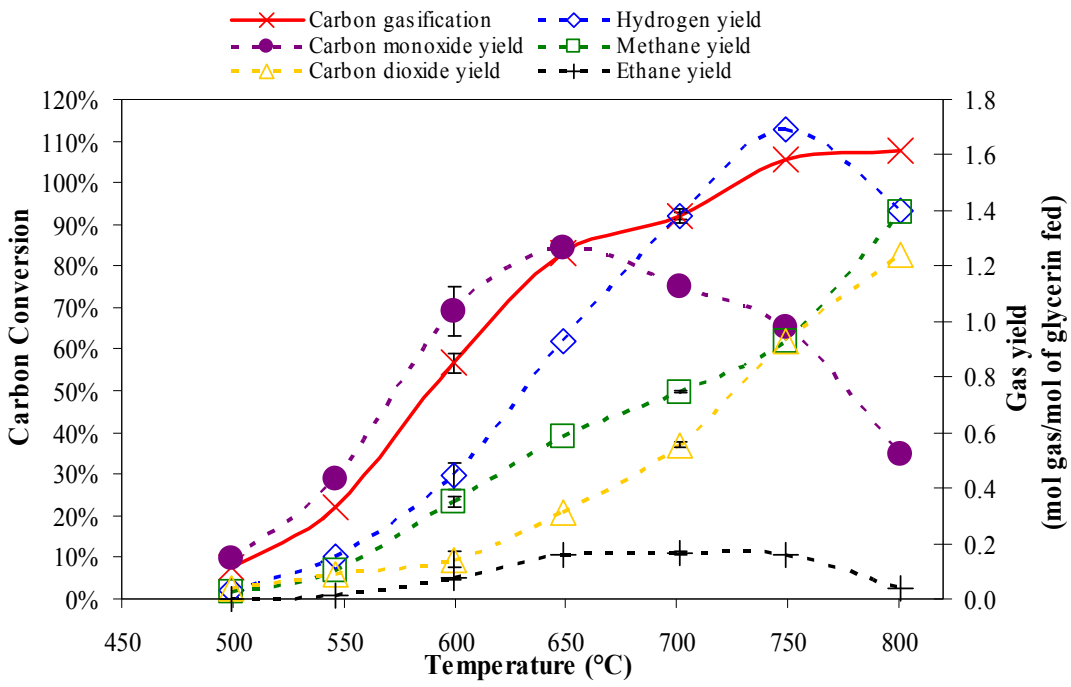

Figure 5-2. Carbon conversion percentage and gas yield for changing temperature at 30.0 ± 0.3 seconds residence time, 3/1 water/glycerin molar ratio, 24.22 ± 0.02 MPa.

In Figure 5-2, it can be seen how the gas yields and carbon conversion changes with temperature at these experimental conditions. The carbon conversion increases with temperature, going from a conversion of 7.6% at 500°C to 105% at 750°C, and remaining above 100% at 800°C. The reason for the conversion to be above 100% is due to inaccuracies in the inlet solution flow rate, the wet test meter reading and the gas chromatograph analysis. It should be assumed that any conversion over 100% in actuality means a conversion of 100%. The conversion increases greatly from 500 to 600 to 650°C, going from 8% to 56.77 ± 0.02% to 83%, after which it increases more slowly to 92.01 ± 0.01% at 700°C.

The hydrogen yield follows a similar trend, going from a very small yield of 0.04 at 500°C and increasing with temperature to 1.7 at 750°C, the highest yield for hydrogen

at these conditions. It decreased to a yield of 1.4 as temperature increased to 800°C. The largest standard error on the hydrogen yield was at 600°C, with a 0.44 ± 0.05 hydrogen yield. Carbon monoxide yield increased with temperature, increasing from 0.15 at 500°C to 1.3 at 650°C, its highest yield at these conditions. Afterwards, with increasing temperature the carbon monoxide yield decreased, ending at a yield of 0.5 at 800°C. Again, the largest standard error was at the 600°C, 1.0 ± 0.09 being the carbon monoxide yield. This is about a 10% error on carbon monoxide at this temperature, while at 700°C the error is only about 1%. Both methane and carbon dioxide increase steadily with temperature. Both begin with small yields, near 0.3, while carbon dioxide increases to 0.55 ± 0.01 at 700°C and continues increasing to 1.2 at 800°C. Methane is similar, 0.745 ± 0.005 at 700°C and 1.4 at 800°C. The ethane yield was near flat, always having a yield below 0.16, going from near zero at 500°C, increasing to 0.16 at 650 to 750°C, decreasing to a yield of 0.04 at 800°C.

The reason for these trends are two-fold; The water gas shift reaction converts more carbon monoxide to carbon dioxide and hydrogen at higher temperatures, leading to an increase in carbon dioxide and hydrogen with a decrease in carbon monoxide. Secondly, the methane formation reaction seems to be more active at the higher temperatures. Methane could be formed from liquid intermediate decomposition, which could produce methane and consume hydrogen. As mentioned previously, these liquid intermediates could include acrolein, hydroxyacetone, acetaldehyde, among others. At 800°C, it may be that the water-gas shift reaction is near equilibrium, and not producing much more hydrogen, while the methane formation is consuming it, leading to an overall decrease in hydrogen.

5.3.2. Experiments at 90 Seconds, 3/1 Water/glycerin Ratio. Experiments were conducted at a residence time of 90 seconds and a 3/1 water/glycerin ratio, the results of which are illustrated in Figure 5-3. For these experiments, three repeats were conducted at 700°C. Again, the carbon conversion increases with temperature, from 18% at 500°C to 107% at 800°C. The largest increase in conversion is from 500 to 650°C, after which the conversion increases but more slowly. From 650 to 800°C, the conversion increases from 94% to 107%. Carbon conversion begins at a higher percentage, and reaches 100% at a lower temperature, for this residence time compared to the 30 second residence time of Figure 5-2. The carbon conversion and standard error at 700°C was 104.3 ± 0.8%. As mentioned earlier, percentages higher than 100% are, in every practical sense, at or close to 100%. The hydrogen yield increased with temperature from a yield of 0.1 at 500 to 1.41 ± 0.09 at 700°C, and decreases with temperature thereafter, having a yield of 1.3 at 800°C. Carbon monoxide again increases with temperature to 650°C, from 0.31 to 1.22, the maximum yield for carbon monoxide at these conditions. It then decreases to 0.40 at 800°C. The yield and standard error at 700°C is 1.07 ± 0.09 for carbon monoxide. Methane and carbon dioxide increase with temperature over the entire temperature range, with methane beginning at a yield of 0.08 at 500°C and ending at 1.55 at 800°C, the highest single gas yield for any gas at these conditions, and the highest methane gas yield seen for any of the 35 experiments. Carbon dioxide increases, but not as linearly as methane. The increase is slow from 500 to 600°C, from a yield of 0.12 to 0.19, but is more rapid from 600 to 750°C, going from 0.12 to 1.20 on carbon dioxide yield.

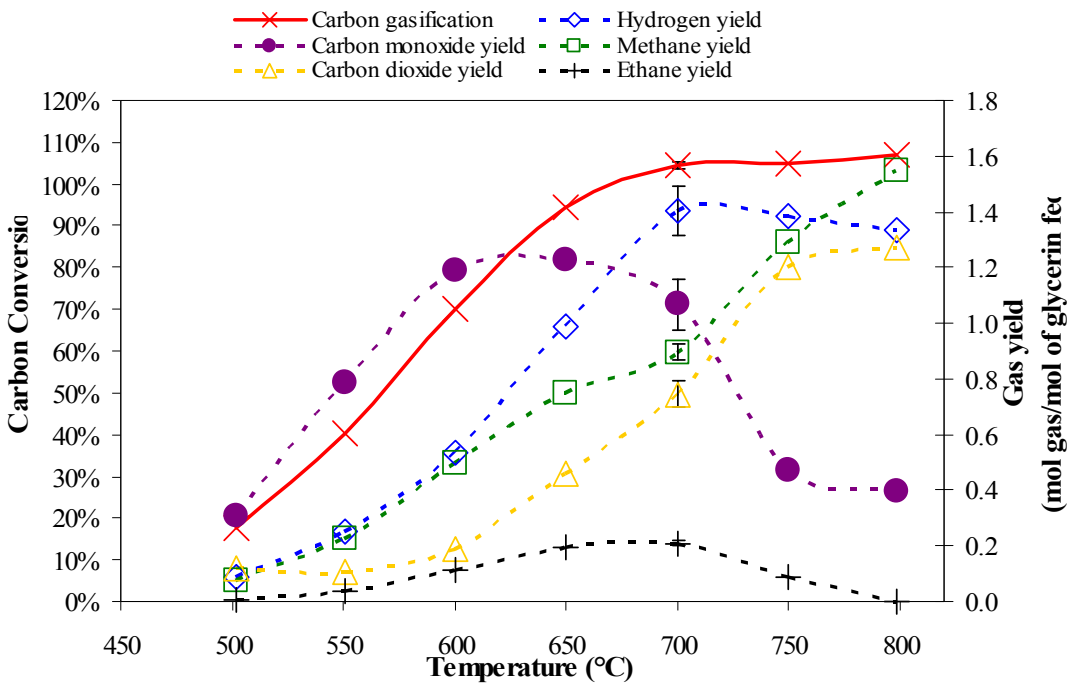

Figure 5-3. Carbon conversion percentage and gas yield for changing temperature at 89 ± 1 seconds residence time, 3/1 water/glycerin molar ratio, 24.28 ± 0.02 MPa.

The yield of carbon dioxide only increases from 1.20 to 1.27 at 800°C. This shows that the water-gas shift reaction is producing most of the carbon dioxide and hydrogen in the 650 to 750°C range, and may be in equilibrium around 800°C. The yield and standard error at 700°C is 0.75 ± 0.05. Again, ethane is near zero at 500°C, increases to 0.21 ± 0.01 at 700°C, and decreases to zero at 800°C. These trends with respect to temperature are very similar to the ones seen at a 30 second residence time, only shifted down by 50°C.

5.3.3. Experiments at 30 Seconds, 13/1 Water/glycerin Ratio. The next two sets of experiments will again be at 30 and 90 seconds residence time, but will have a water/glycerin molar ratio of 13/1 instead of 3/1 like the previous two sets of experiments. These are more dilute experiments, having a glycerin weight percent of

28.2% instead of 63%, and having 4.33 times more moles of water than what is necessary for maximum hydrogen production. Figure 5-4 shows the experiments conducted at 30 seconds residence time and a 13/1 water/glycerin ratio.

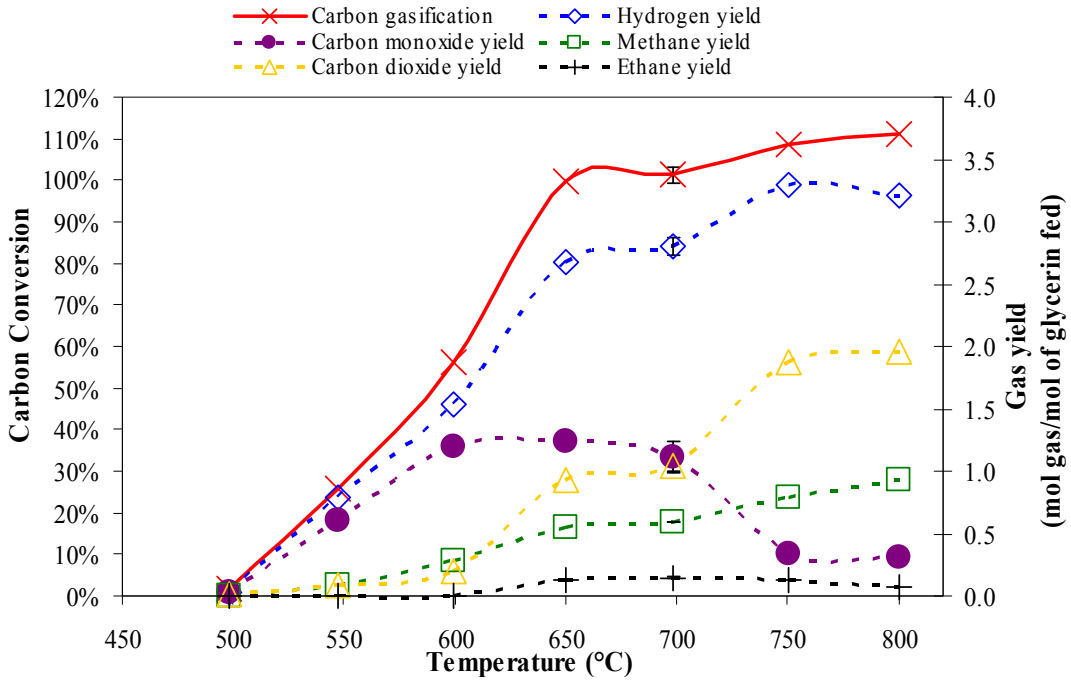

Figure 5-4. Carbon conversion percentage and gas yield for changing temperature at 30.1 ± 0.2 seconds residence time, 13/1 water/glycerin molar ratio, 24.23 ± 0.03 MPa.

The carbon conversion again increases with temperature, from a conversion of only 2% to 100% at 650°C, and increasing to 110% at 800°C. Again, it must be remembered that the reason for the conversion to be above 100% is due to inaccuracies in the inlet solution flow rate, the wet test meter reading and the gas chromatograph analysis. It should be assumed that any conversion over 100% in actuality means a conversion of 100%. If the conversion would have been over 110%, the experiment

would have been repeated, to understand why this was happening. This was the arbitrary cutoff, 110%, but all experiments were at or below this amount.

Hydrogen yield increased rapidly from 0.03 at 500°C to 2.68 at 650°C, and increased more slowly after that. The highest yield was 3.30 at 750°C, decreasing slightly to 3.21 at 800°C. Carbon monoxide again increased from 500 to 650°C, and decreased from 650 to 800°C. Carbon dioxide increased with temperature, but not smoothly, while methane increased with temperature in a more linear fashion. Ethane yield remained very low, always below 0.15.

Comparing these yields to the 3/1 water/glycerin experiments leads to the conclusion that carbon conversion is not affected by water/glycerin ratio, but the gas yields certainly are. Maximum hydrogen yield is about twice as much at 13/1 than 3/1, and carbon dioxide is also much higher. Carbon monoxide is very similar, and methane is much lower for the 13/1 experiments. The larger amount of water could be promoting the water-gas shift, the methane reformation reaction, or the steam reformation of the liquid intermediates, but it has little effect over gasification in general, since the carbon conversion is similar.

5.3.4. Experiments at 90 Seconds, 13/1 Water/glycerin Ratio. The last sets of experiments, shown in Figure 5-5, were performed at the longest residence time and the most dilute water/glycerin molar ratio. This set had the fastest response for the carbon conversion, increasing from 20% at 500°C to 95% at 600°C. None of the other conditions were able to reach a conversion of over 90% by 600°C. The conversion increases slightly with temperature after that, being at or above 100% conversion.

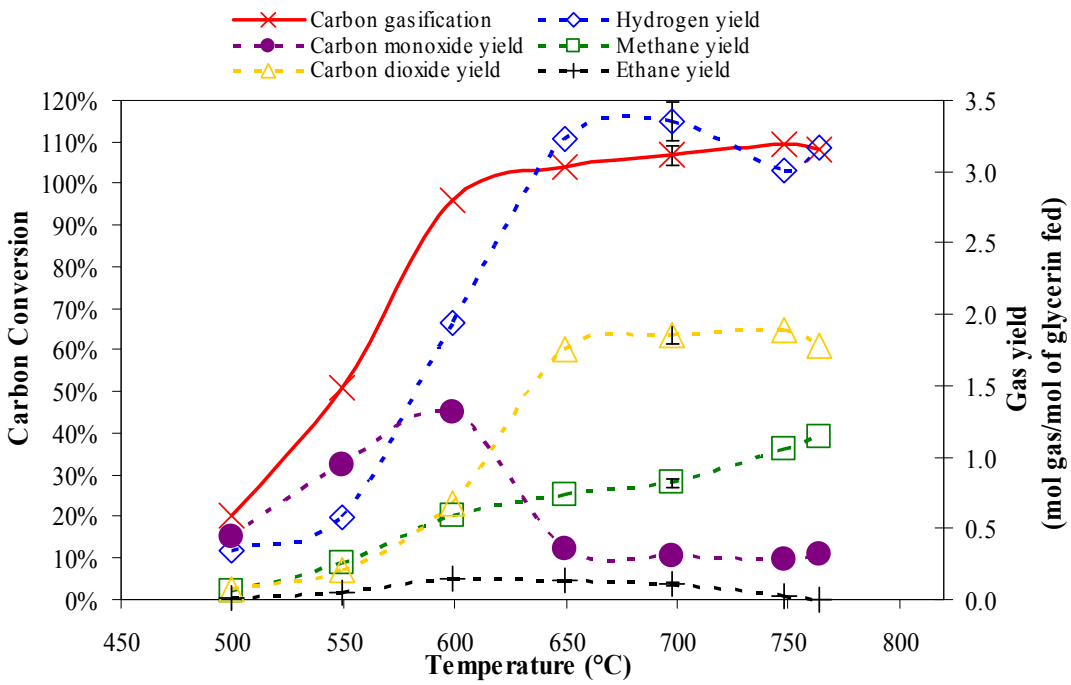

Figure 5-5. Carbon conversion percentage and gas yield for changing temperature at 92 ± 1 seconds residence time, 13/1 water/glycerin molar ratio, 24.32 ± 0.03 MPa.

Hydrogen yield increases greatly with temperature from 500 to 650°C, going from a 0.34 to a 3.23 hydrogen yield over that interval. It increases a little more at 700°C, 3.4 ± 0.1 hydrogen yield. This is the largest hydrogen yield seen for any experiments, and is about half as much as the stoichiometric maximum yield of 7 moles of hydrogen per mole of glycerin fed. Increasing temperatures beyond 700°C decreases the hydrogen yield. Carbon monoxide increases with temperature from 500°C to 600°C, reaching a maximum of 1.31 at 600°C. This is similar to the maximum carbon monoxide yields that were seen for the other experiments, but occurred 50°C earlier at 600°C while the others were at 650°C. This was the maximum amount of carbon monoxide for all the experiments. As the temperature increased further, carbon monoxide dropped to 0.35 and remained at about this level. The methane yield increased with increasing temperature,

reaching a maximum yield of 1.14 at 800°C. Carbon dioxide yield increases from 0.08 at 500°C to 1.76 at 650°C, and remains about level after that. The maximum is 1.90 at 750°C. Ethane is barely detectable at 500°C, has a maximum of 0.15 at 600°C, and is undetectable at 800°C.

It appears that methane formation is limited at these conditions, but increases slowly with temperature. By 600°C, carbon gasification is almost complete, but the water-gas shift reaction has not yet converted much carbon monoxide to hydrogen and carbon dioxide. At higher temperatures it does, leading to the increase in hydrogen and carbon dioxide and the decrease in carbon monoxide. With methane increasing slowly, and gasification already 100%, the hydrogen, carbon monoxide and carbon dioxide yields are stable or trending at a similar rate to methane. The gradual increase in carbon gasification from 600°C to 800°C could be a liquid intermediate decomposing into methane.

For all of the experiments, carbon conversion increases with temperature. The greatest increase is from 500 to 600 or 650°C, where the conversion increases from about 10% to nearly 100%, after which the conversion levels off or increases slowly. Complete gasification is important, because another important goal is to destroy any organic matter completely so that no further treatment of the liquid effluent is necessary. Further analysis would have to be conducted on the liquid to determine if further cleanup was needed, but 100% gasification is an important first step.

After the conversion is 100%, all of the glycerin has become gas and the question becomes what gas is being produced and how is it affected by temperature or the different conditions. In general, hydrogen yield increased with temperature to around

700 to 750°C, and decreased afterwards. This was assumed to be from methane formation at the higher temperatures. The methane formation reaction is assumed to be via liquid intermediates, the decomposition of which consume hydrogen and produce methane. Carbon monoxide yield looked similar for all experimental sets, having a similar shaped trend and similar yields. Generally it increased until 600 or 650°C, and decreased afterwards. Carbon dioxide increased with temperature. Ethane yield was always low, but with maximums near 600°C and minimums at the highest and lowest temperatures.

The effect of residence time at the 3/1 water/glycerin ratio was not very pronounced. The 90-second residence time reached 90% conversion at a lower temperature than at 30 seconds, but overall, the trends and the yields of each gas species were similar. There was less methane and more hydrogen at the 30-second residence time for the 750 and 800°C experiments. For the 13/1 water/glycerin experiments, the 90-second residence time again reached 90% carbon conversion at a lower temperature. At the same water/glycerin ratio, the maximum gas yield produced was similar, but at the longer residence time it was reached at a lower temperature. The same is true of glycerin gasification; the longer residence times reached 100% conversion at temperature that was 50 to 100°C lower than the 30-second residence time experiments.

The effect of water/glycerin ratio at the same residence time was more pronounced than that of residence time. Comparing 30-second experiments at 3/1 and 13/1 water/glycerin molar ratio, it is clear that the 13/1 ratio achieves above 90% conversion at a lower temperature, has a maximum hydrogen yield almost double that of 3/1 with a similar carbon monoxide yield. There is more carbon dioxide in the 13/1 and

less methane, which indicates more water-gas shift and less methane formation. The ethane yields are similar. A similar phenomenon occurs when the residence time is 90 seconds. Water/glycerin ratio had some effect on carbon conversion, in that the more dilute experiments reached full gasification at lower temperature, but the most pronounced effect was in gas yield. The excess of water in the 13/1 water/glycerin ratio promotes water-gas shift over methane formation, leading to these yields.

Gasification seems to be most active from 500 to about 650°C, after which most of the glycerin is gasified. More carbon monoxide is produced from 500 to 650°C as the glycerin is gasified to carbon monoxide, and the concentration reaches a maximum under all conditions. Therefore, gasification is mainly a function of temperature, with all conditions having a similar maximum carbon monoxide yield at a similar temperature up to about 650°C. For all conditions the extent of methane formation is a weak but steady function of temperature, increasing steadily with temperature regardless of conditions.

5.4 ENERGY EFFICIENCY

The efficiency of the experiments was calculated by taking the lower heating value (LHV) of the product gases divided by the LHV of the reactant glycerin plus the heat required to bring the glycerin and water solution to temperature. The cold gas efficiency would give a higher efficiency percentage, because it neglects the amount of heat added to the system. This calculation of efficiency also neglects any heat loss, heat of reaction, or pumping work but also does not take into account energy recovery from the heat exchanger. The specific heat of reaction is not known, because the specific reactions occurring are not known. This is why the heat of reaction is not calculated into

the efficiency. Also unknown is the heat loss of the experiment. Therefore this efficiency is an overestimation, but will give a basis to compare the results of these experiments. The amount of energy necessary to heat water from 25°C to 500°C at 24.2 MPa is 55.0 kJ/mol, and to 800°C it is 70.6 kJ/mol. At 500°C this is 10% less than the amount of energy needed to heat the same amount of water at atmospheric pressure, while at 800°C it is about 3% less (*20*). The amount of energy to heat glycerin must be calculated using a polynomial expression for the heat capacity. The heat capacity is give as

$$C_p = A + B\times T + C\times T^2 + D\times T^3 \quad (25)$$

where A, B, C and D are known (*316*). A correction for the pressure is added,

$$C_p(P_2,T) = C_p(P_1,T) + R\cdot \ln\frac{P_2}{P_1} \quad (26)$$

and the equation is integrated. The result of this is an estimation of the enthalpy, since the constants A through D are for vapor, not supercritical fluid. The values derived from this method are similar to values determined from Aspen simulation. From this, at 500°C 142.3 kJ/mol is needed, and at 800°C 188.2 kJ/mol is needed to heat the glycerin from 25°C. Therefore the minimum energy needed to heat one gram of the 3/1 water/glycerin solution to 800°C is 2.74 kJ, and for the 13/1 it is 3.39 kJ. The efficiency, along with data about the experiment, is given is Table 5-6.

Table 5-6 shows that the efficiency increases dramatically with temperature up to about 650°C, after which it increases more slowly. This mirrors the trend seen in carbon gasification. The 3/1 water/glycerin ratio experiments are more efficient than the more dilute experiments because less water has to be heated to reaction temperature.

Table 5-6. Energy efficiency for the experiments conducted.

Experiment number	Temperature (°C)	Water/glycerin ratio	Energy input (kJ/min)	Energy output (kJ/min)	Efficiency
10	500	3	521.0	23.4	4.5%
13	546	3	414.6	62.1	15.0%
12	599	3	368.4	158.4	43.0%
15	600	3	364.5	166.3	45.6%
17	649	3	343.1	240.8	70.2%
7	701	3	310.7	248.4	80.0%
8	701	3	309.2	246.4	79.7%
11	701	3	309.4	253.4	81.9%
16	749	3	280.3	250.2	89.3%
18	801	3	264.8	233.9	88.3%
9	502	3	176.7	18.8	10.7%
35	551	3	139.9	41.2	29.5%
34	600	3	119.8	67.8	56.5%
33	650	3	109.5	87.7	80.2%
6	699	3	110.2	99.3	90.1%
14	701	3	108.8	99.3	91.3%
29	701	3	100.2	88.7	88.5%
30	750	3	94.6	82.7	87.5%
31	799	3	89.9	80.1	89.1%
4	498	13	167.8	1.5	0.9%
20	547	13	150.9	27.5	18.2%
19	600	13	135.5	53.1	39.2%
23	650	13	120.8	80.0	66.2%
2	698	13	119.3	81.9	68.6%
5	698	13	119.8	78.3	65.3%
21	750	13	107.7	72.1	66.9%
22	801	13	107.2	70.2	65.5%
3	500	13	56.3	6.7	11.8%
32	550	13	48.4	14.2	29.3%
28	599	13	42.6	26.8	63.0%
27	649	13	41.2	27.9	67.7%
1	698	13	40.1	27.4	68.3%
24	699	13	39.3	26.7	68.1%
25	748	13	36.8	24.4	66.2%
26	764	13	35.3	24.4	68.9%

The most efficient experiments by this calculation is 91% for experiment number 14, with a 3/1 water/glycerin ratio, 700°C temperature and a residence time of 85 seconds. The 3/1 water-to-glycerin experiments at 30 seconds residence time reached similar efficiency 50 to 100°C higher than the 90 second experiments. This is a continuation of a similar trend seen with the gas yields, with the shorter residence time experiments requiring higher temperatures for the same result as the longer residence time experiments. Also, the general result is that temperatures above 650 or 700°C do not increase efficiency, and in some experiments the energy required for higher temperature operation decreases the efficiency above this range.

5.5. EQUILIBRIUM MODELING AND COMPARISON

In order to determine the progress possible in glycerin reformation, it is important to have an understanding of the equilibrium conditions for glycerin reformation in supercritical water. Thermodynamic studies provide information on conditions for hydrogen and syngas production that may diverge from practical situations but provide a basis for comparison and theoretical efficiency. The equilibrium yield of all of the products will be determined for various temperatures, pressures, and dilutions, in order to understand which equilibrium conditions would lead to the most hydrogen or synthesis gas. Then, the experimental results will be compared to equilibrium, in order to determine if equilibrium was reached, and if not, how the results compare to equilibrium.

5.5.1. Equilibrium Modeling. Chemical equilibrium is the state in which the concentrations of the reactants and products do not change with time at the given conditions, and can be found from Gibbs free energy minimization (*179*, *235*, *246*, *281*,

301, *309*, *317–322*). Minimization of the Gibbs free energy subject to material balance constraints has been found to be effective for complicated chemical equilibrium problems, and is preferred in fuel reforming analysis, especially when the reaction temperature and pressure can be specified (*300*, *323*). The equilibrium can be calculated by either stoichiometric or non-stoichiometric methods, which will give the same result if done correctly (*247*, *285*, *324*, *325*). Both of these methods are incorporated in the Aspen Plus process simulation software, which has been used for equilibrium analysis is the literature, as well as CHEMCAD and other chemical simulation software (*195*, *235*, *247*, *281*, *300*, *321*, *326–328*). The non-stoichiometric method is based on minimizing the total Gibbs free energy in the system while specifying the possible products, not the possible reactions.

Aspen Plus is a chemical process simulation environment from Aspen Technologies, and will be the simulator used in this dissertation. Its large database of physico-chemical properties and extensive range of unit operations, make Aspen Plus a valuable tool in process modeling and simulation. In Aspen, the RGIBBS unit operation is used to calculate the equilibrium using the non-stoichiometric method. The feed is specified, as well as any of the products that could be produced, and the equilibrium concentration is calculated. The number of compounds in the water-glycerol system, resulting from the atomic combination among C, H and O, could be very high. However, the Gibbs free energy of formation increases with the number of carbon atoms. Compounds with more than three carbon atoms are not likely to exist in the steam-glycerol system (*329*). The possible products used for these simulations were all of the gasses found in the product gas, as well as all the liquid intermediates mentioned in

Section 4.4. Chemical Reactions and the intermediates mentioned in Sections 2.5.1. and 2.5.2. about glycerin gasification. This includes carbon monoxide, carbon dioxide, methane, formaldehyde, methanol, ethylene, ethane, acetaldehyde, ethanol, 1,2-ethanediol, propane, propene, propionaldehyde, acrolein, acetone, allyl alcohol, 2-propanone-1,3-dihydroxy, 2-propanone-1-hydroxy, propanal-2-oxo, 2,3-dihydroxy-propanal, plus glycerol, water and hydrogen. It was found over the experimental operating conditions that the only non-negligible compounds are water, hydrogen, carbon monoxide, methane, carbon dioxide, and ethane. The molar concentrations of the other compounds were always less than 10^{-6}. The amount of ethane was always at least ten times smaller than the next largest concentration. Carbon formation was also considered, with the carbon modeled as graphite. The Gibbs free energy minimization did not form carbon for any of the experimental conditions. The thermodynamic inhibition of carbon formation in supercritical water has also been reported by other groups (*235*, *300*).

From the Gibbs minimization, figures can be made at various conditions to illustrate the effect of water/glycerin ratio, temperature or pressure on the equilibrium yield of the product gas species. Figure 5-6 gives the equilibrium yield of the four main components, hydrogen, carbon monoxide, methane and carbon dioxide at 24.2 MPa and a 3/1 water/glycerin molar ratio. The only other components in equilibrium where ethene and ethane, and they were always in trace amounts. This was true for all of the equilibrium results, not just those in Figure 5-6. Also, for all equilibrium calculations, there was complete gasification.

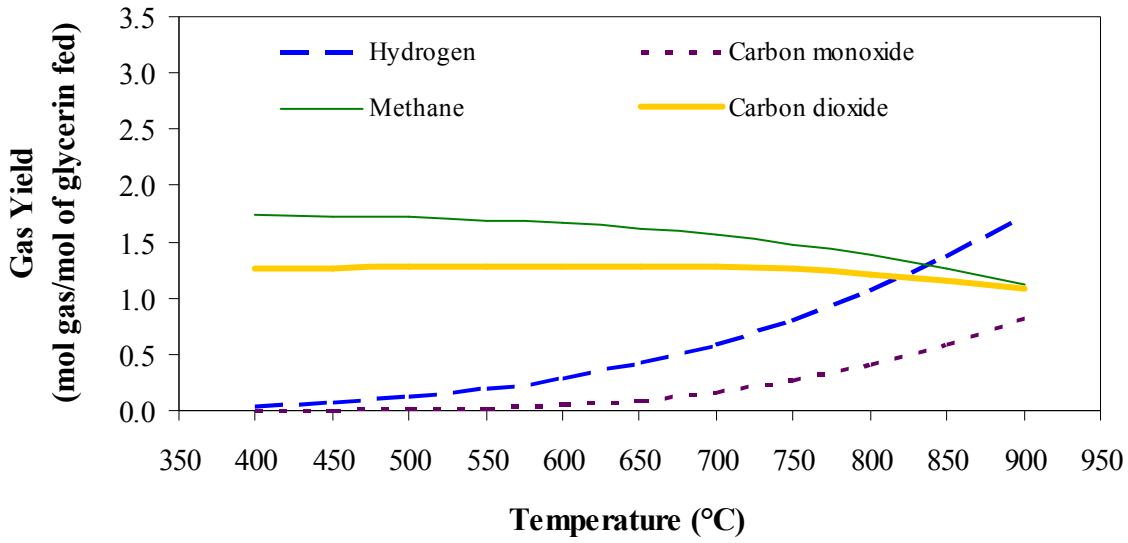

Figure 5-6. Equilibrium gas yield as a function of temperature. Pressure is 24.2 MPa, water/glycerin molar ratio is 3/1.

As a function of temperature, the equilibrium yield at the 3/1 water/glycerin ratio changes very little from 400 to about 600°C, after which the hydrogen and carbon monoxide yield begin to increase and carbon dioxide and methane decrease. As can be seen, there is little to no hydrogen and carbon monoxide at temperatures lower than 600°C. At about 850°C the yield of hydrogen is greater than that of carbon dioxide and methane. Figure 5-7 illustrates the equilibrium yield as a function of temperature for 13/1 water/glycerin ratios. The equilibrium results at a 13/1 water/glycerin ratio are quite different than at a 3/1 ratio. At 400°C the yields of the two ratios are the same, but for 13/1 the hydrogen increases much faster, and carbon dioxide increases instead of decreasing with temperature. Carbon monoxide yield is similar, but slightly smaller for the 13/1 ratio at higher temperatures.

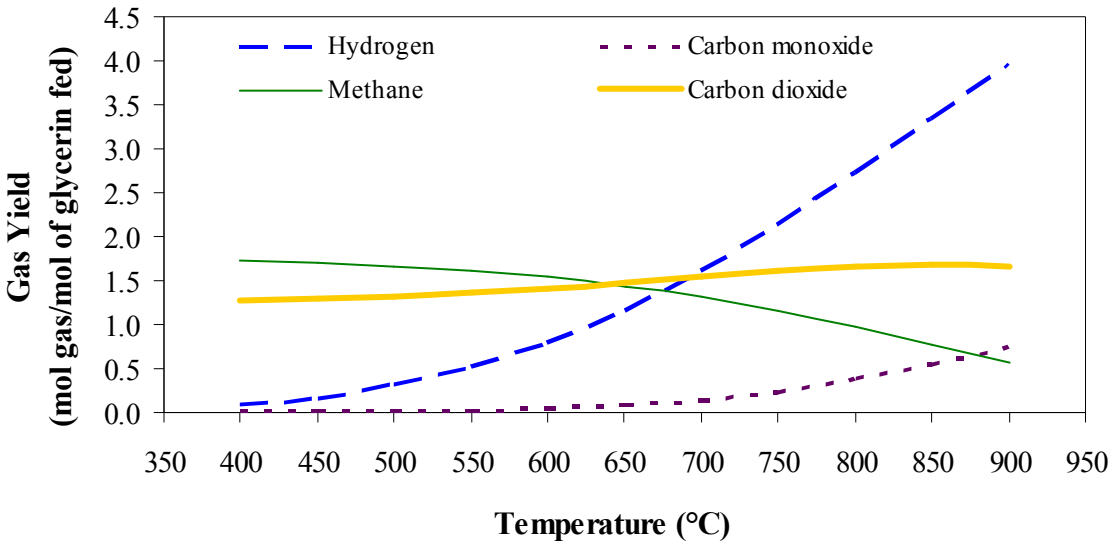

Figure 5-7. Equilibrium gas yield as a function of temperature. Pressure is 24.2 MPa, water/glycerin molar ratio is 13/1.

Hydrogen has the largest increase, from almost nothing to a yield of 3.95 at 900°C. The temperature at which hydrogen yield exceeds carbon dioxide and becomes the dominant species is around 700°C. The increased water concentration means the activity of the water gas shift reaction is increased, and the methane formation reaction is slowed or reversed by steam reformation at temperatures above 700°C (*300*). This results in the increased hydrogen and decreased methane yields with increasing temperature.

Figure 5-8 shows the effect of the water/glycerin molar ratio on the equilibrium gas yields. The pressure was again 24.2 MPa and a temperature of 700°C was used because in the experimental results this produced substantial hydrogen. Figure 5-8 shows that, at these conditions, the water/glycerin ratio strongly affects the hydrogen and

methane yields while carbon dioxide is less affected and carbon monoxide is not affected. The maximum hydrogen yield of almost six is found at the most dilute conditions.

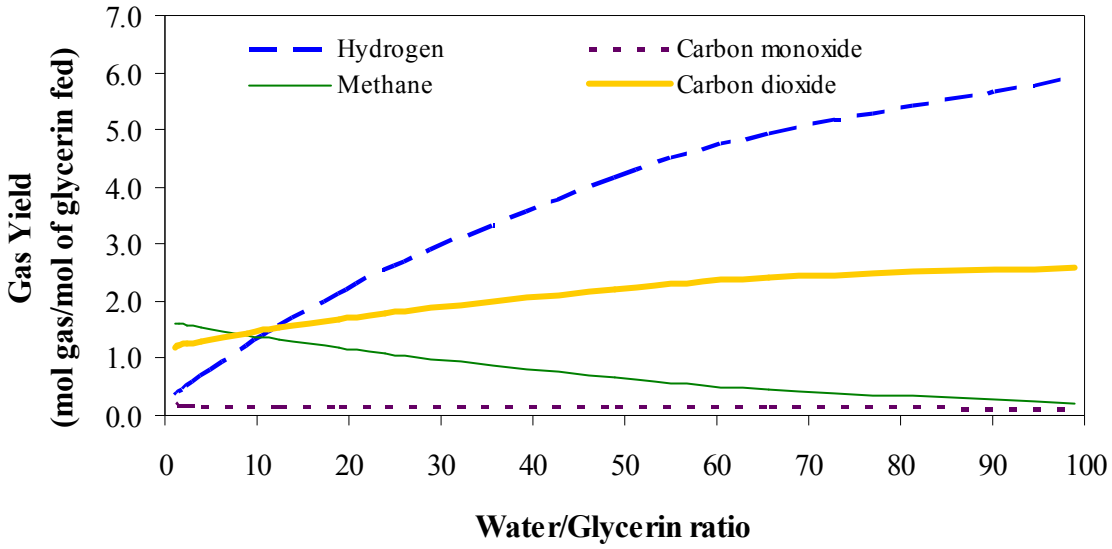

Figure 5-8. Equilibrium gas yield as a function of water/glycerin molar ratio. Pressure is 24.2 MPa, temperature is 700°C.

It appears that at the lower water/glycerin ratios used in these experiments, namely 3/1 and 13/1, methane and carbon dioxide should dominate at equilibrium, and it is not until the solution becomes more dilute that the methane is steam reformed into hydrogen and carbon dioxide. As can be seen in Figures 5-6 and 5-7, there is more equilibrium carbon monoxide at 900°C than at the lower temperatures. In order to see how carbon monoxide changes with water/glycerin ratio, the temperature will be increased to 900°C. Figure 5-9 shows the effect of water/glycerin ratio on the equilibrium yield at 900°C and 24.2 MPa.

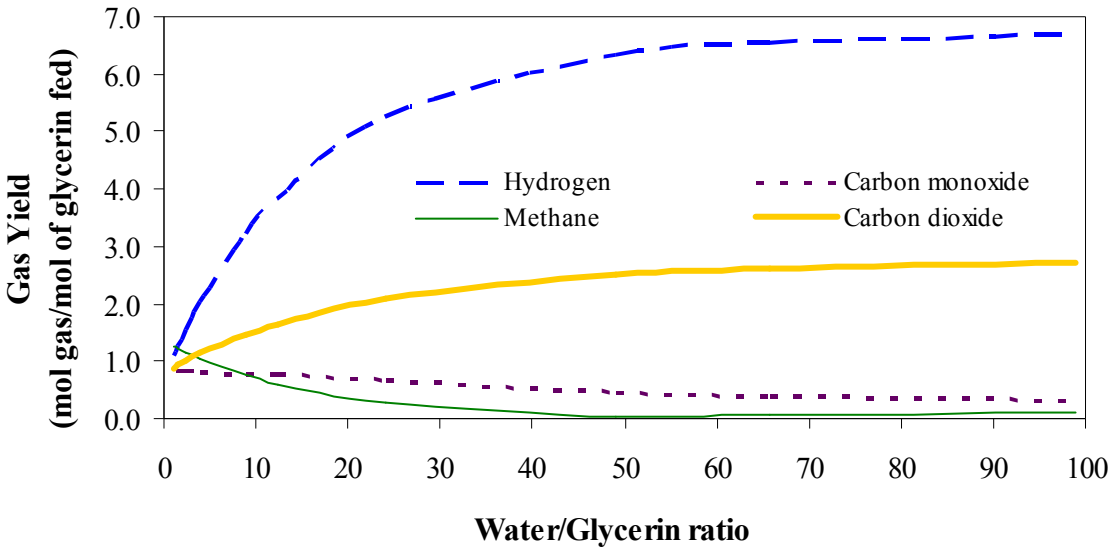

Figure 5-9. Equilibrium gas yield as a function of water/glycerin molar ratio. Pressure is 24.2 MPa, temperature is 900°C.

As can be seen in Figure 5-9, at 900°C the carbon monoxide decreases steadily with increasing water/glycerin ratio. Equilibrium methane yield decreases from 1.3 at a water/glycerin yield of 1 to nearly zero at a water/glycerin ratio of about 40, and remains near zero for increasing dilution. Carbon dioxide yield increases over the same interval, and after remains near a yield of 2.6. Hydrogen yield increases logarithmically with water/glycerin ratio, being about one at a W/G ratio of one, and at a water/glycerin ratio of 50 it has leveled out at about 6.4, increasing slowly to 6.7 at the 99 water/glycerin ratio. This is very close to the stoichiometric maximum hydrogen yield of seven. This effect, that higher temperatures and more dilute feeds increase hydrogen production and inhibit methane, has been seen in another supercritical water glycerin reformation equilibrium analysis (*235*, *300*, *325*).

Figure 5-10 shows the effect of pressure on the equilibrium yield of the product gases at a 13/1 water/glycerin ratio and a 700°C temperature. For all pressures, there was complete gasification of the glycerin. For the atmospheric condition, there was a trace amount of carbon produced. This was the only condition simulated that contained carbon from the RGIBBS non-stoichiometric reactor. As can be seen, at equilibrium the most hydrogen is produced at atmospheric conditions, and decreases logarithmically with increasing pressure. The decrease is fastest from zero to about 7 MPa, and more gradual thereafter. Carbon monoxide decreases from a yield of 0.8 at atmospheric to 0.1 at pressures above 20 MPa.

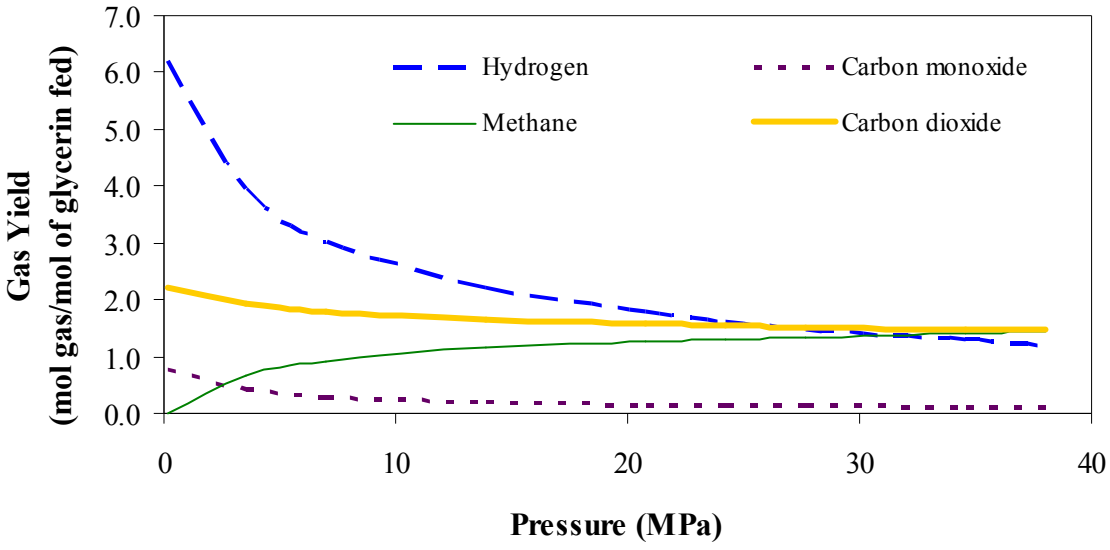

Figure 5-10. Equilibrium gas yield as a function of pressure. Water/glycerin molar ratio is 13/1, temperature is 700°C.

Methane is almost zero at atmospheric pressure, but increases quickly up to about 5 MPa and increases more slowly with pressure thereafter, having a maximum yield of

1.4 at 38 MPa. Carbon dioxide decreases gradually with increasing pressure. The decrease in hydrogen and carbon monoxide and increase in methane at higher pressures is due to methanation, which is driven toward methane and water at higher pressures (*281*). There is little change in the product yield above the critical pressure. These equilibrium results give general trends, and will be compared to the experimental results to see if the experiments are at equilibrium and if not how they differ.

5.5.2. Comparing Equilibrium and Experimental Results. The equilibrium data will be compared to the experimental results to assess how the results compare to equilibrium. Figures 5-11 and 5-12 illustrate the yield of gas as a function of temperature for both the equilibrium and experimental results at a 3/1 water/glycerin and a 30 second residence time.

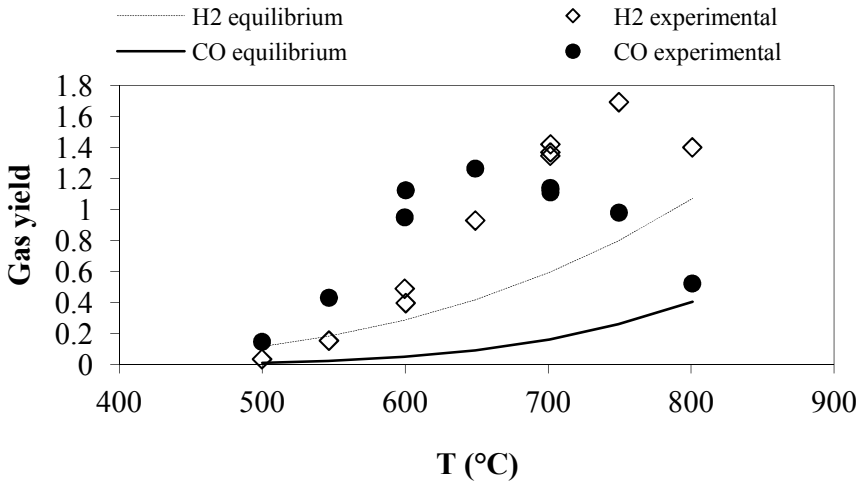

Figure 5-11 Equilibrium and experimental hydrogen and carbon monoxide gas yield as a function of temperature at 30.0 ± 0.3 seconds residence time, 3/1 water/glycerin ratio.

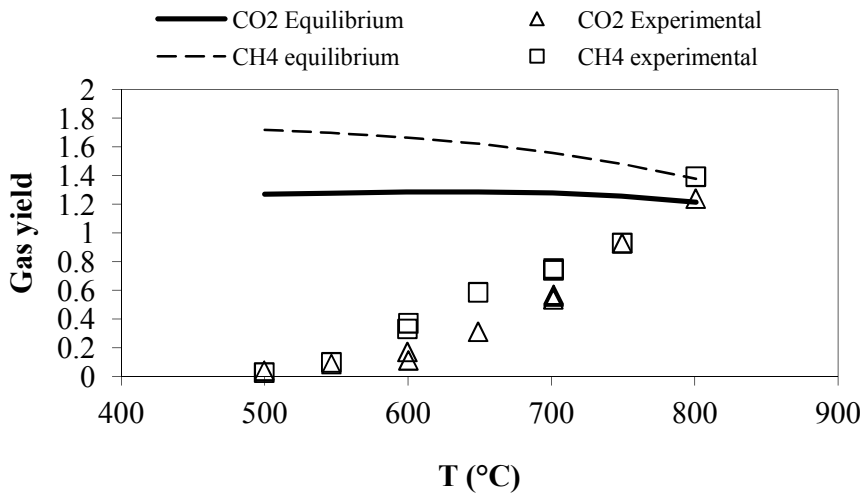

Figure 5-12 Equilibrium and experimental methane and carbon dioxide gas yield as a function of temperature at 30.0 ± 0.3 seconds residence time, 3/1 water/glycerin ratio.

Only the major component gasses of hydrogen, methane, carbon monoxide and carbon dioxide are given. The equilibrium results are given by lines and the experimental results by symbols. As can be seen in these figures, the experimental results and those predicted by equilibrium are quite different at lower temperatures, but nearly merge at the highest temperatures studied. For hydrogen, at temperatures from 500 to 600°C the experimental results are at equilibrium, while from 650 to 750°C the experimental yield of hydrogen is about twice that predicted by equilibrium. At 800°C the two yields are becoming closer. Methane has an experimental yield much lower than that predicted by equilibrium at lower temperatures, but as temperature increases the experimental yields approach equilibrium and at 800°C they are the same. This same trend is witnessed with carbon dioxide. Carbon monoxide has a trend similar to hydrogen, in that the experimental yield is at equilibrium at lower temperatures, increases above equilibrium in the range of 550 to 750°C, but the experimental yield decreases after 650°C and so

approaches equilibrium at 800°C. The results at a water/glycerin ratio of 3/1 and a residence time of 90 seconds illustrated in Figures 5-13 and 5-14.

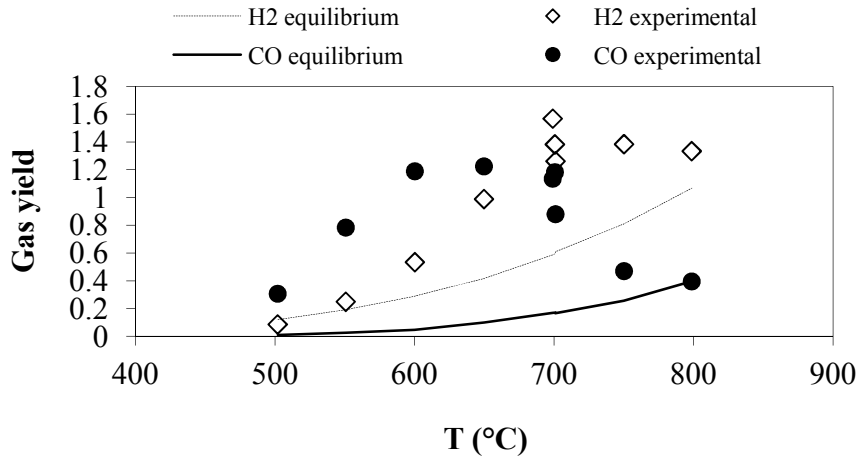

Figure 5-13 Equilibrium and experimental hydrogen and carbon monoxide gas yield as a function of temperature at 89 ± 1 seconds residence time, 3/1 water/glycerin ratio.

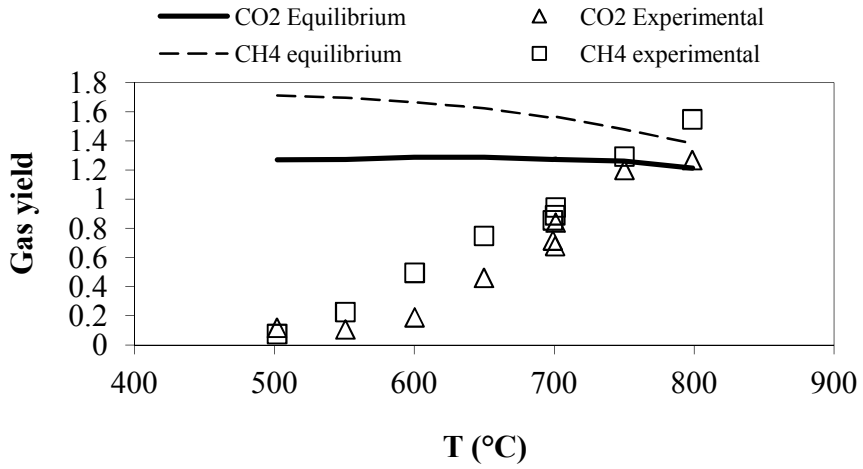

Figure 5-14 Equilibrium and experimental methane and carbon dioxide gas yield as a function of temperature at 89 ± 1 seconds residence time, 3/1 water/glycerin ratio.

The 90 second results are similar to the results at 30 seconds, except that the experimental yield is much closer to equilibrium at 750°C than the shorter residence time experiments. The equilibrium values for both are the same, because equilibrium is independent of the residence time. The equilibrium concentration is changed by the water to glycerin ratio, however.

For the 13/1 water/glycerin experiments, the trends are the same as above, but the yield of hydrogen and carbon dioxide are higher and methane is lower. Figures 5-15 and 5-16 give the equilibrium and experimental results for a 13/1 water/glycerin ratio and a 30 second residence time. Compared to the previous figures of equilibrium and experimental yields, the carbon dioxide yield is higher than predicted by equilibrium for temperatures of 750 and 800°C. This wasn't seen at the 3/1 water/glycerin ratios.

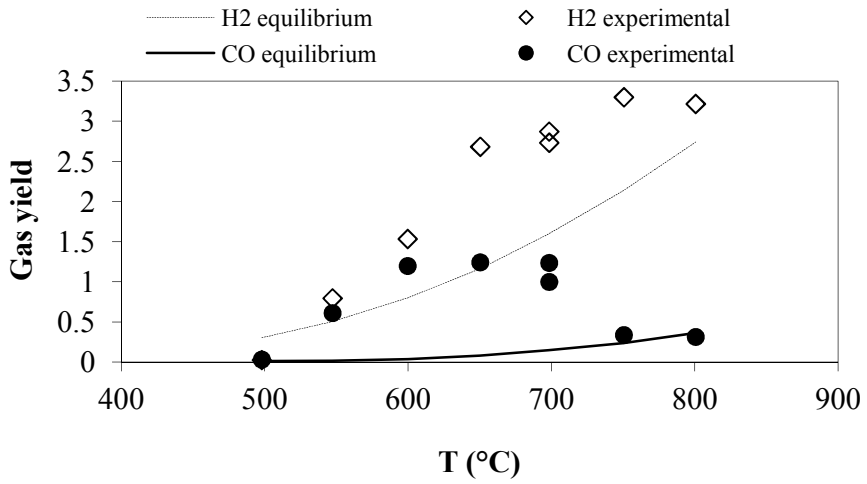

Figure 5-15 Equilibrium and experimental hydrogen and carbon monoxide gas yield as a function of temperature at 30.1 ± 0.2 seconds residence time, 13/1 water/glycerin ratio.

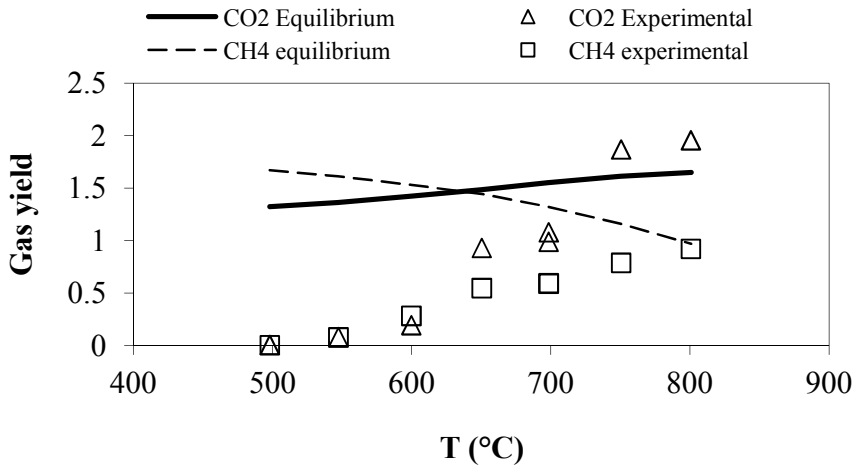

Figure 5-16 Equilibrium and experimental methane and carbon dioxide gas yield as a function of temperature at 30.1 ± 0.2 seconds residence time, 13/1 water/glycerin ratio.

The 13/1 water/glycerin, 90 second residence time results are shown in Figures 5-17 and 5-18. As can be seen in Figure 5-18, the carbon dioxide yield is above the equilibrium yield for temperatures from 650 to 764°C. At the same temperatures, the carbon monoxide yield is at equilibrium, and the hydrogen yield is at a maximum but slightly decreasing with increasing temperature. Methane reaches its predicted equilibrium yield at the highest temperatures.

The experiments conducted at a 13/1 water/glycerin ratio and at a 90 second residence time had the lowest temperature where most of the experimental results had achieved equilibrium. Thermodynamically, higher water/glycerin ratios reduce the amount of methane produced. From these results it appears that methane formation requires a longer residence time than the other reactions, due to the fact that the other species are at or near equilibrium while methane is not. Therefore, methane formation can be kinetically limited by operating at higher product flow rates or using smaller

reactors, reducing the residence time at the highest temperatures (*265*, *281*). Only at the highest temperatures does methane reach equilibrium.

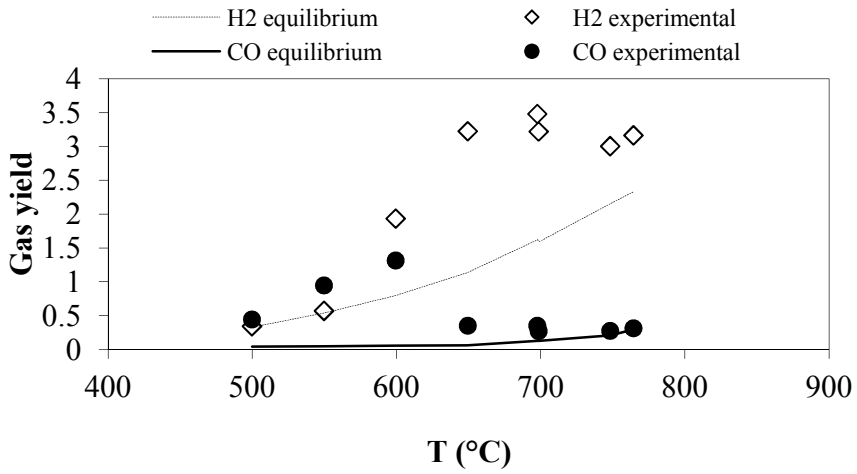

Figure 5-17 Equilibrium and experimental hydrogen and carbon monoxide gas yield as a function of temperature at 92 ± 1 seconds residence time, 13/1 water/glycerin ratio.

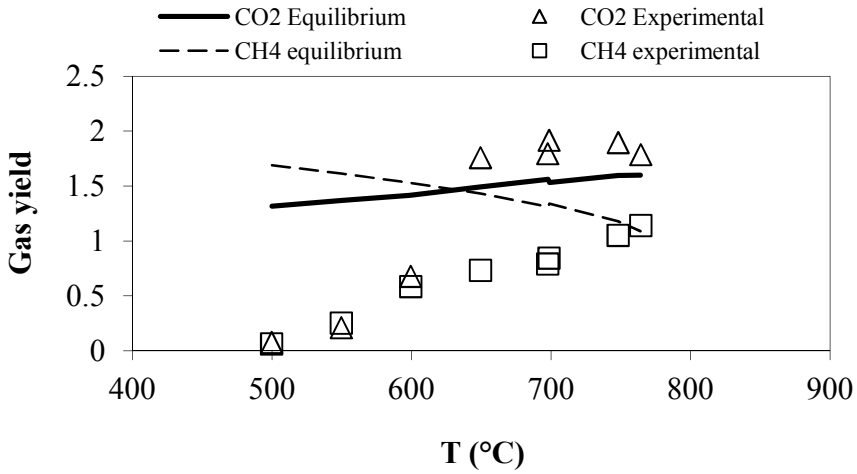

Figure 5-18 Equilibrium and experimental methane and carbon dioxide gas yield as a function of temperature at 92 ± 1 seconds residence time, 13/1 water/glycerin molar ratio.

5.6 KINETIC MODELING

"*It should be noted here that the measured gas composition often is far away from the calculated equilibrium data. Obviously, supercritical water gasification is kinetically driven*"(*14*)

As was seen in the preceding section, a large portion of the experiments were not in chemical equilibrium, so a kinetic model can be useful in understanding the trends at the lower, pre-equilibrium conditions. Two kinetic models will be given. The first is the simplest, a pseudo first order model of the gasification. It gives the simplest model, of how gasification changes with temperature. A more complicated model that takes into account the major gaseous species is given in the next section. This model is used to predict hydrogen production. The section concludes with some of the limitations of the model and possible improvements.

5.6.1. First Order Gasification. It will be assumed that the reaction is first order with respect to carbon content and that water does not play any role in the gasification. This leads to a pseudo first-order kinetic model for the rate of gasification

$$r_g = -k[C] \tag{27}$$

Integration over time yields

$$k = -\ln\left(\frac{C}{C_o}\right)/t \tag{28}$$

where k is the pseudo-first order rate constant, C is carbon in the gas phase, C_o is the initial carbon present in the feed glycerin, and t is the residence time. This is the method used by Chakinala et al, Bennekom et al., and Buhler et al. in studies of the noncatalytic supercritical water gasification of glycerol (*75*, *136*, *267*). The assumption of first order

kinetics have been made by many groups, and proved by some to be accurate (*25*, *26*, *52*, *145*, *269*, *330*, *331*). The idea that water is not present in the reaction rate is usually due to the fact that water is in a large excess compared to the organic, and therefore can be assumed constant. Any factor that is constant can be neglected in the reaction rate because it is a function of time. However, in this study many of the experiments consisted of three moles of water to one mole of glycerin, which is not in excess. In fact, this is the stoichiometric minimum amount of water if complete reformation were to occur. If the gasification of glycerin occurs via liquid intermediates, then water is a product rather than a reactant, and would not appear in the gasification reaction rate. This will be the justification of water not being present in the reaction rate, rather than the more common justification that water is in large excess. The rate constant was calculated, and the results of this study are compared against the results of other groups working in the noncatalytic supercritical water gasification of glycerin in Figure 5-19.

The best fit line and linear equation are for this study only, and from this the activation energy can be determined. These results are from a wide variety of temperatures, pressures, water-to-glycerin ratios and residence times, yet show little scatter and a consistent trend. Although there is little overlap in temperature, the results of the higher temperature experiments appear to extrapolate well to the lower temperature results. The activation energy for this study is 133 kJ/mol, which compares well with the results of Bennekom et al. with 196 kJ/mol and Chakinala et al. with 111 kJ/mol. This is the simplest way of measuring the rate of gasification, but any understanding of the gas production rates would require a more complicated explanation.

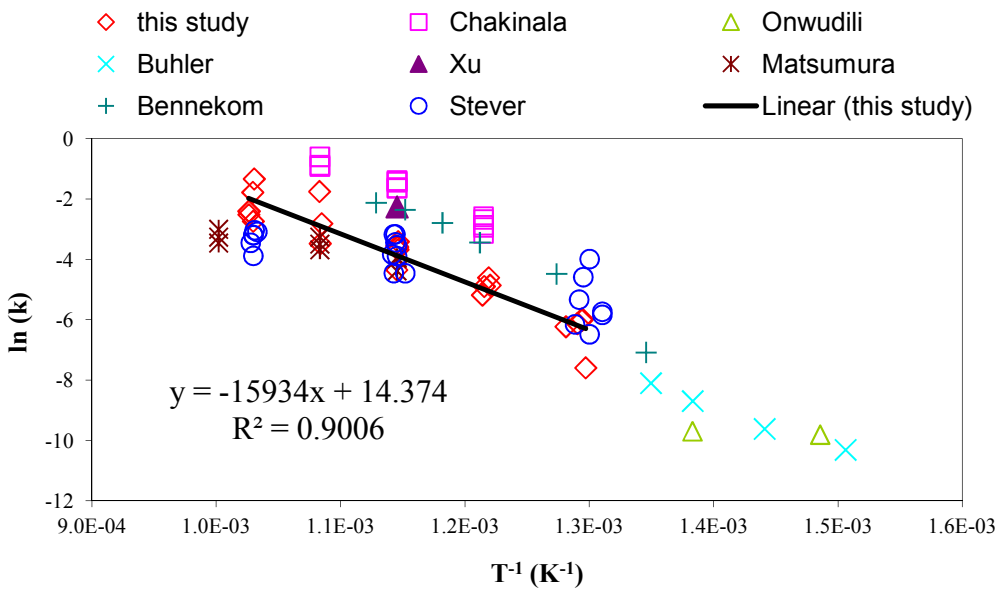

Figure 5-19. Arrhenius plot for the pseudo first order gasification of glycerin in supercritical water. Results are from this study and others in noncatalytic supercritical water gasification of glycerin (*75*, *116*, *136*, *267*, *268*, *270*, *274*).

5.6.2. Simplified Reaction Network. The overall gasification rate given above is unable to model the production of the gaseous products. However, detailed mechanistic approaches involving a large number of species, intermediates and reactions quickly become cumbersome. A simplified kinetic model involving only the gaseous products offers a balance between sophistication and simplicity. These kinetics models are useful and usually acceptable within the ranges of experimental conditions (*52*, *332*). Also, because none of the intermediates could be analyzed, a detailed mechanistic model would be impossible to solve. Many groups have used similar kinetic models when dealing with gasification (*1*, *30*, *50*, *332–339*).

Section 5.5.2. determined that the reaction does proceed to near-equilibrium concentration, especially for the higher temperatures studied, 750°C to 800°C, depending on the reaction conditions. This fact will have to be taken into account when trying to

model the gasification of glycerin in supercritical water. Each reaction will have to be evaluated to determine if it has gas species that are at or near the equilibrium concentration. If an experimental yield value is within 50% of an equilibrium value, those results will not be used for the kinetic analysis. Therefore, all experiments conducted at 750°C to 800°C will be excluded. For the experiments conducted at a residence time of 90 seconds and a 13/1 water/glycerin ratio, all experiments from 650°C to 800°C are excluded.

In order to model the gaseous reactions, a number of different reaction pathways can be envisioned. Many were tried, but the most successful, in that it describes all of the reaction conditions with the highest R^2 values on the Arrhenius plot, is given below. The other pathways, and the resulting Arrhenius plots, are given in Appendix I. All of the models were based on a carbon balance, and the kinetic models were based on glycerin, carbon monoxide, carbon dioxide, methane, and perhaps ethane and ethene. Ethane and ethene were not always included, because they were produced in smaller amounts than the other gaseous carbon species.

The pathway used to model the reaction of glycerin in supercritical water is one in which the glycerin decomposes into either carbon monoxide or methane. Carbon monoxide could then undergo the water gas shift reaction and form carbon dioxide. Using the symbol "*A*" for glycerin, "*B*" for the resulting carbon monoxide, "*C*" for carbon dioxide and "*D*" for methane, the reaction pathway is as follows:

$$A \xrightarrow{k_1} 3B \xrightarrow{k_2} 3C \tag{29}$$

$$A \xrightarrow{k_3} 3D \tag{30}$$

This pathway is a simple model of the gasification of glycerin, and can serve as a starting point for later, more complicated analysis. This pathway assumes that all carbon monoxide and methane is the result of two different glycerin decomposition reactions, and that all carbon dioxide is the result of the water gas shift reaction. It also neglects any ethane or ethene. Reaction 31 is the glycerin to carbon monoxide reaction. Reaction 32 is carbon monoxide to carbon dioxide, the water gas shift reaction. Reaction 33 is the glycerin to methane pathway.

$$C_3H_8O_3 \xrightarrow{k_1} 3CO + 4H_2 \tag{31}$$

$$CO + H_2O \xrightarrow{k_2} CO_2 + H_2 \tag{32}$$

$$C_3H_8O_3 + 5H_2 \xrightarrow{k_3} 3CH_4 + 3H_2O \tag{33}$$

These reactions and this reaction pathway were chosen based on the ability to accurately describe the carbon containing species. These are only approximations of the myriad reactions happening. Integral analysis of the reaction mechanism of Equations 29 and 30, with the further assumption of global first order kinetics gives the following expressions for the molar flow rates of each carbon containing species:

$$C_a = C_{ao} e^{t(-k_1 - k_3)} \tag{34}$$

$$C_b = \frac{-3C_{ao}k_1(e^{-t(k_1+k_3-k_2)} - 1)e^{-k_2 t}}{k_1 + k_3 - k_2} \tag{35}$$

$$C_c = \frac{-3C_{ao}k_1(k_1 e^{-k_2 t} + k_3 e^{-k_2 t} - k_2 e^{-(k_1+k_3)t} - k_1 - k_3 + k_2)}{(k_1 + k_3)(k_1 + k_3 - k_2)} \tag{36}$$

$$C_d = \frac{-3C_{ao}k_3(e^{-t(k_1+k_3)} - 1)}{k_1 + k_3} \tag{37}$$

Where C_{ao} is the molar flow rate of glycerin in the entering water/glycerin solution, and C_a is the remaining, un-reacted glycerin or any liquid intermediates. C_b is the molar flow rate of the product carbon monoxide; C_c represents the molar flow rate of carbon dioxide gas, and C_d the methane molar flow rate. Since the residence time, t, and concentrations are experimentally determined, the rate constants k_1, k_2, and k_3 can be solved for numerically. First order kinetics was used for simplicity. Even if a better correlation could be obtained with more complex reaction kinetics, these simplified rate expressions provide basic information about supercritical water gasification of glycerin under similar reactor systems and experimental conditions. The reactions are not diffusion limited because of the absence of heterogeneous catalysts creating mass transfer resistance, as well as the high diffusivity of supercritical water and the solubility of permanent gasses in supercritical water. Residence time was calculated, as a function of inlet fluid density, using the Peng-Robinson equation of state with Van der Waals' mixing rules. The rate constant of a reaction, especially one in supercritical fluids, can be greatly affected by the pressure (*6*, *25*, *340*). This is overcome in this case by keeping the reactions at the same pressure. From these equations, the rate constants may be calculated, from which the activation energy, E_a, and Arrhenius frequency factor, A, can be regressed using the Arrhenius equation.

The values for C_b, C_c and C_d were calculated from the flow rate of the effluent gas and the gas analysis. For experiments 4, 9, 10 and 13 the concentration of carbon dioxide was so low that the value for C_d was assumed to be zero. This is due to the fact that the

temperatures for these experiments were either 500 or 550°C, which was too low for any significant water gas shift to occur. The value of C_a, the carbon remaining as glycerin in the effluent, was not calculated or used in any calculations because liquid analysis was not performed on the liquid samples.

Using the values for C_b, C_c, and C_d, the rate constants for each reaction can be calculated by solving Equations 35-37 simultaneously and minimizing the difference between the calculated and actual values of C_b, C_c, and C_d by changing the rate constants. This was done in a Microsoft Excel® spreadsheet using the solver tool. The data used for this, the concentrations C_{ao}, C_b, C_c, and C_d along with the calculated rate constants k_1, k_2, and k_3, can be found in Appendix J. The natural log of the rate constants as a function of the inverse temperature for each reaction is illustrated in Figures 5-20 through 5-22.

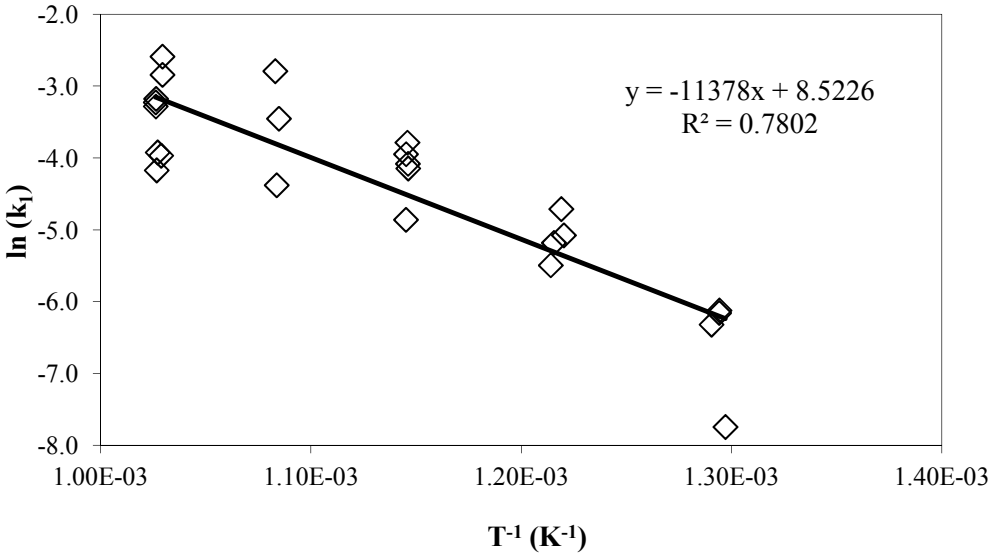

Figure 5-20. First-order Arrhenius plot for reaction 31, glycerin to carbon monoxide.

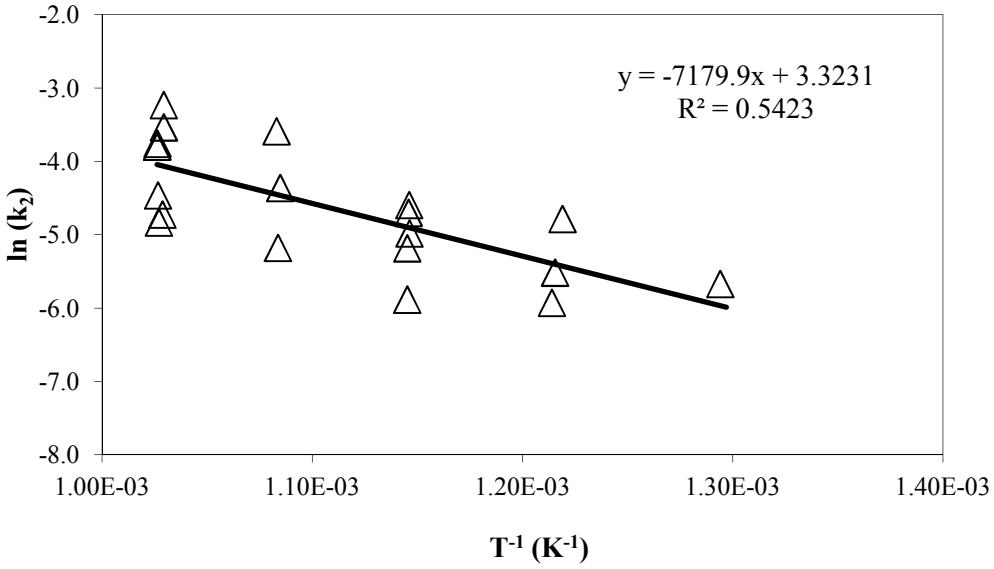

Figure 5-21. First-order Arrhenius plot for reaction 32, carbon monoxide to carbon dioxide.

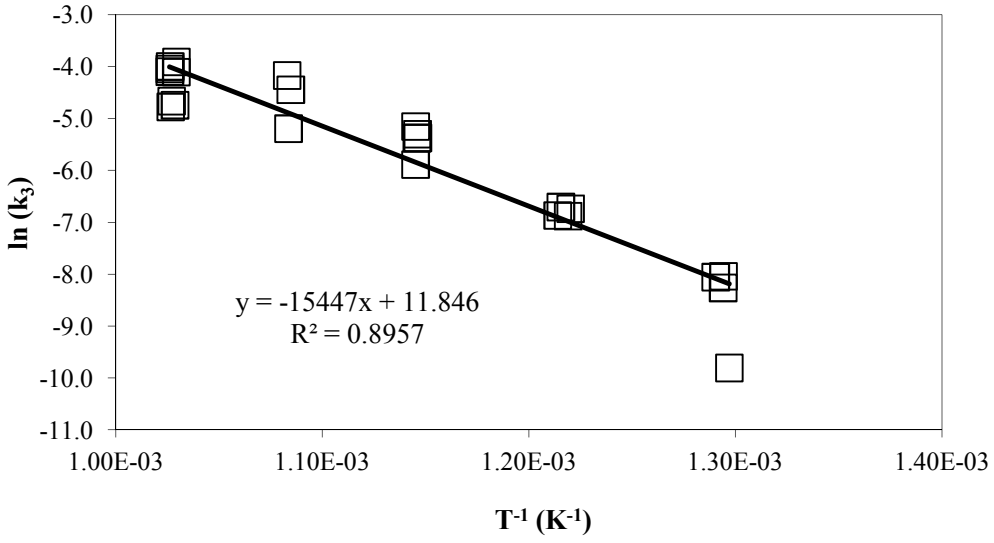

Figure 5-22. First-order Arrhenius plot for reaction 33, glycerin to methane.

When the natural log of the rate constant is plotted against the inverse of the temperature for each experiment, the slope is equal to $-E_a/R$ and the intercept is equal to the natural log of A. The activation energy, Arrhenius frequency factor and the autocorrelation coefficient for each pathway are given in Table 5-7.

Table 5-7. Frequency factor, activation energy and autocorrelation coefficient for the three model reaction pathways for glycerin in supercritical water.

	Arrhenius Frequency Factor, s^{-1}	Activation Energy, kJ/mol	Autocorrelation Coefficient Percent R^2
Reaction (31), glycerin to carbon monoxide	5.03×10^3	94.6	78.0
Reaction (32), water gas shift	27.8	59.7	54.2
Reaction (33), glycerin to methane	1.40×10^5	128.4	89.6

Reaction 33, glycerin to methane, has the largest frequency factor and activation energy, and reaction 31, glycerin to carbon monoxide, has intermediate values. Reaction 32, the water gas shift reaction, has a lower activation energy and a very low frequency factor. The slope of the Arrhenius plot, and hence the activation energy, describe how dependent the reaction is upon temperature. So reaction 33 is the most sensitive to temperature change, followed by reaction 31 then water gas shift. The autocorrelation coefficient for reaction 31 and 33 shows that the Arrhenius plot fits the data well, but reaction 32 is not as good of a fit. From the 2^3 matrix results in Appendix G, it can be seen that the yield of carbon dioxide is affected more by the water/glycerin ratio than any other carbon containing species. Because reaction 32 did not take into account water

concentration, this may be why the autocorrelation coefficient is not as high. Other studies of the non-catalyzed water gas shift reaction in supercritical water have determined activation energies between 67 to 145 kJ/mol (*199*, *294–297*). These studies used pure carbon monoxide as the feed. These previous studies did not always assume first order kinetics, although the reaction order was always near unity. They also neglected the water concentration and the reverse reaction in their analysis.

The error in finding the kinetic model is given in Figure 5-23, which provides a comparison between the measured values of the concentration and those calculated by solving Equations 35-37 simultaneously for all data sets. The maximum error was 3.3%, and the average error in this calculation was 0.02% for all the conditions used for the kinetic analysis. The maximum error was for carbon dioxide, C_c, and occurred at the lowest temperature.

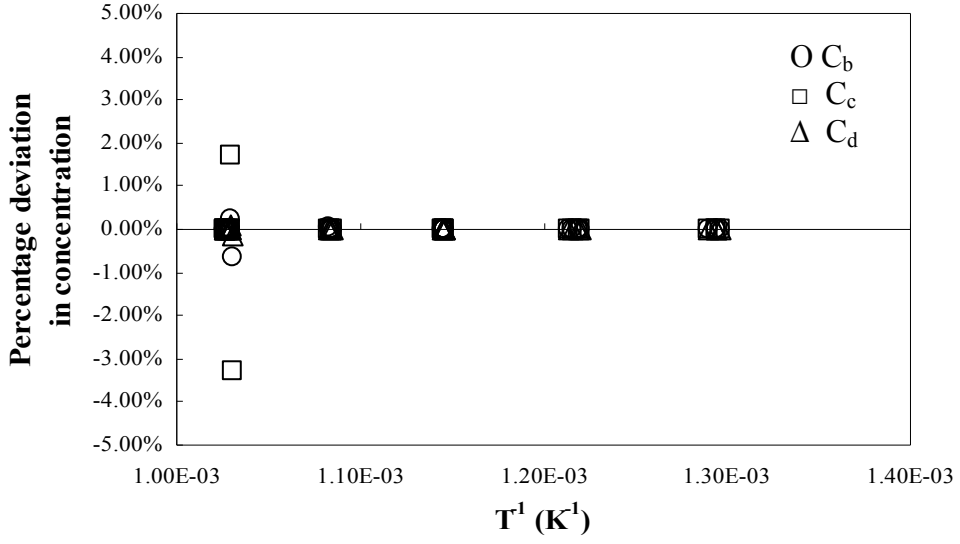

Figure 5-23. Percentage deviations, $(C^{exp}-C^{cal})/C^{exp}$, between experimental results for the concentration and values calculated from the simultaneous solution of equations 35-37.

5.6.3. Modeling Hydrogen Production. The reactions 31-33 should be able to calculate hydrogen production. These reactions are just models of the many reactions occurring during supercritical water reformation of glycerin, but since they can reasonably describe the carbon balance and kinetic models, it is a fair question whether they can also model the hydrogen production. Given the stoichiometry, for every mole of carbon monoxide produced there will be one and $^{1}/_{3}^{rd}$ moles of hydrogen produced. For every mole of carbon dioxide, two and $^{1}/_{3}^{rd}$ moles of hydrogen will be produced. Every mole of methane produced will consume one and $^{2}/_{3}^{rd}$ moles of hydrogen. The experimental yield will be compared to the yield calculated from the stoichiometry. The results will be divided up into groups based on the water/glycerin ratio and residence time used. For the experiments at a 13/1 water/glycerin ratio and 30 second residence time, the results are given in Figure 5-24.

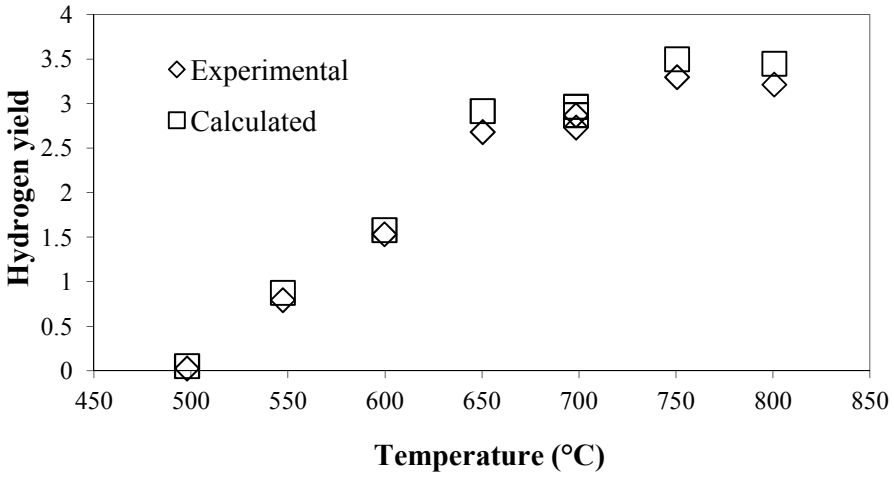

Figure 5-24. Experimental yield of hydrogen and the yield calculated from the stoichiometry of reactions 31-33 as a function of temperature for experiments conducted at a 13/1 water/glycerin ratio and 30 second residence time.

Figure 5-24 shows that there is good agreement between the experimental results and those calculated form the stoichiometry for these conditions. Both the increase from 500 to 650°C, and the subsequent leveling of the yield is accounted for. The largest error is at 500°C, where there is little hydrogen production to begin with.

Figure 5-25 gives the results for the 13/1 water/glycerin ratio and 90 second experiments. Again, the calculated results mirror the experimental ones. The decrease in hydrogen yield above 700°C is accounted for in the calculated results. Here again the largest errors are at the lowest temperatures, 500 or 550°C. The calculated result at 550°C is more than double the experimental result. As temperature increases, the error is lower. Figure 5-26 gives the comparison for experiments conducted at a 3/1 ratio and a 30 second residence time.

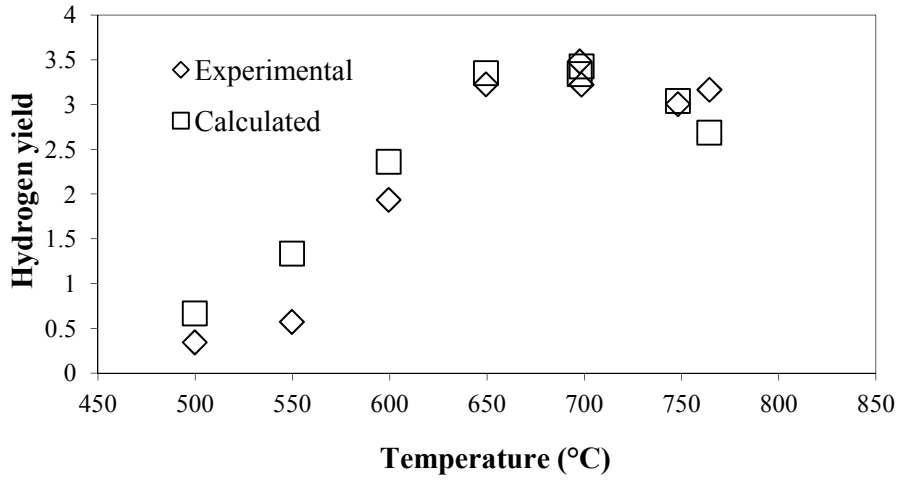

Figure 5-25. Experimental yield of hydrogen and the yield calculated from the stoichiometry of reactions 31-33 as a function of temperature for experiments conducted at a 13/1 water/glycerin ratio and 90 second residence time.

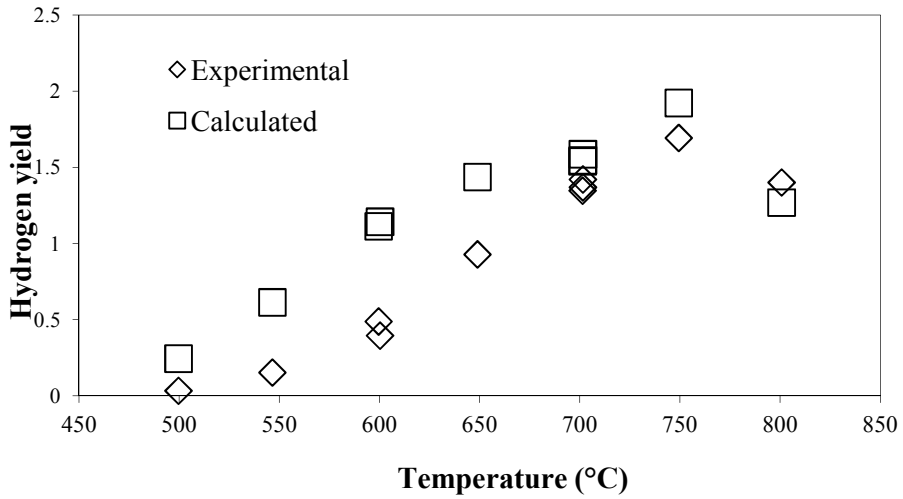

Figure 5-26. Experimental yield of hydrogen and the yield calculated from the stoichiometry of reactions 31-33 as a function of temperature for experiments conducted at a 3/1 water/glycerin ratio and 30 second residence time.

As can be seen in Figure 5-26, the fit is not as good as the previous two experimental sets. From 500 to 650°C the calculated values are always greater than the actual experimental values, from ½ to 4 times larger. From 700 to 800°C the fit is much closer, having a maximum error of 15%. The comparison for experiments at a 3/1 ratio and 90 seconds residence time is given in Figure 5-27.

As shown in Figure 5-27, the calculated results have a similar trend as the experimental results. The calculated hydrogen yields from 500 to 650°C are again larger than the experimental results, from ½ to six times larger. However, at these conditions the values also diverge at the highest temperature. The experimental results level off after 700°C, but the calculated results decrease.

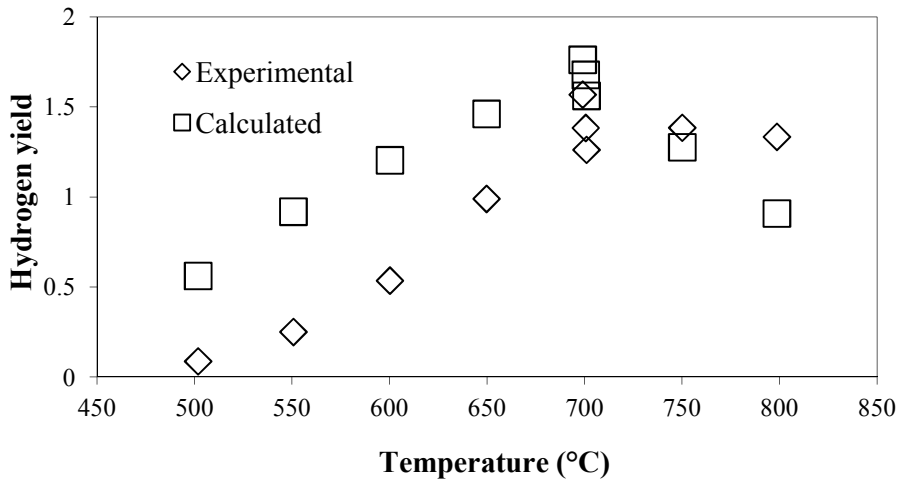

Figure 5-27. Experimental yield of hydrogen and the yield calculated from the stoichiometry of reactions 31-33 as a function of temperature for experiments conducted at a 3/1 water/glycerin ratio and 90 second residence time.

The calculated hydrogen yield is more accurate for experiments conducted at a 13/1 water/glycerin ratio than a 3/1 ratio. For the 3/1 ratio, the error occurs in the range 500 to 650°C. At higher temperatures the calculated results are closer to the experimental ones. The general trends for the 3/1 ratio experiments are correct. In general, the hydrogen production model is more accurate at the higher temperatures where there is complete gasification. This could be because reactions 31-33 are tailored to describe gas phase products, which are dominant when glycerin is completely gasified. Temperatures from 500 to 650˚C do not lead to total gasification, meaning there is either un-reacted glycerin or liquid intermediates, and these are not included in reactions 31-33. It could be there are more intermediates for the 3/1 ratio experiments, making the hydrogen production model even less accurate at these conditions.

5.6.4. Limitations of the Model. During the kinetic modeling of the supercritical water reformation of glycerin, many different pathways or models could

have been used, and many different assumptions were made. It is important to review these choices and discuss what could have been done differently, why certain assumptions were made and how they affected the outcome.

Instead of the kinetic model used in Section 5.6.2., an elementary reaction model could be used. These models require the simultaneous solution of the elementary rate expression for all the reactions that occur between molecules, atoms and radicals. Elementary reaction models are useful in predicting reaction rates outside of the conditions for which they were derived (*297*). They also provide insight into reaction mechanisms (*297*, *341*). However, elementary reaction models contain many reactions. A model for the oxidation of a simple molecule like hydrogen contains seventeen elementary steps and thirty four rate constants (*334*). Researchers, combining physical chemistry with quantum thermodynamics, have created models with 60,000 individual elementary reaction steps (*342*). The simplified kinetics in this study is a balance between a model that is unable to predict gas yields, the first order gasification model, and one that involves a large number of complex equations and simulations to solve.

The models used both in Sections 5.6.1 and 5.6.2. are for gasification only. They either describe overall gasification, Section 5.6.1 or the concentration of the gaseous products, Section 5.6.2. This is because gas products were the only ones measured, and the goal of this study. However, as was mentioned in various articles, the liquid products are both important as gasification intermediates and as products themselves. A better model would include, at the least, the concentrations of formaldehyde, acrolein and acetaldehyde.

All of the reactions were assumed to be first order. Many other groups have made this assumption when modeling supercritical water gasification, as well as other types of gasification. Some groups have experimentally determined the reaction order for the organic species, and they are almost always near unity. The models used in Section 5.6.1 and 5.6.2 would be better if the reaction orders of the constituent reactions could be determined.

Reaction 32, the water gas shift reaction, was modeled as a first order, non-reversible reaction. This reaction is known to be reversible and to include the water concentration. These simplifications may be why the fit of this reaction is less accurate than the others. The reaction can be modeled as non-reversible only when the system is not in equilibrium, as was done in the kinetic model. Since no carbon monoxide or carbon dioxide is initially present, and carbon dioxide is made from the water gas shift reaction, the reaction would only proceed forward, until equilibrium was reached. The water concentration was not included in the model because a rigorous hydrogen or oxygen balance was not conduced, and the correct outlet water concentration is not known. The model would most likely be improved by including water in the reaction.

6. SUMMARY AND CONCLUSION

The supercritical water gasification of glycerin was conducted in a 101 cm^3 tubular reactor at temperatures from 500 to 800°C, 3/1 to 13/1 water/glycerin molar ratios and at 30- and 90-second residence times at a constant pressure of 24 MPa. It was determined, using a 2^3 matrix analysis, that temperature was the dominant variable among the three investigated. Therefore, further experiments were conducted at 50°C intervals. It was found that 100% gasification is possible from 600 to 700°C, and that the maximum hydrogen and carbon monoxide yields also occur in this temperature range. Importantly, methane production always increases with temperature, so that in order to minimize methane production temperatures of 750 or 800°C should not be used.

Water/glycerin ratios of 3/1 can be fully gasified, but produce far less hydrogen than the more dilute 13/1 ratios. The 3/1 ratios also produce more methane. The residence time generally has the effect of shifting the gas yields down the temperature scale by 50°C, so that longer residence times reach maximum conversion and hydrogen yield 50°C before the shorter, 30-second reactions do. Compared to other experimental groups, this work was closer to a pilot-scale study that used no catalysts and had significantly higher glycerin concentrations. The energy efficiency of the process was investigated. The efficiency was an approximation, because many of the parameters needed to correctly calculate the value are unknown for this process. A general trend can be found, in which the efficiency increases dramatically with temperature up to about 650°C, after which it increases more slowly or even decreases. The 3/1 water/glycerin

ratio experiments are thermally more efficient than the more dilute experiments because less water has to be heated to reaction temperature.

The results were compared to chemical equilibrium, as calculated by Gibbs free energy minimization. Hydrogen and carbon monoxide increase with increasing temperature, while methane and carbon dioxide are stable or slightly decrease with temperature at equilibrium. This trend is more pronounced the more dilute the initial glycerin concentration. More hydrogen is produced at the more dilute water/glycerin ratios, with less methane and more carbon dioxide. Lower pressures produce more hydrogen and less methane at equilibrium. It was found that at temperatures from 750°C to 800°C, most of the results were at equilibrium. For experiments conducted at a 13/1 water/glycerin ratio and at a 90 second residence time, equilibrium occurs at a far lower temperature, and all experiments from 650 to 800°C were at or near equilibrium. Experiments were concluded to be near equilibrium if the results were within 50% of an equilibrium value.

Based on this, two kinetic models were developed for experiments not in equilibrium. The first model is a pseudo first order model of the gasification. The amount of carbon entering as glycerin and exiting as carbon in the gas is known, as is the residence time and temperature, so a rate constant and Arrhenius plot can be made. The results of this study were compared to all other non-catalytic supercritical water glycerin reformation articles in the literature. The results of this study compared well with the other studies. Based on this kinetic model, an activation energy for gasification of 133 kJ/mol was calculated. Other studies have calculated activation energies of 111 kJ/mol and 196 kJ/mol (*75*, *267*).

The second kinetic model takes into account the carbon containing gaseous species. Three reactions are used to model the gaseous products: Gasification of the glycerin into carbon monoxide and hydrogen, water gas shift of the resulting carbon monoxide, and a reaction in which glycerin and hydrogen combine to produce methane. The gasification of glycerin into carbon monoxide and the reaction of glycerin to produce methane had better fits to the results than the water gas shift reaction using this pathway. The activation energy of glycerin into carbon monoxide and hydrogen was 95 kJ/mol, the water gas shift was 60 kJ/mol, and the reaction of glycerin and hydrogen to produce methane and water was 128 kJ/mol. Other reaction pathways were tested, and they either did not fit the data as well, or were thermodynamically impossible. The reaction pathway is also capable of predicting hydrogen production for most conditions. The calculated hydrogen yield is more accurate for experiments conducted at a 13/1 water/glycerin ratio than a 3/1 ratio. For the 3/1 ratio, the error occurs in the range 500 to 650°C. At higher temperatures the calculated hydrogen yields are closer to the experimental ones.

In the future, liquid analysis would be instrumental to understanding the pathway of glycerin reformation and in confirming the carbon balance. Future studies could experimentally determine the reaction order of the mechanistic reactions. Also, the water gas shift could be better modeled if the water concentration were incorporated into the reaction, which would necessitate better liquid characterization. In order to test the ability of the system to reform crude glycerin, the consequences of salt in the feed will have to be studied. Salt, more than any other impurity in crude glycerin, would be the impediment to gasification.

APPENDIX A

PHYSICAL DATA FOR PURE AND AQUEOUS GLYCERIN

Table A-1. Viscosity of a glycerin/water solution at various temperatures and glycerin weight percent (*343*).

Glycerin	Temperature (°C)					
weight %	**0**	**20**	**40**	**60**	**80**	**100**
0	1.79	1.01	0.66	0.47	0.36	0.28
10	2.44	1.31	0.83	0.58	–	–
20	3.44	1.76	1.07	0.73	–	–
30	5.14	2.50	1.46	0.96	0.69	–
40	8.25	3.72	2.07	1.30	0.92	0.67
50	14.60	6.00	3.10	1.86	1.25	0.91
60	29.90	10.80	5.08	2.85	1.84	1.28
70	76.00	22.50	9.40	4.86	2.90	1.93
80	255.00	60.10	20.80	9.42	5.13	3.18
90	1310.00	219.00	60.00	22.50	11.00	6.00
100	12070.00	1410.00	284.00	81.30	31.90	14.80

Table A-2. Boiling point and vapor pressure of a glycerin/water solution (*343*).

Glycerin Wt %	Boiling Point at 1 atm (°C)	Vapor Pressure at 100°C (atm)
0	100	1.000
10	100.9	0.974
20	101.8	0.943
25	102.3	0.926
30	102.8	0.908
35	103.4	0.888
40	104	0.864
45	105	0.841
50	106	0.813
55	107.5	0.780
60	109	0.743
65	111.3	0.728
70	113.6	0.653
75	116.7	0.592
80	121	0.521
85	127.5	0.429
90	138	0.325
95	164	0.213
100	290	0.084

Table A-3. Dielectric constant of glycerin/water solutions at $2x10^6$ Hz (*343*).

Glycerin wt %	20°C	40°C	60°C	80°C	100°C
0	80.37	73.12	66.62	60.58	55.1
10	77.55	70.41	63.98	58.31	–
20	74.72	67.7	61.56	56.01	–
30	71.77	64.87	58.97	53.65	–
40	68.76	62.03	56.24	51.17	-
50	65.63	59.55	53.36	48.52	–
60	62.03	55.48	50.17	45.39	41.08
70	57.06	51.41	46.33	41.9	38.07
80	52.27	46.92	42.32	38.3	34.7
90	46.98	42.26	38.19	34.47	31.34
100	41.14	37.3	33.82	30.63	27.88

Table A-4. Density of glycerin/water solutions (*343*).

Glycerin wt %	Density (g/cm^3)			
	15°C	20°C	25°C	30°C
0	0.99913	0.99823	0.99708	0.99568
10	1.02325	1.02210	1.02020	1.01905
20	1.04840	1.04690	1.04525	1.04350
30	1.07455	1.07270	1.07070	1.06855
40	1.10145	1.09930	1.09710	1.09475
50	1.12870	1.12630	1.12375	1.12110
60	1.15650	1.15380	1.15105	1.14830
70	1.18415	1.18250	1.17840	1.17565
80	1.21160	1.20850	1.20545	1.20240
90	1.23810	1.23510	1.23200	1.22890
100	1.26415	1.26108	1.25802	1.25495

APPENDIX B

REACTOR AND HEATER ASSEMBLY AND DIMENSIONS

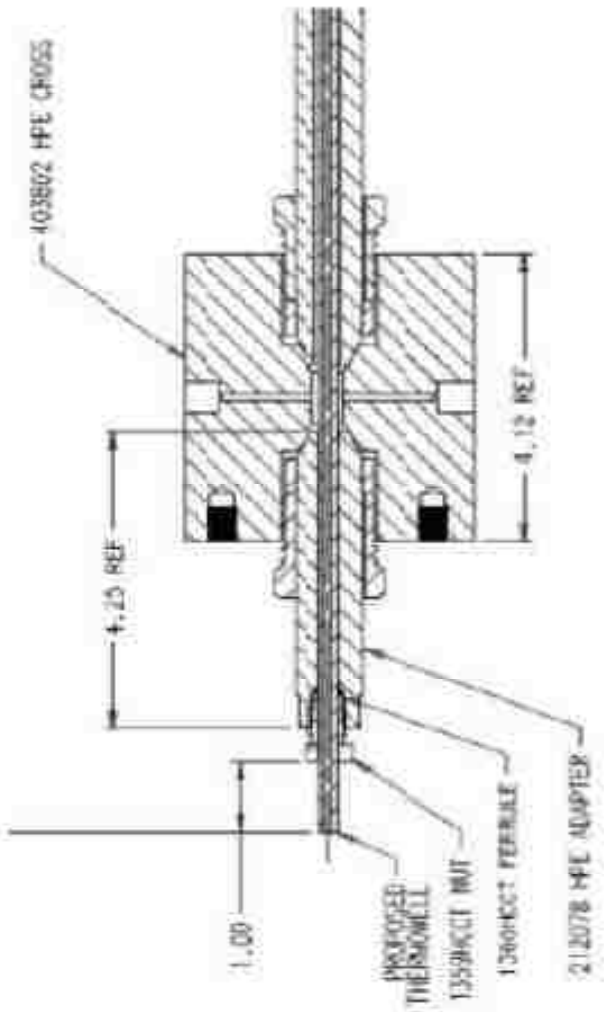

Figure B-1. Inconel 625 adapter cross, reactor and thermowell adapter.

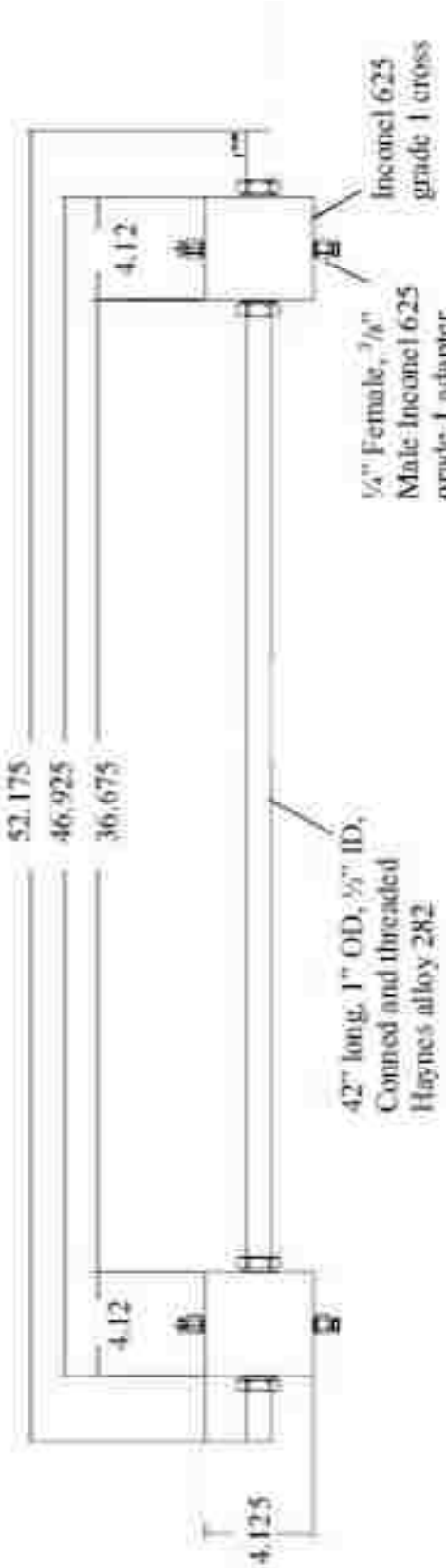

Figure B-2. Schematic of reactor, adapter crosses, thermowell adapters. All dimensions in inches.

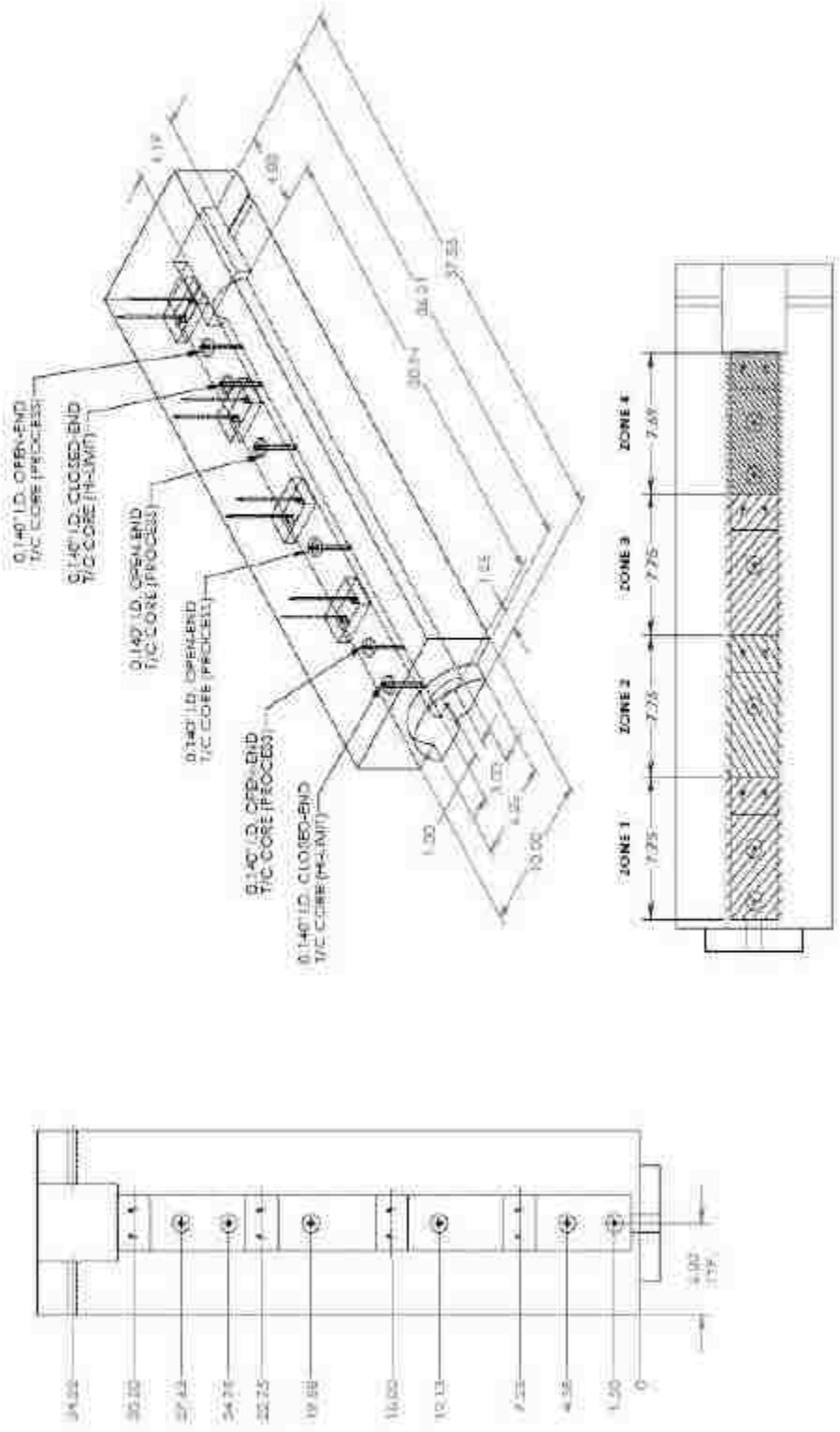

Figure B-3. Watlow heater dimensions and zones.

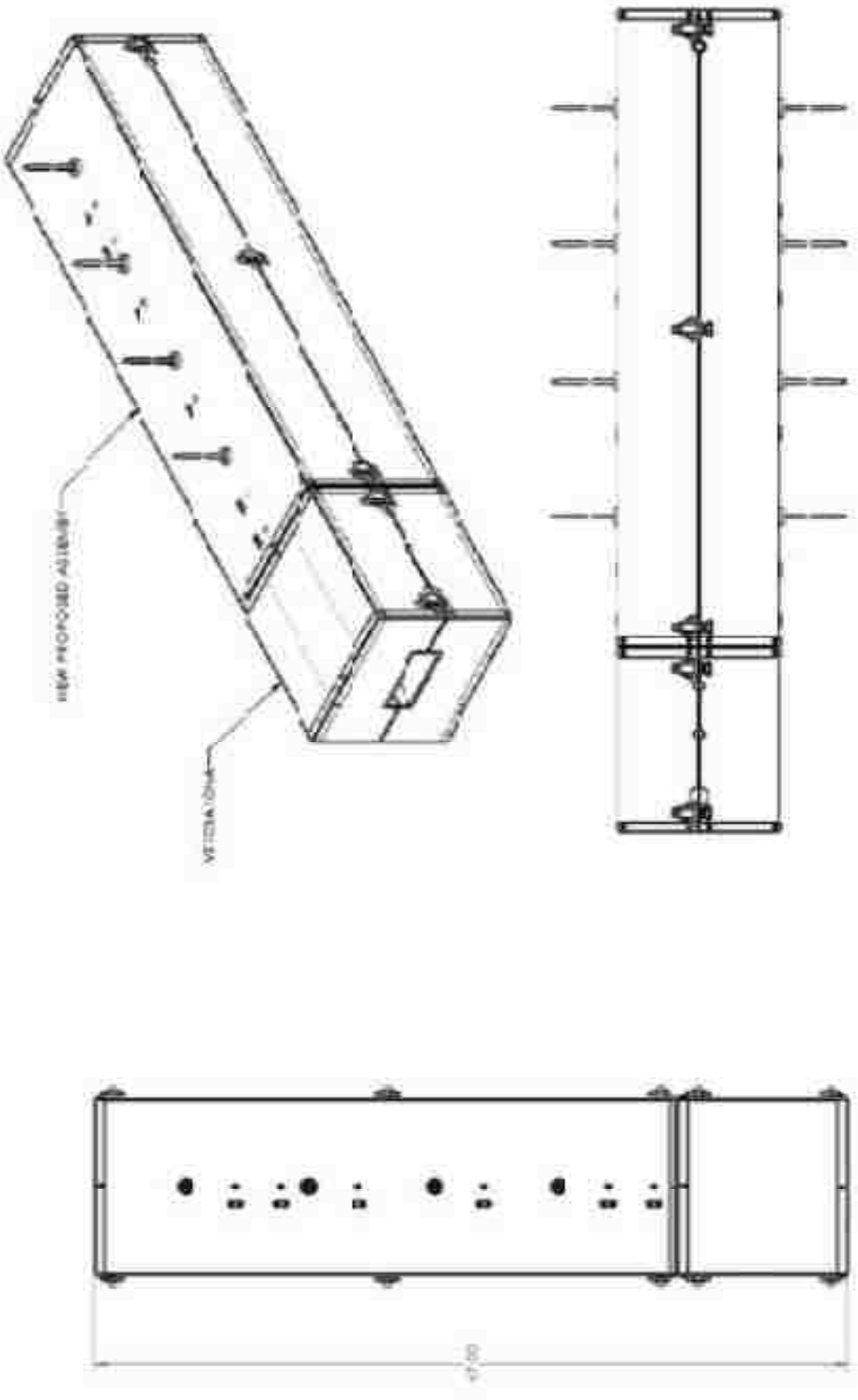

Figure B-4. Full assemble of Watlow heater and outlet insulation.

APPENDIX C

GAS CHROMATOGRAPH CONDITIONS AND CALIBRATION

An HP 5890 Series A gas chromatograph (GC) equipped with a Restek ShinCarbon 100/120 packed column 2 meters in length, 1/16" OD is connected to a thermal conductivity detector (TCD). Three different methods are used when a sample is injected with a syringe: Restek00, Restek01 and Resket02. Each method, with its corresponding GC conditions, is described in Table C-1 below. The injection port on the GC is at a constant temperature of 120°C, and the TCD temperature is 220°C for each method.

Table C-1. GC conditions and times for gas sample methods.

GC Conditions	**Methods**		
	Restek00.M	**Restek01.M**	**Restek02.M**
Initial oven temperature (°C)	30.0	30.0	30.0
Initial time (min)	3.0	3.0	3.0
Oven Heat Rate (°C/min)	8.0	8.0	8.0
Final temperature (°C)	78.0	166.0	250.0
Time at final temp. (min)	0.0	0.0	3.0
Total time (min)	9.0.	20.0	33.5

Restek00 starts with an initial oven temperature of 30°C for 3 minutes, then ramps up to a temperature of 78°C at a rate of 8°C/min. The oven immediately cools back down to 30°C. In this time, hydrogen, oxygen/nitrogen, carbon monoxide, methane and carbon dioxide are eluded from the column. The column was unable to separate oxygen from nitrogen, which is why the peak must be considered oxygen/nitrogen. As can be seen from Table C-1, Restek01 is a continuation of Restek00, with the oven

continuing to increase in temperature until it reaches 166°C. In this time, all of the previously mentioned species elude from the column, along with acetylene, ethylene and ethane. Again, Restek02 is a continuation of the previous method, with the oven increasing to 250°C, and remaining at this temperature for three minutes. This allows all the previous species to elude plus propene and propane. If the gas sample contained a species that did not elude before the method was concluded, that species would remain in the column until a high enough temperature was used to make the species elude. It would elude at an unpredictable time and have characteristics unlike an average gas sample. A skilled GC operator can distinguish when this occurs. To avoid this, during an experiment a longer program is run first, to see if there is significant longer eluding species in the sample. If not, shorter programs can be used. At the conclusion of an experiment, the longest method is used, in case any longer eluding species were present in subsequent gas samples.

The advantage of having all of the methods have the same initial oven temperature is that the method can be changed before it is started without the oven having to come to a new temperature. Additionally, the advantage of having the same oven ramp speed means that during analysis, the method can be changed, to be longer or shorter, merely by changing the final oven temperature. After the method is concluded, the oven must cool down to 30°C before another sample may be injected. Once the oven reaches 30°C, it must remain at this temperature for three minutes, in order to allow the column and all the oven internal parts to reach the correct temperature. The residence times at which all calibrated species elude are given in Table C-2.

Table C-2. Elution times for various species in the HP 5890 Series A gas chromatograph.

Species	Elution time (min)	Standard Deviation
Hydrogen	0.65	0.07
Oxygen/Nitrogen	1.3	0.2
Carbon monoxide	1.8	0.1
Methane	2.7	0.2
Carbon dioxide	6.4	0.3
Acetylene	11.4	0.3
Ethylene	13.0	0.4
Ethane	14.7	0.4
Propene	25.3	0.5
Propane	26.5	0.5

The GC was calibrated for each of the species listed in Table C-2, and the results of that calibration are illustrated in the figures below. The number of moles in the injection was varied by changing the injection size, from 0.01 to 1 mL. The area is the area of the resulting peak, integrated by the HP Chemstation software.

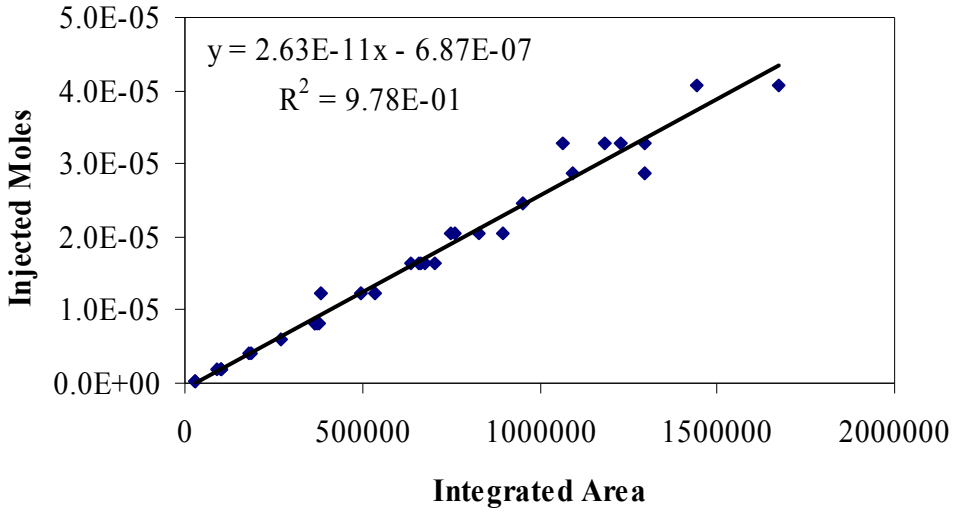

Figure C-1. Hydrogen gas calibration plot.

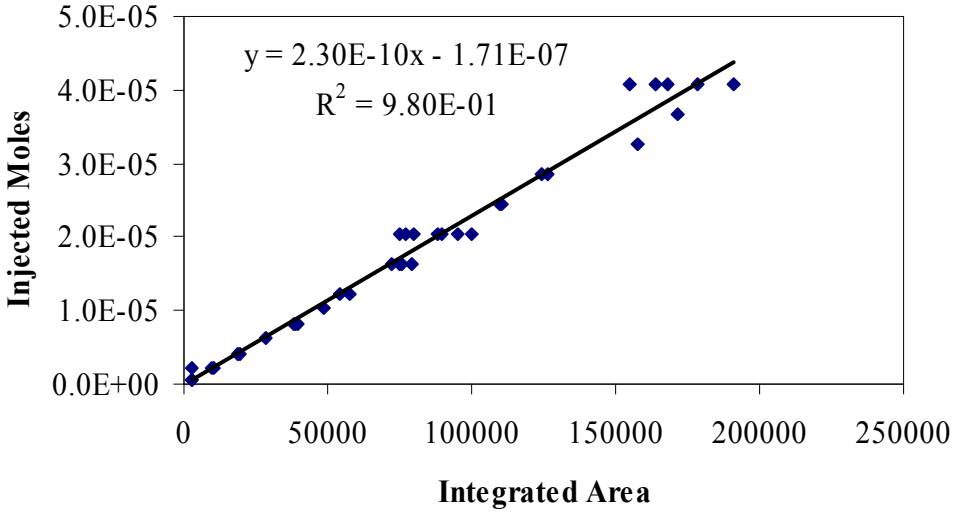

Figure C-2. Nitrogen/oxygen gas calibration plot.

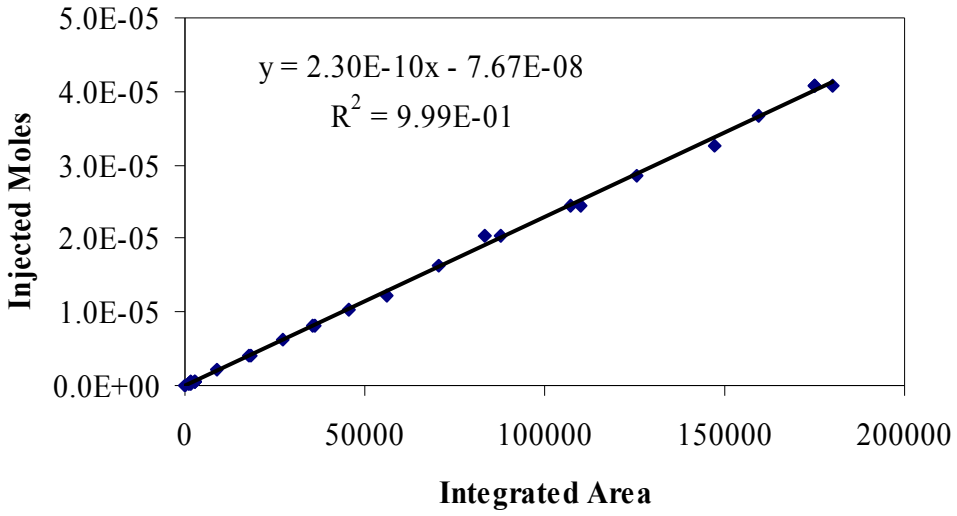

Figure C-3. Carbon monoxide gas calibration plot.

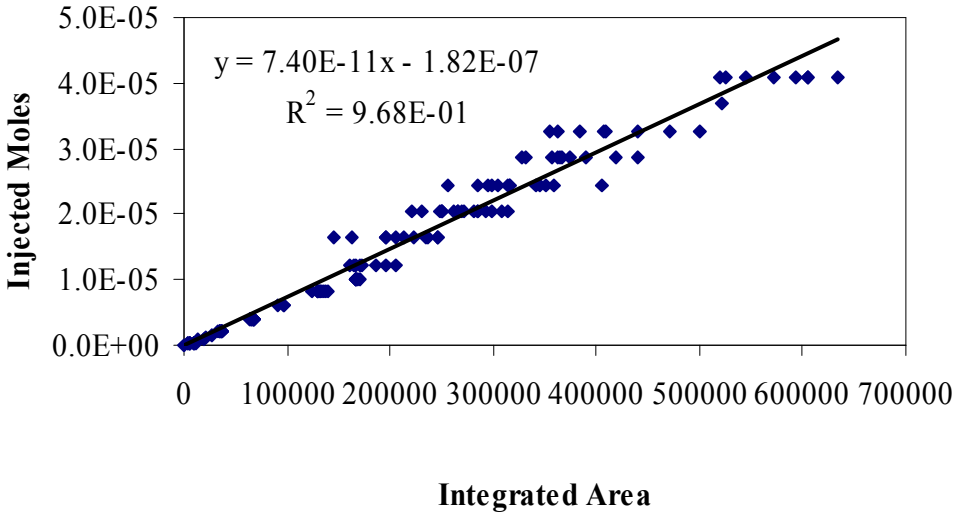

Figure C-4. Methane gas calibration plot.

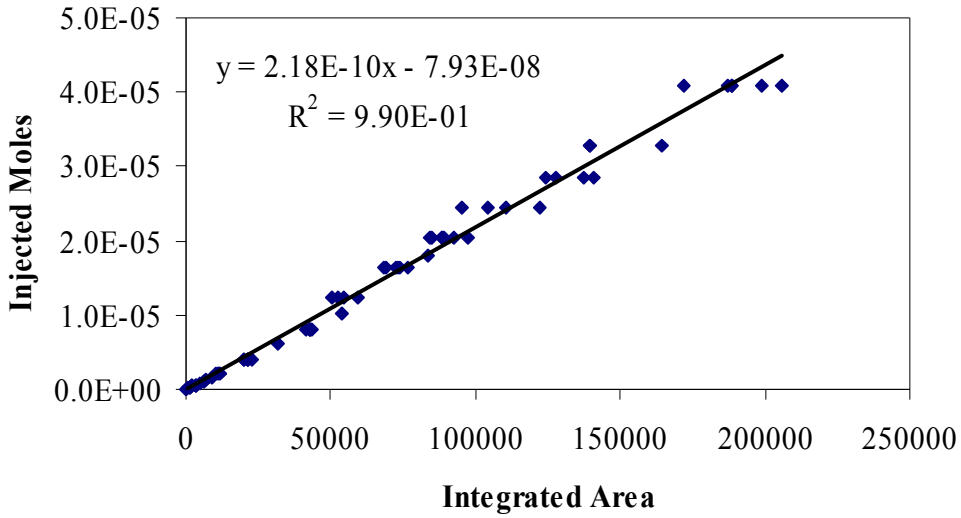

Figure C-5. Carbon dioxide gas calibration plot.

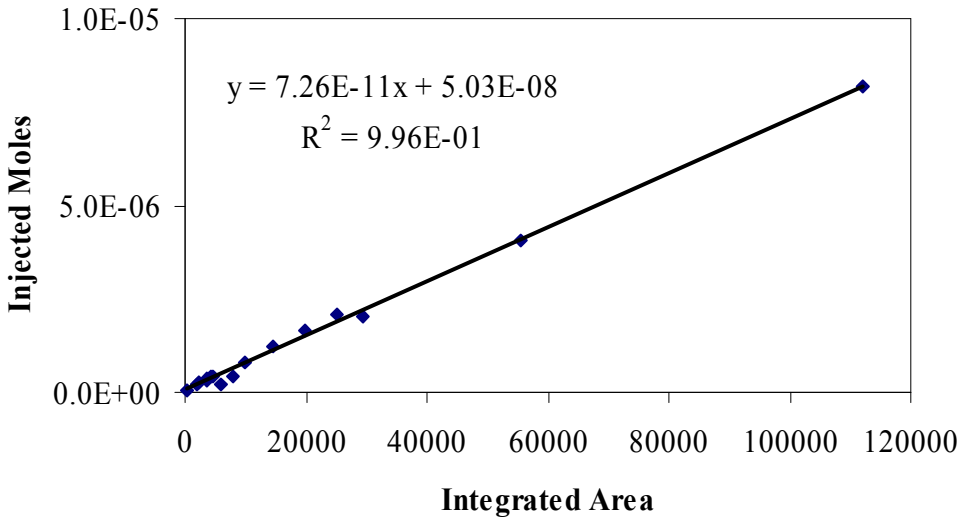

Figure C-6. Acetylene gas calibration plot.

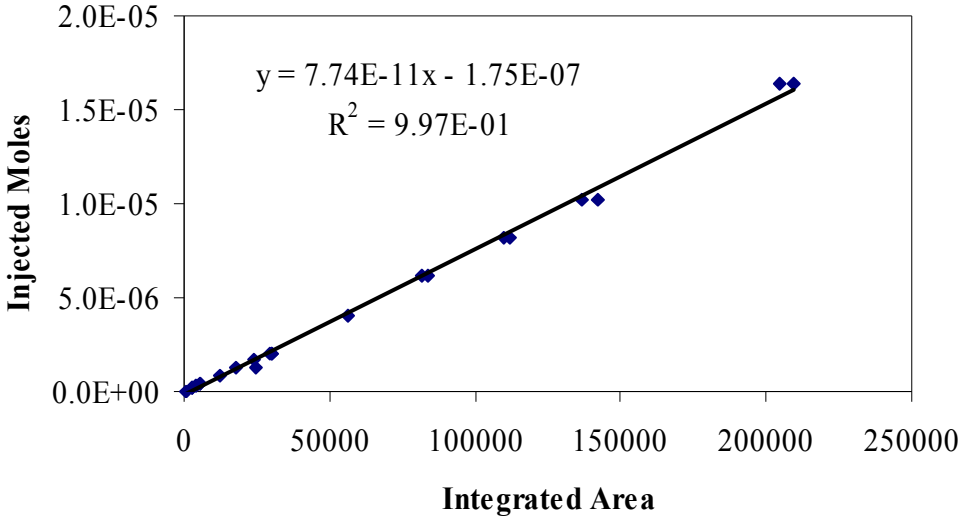

Figure C-7. Ethylene gas calibration plot.

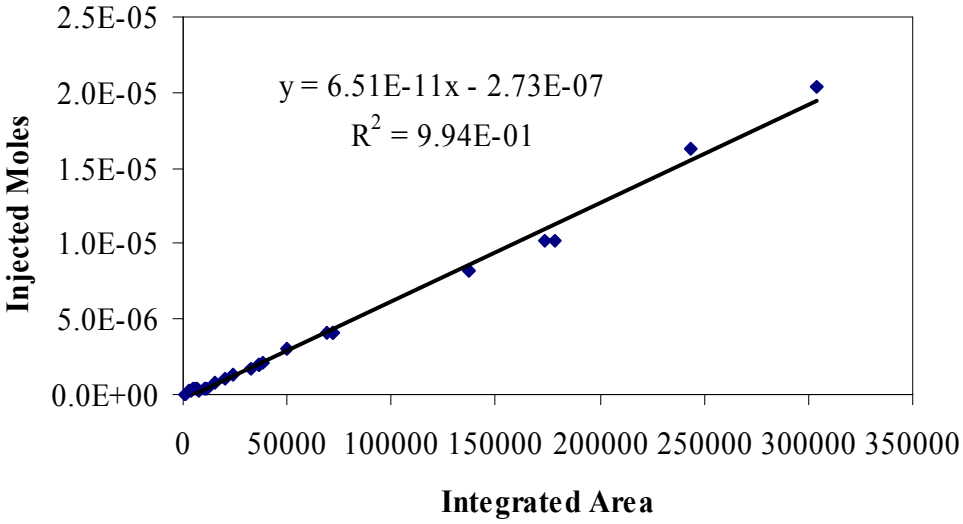

Figure C-8. Ethane gas calibration plot.

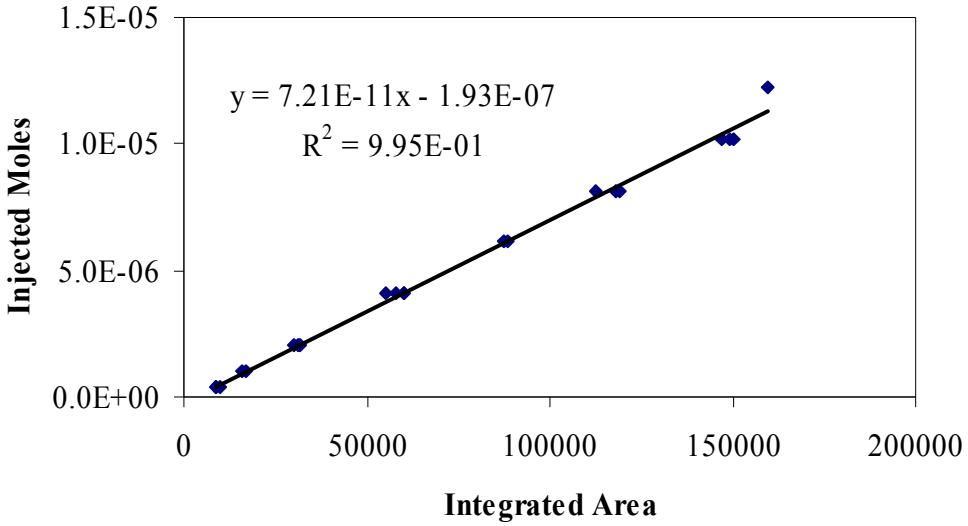

Figure C-9. Propene gas calibration plot.

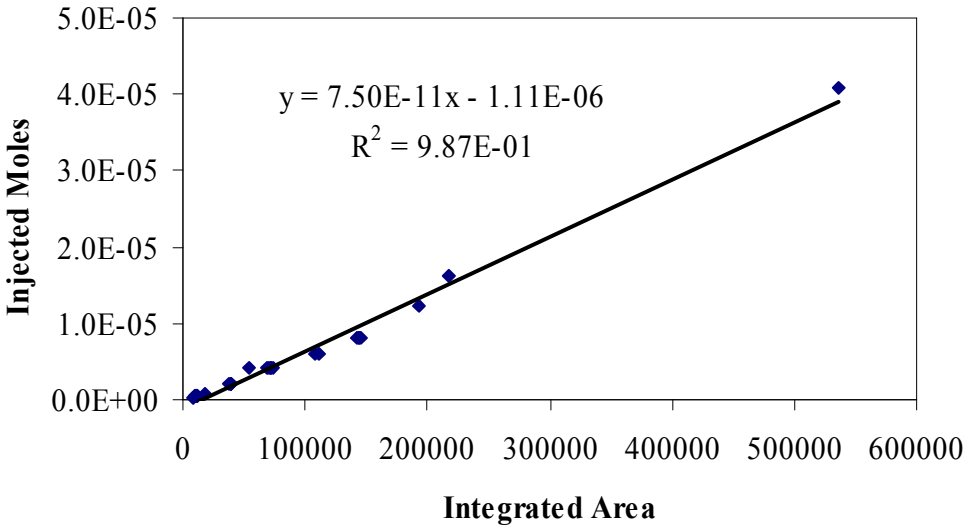

Figure C-10. Propane gas calibration plot.

APPENDIX D

EXAMPLE OF AN HP CHEMSTATION REPORT

Below is an example of the reports that HP Chemstation generates upon completion of an analysis. This particular report is from September 7, 2010 and was the third gas sample syringe taken for experiment number 35. It was analyzed with method Restek01, and from the areas reported here, and the calibrations given above, the mole percentage of each of the gases was calculated. For the TCD, the gas species from left to right are: hydrogen at an elution time of 0.568 minutes, nitrogen/oxygen at 1.102 minutes, carbon monoxide at 1.269 minutes, methane at 2.882 minutes, carbon dioxide at 6.952 minutes, ethene at 13.018 and ethane at 15.055 minutes. The FID was not on, so no peaks were recorded for it.

Data File C:\HPCHEM\1\DATA\SIG25367.D
Instument 1 9/7/10 11:34:32 PM Jason

==========

Injection Date : 9/7/10 11:17:19 PM
Sample Name : Vial : 2
Acq. Operator : Jason
Inj Volume : External
Method : C:\HPCHEM\1\METHODS\RESTEK01.M
Last changed : 9/7/10 10:35:22 PM by Jason
(modified after loading)

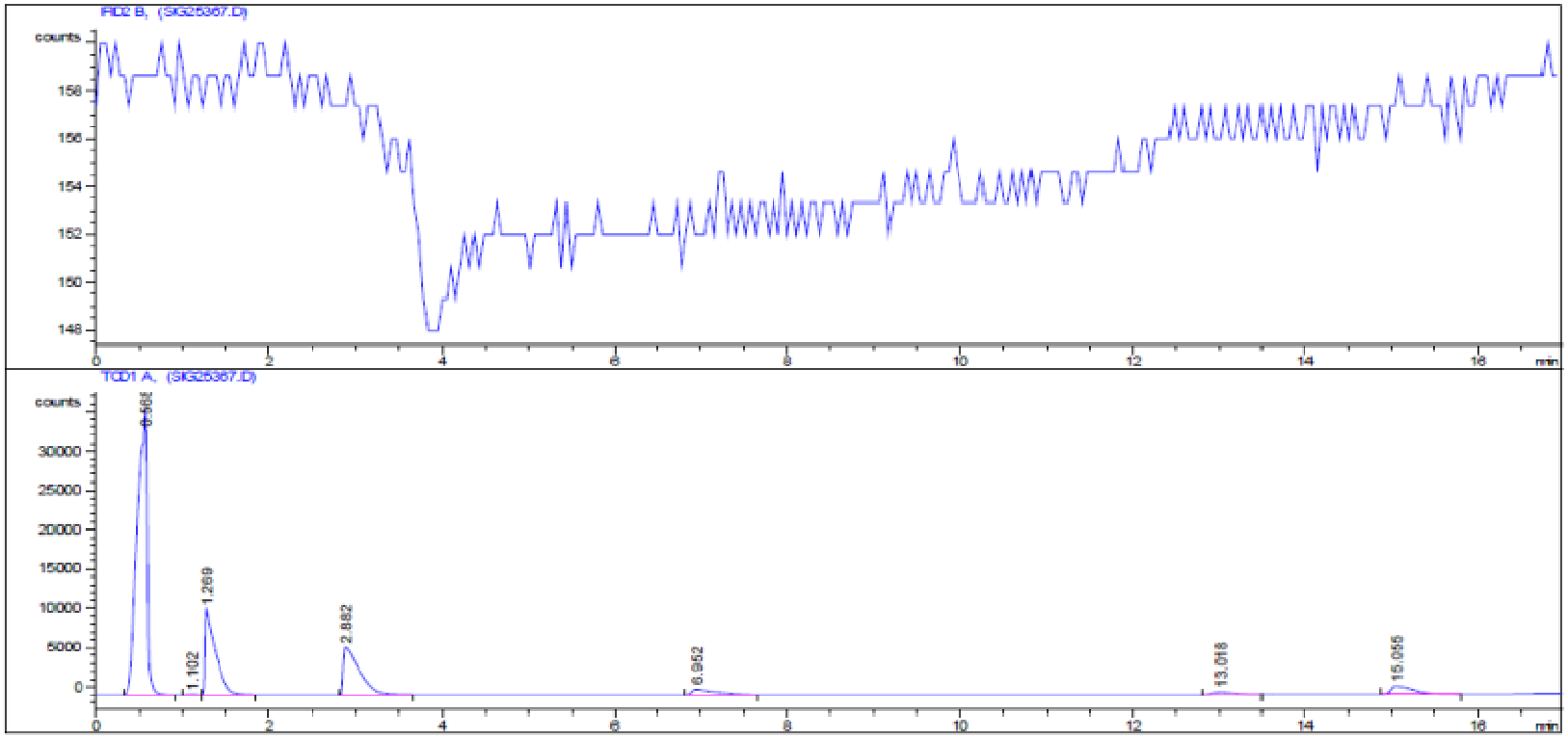

Area Percent Report

Sorted By : Signal
Multiplier : 1.0000
Dilution : 1.0000

Signal 1: FID2 B,

Signal 2: TCD1 A,

Peak #	RetTime [min]	Type	Width [min]	Area counts*s	Height [counts]	Area %
1	0.568	PB	0.0996	2.84154e5	3.78544e4	57.44678
2	1.102	PP	0.0794	236.27097	43.50245	0.04777
3	1.269	VB	0.1162	9.29286e4	1.08215e4	18.78714
4	2.882	PB	0.1805	7.97882e4	6104.12402	16.13057
5	6.952	BB	0.2432	1.28435e4	696.12683	2.59653
6	13.018	BB	0.2053	4637.01709	319.61420	0.93745
7	15.055	BB	0.2374	2.00515e4	1117.04309	4.05376
Totals :					4.94639e5	5.69564e4

Summed Peaks Report

Signal 1: FID2 B,
Signal 2: TCD1 A,

Final Summed Peaks Report

Signal 1: FID2 B,
Signal 2: TCD1 A,

*** End of Report **

APPENDIX E

COMPARISON OF EQUATIONS OF STATE AND MIXING RULES IN SUPERCRITICAL WATER AND SUPERCRITICAL WATER MIXTURES

Equations of state have been used by various groups to determine P-V-T data in supercritical fluids (*304*, *307*, *313*, *344–347*). A literature search was conducted to find data on the P-V-T data of water mixtures, especially water-nitrogen, water-methane, water-glycerin, and water-carbon dioxide (*302*, *348–356*). The only information about water-glycerin mixtures was in regard to glycerin being used to inhibit hydrate formation of water-gas mixtures. The experiments were conducted at low temperatures and pressures, and no P-V-T data was reported that could be compared against (*355*, *356*). Experimental data was found for high temperature, high pressure water-nitrogen and water-carbon dioxide mixtures, along with a large amount of data for water-hydrocarbon systems. This data was compared to the calculated values from a number of equations of state. Again based on the literature, the most promising and most used equations of state are the Peng-Robinson (PR), Soave-Redlick-Kwong (SRK), and the Predictive SRK (PSRK). When mixtures were studied, the PR equation used both the van der Waals (W) and the Huron-Vidal (HV) mixing rules, while the SRK was solved using just the Huron-Vidal (*357*). For mixtures, the PSRK uses a mixing rule proposed by Holderbaum and Gmehling (*358*).

Before the EOS's where compared against mixtures, they were used to calculate the molar volume of pure water and compared against the values from the steam tables (*20*). Temperatures of 400 to 800°C where used at a pressures of 20, 24 and 30 MPa. The percentage error of the calculated molar volume as compared to the steam table values is given in Table E-1 for the pressure of 24 MPa. All of the experiments conducted for this work were performed at a pressure of 24.1 MPa.

Table E-1. Percentage error from steam table values for the molar volume calculated from three equations of state at various temperatures, 24 MPa.

Temperature	Percentage error		
(°C)	PR	SRK	PSRK
400	1.26	6.89	8.36
450	1.46	2.68	3.99
500	1.53	1.95	3.32
550	1.18	1.87	3.29
600	0.78	1.96	3.38
650	0.40	2.08	3.50
700	0.07	2.20	3.58
750	0.22	2.30	3.63
800	0.45	2.38	3.64

As can be seen, the Peng-Robinson equation of state is the most accurate when compared to the steam tables, having an average error of 0.8%. The SRK and PSRK equations are the least accurate at 400°C. With increasing temperature the SRK and PSRK have average errors of about 2% and 3%, respectively. Table E-2 shows the percentage error at the subcritical pressure of 20 MPa.

Table E-2. Percentage error from steam table values for the molar volume calculated from three equations of state at various temperatures, 20 MPa.

Temperature	Percentage error		
(°C)	PR	SRK	PSRK
400	0.39	3.92	4.53
450	1.81	1.58	2.45
500	1.82	1.08	2.09
550	1.54	1.02	2.11
600	1.04	1.27	2.40
650	0.61	1.50	2.64
700	0.10	1.83	2.96
750	0.11	1.88	2.97
800	0.12	1.75	2.79

The results indicate that at subcritical pressures the PR equation of state is the most accurate, having an average error of 0.8%. SRK and PSRK were again the least accurate at 400°C, and had average errors of 1.8% and 2.8% over the temperature range, respectively. Table E-3 shows the percentage error at 30 MPa.

Table E-3. Percentage error from steam table values for the molar volume calculated from three equations of state at various temperatures, 30 MPa.

Temperature	Percentage error		
(°C)	PR	SRK	PSRK
400	29.63	39.12	43.41
450	0.92	6.19	8.50
500	0.45	3.87	5.90
550	0.49	3.27	5.22
600	0.23	3.11	5.01
650	0.07	3.09	4.93
700	0.37	3.12	4.89
750	0.63	3.17	4.85
800	0.85	3.19	4.78

Peng-Robinson is again the most accurate, but it can be seen that at this increased pressure all three equations of state have high error percentages at 400°C. Equations of state are least accurate and should not be used near the critical point, but these tables have shown that for 20 and 24 MPa, the PR equation is capable of producing accurate results above 400°C. At 30 MPa, equations of stat can be used at temperatures above 450°C to correctly predict P-V-T data, but with less accuracy then at 20 and 24 MPa.

Data was used from Greenwood in his study of water-carbon dioxide mixtures at 450 to 750°C, 10 and 50 MPa, mole fractions of 0.2 and 0.5 carbon dioxide, and he reported the molar volume found (*303*). The molar volume was calculated using PR, SRK and PSRK with the Huron Vidal or van der Waals mixing rules. The binary interaction parameter used in the Huron-Vidal was equal to 0.12, while the van der Waals mixing rule did not use a binary interaction parameter. The experimental conditions and values, as well as the percentage error for each EOS are given in Table E-4 below.

Table E-4. Experimental conditions and results from Greenwood, 1969, and the percentage error for each equation of state (*303*).

T	P	Molar fraction CO_2	Percentage error			
°C	MPa	X_{CO2}	PR-HR	SRK-HR	PSRK-HR	PR-W
450	10	0.2	1.94	1.94	0.29	2.33
450	50	0.2	8.04	20.95	15.08	5.59
650	10	0.2	0.44	0.44	1.74	0.29
650	50	0.2	3.87	1.69	9.14	3.23
750	10	0.2	0.75	0.59	1.88	0.65
750	50	0.2	2.86	1.07	7.41	2.46
450	10	0.5	0.19	0.76	1.42	0.73
450	50	0.5	1.51	16.62	7.08	0.51
650	10	0.5	1.32	1.17	2.47	1.10
650	50	0.5	2.91	1.33	7.15	2.14
750	10	0.5	2.69	2.86	1.75	2.83
750	50	0.5	2.83	5.53	0.66	3.31

After taking the absolute value, the PR EOS with the van der Waals mixing rule had the lowest percentage error, with an average error of 2.1%. The PR with HR mixing rule had an error of 2.5%. The SRK and PSRK had average errors of 4-5%. Using PR, the largest error was 6-8%, while the largest for SRK was 21% and PSKR was 15%. Again, the largest errors occurred at elevated pressures and lower temperatures. This approach was also taken with water-nitrogen data from Abdulagatov et al., 1993 (*302*). His data was at 300 and 390°C, 17-40 MPa, and nitrogen molar fractions of 0.18 to 0.88. No binary interaction parameters where used for either mixing rule. Table E-5 gives his experimental results and the percentage error from the equations of state.

Table E-5. Experimental conditions and results from Abdulagatov et al., 19993, and the percentage error for each equation of state (*302*).

T	P	Molar fraction N_2	Percentage error			
°C	MPa	X_{N2}	PR-HR	SRK-HR	PSRK-HR	PR-W
300	32.96	0.8821	1.40	17.19	3.77	1.60
300	24.84	0.8821	1.20	12.05	3.18	1.37
300	16.91	0.8821	0.98	5.82	2.38	1.12
390	31.53	0.0654	6.29	70.92	9.22	5.96
390	20.68	0.0654	1.24	12.52	1.88	1.42
390	39.86	0.1814	4.86	55.46	7.63	4.52
390	29.83	0.1814	0.91	86.86	3.54	0.62
390	19.79	0.1814	1.85	94.10	0.41	2.04
390	39.55	0.3738	0.12	48.97	4.06	0.18
390	29.64	0.3738	1.16	60.75	2.19	1.41
390	19.76	0.3738	1.75	17.39	0.77	1.93

Again, the average error was found for each method. Again PR-HR and PR-W was the lowest, both having an average error of 2%. The PSRK was next at 3.5%, and SRK had an average error of 44%. These results show that SRK coupled with the Huron-Vidal mixing rules are not to be used as an equation of state in supercritical water oxidation systems or any other system were a large percentage of nitrogen is present.

Based on these results, the Peng-Robinson equation of state is the most accurate equation, since it was able to match experimentally determined volumes or densities for water and water mixtures, with average errors of about 2%. It should be noted that the different mixing rules used for the PR EOS, van der Waals and Huron-Vidal, did not change the overall result for the conditions studied. Also, neglecting the binary interaction parameter for the water-nitrogen mixture, and in PR with van der Waals mixing rules for water-carbon dioxide, did not seem to affect the result.

APPENDIX F

MATHEMATICS OF THE MATRIX ANALYSIS

Figure 5-1, the visualization of the 2^3 matrix, will be used for all the calculations. The effect of temperature, residence time and water/glycerin ratio on carbon conversion and all of the gas yields are calculated this way. The numbers on the figure represent the result, either conversion or gas yield, of the experiment conducted at the conditions given by the axis on the figure. The experiments are designated by *E*, then the number of the experiment.

Effect of Temperature:

Average of (*E2*+*E4*+*E6*+*E8*) - Average of (*E1*+*E3*+*E5*+*E7*)

Effect of Residence time:

Average of (*E3*+*E4*+*E7*+*E8*) – Average of (*E1*+*E2*+*E5*+*E6*)

Effect of Water/Glycerin ratio:

Average of (*E5*+*E6*+*E7*+*E8*) – Average of (*E1*+*E2*+*E3*+*E4*)

The two factor interaction is the effect that those two factors have together on the result, which have a coupled influence beyond their individual main effects. It is calculated for each combination by:

Temperature by residence time effect

Average(*E1*+*E5*+*E4*+*E8*) - Average(*E3*+*E7*+*E2*+*E6*)

Temperature by water/glycerin ratio effect

Average (*E1*+*E3*+*E6*+*E8*) – Average (*E2*+*E4*+*E5*+*E7*)

Water/glycerin by residence time effect

Average (*E1*+*E2*+*E7*+*E8*) – Average (*E3*+*E4*+*E5*+*E6*)

For the three-factor interaction, it is calculated by

$$\frac{1}{2} * \left[\frac{(E8 - E7) - (E6 - E5)}{2} - \frac{(E4 - E3) - (E2 - E1)}{2} \right]$$

The standard error for each result is estimated by first taking the summation of the square of each repeat experiment minus the square of the summation divided by the number of repeat experiments performed at that condition. Each experiment is designated by y_x, x being 1, 2, 3, etc. depending on how many repeat experiments were done at that condition. The number of experiments conducted at a specific condition is given by n. This is given by the equation

$$\sum_{1}^{x} y_x^2 - (\sum_{1}^{x} y_x)^2 / n$$

This is the standard error for each experimental point that had duplicate experiments conducted at it. To determine the error of the interaction parameter itself, these separate errors of the experimental points need to be combined. To do this, the summation of the above equations for each repeated condition is divided by the degree of freedom, which is the number of sets of experiments that were repeated. The square root of this number is taken, and this is the estimated standard deviation for the main effects and the interaction effects. To obtain the estimated standard error, this number is divided by the square root of n (*315*).

APPENDIX G

CALCULATED EFFECTS AND ESTIMATED ERROR FOR THE PRODUCT GASES IN THE 2^3 MATRIX

These are the main effects of temperature, residence time and water/glycerin ratio, plus the two-factor and three-factor interaction effects, for carbon monoxide, carbon dioxide, methane and ethane. They were calculated using the method from Appendix F. The estimated error is also included, and is calculated using the methods from Appendix F.

Table G-1. Calculated effects and estimated errors on carbon monoxide and carbon dioxide for the 2^3 matrix.

	Effect on CO yield	**Effect of CO_2 yield**
Main effects		
Temperature, T	0.7 ± 0.1	0.97 ± 0.06
Residence time, R	-0.1 ± 0.1	0.27 ± 0.06
Water/Glycerin ratio, W	-0.2 ± 0.1	0.36 ± 0.06
Two-factor interactions		
T x R	-0.4 ± 0.1	0.20 ± 0.06
T x W	-0.2 ± 0.1	0.40 ± 0.06
R x W	-0.1 ± 0.1	0.14 ± 0.06
Three-factor interaction		
T x R x W	-0.2 ± 0.1	0.14 ± 0.06

Table G-2. Calculated effects and estimated errors methane and ethane for the 2^3 matrix.

	Effect on CH_4 yield	**Effect on C_2H_6 yield**
Main effects		
Temperature, T	0.71 ± 0.03	0.15 ± 0.01
Residence time, R	0.11 ± 0.03	0.00 ± 0.01
Water/Glycerin ratio, W	-0.07 ± 0.03	-0.03 ± 0.01
Two-factor interactions		
T x R	0.06 ± 0.03	0.00 ± 0.01
T x W	-0.06 ± 0.03	-0.03 ± 0.01
R x W	0.01 ± 0.03	-0.02 ± 0.01
Three-factor interaction		
T x R x W	0.01 ± 0.03	-0.02 ± 0.01

APPENDIX H

RESULTS OF THE EXPERIMENTS

In Table H-1 the complete results of the experiments are given; the experiment number, the wet test flow rate, the ambient temperature, the gas composition of all gas species detectable in mole percent, and the carbon conversion. This is the data, in conjunction with the inlet solution flow rate and the water/glycerin ratio, used to calculate the gas yield and the carbon conversion. When the gas composition mole percentage is "trace", that means that the gas was detected but that it was below the calibration limit for the gas chromatograph.

Table H-1. The experiment number, ambient temperature, product gas flow rate, gas molar composition and calculated carbon conversion for all the experiments conducted.

Exp. #	Amb. Temp.	Wet Test	Gas composition (mole %)								Carbon conversion
	(°C)	L/min	H_2	CO	CH_4	CO_2	C_2H_4	C_2H_6	C_3H_6	C_3H_8	%
10	30	1.89	13.3	56.7	10.7	15.8	1.7	0.7	0.0	0.0	7.6%
13	31	4.67	19.0	53.2	12.2	10.8	1.2	1.6	0.3	0.3	22.1%
12	30	10.50	23.6	45.7	16.0	8.3	0.6	3.7	1.2	0.0	54.5%
15	30	10.66	18.6	52.8	17.4	5.3	0.5	3.4	1.1	0.0	59.1%
17	32	15.61	28.0	38.0	17.7	9.4	0.0	4.9	1.2	0.0	82.9%
7	29	16.6	33.9	28.7	18.7	13.6	0.0	4.1	0.0	0.0	91.6%
8	28	16.48	34.4	27.9	18.6	14.0	0.0	4.1	0.0	0.0	91.2%
11	27	16.88	34.7	27.7	18.4	13.9	0.0	4.2	0.0	0.0	93.3%
16	29	17.69	35.7	20.7	19.6	19.6	0.0	3.4	0.0	0.0	105.4%
18	34	16.48	30.2	11.3	30.0	26.7	0.0	0.9	0.0	0.0	107.9%
9	31	1.52	14.3	50.4	12.3	19.3	1.3	1.3	0.0	0.0	17.8%
35	26	2.8	17.4	54.4	15.7	7.4	0.6	2.7	0.6	0.2	40.4%
34	26	4.2	20.7	46.0	19.1	7.3	0.0	4.4	1.6	trace	70.1%
33	26	5.4	27.1	33.5	20.5	12.6	0.0	5.4	0.0	trace	94.3%
6	26	6.6	34.7	25.2	18.9	15.9	0.0	4.3	0.0	0.0	103.2%
14	26	6.35	31.5	26.9	20.3	15.5	0.0	4.8	0.0	0.0	105.9%
29	28	5.6	30.1	21.0	22.5	20.0	0.0	5.4	0.0	0.0	104.0%
30	28	5.6	30.9	10.5	28.8	26.8	0.0	2.0	0.0	0.0	104.7%
31	26	5.4	29.1	8.6	33.7	27.6	0.0	0.0	0.0	0.0	107.1%
4	30	0.1	34.6	43.5	7.0	11.3	1.5	1.1	0.0	0.0	1.6%
20	30	2.52	50.0	38.5	5.0	5.2	0.1	0.0	0.5	0.0	25.9%
19	34	4.61	47.1	36.8	8.7	6.0	0.0	0.2	0.0	0.0	56.3%
23	35	6.95	47.9	22.2	9.8	16.7	0.0	2.4	0.0	0.0	99.5%
2	27	6.9	48.7	21.0	10.1	16.8	0.0	2.4	0.0	0.0	103.3%
5	31	6.7	48.7	17.8	10.5	19.3	0.0	2.8	0.0	0.0	99.3%
21	29	6.79	50.8	5.2	12.2	28.8	0.0	2.0	0.0	0.0	108.4%
22	33	6.77	49.1	4.8	14.1	29.9	0.0	1.0	0.0	0.0	111.0%
3	28	0.6	36.3	46.9	6.7	8.1	0.4	0.7	0.0	0.0	20.2%
32	26	1.0	27.6	45.7	12.2	10.2	0.7	2.2	0.6	trace	51.1%
28	28	2.1	41.1	27.9	12.4	14.4	0.0	3.1	0.0	0.1	95.8%
27	27	2.6	51.4	5.6	11.7	28.0	0.0	2.2	0.0	0.0	104.1%
1	31	2.6	52.9	5.4	12.0	27.3	0.0	1.5	0.0	0.0	104.3%
24	29	2.5	50.0	4.2	13.1	29.8	0.0	1.9	0.0	0.0	109.2%
25	30	2.3	47.5	4.4	16.6	30.0	0.0	0.5	0.0	0.0	109.4%
26	30	2.2	48.9	4.9	17.6	27.6	0.0	0.0	0.0	0.0	108.0%

APPENDIX I

OTHER POSSIBLE GLYCERIN REFORMATION PATHWAYS AND THE RESULTS

Below are the other glycerin reaction pathways that were tried during the course of finding the most accurate and thermodynamically sound pathway. Thermodynamically sound means that the there is a positive activation energy and pre-exponential factor. Each pathway will be described, and the resulting mathematical equations and Arrhenius plot given for each pathway. The same symbols will be used throughout, "*A*" for glycerin, "*B*" for carbon monoxide, "*C*" for carbon dioxide and "*D*" for methane. Any other species included in the pathway will be defined later.

This pathway has glycerin decomposing into carbon monoxide and hydrogen, and the resulting carbon monoxide either undergoing water gas shift to carbon dioxide or methanation. The pathway is

$$A \xrightarrow{k_1} 3B \tag{I-1}$$

$$B \xrightarrow{k_2} C \tag{I-2}$$

$$B \xrightarrow{k_3} D \tag{I-3}$$

The chemical equations would be

$$C_3H_8O_3 \xrightarrow{k_1} 3CO + 4H_2 \tag{I-4}$$

$$CO + H_2O \xrightarrow{k_2} CO_2 + H_2 \tag{I-5}$$

$$CO + 3H_2 \xrightarrow{k_3} CH_4 + H_2O \tag{I-6}$$

Integral analysis of the reaction mechanism of Equations I-1 to I-3, with the further assumption of global first order kinetics gives the following expressions for the molar flow rates of each species:

$$C_a = C_{ao} e^{-k_1 t} \tag{I-7}$$

$$C_b = \frac{-3k_1 C_{ao}(e^{-t(k_1-k_2-k_3)} - 1)e^{-t(k_2+k_3)}}{k_1 - k_2 - k_3} \quad \text{(I-8)}$$

$$C_c = \frac{-3k_2 C_{ao}(k_1 e^{-t(k_2+k_3)} - k_2 e^{-k_1 t} - k_3 e^{-k_1 t} - k_1 + k_2 + k_3)}{(k_1 - k_2 - k_3)(k_2 + k_3)} \quad \text{(I-9)}$$

$$C_d = \frac{-3k_3 C_{ao}(k_1 e^{-t(k_2+k_3)} - k_2 e^{-k_1 t} - k_3 e^{-k_1 t} - k_1 + k_2 + k_3)}{(k_1 - k_2 - k_3)(k_2 + k_3)} \quad \text{(I-10)}$$

Where C_{ao} is the initial concentration of glycerin in the feed. The resulting Arrhenius plots are given in Figures I-1 to I-3 below.

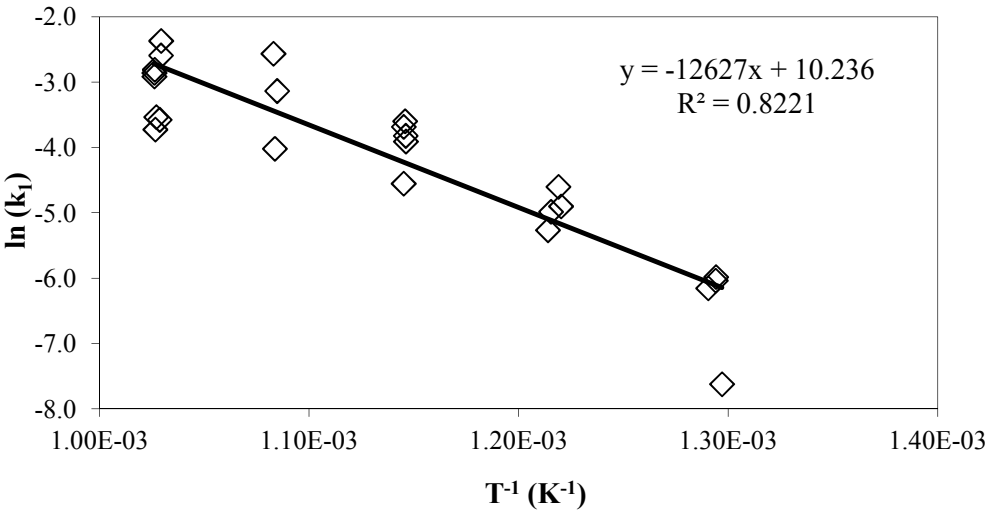

Figure I-1. First-order Arrhenius plot for reaction I-4, glycerin to carbon monoxide.

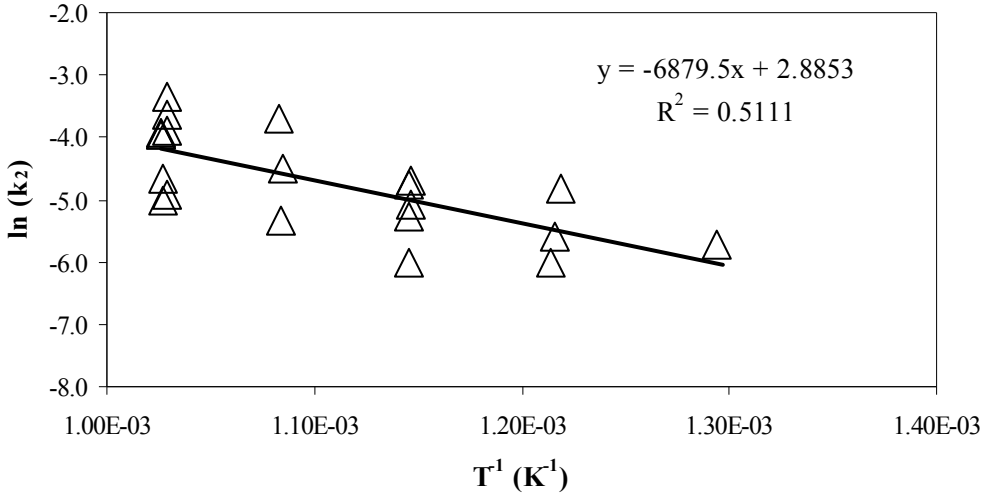

Figure I-2 First-order Arrhenius plot for reaction I-5, carbon monoxide to carbon dioxide.

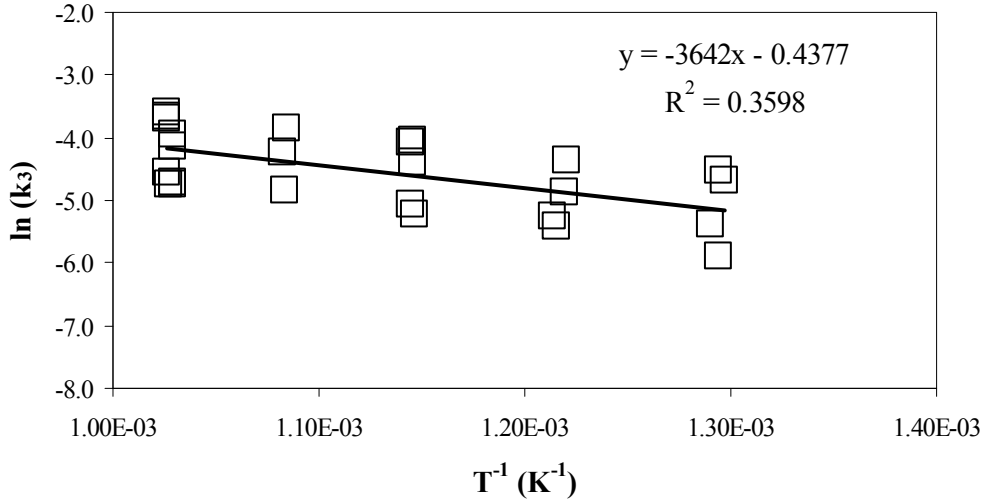

Figure I-3 First-order Arrhenius plot for reaction I-6, carbon monoxide to methane.

The fit for the gasification, k_1 and water gas shift, k_2, is about the same as the chosen pathway, but the fit for methane formation is worse, 36% versus 89.6%. The

activation energies for gasification and water gas shift are in a realistic range, but methanation has a low activation energy and pre-exponential factor. The poor fit for the methanation reaction is likely due to the fact it is a very slow reaction that favors lower temperatures and requires a catalyst (*165*, *299*). This is the most likely alternative pathway of all pathways tested.

Other likely pathways assumed that glycerin reformation could be modeled from the liquid intermediates. The chemical equation would be

$$C_3H_8O_3 \xrightarrow{k_1} 2CO + CH_4 + H_2 + H_2O \qquad \text{(I-11)}$$

$$CO + H_2O \xrightarrow{k_2} CO_2 + H_2 \qquad \text{(I-5)}$$

$$CH_4 + H_2O \xrightarrow{k_3} CO + 3H_2 \qquad \text{(I-12)}$$

Reaction I-11 is the same as that given in Section 4.4, reaction 9, except reaction I-11 has a reaction rate constant associated with it. The reaction pathway would be glycerin decomposing via reaction I-11, and the subsequent carbon monoxide undergoing water gas shift, k_2, to form carbon dioxide. The methane produced from I-11 could undergo steam reformation, reaction I-12, to produce carbon monoxide and hydrogen. After integration and solving for the rate constants, the follow Arrhenius plots, Figures I-4 through I-6 were made.

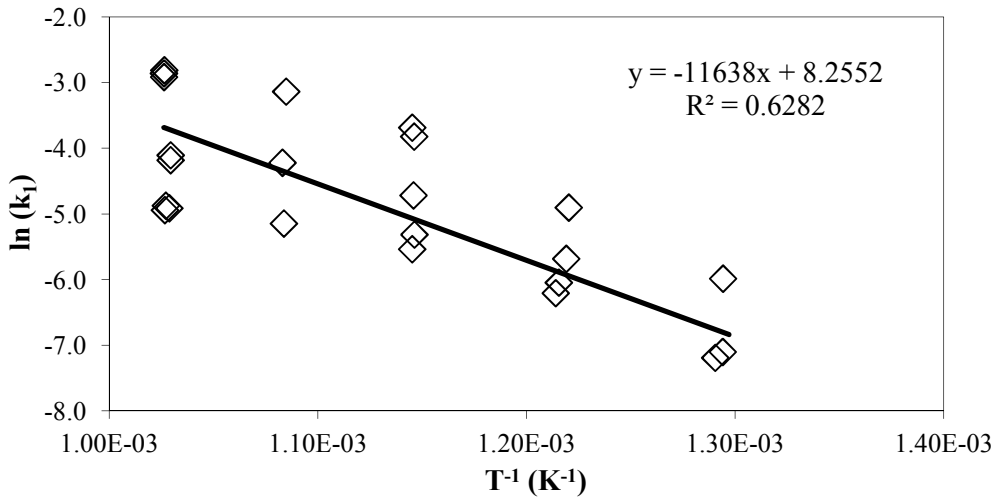

Figure I-4 First-order Arrhenius plot for reaction I-11, glycerin to carbon monoxide and methane.

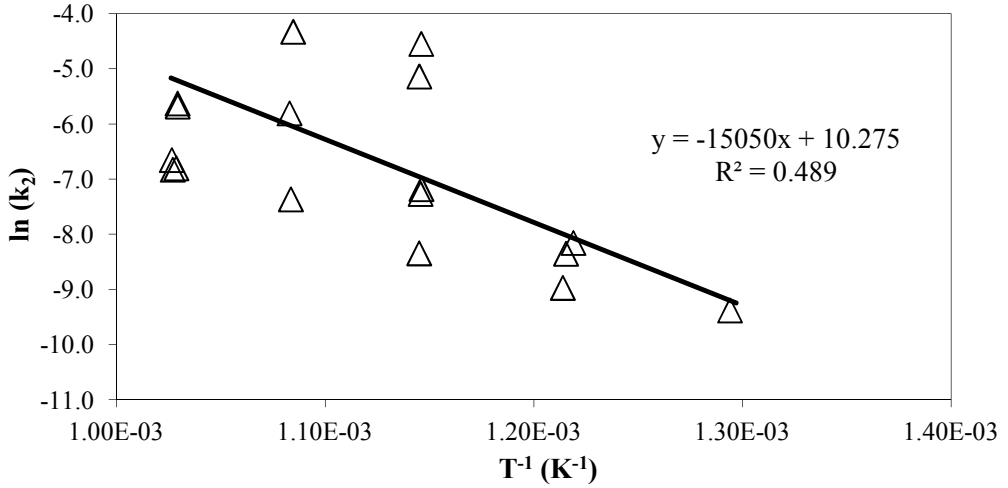

Figure I-5 First-order Arrhenius plot for reaction the water gas shift reaction, carbon monoxide to carbon dioxide.

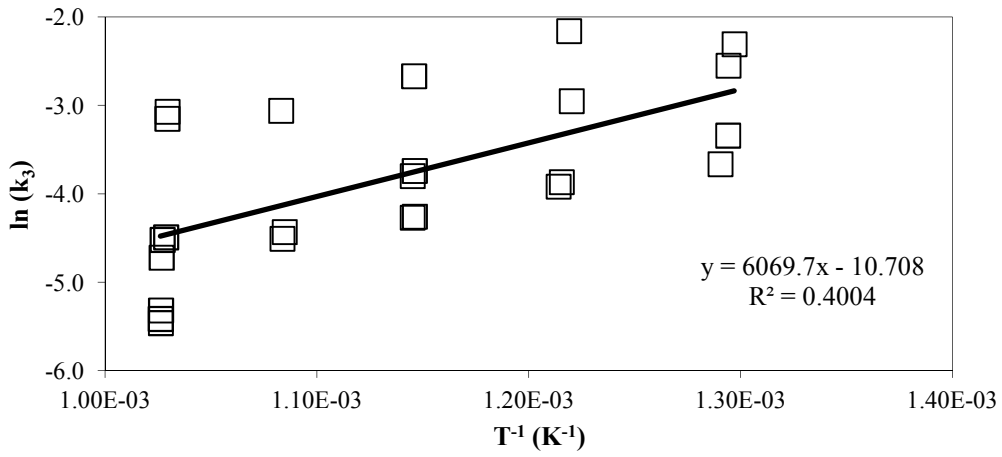

Figure I-6 First-order Arrhenius plot for reaction I-12, steam reformation.

The fit for gasification, k_1, is worse than other models, while water gas shift is better than some. The activation energies and pre-exponential factors are also in a realistic range. However, the slope of the steam reformation Arrhenius plot, Figure I-6, has a positive slope. This means that the activation energy is negative, which is not a thermodynamically valid solution for a kinetic model. Therefore, this pathway is not possible.

Another pathway had the same reactions as the above, I-11 and I-5, except that the steam reformation, I-12, was reversed into the methanation reaction, I-6. The mathematical solutions for the concentrations are

$$C_a = C_{ao} e^{-k_1 t} \tag{I-7}$$

$$C_b = \frac{-2k_1 C_{ao}(e^{-t(k_1-k_2-k_3)} - 1)e^{-t(k_2+k_3)}}{k_1 - k_2 - k_3} \tag{I-13}$$

$$C_c = \frac{-1}{(k_1 - k_2 - k_3)(k_2 + k_3)}(C_{ao}(-4k_3k_2e^{-k_1t} - 3k_3^2e^{-k_1t} + 2k_1k_3e^{-(k_2+k_3)t} + k_1k_2e^{-k_1t} + k_1k_3e^{-k_1t} - k_2^2e^{-k_1t} - 3k_1k_3 + 4k_2k_3 + 3k_3^2 - k_1k_2 + k_2^2)) \quad \text{(I-14)}$$

$$C_d = \frac{-2k_2C_{ao}(k_2e^{-k_1t} - k_3e^{-k_1t} + k_1e^{-(k_2+k_3)t} - k_1 + k_2 + k_3)}{(k_1 - k_2 - k_3)(k_2 + k_3)} \quad \text{(I-15)}$$

This solution ended up giving negative reaction rate constants for half of the k_2 results, and therefore is not a viable reaction pathway.

A pathway in which the liquid intermediate reaction is coupled with a total gasification reaction and the water gas shift reaction was tried.

$$C_3H_8O_3 \xrightarrow{k_1} 2CO + CH_4 + H_2 + H_2O \quad \text{(I-11)}$$

$$C_3H_8O_3 \xrightarrow{k_1} 3CO + 4H_2 \quad \text{(I-4)}$$

$$CO + H_2O \xrightarrow{k_2} CO_2 + H_2 \quad \text{(I-5)}$$

Integral analysis of the reaction mechanism of Equations I-11, I-4 and I-5, with the assumption of global first order kinetics, gives the following expressions for the molar flow rates of each species:

$$C_a = C_{ao}e^{-(k_1+k_2)t} \quad \text{(I-16)}$$

$$C_b = -\frac{C_{ao}(2k_1 + 3k_2)(e^{-t(k_1+k_2-k_3)} - 1)e^{-k_3t}}{k_1 + k_2 - k_3} \quad \text{(I-17)}$$

$$C_c = -\frac{k_1C_{ao}(e^{-t(k_1+k_2)} - 1)}{k_1 + k_2} \quad \text{(I-18)}$$

$$C_d = -\frac{C_{ao}(2k_1 + 3k_2)(k_1e^{-k_3t} + k_2e^{-k_3t} - k_3e^{-t(k_1+k_2)} + k_3 - k_1 - k_2)}{(k_1 + k_2 - k_3)(k_1 + k_2)} \quad \text{(I-19)}$$

The resulting Arrhenius plots are given in Figures I-7 to I-9 below.

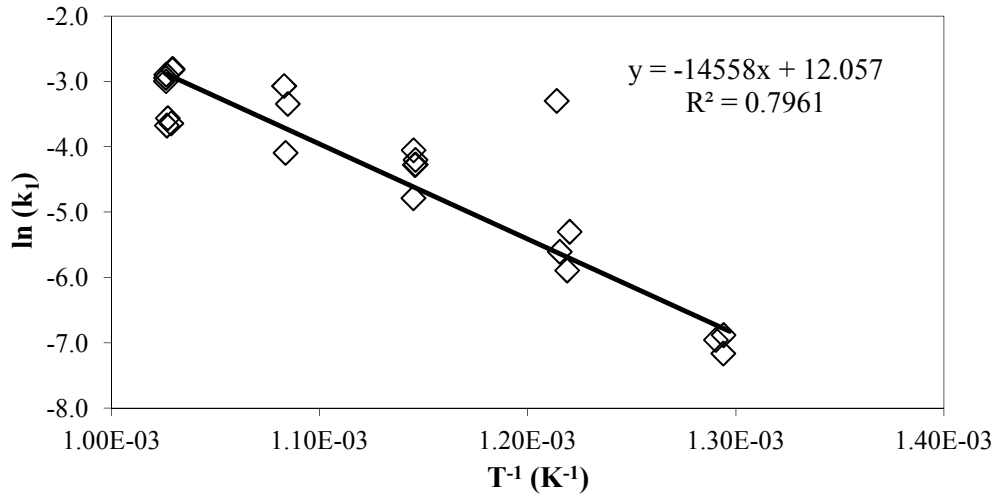

Figure I-7 First-order Arrhenius plot for reaction I-11, glycerin to carbon monoxide and methane.

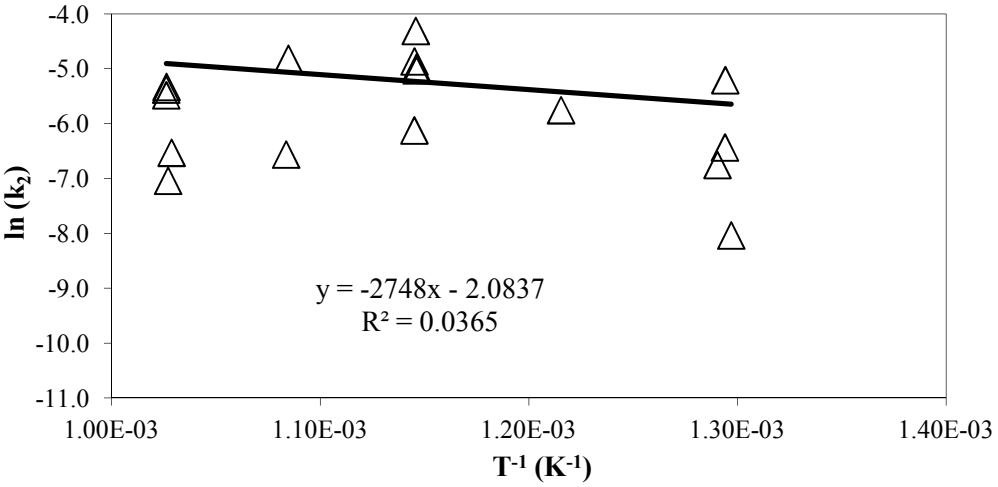

Figure I-8 First-order Arrhenius plot for reaction I-4, glycerin to carbon monoxide.

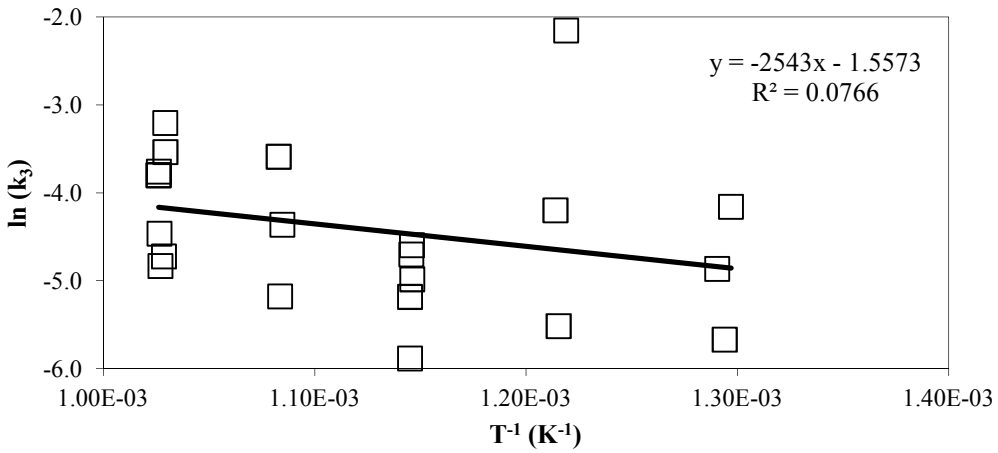

Figure I-9 First-order Arrhenius plot for reaction I-5, the water gas shift reaction.

The fit and trend for P11, the liquid intermediate gasification, is good. The others have very poor fits. Some experiments also gave negative reaction rates, which would be thermodynamically impossible. The best fit using this pathway for reaction I-4, the gasification of glycerin into only carbon monoxide, would have been a parabolic one. More complicated versions of the above reaction pathway were also tried. The first pathway tried with the liquid intermediate reaction included all the following reactions

$$C_3H_8O_3 \xrightarrow{k_1} CO + C_2H_4 + 2H_2O \quad \text{(I-20)}$$

$$C_3H_8O_3 \xrightarrow{k_1} 2CO + CH_4 + H_2 + H_2O \quad \text{(I-11)}$$

$$C_3H_8O_3 \xrightarrow{k_3} 3CO + 4H_2 \quad \text{(I-4)}$$

$$C_2H_4 + H_2 \xrightarrow{k_4} C_2H_6 \quad \text{(I-22)}$$

$$CO + H_2O \xrightarrow{k_5} CO_2 + H_2 \quad \text{(I-5)}$$

$$CO + 3H_2 \xrightarrow{k_6} CH_4 + H_2O \quad \text{(I-6)}$$

Reaction I-20 is the liquid intermediate reaction for ethene formation, and reaction I-22 is the hydrogenation of ethene into ethane. These reactions were first introduced in Section 4.4. The reaction rates would be

$$dC_a/dt = -k_1 C_a - k_2 C_a - k_3 C_a \quad \text{(I-23)}$$

$$dC_b/dt = k_1 C_a + 2k_2 C_a + 3k_3 C_a - k_5 C_b - k_6 C_b \quad \text{(I-24)}$$

$$dC_c/dt = k_5 C_b \quad \text{(I-25)}$$

$$dC_d/dt = k_2 C_a + k_6 C_b \quad \text{(I-26)}$$

$$dC_e/dt = k_1 C_a - k_4 C_e \quad \text{(I-27)}$$

$$dC_f/dt = k_4 C_e \quad \text{(I-28)}$$

Where C_e is the molar flow rate of ethene and C_f is for ethane. The above equations were integrated and solved simultaneously, changing the reaction rate constants so that the correct molar concentration of each species was found. The result was that there was no trend and most of the reaction rate constants were negative. The above pathway was simplified to include only reactions I-11, I-4, I-5 and I-6. The reaction rate constant for the gasification, k_1, and water gas shift, k_3, ended up being negative for almost all conditions for this pathway, and so could not be considered. The carbon dioxide methanation reaction

$$CO_2 + 4H_2 \xrightarrow{k_6} CH_4 + 2H_2O \quad \text{(I-29)}$$

Was also tried in conjunction with many of the pathways given above, but the results were no better. It is because of these results that the model used in Section 5.6.2, in which the glycerin can undergo decomposition into either methane or carbon monoxide, and the resulting carbon monoxide can undergo water gas shift to form carbon dioxide, was chosen.

APPENDIX J

REACTION RATE CONSTANTS AND REACTANT CONCENTRATIONS

In Table J-1 the concentrations and the reaction rate constants are given. The concentrations were used, in conjunction with the rate models and the residence times, to determine the rate constants. C_{ao} is the feed rate of glycerin, C_b is the molar product flow rate of carbon monoxide, C_c is for carbon dioxide and C_d for methane. The reaction rate k_1 is for the decomposition of glycerin into carbon monoxide, k_2 is for the water gas shift of carbon monoxide into carbon dioxide, and k_3 is for the decomposition of glycerin into methane, as given by reactions 31-33.

Table J-1 The experiment number, concentration and the reaction rate constant for all experiments used to calculate the activation energy and pre-exponential factor.

Exp. #	C_{ao} mol of glycerin/ min	C_b mol CO/ min	C_c mol CO_2/ min	C_d mol CH_4/ min	k_1	k_2	k_3
7	0.505	0.1917	0.0906	0.1248	0.04170	0.02331	0.01843
8	0.502	0.1860	0.0934	0.1242	0.03752	0.02242	0.01669
10	0.878	0.0430	0.0120	0.0081	0.00220		0.00032
11	0.503	0.1899	0.0955	0.1262	0.03974	0.02237	0.01757
12	0.610	0.1930	0.0349	0.0675	0.01688	0.01011	0.00500
13	0.693	0.0995	0.0202	0.0228	0.00624		0.00119
15	0.603	0.2261	0.0227	0.0747	0.01931	0.00561	0.00580
17	0.562	0.2371	0.0586	0.1100	0.03165	0.01275	0.01178
2	0.143	0.0588	0.0472	0.0284	0.07513	0.02916	0.02012
4	0.217	0.0023	0.0006	0.0004	0.00043		0.00006
5	0.143	0.0477	0.0517	0.0282	0.05821	0.03949	0.01652
19	0.168	0.0672	0.0110	0.0160	0.02269	0.00910	0.00463
20	0.192	0.0390	0.0053	0.0051	0.00899	0.00836	0.00103
23	0.147	0.0610	0.0458	0.0270	0.06134	0.02765	0.01549
28	0.053	0.0233	0.0120	0.0103	0.01584	0.00686	0.00465
3	0.073	0.0108	0.0019	0.0015	0.00212	0.00345	0.00026
32	0.061	0.0194	0.0043	0.0052	0.00562	0.00403	0.00123
29	0.163	0.0478	0.0456	0.0512	0.01542	0.01153	0.00845
33	0.179	0.0733	0.0275	0.0447	0.01254	0.00564	0.00556
34	0.198	0.0786	0.0125	0.0327	0.00775	0.00279	0.00278
35	0.233	0.0611	0.0083	0.0176	0.00411	0.00267	0.00104
14	0.177	0.0697	0.0400	0.0524	0.01978	0.00797	0.00946
9	0.298	0.0306	0.0117	0.0075	0.00180		0.00032
6	0.179	0.0678	0.0428	0.0511	0.01893	0.00888	0.00873

BIBLIOGRAPHY

1. Boock, L. T., LaMarca, C., and Klein, M. T. (1993) Hydrolysis and oxidation in supercritical water, *Endeavour 17*, 180-185.

2. Levelt Sengers, J. M. H. (1994) Critical behavior of fluids: Concepts and applications. In *Supercritical fluids: Fundamentals for application. NATO Science Series E: Applied Sciences - Vol. 366* (Kiran, E., Debenedetti, P. G., and Peters, C. J., Eds.), pp 3-39, Kluwer Academic Publishers, Dordrecht, The Netherlands.

3. Bunker, C. E., Rollins, H. W., and Sun, Y. (2002) Fundamental Properties of Supercritical Fluids. In *Supercritical Fluid Technology in Materials Science and Engineering: Syntheses, Properties, and Applications* (Sun, Y., Ed.), pp 1-26, Marcel Dekker, Inc., New York, NY.

4. Clifford, A., and Williams, J. R. (2000) Introduction to Supercritical Fluids and Their Applications. In *Supercritical Fluid Methods and Protocols* (William, J. R., and Clifford, A. A., Eds.), pp 1-16, Humana Press, Totowa, NJ.

5. Lilac, W. D. (1999) Controlled Depolymerization of Polypropylene via Selected Partial Oxidation in a Supercritical Water Medium, University of Missouri-Columbia.

6. Savage, P. E., Gopalan, S., Mizan, T. I., Martino, C. J., and Brock, E. E. (1995) Reactions at supercritical conditions: Applications and fundamentals, *AIChE Journal 41*, 1723-1778.

7. Rubin, J. B., Davenhall, L. B., Taylor, C. M. V., Sivils, L. D., Pierce, T., Alamos, L., and Tiefert, K. (1998) CO2-Based Supercritical Fluids as Replacements for Photoresist- Stripping Solvents, pp 1-10, Los Alamos National Laboratory.

8. DeSimone, J. M., Guan, Z., and Elsbernd, C. S. (1992) Synthesis of Fluoropolymers in Supercritical Carbon Dioxide, *Science 257*, 945-947.

9. Gupta, R. B. (2006) Supercritical Fluid Extraction (SFE). In *Encyclopedia of Chemical Processing* (Lee, S., Ed.), pp 2907-2915, Taylor & Francis, New York, NY.

10. Marr, R., and Gamse, T. (2000) Use of supercritical fluids for different processes including new developments—a review, *Chemical Engineering and Processing 39*, 19-28.

11. Jung, J., and Perrut, M. (2001) Particle design using supercritical fluids: Literature and patent survey, *The Journal of Supercritical Fluids 20*, 179-219.

12. Debenedetti, P. G. (1990) Homogeneous nucleation in supercritical fluids, *AIChE Journal 36*, 1289-1298.

13. van der Kraan, M., Fernandez Cid, M. V., Woerlee, G. F., Veugelers, W. J. T., and Witkamp, G. J. (2007) Dyeing of natural and synthetic textiles in supercritical carbon dioxide with disperse reactive dyes, *The Journal of Supercritical Fluids 40*, 470-476.

14. Kruse, A., and Karlsruhe, F. (2008) Supercritical water gasification, *Biofuels, Bioproducts & Biorefining 2*, 415-437.

15. Guo, L., Lu, Y., Zhang, X., Ji, C., Guan, Y., and Pei, A. (2007) Hydrogen production by biomass gasification in supercritical water: A systematic experimental and analytical study, *Catalysis Today 129*, 275-286.

16. Johnston, K. P., and Haynes, C. (1987) Extreme solvent effects on reaction rate constants at supercritical fluid conditions, *AIChE Journal 33*, 2017-2026.

17. Mizan, T. I., Savage, P. E., and Ziff, R. M. (1996) Temperature dependence of hydrogen bonding in supercritical water, *Journal of Physical Chemistry 100*, 403-408.

18. Fernandez-Prini, R. J., Corti, H. R., and Japas, M. L. (1992) High-temperature aqueous solutions: Thermodynamic properties. (Fernandez-Prini, R. J., Ed.), CRC Press, Boca Raton FL.

19. Marshall, W. L., and Frank, E. U. (1981) Ion Product of Water Substance, 0-1000°C, 1-10,000 Bars, *Journal of Physical Chemistry Reference Data 10*, 295-304.

20. Wagner, W., and Kruse, A. (1998) Properties of Water and Steam, pp 236-246, Springer, Berlin.

21. Jessop, P. G., Ikariya, T., and Noyori, R. (1999) Homogeneous Catalysis in Supercritical Fluids, *Chemical Reviews 99*, 475-494.

22. Shaw, R. W., Brill, T. B., Clifford, A. A., Eckert, C. A., and Franck, E. U. (1991) Supercritical Water-A Medium for Chemistry, *Chemical & Engineering News 69*, 26-39.

23. Hong, G. T., and Spritzer, M. H. (2003) Supercritical Water Partial Oxidation. In *Department of Energy Hydrogen Program Annual Review*, Berkeley, CA.

24. Boukis, N., Diem, V., Habicht, W., and Dinjus, E. (2003) Methanol Reforming in Supercritical Water, *Industrial & Engineering Chemistry Research 42*, 728-735.

25. Bröll, D., Kaul, C., Krämer, A., Krammer, P., Richter, T., Jung, M., Vogel, H., and Zehner, P. (1999) Chemistry in Supercritical Water, *Angewandte Chemie (International ed. in English) 38*, 2998-3014.

26. Lee, I.-G., Kim, M.-S., and Ihm, S.-K. (2002) Gasification of Glucose in Supercritical Water, *Industrial & Engineering Chemistry Research 41*, 1182-1188.

27. Yan, B., Wei, C., Hu, C., Xie, C., and Wu, J. (2007) Hydrogen generation from polyvinyl alcohol-contaminated wastewater by a process of supercritical water gasification, *Journal of environmental sciences 19*, 1424-9.

28. Lu, Y., Guo, L., Ji, C., Zhang, X., Hao, X., and Yan, Q. (2006) Hydrogen production by biomass gasification in supercritical water: A parametric study, *International Journal of Hydrogen Energy 31*, 822-831.

29. Pinkwart, K. (2004) Gasification of diesel oil in supercritical water for fuel cells, *Journal of Power Sources 136*, 211-214.

30. Lee, S., Lanterman, H. B., Picou, J. W., and Wenzel, J. E. (2009) Kinetic Modeling of Supercritical Water Reformation of JP-8 Fuel, *Energy Sources, Part A: Recovery, Utilization, and Environmental Effects 31*, 1813-1821.

31. Ikushima, Y., Hatakeda, K., Sato, O., Yokoyama, T., and Arai, M. (1999) Noncatalytic Organic Synthesis Using Supercritical Water: The Peculiarity Near the Critical Point, *Angewandte Chemie (International ed. in English) 38*, 2910-2914.

32. Siskin, M., and Katritzky, A. R. (1991) Reactivity of organic compounds in hot water: geochemical and technological implications, *Science 254*, 231-237.

33. Modell, M., Reid, R. C., and Amin, S. I. (1978) U.S. Patent # 4113446, Gasification process, United States Patent Office.

34. Modell, M. (1982) U.S. Patent # 4338199, Processing methods for the oxidation of organics in supercritical water, United States Patent Office.

35. Cortright, R. D., Davda, R. R., and Dumesic, J. A. (2002) Hydrogen from catalytic reforming of biomass-derived hydrocarbons in liquid water, *Nature 418*, 964-7.

36. Gasafi, E., Meyer, L., and Schebek, L. (2004) Using Life-Cycle Assessment in Process Design Supercritical Water Gasification of Organic Feedstocks, *Journal of Industrial Ecology 7*, 75-91.

37. Picou, J. W. (2008) Autothermal Non-Catalytic Reformation of Jet Fuel in a Supercritical Water Medium, Missouri University of Science and Technology.

38. Gupta, R. B. (2006) Supercritical Water Oxidation. In *Encyclopedia of Chemical Processing* (Lee, S., Ed.), pp 2927-2932, Taylor & Francis, New York, NY.

39. Picou, J. W., Wenzel, J. E., Lanterman, H. B., and Lee, S. (2009) Hydrogen Production by Noncatalytic Autothermal Reformation of Aviation Fuel Using Supercritical Water, *Energy & Fuels 23*, 6089-6094.

40. Svanstrom, M., Froling, M., Olofsson, M., and Lundin, M. (2005) Environmental assessment of supercritical water oxidation and other sewage sludge handling options, *Waste Management & Research 23*, 356-366.

41. Marrone, P., Hodes, M., Smith, K., and Tester, J. (2004) Salt precipitation and scale control in supercritical water oxidation—part B: commercial/full-scale applications, *The Journal of Supercritical Fluids 29*, 289-312.

42. Hodes, M., Marrone, P., Hong, G., Smith, K., and Tester, J. (2004) Salt precipitation and scale control in supercritical water oxidation—Part A: fundamentals and research, *The Journal of Supercritical Fluids 29*, 265-288.

43. Griffith, J. W., and Raymond, D. H. (2002) The first commercial supercritical water oxidation sludge processing plant, *Waste management 22*, 453-9.

44. Masten, D. A., Foy, B. R., Harradine, D. M., and Dyer, R. B. (1993) In Situ Ramam Spectroscopy of Reactions in Supercritical Water, *Journal of Physical Chemistry 97*, 8557-8559.

45. Lavric, E., Weyten, H., Deruyck, J., Plesu, V., and Lavric, V. (2005) Delocalized organic pollutant destruction through a self-sustaining supercritical water oxidation process, *Energy Conversion and Management 46*, 1345-1364.

46. Modell, M. (1989) Supercritical-Water Oxidation. In *Standard Handbook of Hazardous Waste Treatment and Disposal* (Freeman, H. M., Ed.), pp 8.153-8.168, McGraw-Hill, New York, NY.

47. Penninger, J. M. (1988) Reactions of di-n-butylphtalate in water at near-critical temperature and pressure, *Fuel 67*, 490-496.

48. Houser, T. J., Tsao, C. C., Dyla, J. E., Van Atten, M. K., and McCarville, M. E. (1989) The reactivity of tetrahydroquinoline, benzylamine and bibenzyl with supercritical water, *Fuel 68*, 323-327.

49. Thornton, T., and Savage, P. (1990) Phenol oxidation in supercritical water, *The Journal of Supercritical Fluids 3*, 240-248.

50. Picou, J., Wenzel, J., Niemoeller, a., Lee, S., and Lanterman, H. B. (2011) A Kinetic Model Based on the Sequential Reaction Mechanism for the Noncatalytic Reformation of Jet Fuel in Supercritical Water, *Energy Sources, Part A: Recovery, Utilization, and Environmental Effects 33*, 785-794.

51. Savage, P. E. (1999) Organic Chemical Reactions in Supercritical Water, *Chemical Reviews 99*, 603-622.

52. Ding, Z. Y., Frisch, M. A., Li, L., and Gloyna, E. F. (1996) Catalytic Oxidation in Supercritical Water, *Industrial & Engineering Chemistry Research 35*, 3257-3279.

53. Arai, K., and Adschiri, T. (1999) Importance of phase equilibria for understanding supercritical fluid environments, *Fluid Phase Equilibria 158-160*, 673-684.

54. Kruse, A. (2009) Hydrothermal biomass gasification, *The Journal of Supercritical Fluids 47*, 391-399.

55. Griffith, J. W., Wofford III, W. T., and Griffith, J. R. (2000) U.S. Patent # 6051145, Method for Handling and Effluent in a Hydrothermal Process, United States Patent Office.

56. Griffith, J. W., Wofford III, W. T., and Griffith, J. R. (1999) U.S. Patent # 5888389, Apparatus for Oxidizing Undigested Wastewater Sludges, United States Patent Office.

57. Yoo, J., Ishiwatari, Y., Oka, Y., and Liu, J. (2006) Conceptual design of compact supercritical water-cooled fast reactor with thermal hydraulic coupling, *Annals of Nuclear Energy 33*, 945-956.

58. Mukohara, T. (1999) Core design of a high-temperature fast reactor cooled by supercritical light water, *Annals of Nuclear Energy 26*, 1423-1436.

59. Bugge, J., Kjar, S., and Blum, R. (2006) High-efficiency coal-fired power plants development and perspectives, *Energy 31*, 1437-1445.

60. Viswanathan, R., Coleman, K., and Rao, U. (2006) Materials for ultra-supercritical coal-fired power plant boilers, *International Journal of Pressure Vessels and Piping 83*, 778-783.

61. Downey, K. W., Snow, R. H., Hazlebeck, D. A., and Roberts, A. J. (1995) Corrosion and chemical agent destruction: Research on supercritical water oxidation of hazardous military wastes. In *ACS Symp. Ser. 608, Innovations in Supercritical Fluids - Science and Technology* (Hutchenson, K. W., and Foster, N. R., Eds.), pp 313-326, American Chemical Society, Washington, D.C.

62. Konys, J., Fodi, S., Hausselt, J., Schmidt, H., and Casal, V. (1999) Corrosion of High-Temperature Alloys in Chloride-Containing Supercritical Water Oxidation Systems, *Corrosion 55*, 45-51.

63. Mitton, D. B., Yoon, J.-H., Cline, J., Kim, H.-S., Eliaz, N., and Latanision, R. M. (2000) Corrosion Behavior of Nickel-Based Alloys in Supercritical Water Oxidation Systems, *Industrial & Engineering Chemistry Research 39*, 4689-4696.

64. Kritzer, P. (2004) Corrosion in high-temperature and supercritical water and aqueous solutions: a review, *The Journal of Supercritical Fluids 29*, 1-29.

65. Kritzer, P. (2001) An assessment of supercritical water oxidation (SCWO) Existing problems, possible solutions and new reactor concepts, *Chemical Engineering Journal 83*, 207-214.

66. Wang, J. (2003) Phase behaviour of binary fluid mixtures: a global phase diagram solely in terms of pure component properties, *Fluid Phase Equilibria 214*, 67-78.

67. Sadus, R. J. (1993) Novel high pressure critical phase transitions in multicomponent fluid mixtures, *Fluid Phase Equilibria 83*, 101-108.

68. Kawasaki, S., Oe, T., Itoh, S., Suzuki, A., Sue, K., and Arai, K. (2007) Flow characteristics of aqueous salt solutions for applications in supercritical water oxidation, *The Journal of Supercritical Fluids 42*, 241-254.

69. Antal,, M. J., Allen, S. G., Schulman, D., Xu, X., and Divilio, R. J. (2000) Biomass Gasification in Supercritical Water, *Industrial & Engineering Chemistry Research 39*, 4040-4053.

70. Loppinet-Serani, A., Aymonier, C., and Cansell, F. (2008) Current and foreseeable applications of supercritical water for energy and the environment, *ChemSusChem 1*, 486-503.

71. Osada, M., Hiyoshi, N., Sato, O., Arai, K., and Shirai, M. (2007) Reaction Pathway for Catalytic Gasification of Lignin in Presence of Sulfur in Supercritical Water, *Energy & Fuels 21*, 1854-1858.

72. Elliott, D. C., Peterson, K. L., Muzatko, D. S., Alderson, E. V., Hart, T. R., and Neuenschwander, G. G. (2004) Effects of trace contaminants on catalytic processing of biomass-derived feedstocks., *Applied Biochemistry and Biotechnology 113-116*, 807-25.

73. Ro, K. S., Cantrell, K., Elliott, D., and Hunt, P. G. (2007) Catalytic Wet Gasification of Municipal and Animal Wastes, *Industrial & Engineering Chemistry Research 46*, 8839-8845.

74. Kruse, A., and Dinjus, E. (2005) Influence of salts during hydrothermal biomass gasification: The role of the catalyzed water-gas shift reaction, *Zeitschrift fur physikalische Chemie*, Oldenbourg *219*, 341-366.

75. van Bennekom, J. G., Venderbosch, R. H., Assink, D., and Heeres, H. J. (2011) Reforming of methanol and glycerol in supercritical water, *The Journal of Supercritical Fluids 58*, 99-113.

76. Jungermann, E. (1991) Introduction. In *Glycerine: a Key Cosmetic Ingredient* (Jungermann, E., and Sonntag, N. O. V., Eds.), pp 1-6, Marcel Dekker, Inc., New York, NY.

77. (2005) Chemical Safety Data: Glycerol, Sigma-Aldrich.

78. (2003) Material Safety Data Sheet - Glycerin, Fisher Scientific.

79. Shimoyama, Y., Iwai, Y., Jin, B., Hirayama, T., and Arai, Y. (2007) Measurement and correlation of vapor–liquid equilibria for methanol+methyl laurate and methanol+methyl myristate systems near critical temperature of methanol, *Fluid Phase Equilibria 257*, 217-222.

80. Brown, R. L., and Stein, S. . (2011) Boiling Point Data. In *NIST Chemistry WebBook, NIST Standard Reference Database Number 69* (Linstrom, P. J., and Mallard, W. G., Eds.), National Institute of Standards and Technology, Gaithersburg, MD.

81. Bondioli, P. (2005) Overview from oil seeds to industrial products: Present and future oleochemistry, *Journal of Synthetic Lubrication 21*, 331-343.

82. Garti, N., Aserin, a., and Zaidman, B. (1981) Polyglycerol esters: Optimization and techno-economic evaluation, *Journal of the American Oil Chemists' Society 58*, 878-883.

83. (2001) Polyglycerol esters of Fatty Acids. In *Food Chemicals Codex, Institute of Medicine of the National Academies* 5th ed., p 343, The National Academic Press, Washington, D.C.

84. Niessner, M., Nilz, C., Hossel, P., Korthrade, S., and Sanner, A. (2001) U.S. Patent # 6231876, Use of water-soluble copolymers as active ingredients in cosmetics, United States Patent Office.

85. Holmberg, K. (1987) High Solids Alkyd Resins, pp 57-72, Marcel Dekker, Inc., New York, NY.

86. Johnson, D. T., and Taconi, K. A. (2009) The Glycerin Glut: Options for the Value-Added Conversion of Crude Glycerol Resulting from Biodiesel Production, *Environmental Progress 26*, 338-348.

87. Pagliaro, M., and Rossi, M. (2010) Glycerol: Properties and Production. In *The Future of Glycerol* 2nd ed., p 7, RSC Publishing, Cambridge, UK.

88. Demirbas, A. (2008) Biodiesel: A Realistic Fuel Alternative for Diesel Engines, p 166, Springer, New York, NY.

89. Huber, G. W., Iborra, S., and Corma, A. (2006) Synthesis of transportation fuels from biomass: chemistry, catalysts, and engineering, *Chemical Reviews 106*, 4044-98.

90. Ma, F., and Hanna, M. A. (1999) Biodiesel production: a review, *Bioresource Technology 70*, 1-15.

91. Knothe, G. (2001) Historical perspectives on vegetable oil-based diesel fuels, *Inform 12*, 1103-1107.

92. Wiltsee, G. (1998) Urban Waste Grease Resource Assessment. In *Report No. NREL/SR-570-26141*, pp 1-10, National Renewable Energy Laboratory, Golden, CO.

93. Gerpen, J. (2005) Biodiesel processing and production, *Fuel Processing Technology 86*, 1097-1107.

94. de Souza, A. C. C., and Silveira, J. L. (2011) Hydrogen production utilizing glycerol from renewable feedstocks—The case of Brazil, *Renewable and Sustainable Energy Reviews*, Elsevier Ltd *15*, 1835-1850.

95. Aimaretti, N., Manuale, D. L., Mazzieri, V. M., Vera, C. R., and Yori, J. C. (2009) Batch Study of Glycerol Decomposition in One-Stage Supercritical Production of Biodiesel, *Energy & Fuels 23*, 1076-1080.

96. Pinnarat, T., and Savage, P. E. (2008) Assessment of Noncatalytic Biodiesel Synthesis Using Supercritical Reaction Conditions, *Industrial & Engineering Chemistry Research 47*, 6801-6808.

97. Haas, M. J., and Foglia, T. A. (2004) Alternate Feedstocks and Technologies for Biodiesel Production. In *The Biodiesel Handbook* (Knothe, G., Gerpen, J., and Krahl, J., Eds.), pp 42-60, AOCS Press, Urbana, IL.

98. Mata, T., Martins, A., and Caetano, N. (2010) Microalgae for biodiesel production and other applications: A review, *Renewable and Sustainable Energy Reviews 14*, 217-232.

99. Kumar, A., Ergas, S., Yuan, X., Sahu, A., Zhang, Q., Dewulf, J., Malcata, F. X., and van Langenhove, H. (2010) Enhanced CO2 fixation and biofuel production via microalgae: recent developments and future directions, *Trends in biotechnology*, Elsevier Ltd *28*, 371-380.

100. Liu, Z.-Y., Wang, G.-C., and Zhou, B.-C. (2008) Effect of iron on growth and lipid accumulation in Chlorella vulgaris, *Bioresource Technology 99*, 4717-22.

101. Hossain, A. B. M. S., Salleh, A., Boyce, A. N., Chowdhury, P., and Naqiuddin, M. (2008) Biodiesel Fuel Production from Algae as Renewable Energy, *American Journal of Biochemistry and Biotechnology 4*, 250-254.

102. Klass, D. L. (1998) Biomass for Renewable Energy, Fuels and Chemicals, pp 341-342, Academic Press, San Diego, CA.

103. Molina Grima, E., Belarbi, E.-H., Acién Fernández, F. G., Robles Medina, A., and Chisti, Y. (2003) Recovery of microalgal biomass and metabolites: process options and economics, *Biotechnology Advances 20*, 491-515.

104. Wang, B., Li, Y., Wu, N., and Lan, C. Q. (2008) CO(2) bio-mitigation using microalgae, *Applied Microbiology and Biotechnology 79*, 707-18.

105. Spolaore, P., Joannis-Cassan, C., Duran, E., and Isambert, A. (2006) Commercial applications of microalgae, *Journal of Bioscience and Bioengineering 101*, 87-96.

106. Pulz, O., and Gross, W. (2004) Valuable products from biotechnology of microalgae, *Applied Microbiology and Biotechnology 65*, 635-48.

107. Sheehan, J., Dunahay, T., Benemann, J., and Roessler, P. (1998) A Look Back at the U.S. Department of Energy ' s Aquatic Species Program - Biodiesel from Algae. In *Report No. NREL/TP-580-24190*, pp 1-13, National Renewable Energy Laboratory, Golden, CO.

108. Pachauri, N., and He, B. (2006) Value-added Utilization of Crude Glycerol from Biodiesel Production: A Survey of Current Research Activities. In *An American society of agricultural and biological engineers (ASABE) meeting presentation*, pp 1-16, Paper # 066223, Portland, OR.

109. (2011) Biodiesel Statistics, *U.S. Department of Energy, Alternative Fuels & Advanced Vehicles Data Center*.

110. (2011) Statistics: The EU biodiesel industry, *European Biodiesel Board*.

111. Bendz, K. (2005) EU-25 Oilseeds and products Biofuels Situation in the European Union 2005. In *GAIN Report No. E35058*, pp 1-11, USDA Foreign Agriculture Service, Washington, D.C.

112. Carriquiry, M. (2007) U.S. Biodiesel Production: Recent Developments and Prospects, *Iowa Ag. Review 13*, 8-9.

113. Bournay, L., Casanave, D., Delfort, B., Hillion, G., and Chodorge, J. (2005) New heterogeneous process for biodiesel production: A way to improve the quality and the value of the crude glycerin produced by biodiesel plants, *Catalysis Today 106*, 190-192.

114. Haas, M. J., McAloon, A. J., Yee, W. C., and Foglia, T. a. (2006) A process model to estimate biodiesel production costs, *Bioresource Technology 97*, 671-8.

115. Thompson, J. C., and He, B. B. (2006) Characterization of Crude Glycerol from Biodiesel Production from Multiple Feedstocks, *Applied Engineering in Agriculture 22*, 261-265.

116. Onwudili, J. A., and Williams, P. T. (2010) Hydrothermal reforming of bio-diesel plant waste: Products distribution and characterization, *Fuel 89*, 501-509.

117. Vaidya, P. D., and Rodrigues, A. E. (2009) Glycerol Reforming for Hydrogen Production: A Review, *Chemical Engineering & Technology 32*, 1463-1469.

118. Dou, B., Dupont, V., Williams, P. T., Chen, H., and Ding, Y. (2009) Thermogravimetric kinetics of crude glycerol, *Bioresource Technology 100*, 2613-20.

119. Pagliaro, M., Ciriminna, R., Kimura, H., Rossi, M., and Della Pina, C. (2007) From glycerol to value-added products, *Angewandte Chemie (International ed. in English) 46*, 4434-40.

120. Stelmachowski, M. (2011) Utilization of Glycerol, A by-product of the transesterification process of vegetable oils: A review, *Ecological Chemistry and Engineering 18*, 9-30.

121. Werpy, T., and Peterson, G. (2004) Top Value Added Chemicals from Biomass. In *Volume 1 — Results of Screening for Potential Candidates from Sugars and Synthesis Gas*, pp 1-68, U.S. Department of Energy, Oak Ridge, TN.

122. Atong, D., Pechyen, C., Aht-Ong, D., and Sricharoenchaikul, V. (2011) Synthetic olivine supported nickel catalysts for gasification of glycerol, *Applied Clay Science*, Elsevier B.V. *53*, 244-253.

123. Demirel-Gulen, S., Lucas, M., and Claus, P. (2005) Liquid phase oxidation of glycerol over carbon supported gold catalysts, *Catalysis Today 102-103*, 166-172.

124. Garcia, R., Besson, M., and Gallezot, P. (1995) Chemoselective catalytic oxidation of glycerol with air on platinum metals, *Applied Catalysis A: General 127*, 165-176.

125. Ciriminna, R., and Pagliaro, M. (2003) One-Pot Homogeneous and Heterogeneous Oxidation of Glycerol to Ketomalonic Acid Mediated by TEMPO, *Advanced Synthesis Catalysis 345*, 383-388.

126. Kimura, H. (2001) Oxidation Assisted New Reaction of Glycerol, *Polymers for Advanced Technologies 12*, 697-710.

127. Aresta, M., Dibenedetto, A., Nocito, F., and Pastore, C. (2006) A study on the carboxylation of glycerol to glycerol carbonate with carbon dioxide: The role of the catalyst, solvent and reaction conditions, *Journal of Molecular Catalysis A: Chemical 257*, 149-153.

128. Okutsa, M., and Kitsuki, T. (2002) U.S. Patent # 6495703, Process for the Preparation of Glycerol Carbonate, United States Patent Office.

129. Kesling Jr., H. S., Karas, L. J., and Liotta Jr., F. J. (1994) U.S. Patent # 5308365, Diesel Fuel, United States Patent Office.

130. Gupta, V. P. (1995) U.S. Patent # 5476971, Glycerine Ditertiary Butyl Ether Preparation, United States Patent Office.

131. Noureddlni, H., Dailey, W. R., and Hunt, B. A. (1998) Production of Ethers of Glycerol from Crude Glycerol: The By-Product of Biodiesel Production. In *Chemical and Biomolecular Engineering Research and Publications, Papers in Biomaterials*, pp 1-14, University of Nebraska - Lincoln, Lincoln, NE.

132. Schwenk, E., Gehrke, M., and Aichner, F. (1933) U.S. Patent # 1916743, Production of Acrolein, United States Patent Office.

133. Kusunoki, Y., Miyazawa, T., Kunimori, K., and Tomishige, K. (2005) Highly active metal–acid bifunctional catalyst system for hydrogenolysis of glycerol under mild reaction conditions, *Catalysis Communications 6*, 645-649.

134. Miyazawa, T., Kusunoki, Y., Kunimori, K., and Tomishige, K. (2006) Glycerol conversion in the aqueous solution under hydrogen over Ru/C + an ion-exchange resin and its reaction mechanism, *Journal of Catalysis 240*, 213-221.

135. Maglinao, R. L., and He, B. B. (2011) Catalytic Thermochemical Conversion of Glycerol to Simple and Polyhydric Alcohols Using Raney Nickel Catalyst, *Industrial & Engineering Chemistry Research* 6028-6033.

136. Buhler, W., Dinjus, E., Ederer, H., Kruse, A., and Mas, C. (2002) Ionic reactions and pyrolysis of glycerol as competing reaction pathways in near- and supercritical water, *The Journal of Supercritical Fluids 22*, 37-53.

137. Ott, L., Bicker, M., and Vogel, H. (2006) Catalytic dehydration of glycerol in sub- and supercritical water: a new chemical process for acrolein production, *Green Chemistry 8*, 214-220.

138. Ramayya, S., Brittain, A., DeAlmeida, C., Mok, W., and Antal, M. J. J. (1987) Acid-catalysed dehydration of alcohols in supercritical water, *Fuel 66*, 1364-1371.

139. Watanabe, M., Iida, T., Aizawa, Y., Aida, T. M., and Inomata, H. (2007) Acrolein synthesis from glycerol in hot-compressed water, *Bioresource technology 98*, 1285-90.

140. Chai, S., Wang, H., Liang, Y., and Xu, B. (2007) Sustainable production of acrolein: Gas-phase dehydration of glycerol over Nb2O5 catalyst, *Journal of Catalysis 250*, 342-349.

141. Ning, L., Ding, Y., Chen, W., Gong, L., Lin, R., Yuan, L., and Xin, Q. (2008) Glycerol dehydration to acrolein over activated carbon-supported silicotungstic acids, *Chinese Journal of Catalysis 29*, 212-214.

142. Ulgen, A., and Hoelderich, W. (2009) Conversion of Glycerol to Acrolein in the Presence of WO3/ZrO2 Catalysts, *Catalysis Letters 131*, 122-128.

143. Tsukuda, E., Sato, S., Takahashi, R., and Sodesawa, T. (2007) Production of acrolein from glycerol over silica-supported heteropoly acids, *Catalysis Communications 8*, 1349-1353.

144. Wright, C. R. A. (1894) Fixed Oils, Fats, Butters and Waxes: Their Preperation and Properties, and the Manufacture therefrom of Candles, Soaps, and other Products, p 513, Charles Griffin & Co., London.

145. Qadariyah, L., Mahfud, Sumarno, Machmudah, S., Wahyudiono, Sasaki, M., and Goto, M. (2011) Degradation of glycerol using hydrothermal process, *Bioresource technology 102*, 9267-71.

146. Antal, M. J. J., Mok, W. S. L., Roy, J. C., and Raissi, A. T. (1985) Pyrolytic sources of hydrocarbons from biomass, *Journal of Analytical and Applied Pyrolysis 8*, 291-303.

147. Stein, Y. S., Antal, M. J. J., and Jones Jr., M. (1983) A study of the gas-phase pyrolysis of glycerol, *Journal of Analytical and Applied Pyrolysis 4*, 283-296.

148. Pathak, K., Reddy, K. M., Bakhshi, N. N., and Dalai, a. K. (2010) Catalytic conversion of glycerol to value added liquid products, *Applied Catalysis A: General 372*, 224-238.

149. Nimlos, M. R., Blanksby, S. J., Qian, X., Himmel, M. E., and Johnson, D. K. (2006) Mechanisms of glycerol dehydration, *The journal of physical chemistry. A 110*, 6145-56.

150. Paine, J. B. I., Pithawalla, Y. B., Naworal, J. D., and Thomas, C. E. J. (2007) Carbohydrate pyrolysis mechanisms from isotopic labeling Part 1: The pyrolysis of glycerin: Discovery of competing fragmentation mechanisms affording acetaldehyde and formaldehyde and the implications for carbohydrate pyrolysis, *Journal of Analytical and Applied Pyrolysis 80*, 297-311.

151. Bieble, H., Menzel, A. P., Zeng, A. P., and Deckwer, W. D. (1999) Microbial production of 1,3-propanediol, *Applied Microbiology and Biotechnology 52*, 289-297.

152. Deckwer, W. D. (1995) Microbial conversion of glycerol to 1,3-propanediol, *FEMS Microbiology Reviews 16*, 143-149.

153. Zeng, A. P. (1996) Pathway and kinetic analysis of 1,3-propanediol production from glycerol fermentation by Clostridium butyricum, *Bioprocess Engineering 14*, 169-175.

154. Ashby, R. D., Nuñez, A., Solaiman, D. K. Y., and Foglia, T. A. (2005) Sophorolipid biosynthesis from a biodiesel co-product stream, *Journal of the American Oil Chemists Society 82*, 625-630.

155. Papanikolaou, S., and Aggelis, G. (2002) Lipid production by Yarrowia lipolytica growing on industrial glycerol in a single-stage continuous culture, *Bioresource Technology 82*, 43-49.

156. Papanikolaou, S., Muniglia, L., Chevalot, I., Aggelis, G., and Marc, I. (2002) Yarrowia lipolytica as a potential producer of citric acid from raw glycerol, *Journal of Applied Microbiology 92*, 737-44.

157. Forsberg, C. (1987) Production of 1,3-propanediol from glycerol by Clostridium acetobutylicum and Other clostridium species, *Applied and Environmental Microbiology 53*, 639-643.

158. Bieble, H. (2001) Fermentation of glycerol by Clostridium pasteurianum— Batch and continuous culture studies, *Journal of Industrial Microbiology and Biotechnology 27*, 18-26.

159. Dabrock, B., Bahl, H., and Gottschalk, G. (1992) Parameters affecting solvent production by Clostridium pasteurianum, *Applied and Environmental Microbiology 58*, 1233-1239.

160. Saint-Amans, S., Perlot, P., Goma, G., and Soucaille, P. (1994) High production of 1,3-propanediol from glycerol by Clostridium butyricum VPI 3266 in a simply controlled fed-batch system, *Biotechnology Letters 16*, 831-836.

161. Himmi, E. H., Bories, A., and Barbirato, F. (1999) Nutrient requirements for glycerol conversion to 1,3-propanediol by Clostridium butyricum, *Bioresource Technology 67*, 123-128.

162. Sheldon, R. A. (1983) Chemicals from synthesis gas: Catalytic reactions of CO and H2, pp 1-6, D. Reidel Publishing Co., Dordrecht, The Netherlands.

163. Song, C. (2010) Introduction to Hydrogen and Syngas Production and Purification Technologies. In *Hydrogen and Syngas Production and Purification Technologies* (Lu, K., Song, C., and Subramani, V., Eds.), pp 1-12, John Wiley & Sons, Inc., Hoboken, NJ.

164. Muradov, N. Z. (2009) Production of Hydrogen from Hydrocarbons. In *Hydrogen Fuel: Production, Storage and Transport* (Gupta, R. B., Ed.), pp 33-47, Taylor & Francis, Boca Raton FL.

165. Lee, S. (1997) Methane and its Derivatives, pp 33-50, Marcel Dekker, Inc., New York, NY.

166. Mueller-Langer, F., Tzimas, E., Kaltschmitt, M., and Peteves, S. (2007) Techno-economic assessment of hydrogen production processes for the hydrogen economy for the short and medium term, *International Journal of Hydrogen Energy 32*, 3797-3810.

167. Rostrup-Nielsen, J. R., Dybkjaer, I., and Christiansen, L. J. (1992) Steam reforming opportunities and limits of the technology. In *Chemical Reactor Technology for Environmentally Safe Reactors and Products* (De Lasa, H. I., Dogu, G., and Ravella, A., Eds.), pp 249-281, Kluwer Academic Publishers, Dordrecht, The Netherlands.

168. Contadini, J. F., Diniz, C. V., Sperling, D., and Moore, R. M. (2000) Hydrogen production plants: emissions and thermal efficiency analysis. In *Institute of Transportation Studies*, pp 1-12, Ref# UCD-ITS-RR-00-16, Unviersity of California.

169. Aasberg-Petersen, K. (2006) Synthesis Gas. In *Encyclopedia of Chemical Processing* (Lee, S., Ed.), pp 2933-2946, Taylor & Francis, New York, NY.

170. Dogan, M., Posarac, D., and Grace, J. (2003) Modeling of Autothermal Steam Methane Reforming in a Fluidized Bed Membrane Reactor, *International Journal of Chemical Reactor Engineering 1*, 1-12.

171. Spath, P. L., and Dayton, D. C. (2003) Preliminary Screening — Technical and Economic Assessment of Synthesis Gas to Fuels and Chemicals with Emphasis on the Potential for Biomass-Derived Syngas. In *Report No. NREL/TP-510-34929*, p 3, National Renewable Energy Laboratory, Golden, CO.

172. Lee, S. (1996) Alternative Fuels, Taylor & Francis, Philadelphia, PA.

173. Liu, K., Cui, Z., and Fletcher, T. H. (2010) Coal Gasification. In *Hydrogen and Syngas Production and Purification Technologies* (Liu, K., Song, C., and Subramani, V., Eds.), pp 156-178, John Wiley & Sons, Inc., Hoboken, NJ.

174. Nath, K., and Das, D. (2003) Hydrogen from biomass, *Current Science 85*, 265-271.

175. Chen, G., and Zhao, L. (2011) Preliminary investigation on hydrogen-rich gas production by co-steam-reforming of biomass and crude glycerin, *International Journal of Hydrogen Energy*, Elsevier Ltd 1-9.

176. Rapagna, S., Jand, N., Kiennemann, A., and Foscolo, P. U. (2000) Steam-gasification of biomass in a fluidised-bed of olivine particles, *Biomass and Bioenergy 19*, 187-197.

177. Saha, R. K., Gupta, B. R., and Sen, P. (1984) Production of hydrogen in an autothermal fluidized gasifier, *International Journal of Hydrogen Energy 9*, 483-486.

178. Milne, T. A., Evans, R. J., and Abatzoglou, N. (1998) Biomass Gasifier " Tars ": Their Nature, Formation , and Conversion. In *Report No. NREL/TP-570-25357*, p v, National Renewable Energy Laboratory, Golden, CO.

179. Calzavara, Y., Joussot-Dubien, C., Boissonnet, G., and Sarrade, S. (2005) Evaluation of biomass gasification in supercritical water process for hydrogen production, *Energy Conversion and Management 46*, 615-631.

180. Rustamov, V. R., Abdullayev, K. M., Aliyev, F. G., and Kerimov, V. K. (1998) Hydrogen formation from biomass using solar energy, *International Journal of Hydrogen Energy 23*, 649-652.

181. Hathaway, B. J., Davidson, J. H., and Kittelson, D. B. (2011) Solar Gasification of Biomass: Kinetics of Pyrolysis and Steam Gasification in Molten Salt, *Journal of Solar Energy Engineering 133*, 1-9.

182. Caglar, A., and Demirbas, A. (2001) Hydrogen-Rich Gaseous Products from Tea Waste by Pyrolysis, *Energy Sources, Part A: Recovery, Utilization, and Environmental Effects 23*, 739-746.

183. Wang, D., Czernik, S., and Chornet, E. (1998) Production of Hydrogen from Biomass by Catalytic Steam Reforming of Fast Pyrolysis Oils, *Energy & Fuels 12*, 19-24.

184. Wang, X., Wang, N., Zhao, J., and Wang, L. (2010) Thermodynamic analysis of propane dry and steam reforming for synthesis gas or hydrogen production, *International Journal of Hydrogen Energy 35*, 12800-12807.

185. Wang, X., Li, M., Wang, M., Wang, H., Li, S., Wang, S., and Ma, X. (2009) Thermodynamic analysis of glycerol dry reforming for hydrogen and synthesis gas production, *Fuel 88*, 2148-2153.

186. García-Serna, J., García-Merino, E., and Cocero, M. J. (2007) Gasification of charcoal using supercritical CO2 at high pressures, *The Journal of Supercritical Fluids 43*, 228-235.

187. Matos, J., Díaz, K., García, V., Cordero, T. C., and Brito, J. L. (2006) Methane Transformation in Presence of Carbon Dioxide on Activated Carbon Supported Nickel–calcium Catalysts, *Catalysis Letters 109*, 163-169.

188. Courson, C., Makaga, E., Petit, C., and Kiennemann, a. (2000) Development of Ni catalysts for gas production from biomass gasification. Reactivity in steam- and dry-reforming, *Catalysis Today 63*, 427-437.

189. Jankhah, S., Abatzoglou, N., and Gitzhofer, F. (2008) Thermal and catalytic dry reforming and cracking of ethanol for hydrogen and carbon nanofilaments' production, *International Journal of Hydrogen Energy 33*, 4769-4779.

190. De Oliveira-Vigier, K., Abatzoglou, N., and Gitzhofer, F. (2005) Dry-Reforming of Ethanol in the Presence of a 316 Stainless Steel Catalyst, *Canadian Journal of Chemical Engineering 83*, 978-984.

191. Datar, R., Huang, J., Maness, P., Mohagheghi, A., Czernik, S., and Chornet, E. (2007) Hydrogen production from the fermentation of corn stover biomass pretreated with a steam-explosion process, *International Journal of Hydrogen Energy 32*, 932-939.

192. Ntaikou, I., Gavala, H., Kornaros, M., and Lyberatos, G. (2008) Hydrogen production from sugars and sweet sorghum biomass using Ruminococcus albus, *International Journal of Hydrogen Energy 33*, 1153 - 1163.

193. Geng, A., He, Y., Qian, C., Yan, X., and Zhou, Z. (2010) Effect of key factors on hydrogen production from cellulose in a co-culture of Clostridium thermocellum and Clostridium thermopalmarium, *Bioresource Technology 101*, 4029-33.

194. Kivisto, A., Santala, V., and Karp, M. (101AD) Hydrogen production from glycerol using halophilic fermentative bacteria, *Bioresource Technology 22*, 8671-8677.

195. Kruse, A., Meier, D., Rimbrecht, P., and Schacht, M. (2000) Gasification of Pyrocatechol in Supercritical Water in the Presence of Potassium Hydroxide, *Industrial & Engineering Chemistry Research 39*, 4842-4848.

196. Biloen, P., and Sachtler, W. M. H. (1981) Mechanism of Hydrocarbon Synthesis over Fischer-Tropsch Catalysts, *Advances in Catalysis 30*, 165-214.

197. Dry, M. (2002) The Fischer–Tropsch process: 1950–2000, *Catalysis Today 71*, 227-241.

198. Ahmed, S. (2005) Water-Gas Shift Reaction over Cu-Based Mixed Oxide Catalysts. In *15th Saudi-Japan Joint Symposium*, pp 1-6, Dhahran, Saudi Arabia.

199. Picou, J. W., Stever, M. S., Bouquet, J., Wenzel, J. E., and Lee, S. (2011) Kinetics of the noncatalytic water gas shift reaction in supercritical water, *Energy Sources, Part A: Recovery, Utilization, and Environmental Effects* In Press.

200. Yokota, K., and Fujimoto, K. (1989) Supercritical phase Fischer-Tropsch synthesis reaction, *Fuel 68*, 255-256.

201. Yokota, K., and Fujimoto, K. (1991) Supercritical-phase Fischer-Tropsch synthesis reaction. 2. The effective diffusion of reactant and products in the supercritical-phase reaction, *Industrial & Engineering Chemistry Research 30*, 95-100.

202. Leckel, D. (2009) Diesel Production from Fischer-Tropsch: The Past, the Present, and New Concepts, *Energy & Fuels 23*, 2342-2358.

203. Soares, R. R., Simonetti, D. A., and Dumesic, J. A. (2006) Glycerol as a source for fuels and chemicals by low-temperature catalytic processing., *Angewandte Chemie (International ed. in English) 45*, 3982-5.

204. Hamelinck, C., Faaij, A., Denuil, H., and Boerrigter, H. (2004) Production of FT transportation fuels from biomass; technical options, process analysis and optimization, and development potential, *Energy 29*, 1743-1771.

205. LeBlanc, J. R., Schneider III, R. V., and Strait, R. B. (1994) Production of Methanol. In *Methanol Production and Use* (Cheng, W. H., and Kung, H. H., Eds.), pp 51-122, Marcel Dekker, Inc., New York, NY.

206. Lee, S. (1990) Methanol Synthesis Technology, CRC Press, Boca Raton FL.

207. Klier, K., Chatikavanij, V., Herman, R. G., and Simmons, G. W. (1982) Catalytic synthesis of methanol from CO/H2: IV. The effects of carbon dioxide, *Journal of Catalysis 74*, 343-360.

208. Olah, G. A., Goeppert, A., and Prakash, G. K. S. (2009) Chemical recycling of carbon dioxide to methanol and dimethyl ether: from greenhouse gas to renewable, environmentally carbon neutral fuels and synthetic hydrocarbons, *The Journal of Organic Chemistry 74*, 487-98.

209. Kung, H. H., and Smith, K. J. (1994) Methanol to Chemicals. In *Methanol Production and Use* (Cheng, W.-H., and Kung, H. H., Eds.), pp 175-204, Marcel Dekker, Inc., New York, NY.

210. Mao, D., Yang, W., Xia, J., Zhang, B., Song, Q., and Chen, Q. (2005) Highly effective hybrid catalyst for the direct synthesis of dimethyl ether from syngas with magnesium oxide-modified HZSM-5 as a dehydration component, *Journal of Catalysis 230*, 140-149.

211. Aguayo, a, Erena, J., Sierra, I., Olazar, M., and Bilbao, J. (2005) Deactivation and regeneration of hybrid catalysts in the single-step synthesis of dimethyl ether from syngas and CO, *Catalysis Today 106*, 265-270.

212. Arcoumanis, C., Bae, C., Crookes, R., and Kinoshita, E. (2008) The potential of di-methyl ether (DME) as an alternative fuel for compression-ignition engines: A review, *Fuel 87*, 1014-1030.

213. Hammond, C. R. (1976) The Elements. In *CRC Handbook of Chemistry and Physics* (Weast, R. C., Ed.) 57th ed., p B-26, CRC Press, Cleveland, OH.

214. (2011) Hydrogen Production, *U.S. Department of Energy, Hydrogen Analysis Research Center*.

215. Roy, A., Watson, S., and Infield, D. (2006) Comparison of electrical energy efficiency of atmospheric and high-pressure electrolysers, *International Journal of Hydrogen Energy 31*, 1964-1979.

216. Szklo, A., and Schaeffer, R. (2007) Fuel specification, energy consumption and CO2 emission in oil refineries, *Energy 32*, 1075-1092.

217. Lapinski, M., Baird, L., and James, R. (2004) UOP Platforming Process. In *Handbook of Petroleum Refining Processes* (Meyers, R. A., Ed.) 3rd ed., pp 4.01-4.31, McGraw-Hill, New York, NY.

218. Liu, K., Deluga, G. D., Bitsch-Larsen, A., Schmidt, L. D., and Zhang, L. (2010) Catalytic Partial Oxidation and Autothermal Reforming. In *Hydrogen and Syngas Production and Purification Technologies* (Lu, K., Song, C., and Subramani, V., Eds.), pp 127-130, John Wiley & Sons, Inc., Hoboken, NJ.

219. Hager, T. (2008) The Alchemy of Air, pp 1-42, Harmony Books, New York, NY.

220. Evans, L. T. (1998) Feeding the Ten Billion - Plants and Population Growth, p 127, Cambridge University Press, Cambridge, UK.

221. Trewavas, A. (2002) Malthus foiled again and again, *Nature 418*, 668-70.

222. Perkins, J. H. (1997) Geopolitics and the Green Revolution: Wheat, Genes and the Cold War, pp 210-255, Oxford University Press, New York, NY.

223. Joshi, M. V. (1999) Green Revolution and its Impacts, pp 1-24, A.P.H Publishing Co., New Delhi.

224. Chiras, D. D. (2001) Environmental Science. Creating a Sustainable Future (Hauck, J. H., Ed.) 6th ed., pp 148-167, Jones and Bartlett Publishers, Sudbury, MA.

225. (2010) Historical Estimates of World Population, *US Census Bureau*.

226. Appl, M. (2006) Ammonia, *Ullmann's Encyclopedia of Industrial Chemistry*, Wiley Online Library.

227. (2011) Mineral Commodity Summaries 2011, *US Geological Survey* 112.

228. Huang, W. (2007) Impact of Rising Natural Gas Prices on U.S. Ammonia Supply, Economic Research Service, U.S. Department of Agriculture.

229. White, C., Steeper, R., and Lutz, A. (2006) The hydrogen-fueled internal combustion engine: a technical review, *International Journal of Hydrogen Energy 31*, 1292-1305.

230. Carrette, L., Friedrich, K. A., and Stimming, U. (2001) Fuel Cells - Fundamentals and Applications, *Fuel Cells 1*, 5-39.

231. Sammes, N. ., Bove, R., and Pusz, J. (2006) Solid Oxide Fuel Cells. In *Fuel Cell Technology: Reaching towards commercialization* (Sammes, N. M., Ed.), pp 1-20, Springer, London.

232. Slinn, M., Kendall, K., Mallon, C., and Andrews, J. (2008) Steam reforming of biodiesel by-product to make renewable hydrogen, *Bioresource Technology 99*, 5851-8.

233. Hirscher, M. (2010) Handbook of Hydrogen Storage: New Materials for Future Energy Storage, Wiley-VCH, Weinheim, Germany.

234. (2011) Fuel Cells, *US Department of Energy, Energy Efficiency & Renewable Energy*.

235. Gutiérrez Ortiz, F. J., Ollero, P., and Serrera, A. (2011) Thermodynamic analysis of the autothermal reforming of glycerol using supercritical water, *International Journal of Hydrogen Energy 36*, 12186-12199.

236. (2011) Green Hydrogen, *The Linde Group, Biomass to Hydrogen (BTH) - Corporate Responsibility, Engineering Division, Biomass*.

237. Adhikari, S., Fernando, S., and Haryanto, A. (2007) Production of hydrogen by steam reforming of glycerin over alumina-supported metal catalysts, *Catalysis Today 129*, 355-364.

238. Adhikari, S., Fernando, S. D., To, S. D. F., Bricka, R. M., Steele, P. H., and Haryanto, A. (2008) Conversion of Glycerol to Hydrogen via a Steam Reforming Process over Nickel Catalysts, *Energy & Fuels 22*, 1220-1226.

239. Fierro, V., Klouz, V., Akdim, O., and Mirodatos, C. (2002) Oxidative reforming of biomass derived ethanol for hydrogen production in fuel cell applications, *Catalysis Today 75*, 141-144.

240. Ramírez de la Piscina, P., and Homs, N. (2008) Use of biofuels to produce hydrogen (reformation processes), *Chemical Society Reviews 37*, 2459-67.

241. Buffoni, I. N., Pompeo, F., Santori, G. F., and Nichio, N. N. (2009) Nickel catalysts applied in steam reforming of glycerol for hydrogen production, *Catalysis Communications 10*, 1656-1660.

242. Davda, R. R., Shabaker, J. W., Huber, G. W., Cortright, R. D., and Dumesic, J. A. (2005) A review of catalytic issues and process conditions for renewable hydrogen and alkanes by aqueous-phase reforming of oxygenated hydrocarbons over supported metal catalysts, *Applied Catalysis B: Environmental 56*, 171-186.

243. Adhikari, S., Fernando, S., and Haryanto, A. (2007) A Comparative Thermodynamic and Experimental Analysis on Hydrogen Production by Steam Reforming of Glycerin, *Energy & Fuels 21*, 2306-2310.

244. Adhikari, S., Fernando, S., Gwaltney, S., Filipto, S., Markbricka, R., Steele, P., and Haryanto, A. (2007) A thermodynamic analysis of hydrogen production by steam reforming of glycerol, *International Journal of Hydrogen Energy 32*, 2875-2880.

245. Rossi, C., Alonso, C., Antunes, O., Guirardello, R., and Cardozofilho, L. (2009) Thermodynamic analysis of steam reforming of ethanol and glycerine for hydrogen production, *International Journal of Hydrogen Energy 34*, 323-332.

246. Wang, X., Li, S., Wang, H., Liu, B., and Ma, X. (2008) Thermodynamic Analysis of Glycerin Steam Reforming, *Energy & Fuels 22*, 4285-4291.

247. Pairojpiriyakul, T., Kiatkittipong, W., Wiyaratn, W., Soottitantawat, A., Arpornwichanop, A., Laosiripojana, N., Croiset, E., and Assabumrungrat, S. (2010) Effect of mode of operation on hydrogen production from glycerol at thermal neutral conditions: Thermodynamic analysis, *International Journal of Hydrogen Energy 35*, 10257-10270.

248. Kunkes, E. L., Soares, R. R., Simonetti, D. A., and Dumesic, J. A. (2009) An integrated catalytic approach for the production of hydrogen by glycerol reforming coupled with water-gas shift, *Applied Catalysis B: Environmental 90*, 693-698.

249. Hirai, T., Ikenaga, N., Miyake, T., and Suzuki, T. (2005) Production of Hydrogen by Steam Reforming of Glycerin on Ruthenium Catalyst, *Energy & Fuels 19*, 1761-1762.

250. Zhang, B., Tang, X., Li, Y., Xu, Y., and Shen, W. (2007) Hydrogen production from steam reforming of ethanol and glycerol over ceria-supported metal catalysts, *International Journal of Hydrogen Energy 32*, 2367-2373.

251. Dou, B., Rickett, G. L., Dupont, V., Williams, P. T., Chen, H., Ding, Y., and Ghadiri, M. (2010) Steam reforming of crude glycerol with in situ CO2 sorption., *Bioresource Technology 101*, 2436-42.

252. Dou, B., Dupont, V., Rickett, G., Blakeman, N., Williams, P. T., Chen, H., Ding, Y., and Ghadiri, M. (2009) Hydrogen production by sorption-enhanced steam reforming of glycerol, *Bioresource Technology 100*, 3540-3547.

253. Iulianelli, A., Longo, T., Liguori, S., and Basile, A. (2010) Production of hydrogen via glycerol steam reforming in a Pd-Ag membrane reactor over Co-Al 2 O 3 catalyst, *Asia-Pacific Journal of Chemical Engineering 5*, 138-145.

254. Cortright, R. D., and Dumesic, J. A. (2011) Method for producing bio-fuel that integrates heat from carbon-carbon bond-forming reactions to drive biomass gasification reactions, U.S. Patent Application Publication, Pub. No. US 2011/0086927 A1, United States Patent Office.

255. Lehnert, K., and Claus, P. (2008) Influence of Pt particle size and support type on the aqueous-phase reforming of glycerol, *Catalysis Communications 9*, 2543-2546.

256. Huber, G. W., Shabaker, J. W., and Dumesic, J. (2003) Raney Ni-Sn catalyst for H2 production from biomass-derived hydrocarbons, *Science 300*, 2075-7.

257. Menezes, A. O., Rodrigues, M. T., Zimmaro, A., Borges, L. E. P., and Fraga, M. A. (2011) Production of renewable hydrogen from aqueous-phase reforming of glycerol over Pt catalysts supported on different oxides, *Renewable Energy 36*, 595-599.

258. Pompeo, F., Santori, G., and Nichio, N. N. (2010) Hydrogen and/or syngas from steam reforming of glycerol. Study of platinum catalysts, *International Journal of Hydrogen Energy 35*, 8912-8920.

259. Shabaker, J. ., Huber, G. ., and Dumesic, J. (2004) Aqueous-phase reforming of oxygenated hydrocarbons over Sn-modified Ni catalysts, *Journal of Catalysis 222*, 180-191.

260. Cheng, C. K., Foo, S. Y., and Adesina, A. A. (2010) Hydrogen rich synthesis gas production over Co/Al2O3 catalyst via glycerol steam reforming, *Catalysis Communications 12*, 292-298.

261. King, D. L., Zhang, L., Xia, G., Karim, A. M., Heldebrant, D. J., Wang, X., Peterson, T., and Wang, Y. (2010) Aqueous phase reforming of glycerol for hydrogen production over Pt–Re supported on carbon, *Applied Catalysis B: Environmental 99*, 206-213.

262. Atong, D., Ausadasuk, S., and Sricharoenchaikul, V. (2010) Fuel gas production by gasification of glycerol waste over perovskite type oxide catalysts, *International Journal of Chemical Reactor Engineering 8*, A49.

263. Wen, G., Xu, Y., Ma, H., Xu, Z., and Tian, Z. (2008) Production of hydrogen by aqueous-phase reforming of glycerol, *International Journal of Hydrogen Energy*, Elsevier Ltd *33*, 6657-6666.

264. Wawrzetz, A., Peng, B., Hrabar, A., Jentys, A., Lemonidou, A. A., and Lercher, J. A. (2010) Towards understanding the bifunctional hydrodeoxygenation and aqueous phase reforming of glycerol, *Journal of Catalysis 269*, 411-420.

265. Luo, N., Zhao, X., Cao, F., Xiao, T., and Fang, D. (2007) Thermodynamic Study on Hydrogen Generation from Different Glycerol Reforming Processes, *Energy & Fuels 21*, 3505-3512.

266. Valliyappan, T. (2004) Hydrogen or Syn Gas Production from Glycerol Using Pyrolysis and Steam Gasification Process, University of Saskatchewan.

267. Chakinala, A. G., Brilman, D. W. F. (Wim), van Swaaij, W. P. M., and Kersten, S. R. A. (2010) Catalytic and Non-catalytic Supercritical Water Gasification of Microalgae and Glycerol, *Industrial & Engineering Chemistry Research 49*, 1113-1122.

268. Xu, X., Matsumura, Y., Stenberg, J., and Antal, M. J. (1996) Carbon-Catalyzed Gasification of Organic Feedstocks in Supercritical Water, *Industrial & Engineering Chemistry Research 35*, 2522-2530.

269. Byrd, A., Pant, K., and Gupta, R. (2008) Hydrogen production from glycerol by reforming in supercritical water over Ru/Al2O3 catalyst, *Fuel 87*, 2956-2960.

270. Matsumura, Y., Minowa, T., Potic, B., Kersten, S., Prins, W., Vanswaaij, W., Vandebeld, B., Elliott, D., Neuenschwander, G., and Kruse, A. (2005) Biomass gasification in near- and super-critical water: Status and prospects, *Biomass and Bioenergy 29*, 269-292.

271. Kersten, S. R. A., Potic, B., Prins, W., and Van Swaaij, W. P. M. (2006) Gasification of Model Compounds and Wood in Hot Compressed Water, *Industrial & Engineering Chemistry Research 45*, 4169-4177.

272. May, A., Salvadó, J., Torras, C., and Montané, D. (2010) Catalytic gasification of glycerol in supercritical water, *Chemical Engineering Journal 160*, 751-759.

273. Xu, D., Wang, S., Hu, X., Chen, C., Zhang, Q., and Gong, Y. (2009) Catalytic gasification of glycine and glycerol in supercritical water, *International Journal of Hydrogen Energy 34*, 5357-5364.

274. Stever, M. S. (2011) Effects of a nickel reactor liner and other reaction variables during supercritical water reformation of glycerin, Missouri University of Science and Technology.

275. Yu, D., Aihara, M., and Antal, M. J. (1993) Hydrogen production by steam reforming glucose in supercritical water, *Energy & Fuels 7*, 574-577.

276. Arita, T., Nakahara, K., Nagami, K., and Kajimoto, O. (2003) Hydrogen generation from ethanol in supercritical water without catalyst, *Tetrahedron Letters 44*, 1083-1086.

277. Lachance, R. P. (2005) A Fundamental Study of Model Fuel Conversion Reactions in Sub and Supercritical Water, Massachusetts Institute of Technology.

278. Yang, H. H., and Eckert, C. A. (1988) Homogeneous catalysis in the oxidation of p-chlorophenol in supercritical water, *Industrial & Engineering Chemistry Research 27*, 2009-2014.

279. Bustamante, F., Enick, R. M., Killmeyer, R. P., Howard, B. H., Rothenberger, K. S., Cugini, A. V., Morreale, B. D., and Ciocco, M. V. (2005) Uncatalyzed and wall-catalyzed forward water-gas shift reaction kinetics, *AIChE Journal 51*, 1440-1454.

280. Benjamin, K. M., and Savage, P. E. (2005) Supercritical Water Oxidation of Methylamine, *Industrial & Engineering Chemistry Research 44*, 5318-5324.

281. Gadhe, J. B., and Gupta, R. B. (2005) Hydrogen Production by Methanol Reforming in Supercritical Water: Suppression of Methane Formation, *Industrial & Engineering Chemistry Research 44*, 4577-4585.

282. (2001) Hastelloy C-276 Alloy, Report H-2002D, Haynes International Corrosion-Resistant Alloys.

283. (2008) Haynes 282 Alloy, Report H-3173, p 3, Haynes International Corrosion-Resistant Alloys.

284. (2006) Inconel alloy 625, Publication Number SMC-063, Special Metals Corporation.

285. Chen, H., Ding, Y., Cong, N. T., Dou, B., Dupont, V., Ghadiri, M., and Williams, P. T. (2011) A comparative study on hydrogen production from steam-glycerol reforming: thermodynamics and experimental, *Renewable Energy 36*, 779-788.

286. Adhikari, S., Fernando, S. D., and Haryanto, A. (2009) Hydrogen production from glycerol: An update, *Energy Conversion and Management 50*, 2600-2604.

287. Klein, M. T., Mentha, Y. G., and Torry, L. A. (1992) Decoupling substituent and solvent effects during hydrolysis of substituted anisoles in supercritical water, *Industrial & Engineering Chemistry Research 31*, 182-187.

288. Laino, T., Tuma, C., Curioni, A., Jochnowitz, E., and Stolz, S. (2011) A revisited picture of the mechanism of glycerol dehydration, *The journal of physical chemistry. A 115*, 3592-5.

289. Castro, C. E., and Rust, F. F. (1961) Thermal Decomposition of Acrolein. The Attack of Methyl and t-Butoxy Free Radicals on Acrolein, *Journal of the American Chemical Society 83*, 4928-4932.

290. de Jesus, P., Boukis, N., Kraushaarczarnetzki, B., and Dinjus, E. (2006) Gasification of corn and clover grass in supercritical water, *Fuel 85*, 1032-1038.

291. Nagai, Y., Morooka, S., Matubayasi, N., and Nakahara, M. (2004) Mechanisms and Kinetics of Acetaldehyde Reaction in Supercritical Water: Noncatalytic Disproportionation, Condensation, and Decarbonylation, *The Journal of Physical Chemistry A 108*, 11635-11643.

292. Klein, R., Scheer, M. D., and Schoen, L. J. (1955) The Pyrolysis of Formaldehyde, *Journal of American Chemistry Society 78*, 50-52.

293. Watanabe, M. (2003) Acidity and basicity of metal oxide catalysts for formaldehyde reaction in supercritical water at 673 K, *Applied Catalysis A: General 245*, 333-341.

294. Holgate, H. R., Webley, P. A., Tester, J. W., and Helling, R. K. (1992) Carbon monoxide oxidation in supercritical water: the effects of heat transfer and the water-gas shift reaction on observed kinetics, *Energy & Fuels 6*, 586-597.

295. Rice, S. F., Steeper, R. R., and Aiken, J. D. (1998) Water Density Effects on Homogeneous Water-Gas Shift Reaction Kinetics, *The Journal of Physical Chemistry A 102*, 2673-2678.

296. Sato, T., Kurosawa, S., Smith, R., Adschiri, T., and Arai, K. (2004) Water gas shift reaction kinetics under noncatalytic conditions in supercritical water, *The Journal of Supercritical Fluids 29*, 113-119.

297. Helling, R. K., and Tester, J. W. (1987) Oxidation kinetics of carbon monoxide in supercritical water, *Energy & Fuels 1*, 417-423.

298. Fatsikostas, A. (2004) Reaction network of steam reforming of ethanol over Ni-based catalysts, *Journal of Catalysis 225*, 439-452.

299. Kolb, G. (2008) Fuel Processing for Fuel Cells, p 51, Wiley-VCH, Weinheim, Germany.

300. Gutiérrez Ortiz, F. J., Ollero, P., Serrera, A., and Sanz, A. (2011) Thermodynamic study of the supercritical water reforming of glycerol, *International Journal of Hydrogen Energy 36*, 8994-9013.

301. Authayanun, S., Arpornwichanop, A., Paengjuntuek, W., and Assabumrungrat, S. (2010) Thermodynamic study of hydrogen production from crude glycerol autothermal reforming for fuel cell applications, *International Journal of Hydrogen Energy*, Elsevier Ltd *35*, 6617-6623.

302. Abdulagatov, I. M., Bazaev, A. R., and Ramazanova, A. E. (1993) P-V-T-x measurements of aqueous mixtures at supercritical conditions, *International Journal of Thermophysics 14*, 231-250.

303. Greenwood, H. G. (1969) The Compressibility of Gaseous Mixtures of Carbon Dioxide and Water Between 0 and 500 Bars Pressure and 450 and 800 Centigrade, *American Journal of Science 267-A*, 191-208.

304. Cocero, M., Alonso, E., Sanz, M., and Fdzpolanco, F. (2002) Supercritical water oxidation process under energetically self-sufficient operation, *The Journal of Supercritical Fluids 24*, 37-46.

305. Brennecke, J. F., Tomasko, D. L., and Eckert, C. A. (1990) Naphthalene/triethylamine exciplex and pyrene excimer formation in supercritical fluid solutions, *Journal of Physical Chemistry 94*, 7692-7700.

306. Roberts, C. B., Chateauneuf, J. E., and Brennecke, J. F. (1992) Unique Pressure Effects on the Absolute Kinetics of Triplet Benzophenone Photoreduction in Supercritcal CO2, *Journal of American Chemistry Society 114*, 8455-8463.

307. Wenzel, J. E., Lanterman, H. B., and Lee, S. (2005) Experimental $P - T - \rho$ Measurements of Carbon Dioxide and 1,1-Difluoroethene Mixtures, *Journal of Chemical & Engineering Data 50*, 774-776.

308. Lavric, E., Weyten, H., Deruyck, J., Plesu, V., and Lavric, V. (2006) Supercritical water oxidation improvements through chemical reactors energy integration, *Applied Thermal Engineering 26*, 1385-1392.

309. Tang, H., and Kitagawa, K. (2005) Supercritical water gasification of biomass: thermodynamic analysis with direct Gibbs free energy minimization, *Chemical Engineering Journal 106*, 261-267.

310. Van Konynenburg, P. H., and Scott, R. L. (1980) Critical Lines and Phase Equilibria in Binary Van Der Waals Mixtures, *Philosophical Transactions of the Royal Society of London. Series A, Mathematical and Physical Sciences 298*, 495-540.

311. Schneider, G. M., Scheidgen, A. L., and Klante, D. (2000) Complex Phase Equilibrium Phenomena in Fluid Mixtures up to 2 GPa−Cosolvency, Holes, Windows, Closed Loops, High-Pressure Immiscibility, Barotropy, and Related Effects, *Industrial & Engineering Chemistry Research 39*, 4476-4480.

312. Sadus, R. J. (1994) Calculating critical transitions of fluid mixtures: Theory vs. experiment, *AIChE Journal 40*, 1376-1403.

313. Ke, J., Han, B., George, M. W., Yan, H., and Poliakoff, M. (2001) How does the critical point change during a chemical reaction in supercritical fluids? A study of the hydroformylation of propene in supercritical CO(2), *Journal of the American Chemical Society 123*, 3661-70.

314. Byrd, A. J., Pant, K. K., and Gupta, R. B. (2007) Hydrogen Production from Ethanol by Reforming in Supercritical Water Using Ru/Al2O3 Catalyst, *Energy & Fuels 21*, 3541-3547.

315. Box, G. E. P., Hunter, J. S., and Hunter, W. G. (2005) Statistics for Experimenters: Design, Innovation, and Discovery 2nd ed., John Wiley & Sons, Inc., Hoboken, NJ.

316. Yaws, C. L. (1999) Chemical Properties Handbook: Physical, Thermodynamic, Environmental, Transport, Safety and Health related properties for Organic and Inorganic Chemicals, McGraw-Hill, New York, NY.

317. Cairns, E. J., and Tevebaugh, A. D. (1964) CHO gas phase compositions in equilibrium with carbon, and carbon deposition boundaries at one atmosphere, *Journal of Chemical and Engineering Data 9*, 453–462.

318. Baron, R. E., Porter, S. H., and Hammond, O. H. (1976) Chemical equilibria in carbon–hydrogen–oxygen systems., MIT Press, Cambridge, Mass.

319. Buragohain, B., Mahanta, P., and Moholkar, V. S. (2011) Investigations in gasification of biomass mixtures using thermodynamic equilibrium and semi–equilibrium model, *International Journal of Energy and Environment 2*, 551-578.

320. Castello, D., and Fiori, L. (2011) Supercritical water gasification of biomass: Thermodynamic constraints, *Bioresource technology*, Elsevier Ltd *102*, 7574-82.

321. Wang, X., Li, M., Li, S., Wang, H., Wang, S., and Ma, X. (2010) Hydrogen production by glycerol steam reforming with/without calcium oxide sorbent: A comparative study of thermodynamic and experimental work, *Fuel Processing Technology 91*, 1812-1818.

322. Wang, X., Wang, N., Li, M., Li, S., Wang, S., and Ma, X. (2010) Hydrogen production by glycerol steam reforming with in situ hydrogen separation: A thermodynamic investigation, *International Journal of Hydrogen Energy*, Elsevier Ltd *35*, 10252-10256.

323. Nichita, D., Gomez, S., and Luna, E. (2002) Multiphase equilibria calculation by direct minimization of Gibbs free energy with a global optimization method, *Computers & Chemical Engineering 26*, 1703-1724.

324. Prins, M. J., Ptasinski, K. J., and Janssen, F. J. J. . (2003) Thermodynamics of gas-char reactions: first and second law analysis, *Chemical Engineering Science 58*, 1003-1011.

325. Voll, F. A. P., Rossi, C. C. R. S., Silva, C., Guirardello, R., Souza, R. O. M. A., Cabral, V. F., and Cardozo-Filho, L. (2009) Thermodynamic analysis of supercritical water gasification of methanol, ethanol, glycerol, glucose and cellulose, *International Journal of Hydrogen Energy 34*, 9737-9744.

326. Wang, H., Wang, X., Li, M., Li, S., Wang, S., and Ma, X. (2009) Thermodynamic analysis of hydrogen production from glycerol autothermal reforming, *International Journal of Hydrogen Energy 34*, 5683-5690.

327. Li, Y., Wang, Y., Zhang, X., and Mi, Z. (2008) Thermodynamic analysis of autothermal steam and CO2 reforming of methane, *International Journal of Hydrogen Energy 33*, 2507-2514.

328. Mathieu, P., and Dubuisson, R. (2002) Performance analysis of a biomass gasifier, *Energy Conversion and Management 43*, 1291-1299.

329. Garcia, E. Y., and Larorde, M. A. (1991) Hydrogen production by the steam reforming of ethanol: thermodynamic analysis, *International Journal of Hydrogen Energy 16*, 307-312.

330. Rice, S. F. (1999) Kinetics of Supercritical Water Oxidation. Sandia National Laboratories Combustion Research Facility Final Report. Project 364-DOE.

331. Rice, S. F., and Steeper, R. R. (1998) Oxidation rates of common organic compounds in supercritical water, *Journal of Hazardous Materials 59*, 261-278.

332. Belkacemi, K., Larachi, F., and Sayari, A. (2000) Lumped Kinetics for Solid-Catalyzed Wet Oxidation: A Versatile Model, *Journal of Catalysis 193*, 224-237.

333. Wenzel, J. (2008) The Kinetics of Non-Catalyzed Supercritical Water Reforming of Ethanol, University of Missouri-Columbia.

334. Boock, L. T., and Klein, M. T. (1993) Lumping strategy for modeling the oxidation of C1-C3 alcohols and acetic acid in high-temperature water, *Industrial & Engineering Chemistry Research 32*, 2464-2473.

335. Webley, P. A., Tester, J. W., and Holgate, H. R. (1991) Oxidation Kinetics of Ammonia and Ammonia-Methanol Mixtures in Supercritical Water in the Temperature Range 530-700 C at 246 bar, *Industrial & Engineering Chemistry Research 30*, 1745-1754.

336. Cui, B., Liu, S., Cui, F., Jing, G., and Liu, X. (2011) Lumped kinetics for supercritical water oxidation of oily sludge, *Process Safety and Environmental Protection 89*, 198-203.

337. Corella, J., Toledo, M., and Aznar, M. (2002) Improving the Modeling of the Kinetics of the Catalytic Tar Elimination in Biomass Gasification, *Industrial & Engineering Chemistry Research 41*, 3351-3356.

338. Galtier, P. (2007) Kinetic Methods in Petroleum Process Engineering. In *Advances in Chemical Engineering, Volume 32* (Marin, G. B., Ed.), pp 259-302, Academic Press, Burlington, MA.

339. Ayasse, A. R., Nagaishi, H., Chan, E. W., and Gray, M. R. (1997) Lumped Kinetics of hydrocracking of bitumen, *Fuel 76*, 1025-1033.

340. Adschiri, T. (2002) Supercritical Fluid Technology. In *The Expanding World of Chemical Engineering* (Furusaki, S., Garside, J., and Fan, L. S., Eds.) 2nd ed., pp 105-124, Taylor & Francis, New York, NY.

341. Westbrook, C. K., Creighton, J., Lund, C., and Dryer, F. L. (1977) A numerical model of chemical kinetics of combustion in a turbulent flow reactor, *The Journal of Physical Chemistry 81*, 2542-2554.

342. Levenspiel, O. (1999) Chemical Reaction Engineering, *Industrial & Engineering Chemistry Research 38*, 4140-4143.

343. (2011) Dow, OPIM TM Glycerine, Physical Properties.

344. Duan, Z., Moller, N., and Weare, J. (1996) A general equation of state for supercritical fluid mixtures and molecular dynamics simulation of mixture PVTX properties, *Geochimica et Cosmochimica Acta 60*, 1209-1216.

345. Haruki, M., Yahiro, Y., Higashi, H., Iwai, Y., and Arai, Y. (1999) Correlation of Phase Equilibria for Water + Hydrocarbon Systems at High Temperatures and Pressures by Cubic Equation of State., *Journal of Chemical Engineering of Japan 32*, 535-539.

346. Tester, J. W., and Cline, J. A. (1999) Hydrolysis and Oxidation in Subcritical and Supercritical Water: Connecting Process Engineering Science to Molecular Interactions, *Corrosion 55*, 1088.

347. Valderrama, J., and Zavaleta, J. (2005) Generalized binary interaction parameters in the Wong–Sandler mixing rules for mixtures containing -alkanols and carbon dioxide, *Fluid Phase Equilibria 234*, 136-143.

348. Fornari, R. E., Alessi, P., and Kikic, I. (1990) High pressure fluid phase equilibria: experimental methods and systems investigated (1978–1987), *Fluid Phase Equilibria 57*, 1-33.

349. Dohrn, R., and Brunner, G. (1995) High-pressure fluid phase equilibria: Experimental methods and systems investigated (1988–1993), *Fluid Phase Equilibria 106*, 213-283.

350. Christov, M. (2002) High-pressure fluid phase equilibria Experimental methods and systems investigated (1994–1999), *Fluid Phase Equilibria 202*, 153-218.

351. Dohrn, R., Peper, S., and Fonseca, J. M. S. (2010) High-pressure fluid-phase equilibria: Experimental methods and systems investigated (2000–2004), *Fluid Phase Equilibria 288*, 1-54.

352. Fonseca, J. M. S., Dohrn, R., and Peper, S. (2011) High-pressure fluid-phase equilibria: Experimental methods and systems investigated (2005–2008), *Fluid Phase Equilibria 300*, 1-69.

353. Bazaev, A. R., Abdulagatov, I. M., Magee, J. W., Bazaev, E. A., Ramazanova, A. E., and Abdurashidova, A. A. (2004) PVTx Measurements for a H2O + Methanol Mixture in the Subcritical and Supercritical Regions, *International Journal of Thermophysics 25*, 805-838.

354. Abdulagatov, I., Bazaev, E., Bazev, A., and Rabezkii, M. (2001) PVTx measurements for dilute water+n-hexane mixtures in the near-critical and supercritical regions, *The Journal of Supercritical Fluids 19*, 219-237.

355. Breland, E., and Englezos, P. (1996) Equilibrium Hydrate Formation Data for Carbon Dioxide in Aqueous Glycerol Solutions, *Journal of Chemical & Engineering Data 41*, 11-13.

356. Mohammadi, A. H., Kraouti, I., and Richon, D. (2008) Experimental Data and Predictions of Dissociation Conditions for Methane, Ethane, Propane, and Carbon Dioxide Simple Hydrates in the Presence of Glycerol Aqueous Solutions, *Industrial & Engineering Chemistry Research 47*, 8492-8495.

357. Huron, M. J., and Vidal, J. (1979) New mixing rules in simple equations of state for representing vapour-liquid equilibria of strongly non-ideal mixtures, *Fluid Phase Equilibria 3*, 255-271.

358. Holderbaum, T., and Gmehling, J. (1991) PSRK: A Group Contribution Equation of State Based on UNIFAC, *Fluid Phase Equilibria 70*, 251-265.

VITA

Jason Wade Picou was born in St. Louis, Missouri in November 1982. Jason graduated from Ste. Genevieve High School in May of 2001. In December of 2005 he graduated from the University of Missouri-Columbia with a B.S. in Chemical Engineering. Jason transferred to Missouri University of Science and Technology and graduated with his Master's Degree in Chemical Engineering in August 2008.